Department of Carbohydrates
and Cereals, UCT Prague

UNIVERSITY OF
CHEMISTRY AND TECHNOLOGY
PRAGUE

Czech Chemical Society

Proceedings of the 19th International Conference on Polysaccharides-Glycoscience

Prague, Czech Republic
November 8 – 10, 2023

ICPG 2023

ISBN 978-80-88307-17-4
ISSN 2336-6796

EuChemS
European Chemical Society

Chem Plus Chem
Chemistry Europe

Proceedings of the 19th International Conference on Polysaccharides-Glycoscience

Prague, Czech Republic
November 8 – 10, 2023

EDITOR

Ing. Roman Bleha, Ph.D.
UCT Prague
Department of Carbohydrates and Cereals
Technická 3, Prague
Czech Republic

PUBLISHED AND DISTRIBUTED BY

Czech Chemical Society
Novotného Lávka 5
116 68 Prague, Czech Republic

ISBN 978-80-88307-17-4
ISSN 2336-6796

The conference is sponsored by

Organising Committee

Dr. Helena Pokorná
Czech Chemical Society

Ing. Alena Vlková
Czech Chemical Society

Ing. Radmila Řápková
Chemické listy journal

Ing. Ivan Jablonský, CSc.
Czech University of Life Sciences, Prague

Ing. Roman Bleha, Ph.D.
Department of Carbohydrates and Cereals, UCT Prague

Scientific Committee

Ing. Roman Bleha, Ph.D.,
Department of Carbohydrates and Cereals, UCT Prague

Prof. Jana Čopíková, CSc.
Department of Carbohydrates and Cereals, UCT Prague

Assoc. prof. Evžen Šárka, CSc.
Department of Carbohydrates and Cereals, UCT Prague

Assoc. prof. Manuel Antonio Coimbra, Ph.D.
Department of Biochemistry and Food Chemistry, Universidade de Aveiro

Prof. Krzysztof Surówka
Department of Refrigeration and Food Concentrates, University of Agriculture, Kraków, Poland

Prof. Richard Tester
Glycologic Limited, Reading, UK

Dr. Triinu Visnapuu
Institute of Molecular and Cell Biology, University of Tartu, Estonia

Ing. Zuzana Košťálová, Ph.D.
Institute of Chemistry, Slovak Academy of Sciences, Bratislava, Slovak Republic

Ing. Ján Hirsch, DrSc.
Institute of Chemistry, Slovak Academy of Sciences, Bratislava, Slovak Republic

Assoc. prof. Andrej Sinica, Ph.D.
Department of Carbohydrates and Cereals, UCT Prague

Ing. Petra Smrčková, Ph.D.
Department of Carbohydrates and Cereals, UCT Prague

Contents

DEVELOPMENT OF A TECHNOLOGY FOR CRYSTALLIZATION AND SPRAY DRYING OF SACCHARIDES IN THE FOOD INDUSTRY

DAMLA AVCI*, SVATOPLUK HENKE, SIMONA GILLAROVÁ, ZDENĚK BUBNÍK

Department of Carbohydrates and Cereals, University of Chemistry and Technology, Prague, Technická 5, 16628 Prague 6

avcid@vscht.cz

Abstract

This work presents the purification and separation of sucrose from solution with optimal experimental techniques by cooling crystallization, spray drying, and image analysis. Key parameters including supersaturation, nucleation, metastable zone width, and cooling rate were determined through a series of batch crystallization experiments. Subsequently, spray drying of the sucrose solution was performed to yield dried crystals. Furthermore, the characterization of the resulting crystals, encompassing both their quality and size distribution, was conducted via LUCIA image analysis after the crystallization processes.

Introduction

The principle of this work is based on performing and determining the optimal design of crystallization and drying methods on food products, especially on sucrose, to evaluate the newly designed technology for industrial process engineering. One of the key subjects of experimentation in this research was to focus on crystallization process design to determine the optimal experimental conditions yielding the most informative procedural data, which can be used to accurately identify the supersaturation, nucleation, crystal growth, metastable zone width, and other essential parameters. Another central aspect was achieving an efficient spray drying on pre-existing crystals in solutions of sucrose for a comprehensive range of applications within a practical processing time.

Sucrose (sugar, saccharose, Sac, $C_{12}H_{22}O_{11}$) is a carbohydrate generally found as a mixture form in food products. Sucrose is a disaccharide consisting of dimmer glucose-fructose monosaccharides linked by one oxygen atom (see Figure 1), the main composition of table sugar (granulated-refined sugar). It does not only provide a sweet taste for edible materials but also gives them a distinctive texture.[1,2,3] In addition, sucrose improves the color, flavour, shelf-life, and preserving properties of food products. Moreover, it can increase yeast fermentation activity and the rising baking products in the food industry. Besides food manufacturing, sucrose is also commonly used in biotechnological industries such as ethanol production.[4,5]

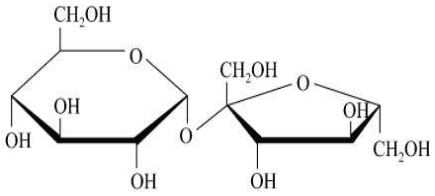

Figure 1: **Structure of sucrose**

To enhance the automation of industries, control techniques, and image classification systems have to be accurate and efficient in crystallization processes. Since the crystallization step in the sugar production flow will affect the quality of the final product, it is necessary to control the critical parameters and keep them at an optimal level. It should also be considered that controlling produce the final crystals in high quality will affect further downstream processes such as washing, filtration, or drying.[6]

The formation of supersaturation, nucleation, crystal growth, and metastable zone width are the essential points in the sucrose crystallization process. To produce pure crystalline solids efficiently, the designer of crystallization equipment takes steps to ensure the control of the supersaturated solution formation, the first crystal nuclei appearance, and growth of the nuclei in desired size. Determination of the process kinetics of a solution system is crucial to obtain an explanation for the crystallization processes. The thermodynamic driving force for crystallization arises once the melt or solution has become supersaturated. In other words, the shift of molecules

occurs through a crystalline form to reduce the energy level of the system. In addition, nucleation or subsequent development of the solute nuclei and crystal growth are essential two stages in the crystallization process, with the relative magnitudes of the competing processes for supersaturation consumption defining the size of the crystal, distribution, and yield of the end product.[7,8]

Spray drying is one of the well-known methods for producing particles with a special equipment, invented in the 1870s.[9] The basic principle is removing moisture from the feed product by applying heat and controlling humidity. This process mainly results in amorphous (non-crystalline) solids due to the rapid transition between liquid and solid phases. However, crystalline substances also can be produced by this method. Spray drying accurately feeds the crystals, allowing fine-tuning of the final content of residual solvents and crystal size distribution.[10]

LUCIA (Laboratory Universal Computer Image Analysis) is a powerful digital image analysis used mainly in the food and chemical industries. The instrument provides a computer vision to determine the various parameters, including particle size, texture, structure, and geometric properties of samples such as sugars. Moreover, the system consists of up-to-date software and a camera with high-resolution objective lenses on a microscope which provides high-quality images. Image data acquired by the system of computer can be saved, analysed, and presented in the form of matrices, the units of which are referred to as pixels for purposes of image processing, with the information stored as visual features.[11] In addition, this technique can determine the crystal size and shape in various samples such as saccharides, and it provides clear images for research and industrial analysis. Furthermore, the output of the program provides the data for statistical and mathematical measurements, including histogram plots to assess crystal size distribution.[12]

Materials, equipment, and methods

Crystallization processes

75.62 % (*w*/*w*) sucrose solutions were prepared by dissolving 2053 g of white crystal table sugar (AGRANA® Sales & Marketing GmbH Company, A-1020, Wien) in 662 g of demineralized water at 77 °C on an induction heater (Model: R-223, Rohnson®, Czech Republic), respectively. The program of the thermostat was set according to the Table I and Table II for all measurements. Subsequently, prepared sucrose solution was put in a 3.0 L of jacketed glass reactor vessel. The impeller speed was set to 70.0 rpm. A low-power ultrasonic sensor (LiquiSonic ®: SensoTech GmbH, Germany) and a temperature sensor data logger (ALMEMO® 2590-9 V5) inside the solution were connected to the personal computer (PC). The thermostat program was run.

Seeding technique was applied only for measurement Sac-6. 2 g of sucrose was mixed with 2 ml of isopropanol (PENTA®, Czech Republic) in a small beaker. The mixture was added inside the 75.62 % (*w*/*w*) sucrose solution in three steps according to Table II. Temperature was manually lowered by thermostat until the crystals remained undissolved in the solution. After the program was ended for all six measurements, all data was collected *on the PC*. The ultrasound velocity vs. temperature and temperature vs. time graphs were determined and examined on Microsoft Excel Office 365 software.

Table I: **Thermostat program of Sac crystallization experiments; measurement Sac-1 to 5.**

Measure-ment number	**Time t_1 in min**	**Time t_2 in min**	**Time t_3 in min**	**Time t_4 in min**	**Time t_5 in min**	**Time t_6 in min**	**Temper a-ture T_1 in °C**	**Tempera-ture T_2 in °C**
Sac-1	15	120	15	120	15	0.03	57	77
Sac-2	15	60	15	60	15	0.03	47	77
Sac-3	15	120	15	120	15	0.03	57	77
Sac-4	15	120	15	120	15	0.03	57	77
Sac-5	15	120	15	120	15	0.03	57	77

Table II: **Thermostat program of Sac crystallization experiment; measurement Sac-6.**

Steps	**1**	**2**	**3***	**4**	**5***	**6**	**7***
Time t in min	6	7	27	9	74	9	48
Temperature T_2 in °C	80	77	77	73	73	70	70

***** Seeding process applied.

Spray drying processes.

Before the experiment, sucrose solutions were dissolved in demineralized water at 65 °C on the induction heater according to Table III. Prepared samples at room temperature were dried according to operation conditions shown in Table IV. Dried powders were collected in 250 mL reusable glass media bottles and analysed for the further image analysis.

Table III: **The weight percents in mass of dried sucrose aqueous solutions.**

Measurement number	**1**	**2**	**3**	**4**	**6**
Aqueous solutions in weight percent (% (*w/w*) of sucrose)	67	60	60	20	30
Mass in kg	0.5	0.5	0.5	0.5	0.5

Table IV: **Operating conditions of spray drying processes; measurements SD-1 to SD-5.**

Measurement number	**Time (min)**	**T_{inlet} °C)**	**T_{outlet} (°C)**	**Pump Flow Rate (%)**	**Air Flow Rate in L s^{-1}**	**Compressor / Air Pump (mL L^{-1})**
SD-1	0 - 180	231	132	8	24	0.6
SD-2	0-39	251-85	124-68	11	24-25	0.6
SD-3	0-6	196-222	113-110	113-110	11-9	21-8
SD-4	15	120	15	120	15	0.03
SD-5	-	250	132	12	21	0.9

LUCIA image analysis

LUCIA image analysis was executed with the 12X optical zoom microscope (Navitar Ametek®, USA) and Nikon imaging software NIS-Elements (Version AR 5.11.01 64-bit) for evaluating the crystals on the PC. The products from crystallization and spray drying were prepared for the microscopy analysis according to Table V. Samples with a few drops of isopropanol on the slides were observed by 0.5X or 2X lenses (Navitar Ametek®, USA) and light with a cold light source (Schott KL 2500 LCD, SCHOTT®, Mainz). The statistical data was collected and exported to MS Excel.

Table V: **Operating conditions of the samples in LUCIA image analysis; sample E to F.**

Sample Name	**Process Type**	**Lens Magnitude**	**Isopropanol**
E	Spray Drying	0.5X	+
F	Spray Drying	0.5X	+
G	Crystallization	2X	+

Results and discussion

Crystallization processes

Crystallization experiments were analyzed qualitatively. Figure 2a demonstrates the cooling and heating cycle of batch process for the measurement Sac-5, and Figure 2b shows the measurement Sac-6. At the beginning, solutions were dissolved completely at 77.0 °C and 80.0 °C, respectively. During cooling process, slight haze which represents the first crystals appeared at 64.8 °C in 107.5 minutes for the measurement Sac-5. As the system cooled down more, white sugar crystals were visible as a slurry at 58.2 °C (see Figure 2a). After 5.5 hours, all the crystals were dissolved at the solubility temperature.

In the measurement Sac-6, seeding process started the crystallization in the field of supersaturating metastable by adding an amount of seeds in the concentrated solution by the temperature was lowered step by step until it reached to 70.3 °C in 3 hours (see Figure 2a and Figure 2b).[13] Seeding process provided more uniform and faster results than the experiments with normal development of nuclei.

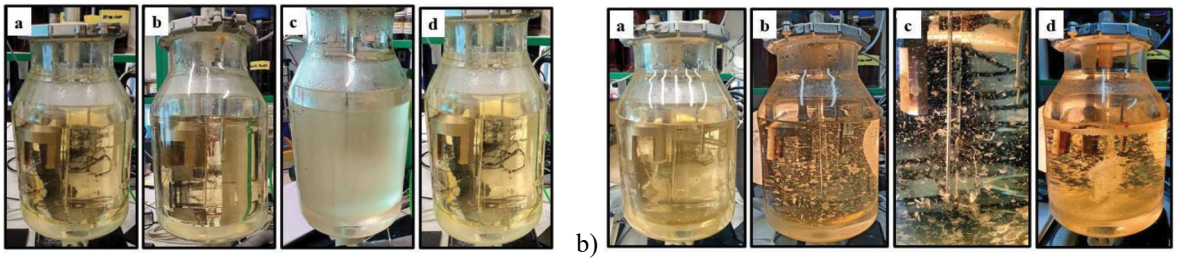

Figure 2: **Crystallization processes with the cooling and heating cycles; a) measurement Sac-5, b) measurement Sac-6.**

The key variables were determined by quantitative measurements for developing industrial crystallization operations shown in Figure 3. Figure 3a illustrates that the MSZW is between 64.5-67.09 °C which can be verified in accuracy by qualitative analysis while slight haze appeared at 64.8 °C due to the nucleation during the cooling process in Figure 2a. In addition, temperature sensor represents a slight shift from the heating side after 65 °C due to the dissolving of solution, and it can be a sign for the end of the nucleation point (see Figure 3b). From Figure 3c, it can be seen that linear cooling and supersaturation control was initiated to start crystallization by seeding. The experimental supersaturation point is almost equal to the theoretical point that indicates a successful result with optimal parameters. Temperature-time shows the gradual temperature in three steps (see Figure 3d).

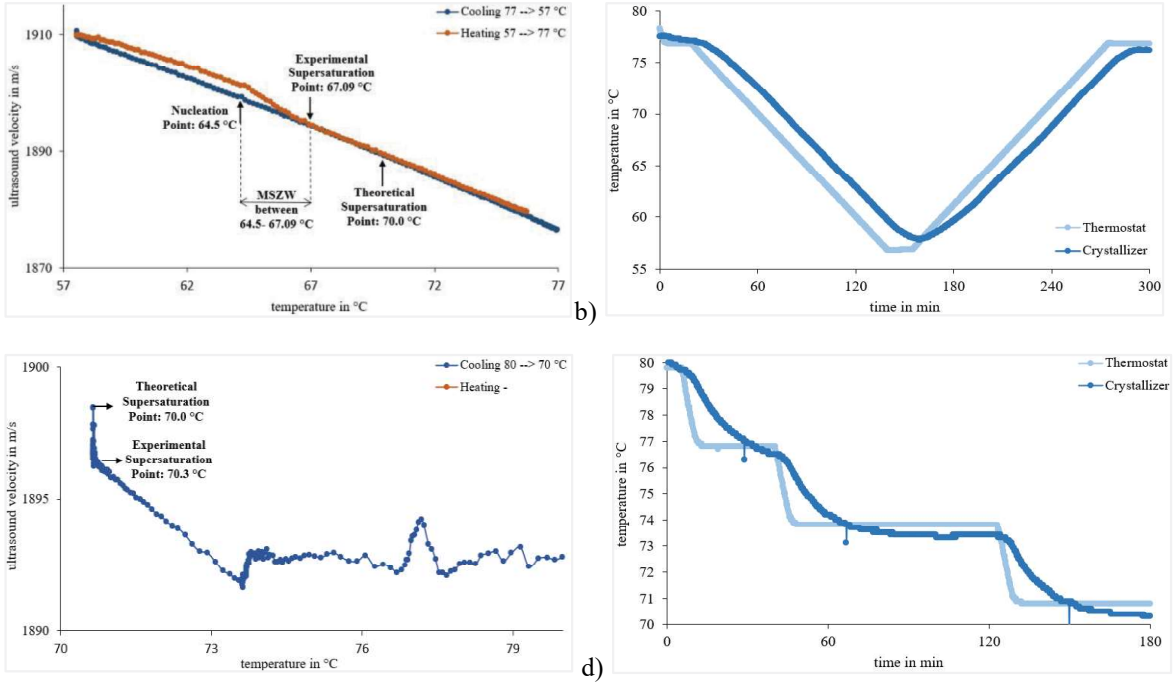

Figure 3: **The variations of ultrasound velocity versus temperature and temperature versus time during the cooling/heating cycles.**

As a result, especially these optimized parameters can be verifiable and approvable for availability of usage as setpoints in the development of industrial progress by comparing the study by Bubnik et al., which had the same experimental conditions with the identical analytical sensors.[14] However, similar to the study by Belca et al., it was achieved that seeding technique compared to spontaneous crystallization measurements, the seeding technique gives better results, provides more control, and eliminates waste of time, especially for confirming the experimental supersaturation point.[15]

Spray drying processes.

Crystalline products were gained under controlled airflow and temperature conditions. In this way, it was attempted to find the optimal operation method. However, stickiness of dried sucrose is a common due to its hygroscopicity feature. While sucrose was exposed to moisture, sticky form occurred due to higher solubility in water. The product sticked to the wall of dryer chamber and the less amount of product was collected (see Figure 4a). To avoid from this problem, a wide range of inlet temperature was applied. In the end, it was observed that this issue was caused by clogged nozzle by agglomeration of the sample. Drying aids such as Arabic gum can be a solution to obtain less sticky product. Also, a new nozzle can be used.

Figure 4c shows the difference between dried samples from two measurements. While the inlet temperature T_{inlet} was kept between 196 °C and 215 °C, white sucrose particles were collected as desired. With higher temperature exposure at 250 °C, sugar degradation has occurred. Therefore, the undesired brownish product was collected (see Figure 4b and 4c).

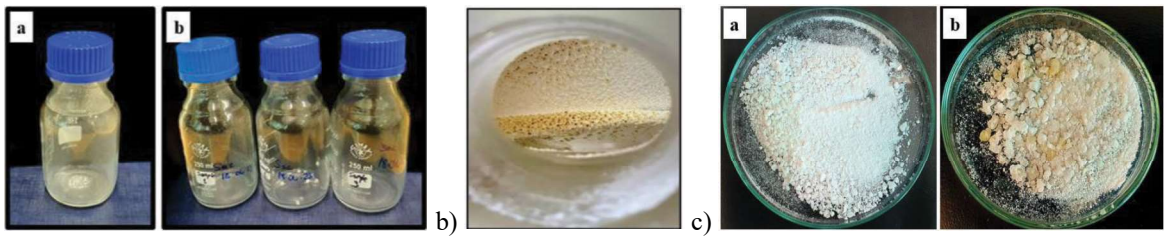

Figure 4: **Collected dried samples; a) measurement SD-1 and measurement SD-2, b) Caramelization in the chamber from measurement SD-5, c) White powder from measurement SD-3 and SD-4, and caramel powder from SD-5.**

In traditional production processes, the crystallization process is applied before drying. The goal is to form crystals from the crystallizer and then remove the water using drying. However, there is no reason that why this sequence of operations, in which spray drying and crystallization are not carried out together, should not be combined in a single step. Therefore, this process can be used for future studies. Moreover, although converting amorphous to crystalline products has been widely studied, especially for sucrose, understanding the impact of operating conditions on the crystallization and spray drying process remains a significant point in industries.

LUCIA image analysis

Qualitative and quantitative characterization results of the individual sucrose particles were investigated based on microscopic image analysis. Qualitatively, the surface morphology of the crystals was analyzed. Quantitatively, the critical size distribution was determined by the statistical analysis.

The image analysis of the sucrose crystals obtained from crystallization and spray drying processes were examined (see Figure 5). Figure 5a shows 67 % (*w*/*w*) of sucrose particles of sample E collected from spray drying. Due to the unfixed sample, amorphous particles were randomly ordered, and without a distinctive shape. Figure 5b demonstrates the spray dried 30 % (*w*/*w*) sucrose particles of sample F fixed with isopropanol to get a clear visualization. It shows the shape of the sample, which seems like broken pieces of assembled sugar particles. Figure 5c represents the sucrose crystals obtained from the solution inside the reactor at room temperature. A cubic shaped crystals were observed after crystallization. Large and small particles appear to be uniform in size and shape in this sample, although it is difficult to obtain the desired uniform shape and size in crystals due to the easily changeable feature of the nucleation and growth phases.[16]

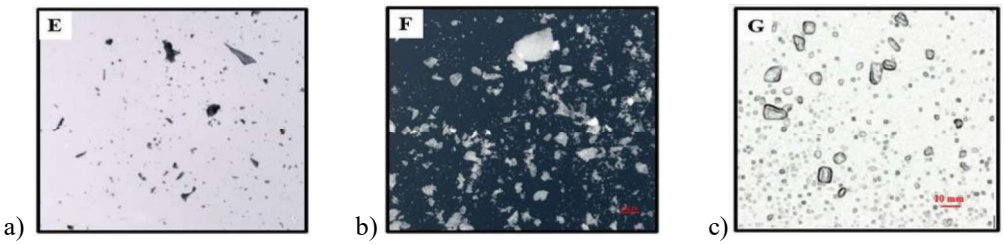

a) b) c)

Figure 5: **Spray dried sucrose particles; a) 67 % (*w/w*) of sucrose without isopropanol fixation (no included scalebar), b) 30 % (*w/w*) of sucrose with isopropanol fixation (scalebar: 500 µm), c) Sucrose crystals obtained after crystallization at room temperature with isopropanol fixation (scalebar: 1000 µm).**

The histogram graphs shown in Figure 6 represents crystal size distribution (CSD) analysis from obtained statistical data with various parameters such as Feret diameter, volume fraction, cumulative curve, and equivalent diameter of the measured particles.

67% (w/w) sucrose particles obtained via spray drying had a size range between 550-1450 µm, with an average length of 850 µm for 81 particles according to Figure 6a. This increased length is attributed to agglomeration resulting from a high concentration, where particles collide and stick together, forming larger pieces.

30% (w/w) sucrose revealed a size range between 10-1070 µm (see Figure 6b). The first quartile Q1 refers to 90 µm, which means the 25 % of the length of all particles are less than 90 µm. The mean is 63.41 µm which is the average of the number of the sample. Also, second quartile (Q2, median) is equal to the interquartile area between Q1-Q3, which means that the 50 % of the length of all particles are in the range between 90-330 µm. The third quartile Q3 starts from 330 µm, which means the 25 % of the length of all particles are more than 330 µm. In addition, the right from 710 µm bar represents the 4 % of all particles, and the large size particles are included in this area.

The length of the samples obtained from the aqueous solution after crystallization process at room temperature were measured in size interval that was between 2.8-11.8 µm (see Fig 6c). The average length was 6.4 ± 2 µm. Q1 was 4.8 µm, mean was 6.3 µm, Q2 was between 4.8-7.3 µm, and Q3 was 7.3 µm for this distribution.

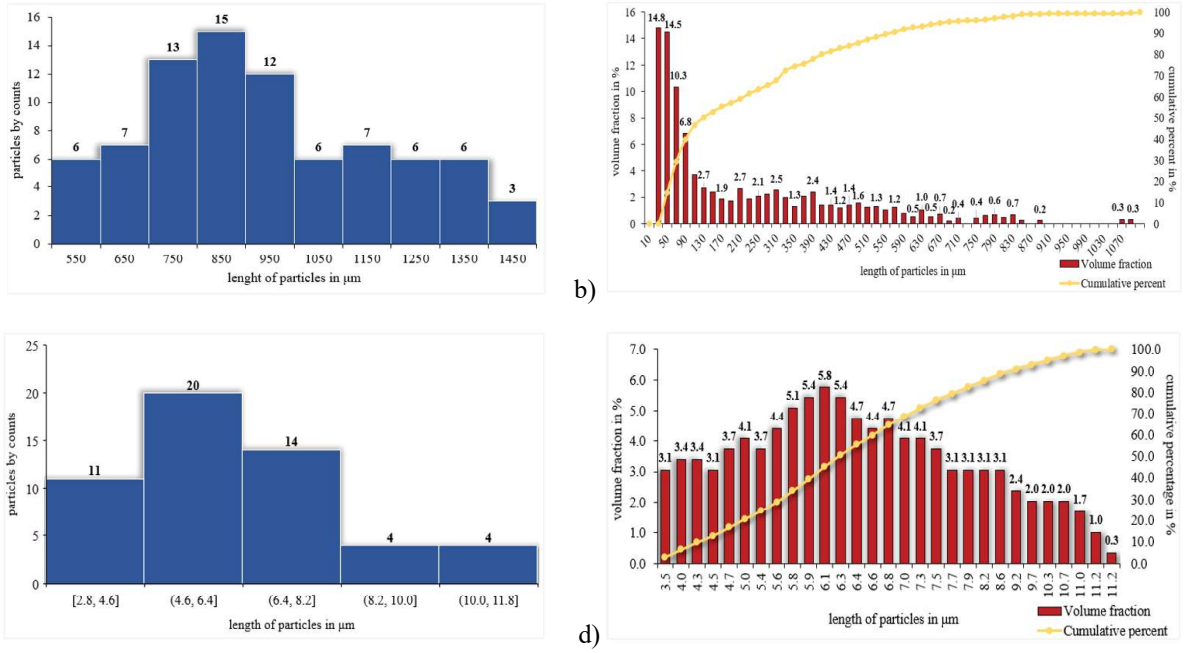

a) b) c) d)

Figure 6: **CSD histograms according to the particles by counts versus length, and cumulative and frequency particle size distributions; a) CSD of sample-E, b) cumulative curve of sample-F, c) CSD of sample-G, d) cumulative curve of sample-G.**

Particle characterization is crucial for understanding the properties of food substances, encompassing factors such as shape and size. While particle technology is complex and less prevalent in various fields, their properties are extensively used for qualitative and quantitative analyses, aiding in the assessment of powder and suspension behaviour. It also serves as valuable guidance for equipment selection in many studies. As a result, obtained image analysis results indicate that surface morphology and length size of the sucrose and sodium acetate particles which were affected by the crystallization and spray drying operating conditions has powerful impact on the modelling process. Thus, the obtained results can be considered in the development of the crystallization and drying processes.

Conclusion

In the crystallization process of 75.62 % (*w*/*w*) sucrose aqueous solution, since the first crystals are seen at 64.8 °C, the lowest thermostat temperature can be kept at these levels. Thus, excess crystallization with over-cooling can be prevented, and the growth of the obtained crystals can be achieved in a controlled manner. In addition, metastable zone width was measured between 64.5-67.1 °C.

Experiments under certain circumstances demonstrated that seeding technique and temperature are certainly essential when crystallizing the sucrose via cooling batch processing. It helped to promote crystal formation, to detect the experimental supersaturation point and to avoid the loss of time for crystal growth. Subsequently, the key parameters (supersaturation point, nucleation point, crystal growth, and metastable zone width) has been investigated by analytical sensors which provided the graphical data. Especially, low-power ultrasonic sensor had provided a sensitive measurement to measure these parameters. This sensor can be used to improve product quality by controlling and maintaining supersaturation and crystal growth in the industries.

It was determined that the concentration of the feed, drying parameters, and nozzle diameter affect the drying performance and amount and of the final product during the experimental process of spray drying. In addition, the high inlet temperature at 250 °C leads to caramelization of sucrose. The stickiness problem of sucrose during the experiments can be solved by adding substances which are preventing the agglomeration or changing the nozzle in diameter in further analysis.

In LUCIA image analysis, the typical cubic shape of sucrose was determined. According to crystal size distribution, it was observed that the size of the particles obtained from spray drying is smaller than the obtained particles from crystallization. In future studies, detected situations such as agglomeration can be investigated to design particles and to better understand crystallization and drying processes. As a result, the obtained data of this study leads to the unveils all benefits of having real-time process analytical data in industrial processes which can be in the food industry to improve long-term monitoring, assessment and performance of the crystallization and drying processes.

REFERENCES

1. Da Costa, Z., Pontuschka, W., Campos, L. et al.: Appl Radiat and Isot, *62*(2), 331-336 (2005).
2. Hartel, R. W., Shastry, A. V. et al.: Crit Rev Food Sci Nutr, *30*(1), 49-112 (1991).
3. Honig, P. et al.: Princ Sugar Technol, (2013).
4. Asadi, M. et al.: Beet-Sugar Handb, (2006).
5. Xingchu, G., Shanshan, W., Haibin, Q. et al.: Chinese J Chem Eng, *19*(2), 217-222 (2011).
6. Terdenge, L. M., Wohlgemuth, K. et al.: Cryst Res Technol, *51*(9), 513-523 (2016).
7. Mitchell, N. A., Ó'Ciardhá, C. T., & Frawley, P. J. et al.: J Cryst Growth, *328*(1), 39-49 (2011).
8. Laos, A. K., Kirs, B. E., Kikkas, C. A., Paalme, D. T. et al.: Proceedings Eur Congr Chem Eng, (2007).
9. MP, W. et al.: Rev Spray Dry Technol, *4*(2) (2014).
10. Patel, R., Patel, M., Suthar, A. et al.: Indian J Sci Technol, *2*(10), 44-47 (2009).
11. Fıratlıgil-Durmuş, E., Šárka, E., Bubník, Z. et al.: Czech J Food Sci, *26*(2), 109-116 (2008).
12. Engineers, I. o. C. et al.: 14th Int Sym Ind Cryst, (1999).
13. Gh, S., & Cheregi, V. et al.: Res Seed Agents Sugar Cryst, (2010).
14. Bubnik, Z., Kadlec, P., Hinkova, A. et al.: Rec Prog Cryst Sugar, *3*(3), 141-145 (2003).
15. Belca, L. M., Ručigaj, A., Teslič, D. et al.: Ultrason Sonochem, *58*, 104642 (2019).
16. Deora, N., Misra, N., Deswal, A., et al.: Food Eng Rev, *5*, 36-44 (2013).

AN ENVIRONMENTALLY FRIENDLY APPROACH TO THE ISOLATION OF CHONDROITIN SULPHATES FROM ANIMAL CARTILAGES

TAMILLA BABAYEVA*, ANDREJ SINICA

Department of Carbohydrates and Cereals, University of Chemistry and Technology Prague, Technická 5, 166 28 Prague, Czech Republic

mirzayet@vscht.cz

Abstract

Chondroitin sulphates are components of cartilage tissue in vertebrates that provide integrity, elasticity, and lubrication of the cartilage matrix. Current industrial methods for obtaining these polysaccharides from animal cartilage involve harmful chemicals and processes. An alternative environmentally sustainable approach, based on enzymatic hydrolysis of collagens with proteases and dialysis, was tested on pork, duck, and shark cartilages. The obtained products were pure chondroitin sulphates suitable for food and feed supplementation.

Introduction

Chondroitin sulphates (CS) are natural non-branched sulphated glycosaminoglycans composed of repeating 1,4-linked *β*-D-glucuronic acid and 1,3-linked *N*-acetyl-*β*-D-galactosamine residues. Individual types of chondroitin sulphate are distinguished based on the position of sulphate substitution, e.g., non-sulphated chondroitin (CS-0), chondroitin-2-sulphate (CS-2), chondroitin-4-sulphate (CS-A or CS-4), chondroitin-2,4-disulphate (CS-B), chondroitin-6-sulphate (CS-C or CS-6), chondroitin-2,6-disulphate (CS-D), chondroitin-4,6-disulphate (CS-E), chondroitin-2,4,6-trisulphate[1] (Fig. 1). CS demonstrate a wide structural diversity depending on the biological species (mammals, birds, fishes, or invertebrates) and body localization.

CS are the main component of the extracellular matrix and, together with other biopolymers, ensure the structural integrity of the tissues. They are plentiful in various connective tissues, especially in the cartilage, where it is free or associated with proteins. In mammals, CS is highly sulphated. Sulphate groups generate an electrostatic repulsion, providing resistance to cartilage compression and allowing complexation with proteins. The sulphated domains of CS act as ligands for proteins and mediate various physiological functions.

Commercial applications for CS are growing, e.g., use in osteoarthritis treatment[2,3] and cartilage regeneration[4]. Other applications include designing slow and controlled biodegradable scaffolds for wound healing[5]. CS is part of dietary supplements usually sold as a mixture with glucosamine[6].

The preparative methods used for isolation of CS from various natural sources were previously reviewed[7-9]. Generally, the preparative methods are based on the chemical hydrolysis of the dried defatted cartilage or another source to destroy the proteoglycan core, eliminate proteins and thus recover polysaccharides, including CS. First step uses proteases or chemical reagents to remove proteins. Ultrafiltration, dialysis, and ion exchange are the methods used for purification of crude CS extracts. Current industrial methods for obtaining these polysaccharides from animal cartilage involve harmful chemicals and processes. An alternative environmentally sustainable approach, based on enzymatic hydrolysis of collagens with proteases and dialysis, was tested on pork, duck, and shark cartilages.

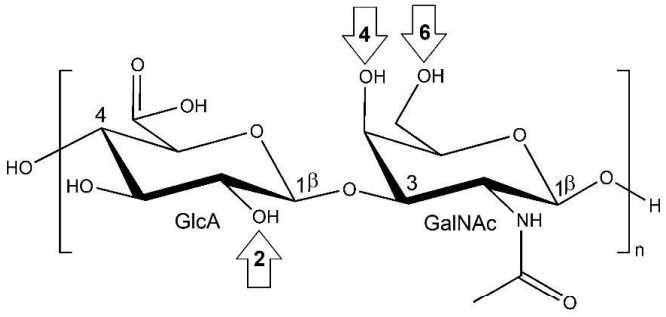

Figure 1: **Basic structure of CS. Arrows shows possible positions of sulphation.**

Experimental

Materials

Animal cartilages from pig ribs, duck keels and shark vertebrae were obtained from the chain store. Pepsin from porcine gastric mucosa and pronase from *Streptomyces griseus* were purchased from Sigma-Aldrich (USA). Organic solvents were purchased from Penta s.r.o., Czech Republic. Other chemicals and solvents used, like ethanol and deionised water, were of laboratory grade and prepared or ordered locally.

Isolation of CS from cartilages

The scheme of CS isolation from cartilages is shown in Fig. 3. The cartilage samples were washed with ethanol and freed of fat and soft tissue, then ground in an IKA laboratory grinder (IKA, Germany), washed with hexane to completely remove fat, and air-dried. The material processed in this way is shown in Fig. 2. It is a fibrous or flaky mass, so a Retsch MM 301 ball mill (Retch, Germany) was used to completely pulverize it. The cartilage proteins were hydrolysed using pepsin (pH 3) and pronase (pH 7) at 40°C overnight with magnetic stirring. This process resulted in the fragmentation of collagens, other proteins, and proteoglycans into peptides and free amino acids, and the solubilisation of polysaccharides occurred. Although most cartilage mass dissolved entirely, an insoluble fraction recovered in all three cases. Therefore, pepsin hydrolysis was repeated to achieve complete dissolution. Then the hydrolysates were dialysed (cut off 20 kDa) against distilled water and freeze dried yielding the macromolecular fractions. Purity of CS preparation was checked by organic elemental analysis and FTIR spectroscopy, and the structure and type of CS were defined by ^{1}H and ^{13}C APT NMR spectra.

Analytical methods

The organic elemental analysis (OEA) was performed on an Elementar Vario EL Cube instrument in central laboratories at the University of Chemical Technology in Prague. FTIR spectra (400–4000 cm^{-1}) of the fractions were recorded in KBr pellets using a Nicolet 6700 FTIR spectrometer (Thermoscientific, USA); 64 scans were accumulated with a spectral resolution of 2.0 cm^{-1}. The spectra were smoothed, and the baseline was corrected using Omnic 8.0 and 9.0 (ThermoScientific, USA) software and exported in ASCII format to Origin 2019b software (OriginLab Inc., USA) for graph preparation. The NMR spectra were recorded on a Bruker Avance III TM 600 MHz (Bruker, USA) in D_2O or with the addition of NaOD solutions and processed in MestReNova 10.0 software (Mestrelab Research S.L., Spain) software. All the spectra were exported to Origin 6.0 software (Microcal Origin, USA) software for graph preparation.

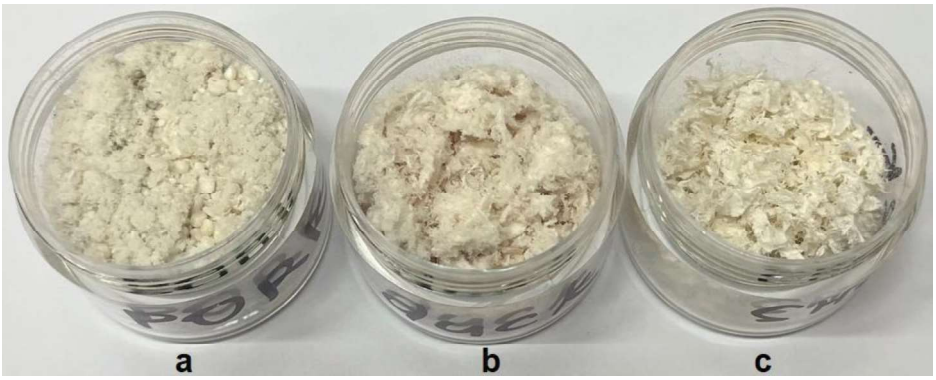

Figure 2: **Ground defatted cartilages from pork ribs (a), duck keel (b) and shark vertebrae (c).**

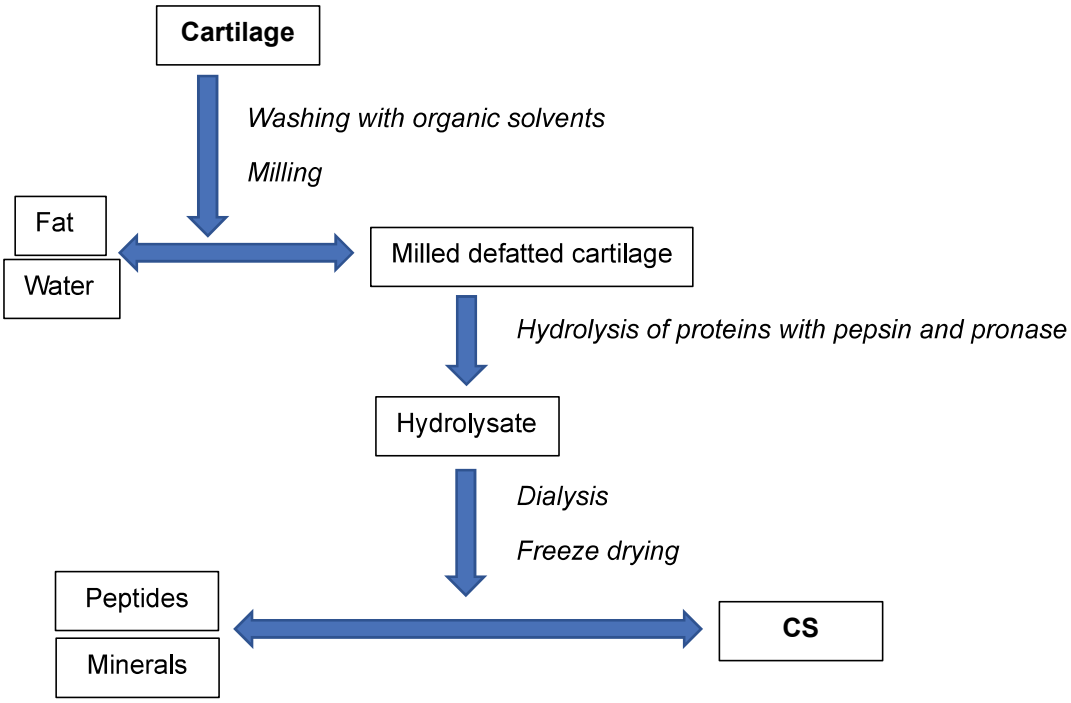

Figure 3: **Isolation of CS from cartilages.**

Results and discussion

FTIR spectra of defatted and dried ground cartilage samples are shown in Fig. 4. The presence of proteins is evident from intense amide bands at 1653-1657 and 1545-1552 cm^{-1} in all samples. Sulphate groups attached to CS are confirmed by prominent bands around 1238-1242 and 850-872 cm^{-1}. The stretching vibrations of C-O and C-C bonds of polysaccharides correspond to the bands in the region of 950-1200 cm^{-1}. The spectra of duck cartilage showed more intense bands assigned to vibrations of polysaccharides and sulphate ester groups. In contrast, protein bands were predominant in the spectrum of pig cartilage. In the case of shark cartilage, intense bands found at 1111, 602, and 557 cm^{-1} arose from inorganic components such as phosphates and carbonates. The differences in cartilage composition detected by FTIR spectroscopy suggest that they will affect the extraction and purification process.

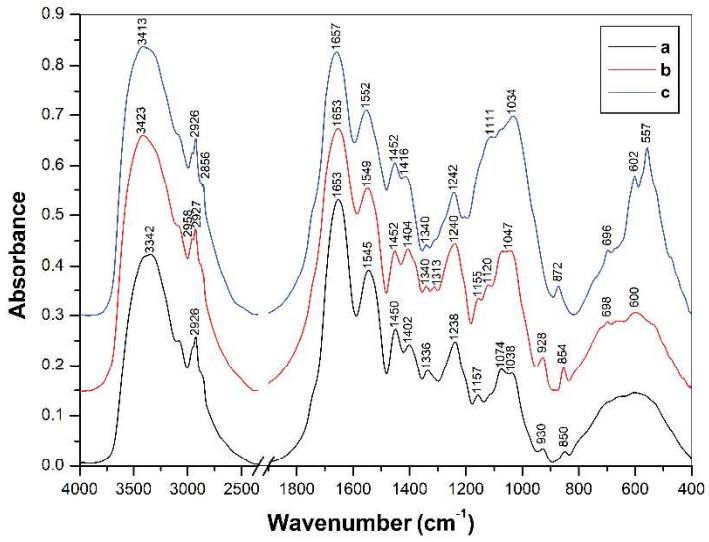

Figure 4: **FTIR spectra of defatted cartilages from pork ribs (a), duck keel (b) and shark vertebrae (c).**

The yields of soluble and insoluble cartilage fractions after the treatment with pepsin are summarized in Table I. The best dissolution of the sample occurred in the case of pig cartilage (78.7 % in total). On the other hand, shark

cartilage was the most resistant to hydrolysis (1.5 %), probably due to the presence of mineral components. Further steps of enzymatic hydrolysis of proteins led to complete dissolution of pig and duck cartilages, while in the case of shark cartilage, mineral compounds retained in the solid state and was removed from the hydrolysate.

The FTIR spectra of the fractions obtained by pepsin hydrolysis are shown in Fig. 5. The spectra were normalized according to the amide I band around 1650 cm^{-1}. The CS contribution to the fractions was indicated by the intensity of the vibrational bands of sulphate groups around 1240 cm^{-1} and polysaccharides in the region of 950–1200 cm^{-1}. The spectra showed that both fractions of porcine cartilage contain comparable amounts of polysaccharides. However, the hydrolysate of duck cartilage included significantly more CS than the solid fraction. In the case of shark cartilage, it is evident that the hydrolysate mainly contained protein residues, while the insoluble part had distinct IR bands of inorganic components. The insoluble part of the shark cartilage was soaked with an acidic solution to remove mineral compounds. This process eliminated most of them; the rest was removed as sediment during dialysis.

Dialysis of the hydrolysates resulted in purified polysaccharides identified as CS. Proton NMR spectra of CS derived from pig, duck and shark cartilage are shown in Fig. 6. From the spectra, it is clear that CS-A obtained from pig and duck cartilage were similar and different from CS-A obtained from shark cartilage. The strong resonance signals at 1.9–2.0 ppm correspond to the CH_3 protons in *N*-acetyl groups of β-GalNAc, and the signals at 4.3–4.6 ppm arose from anomeric H1β protons of both types of units. The signal at 4.68 ppm was assigned to the H5 of β-GlcA. The signals of the other carbohydrate protons were found in the region of 3.2 – 4.2 ppm. An intense signal near 3.92 ppm observed for CS from duck cartilage was similar to that found for CS isolated from industrial poultry waste[10]. Possibly this band correspond to the CS domain specific for poultries.

Table I: **Yields of soluble and insoluble cartilage fractions after the treatment with pepsin.**

Source	Fraction	Mass (g)	Yield (% w/w)
pork ribs	Raw material	9.18	100
	Hydrolysate 1	7.01	76.4
	Solids 1	1.92	20.9
	Hydrolysate 2	0.21	2.3
	Solids 2	0.27	2.9
duck keel	Raw material	3.00	100
	Hydrolysate	0.11	3.7
	Solids	0.38	12.7
shark vertebrae	Raw material	1.30	100
	Hydrolysate	0.02	1.5
	Solids	0.45	34.6

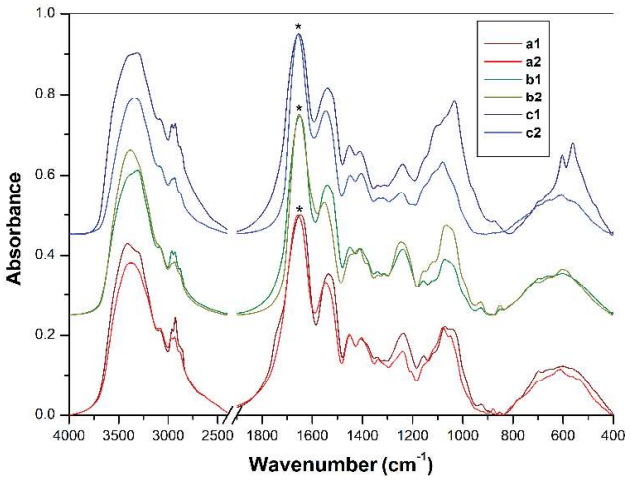

Figure 5: **FTIR spectra of soluble (1) and insoluble (2) cartilage fractions obtained by the treatment with pepsin: pork ribs (a), duck keel (b) and shark vertebrae (c).**

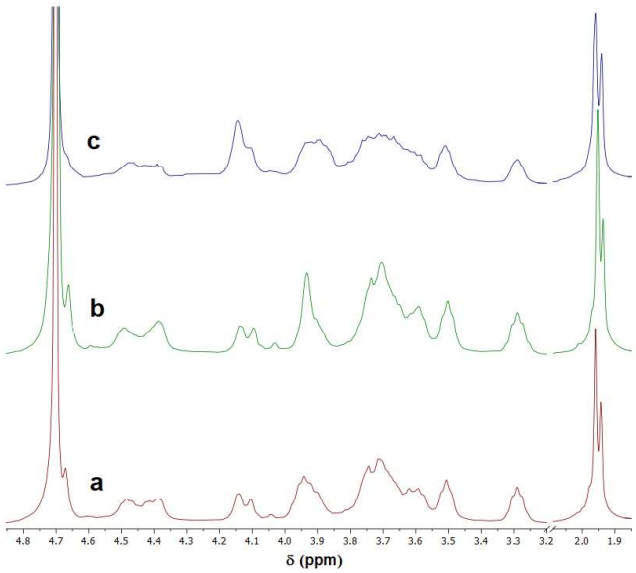

Figure 6: **^{1}H NMR spectra of CS from pork (a), duck (b) and shark (c) cartilages.**

Conclusions

Waste or by-products of animal processing is a source of CS as the main glycosaminoglycan of cartilage and other tissues. The presented results are useful to establish waste-free production order to dispose of the waste and prevent environmental problems. The preparative approach presented here leads to obtain this polysaccharide for food, feed, and pharmaceutical applications.

This work was supported from the grant of Specific university research – grant No A1_FPBT_2023_006.

REFERENCES

1. Volpi N.: Molecules, *24*, 1447 (2019).
2. Martel-Pelletier J., Farran A., Montell E., Vergés J., Pelletier J. P.: Molecules, *20*, 4277 (2015).
3. Brito R., Costa D., Dias C., Cruz P., Barros P.: Cureus *15*, e40192 (2023).
4. Muzzarelli R. A., Greco F., Busilacchi A., Sollazzo V., Gigante A.: Carbohydr. Polym. *89*, 723 (2012).
5. Zhang H., Xu R., Yin Z., Yu J., Liang N., Geng Q.: Macromol. Res. *30*, 36 (2022).
6. Restaino O. F., Finamore R., Stellavato A., Diana P., Bedini E., Trifuoggi M., De Rosa, M., Schiraldi C.: Carbohydr. Polym. 222, 114984 (2019).

7. Abdallah M. M., Fernández N., Matias A. A., do Rosário Bronze M.: Carbohydrate Polymers, 243, 116441. (2020).
8. Urbi Z., Azmi N. S., Ming L. C., Hossain M. S.: Curr. Issues Mol. Biol. *44*, 3905 (2022).
9. Nakano T., Pietrasik, Z., Ozimek L., Betti M.: Proc. Biochem. *47*, 1909 (2012).
10. Babayeva T., Sinica A., Kvasnička F., Bleha R., Demnerová K.: Proc. 18th Int. Conf. Polysac. Glycosci. 18, 48 (2022).

EXTRACTION AND CHARACTERIZATION OF NON-STARCH POLYSACCHARIDES FROM MILK THISTLE, HEMP AND SWEET BASIL SEEDS

ANGELIKA BIENIEK*, KRZYSZTOF BUKSA

University of Agriculture in Krakow, Faculty of Food Technology, Department of Carbohydrate Technology and Cereal Processing, ul. Balicka 122, 30-149 Kraków, Poland

angelika.bieniek@student.urk.edu.pl

Abstract

The aim of this study was to develop efficient methods of extraction of non-starch polysaccharides from the seeds of milk thistle, hemp, and sweet basil, and to determine their basic composition and molecular properties under standardized conditions. The highest yield of polysaccharides (43.9%) was obtained by extraction of ground sweet basil seeds at 70°C. In all of the seeds tested, whole seeds subjected to water extraction at 70°C had the highest content of sugar residues. Among all samples examined, the polysaccharides extracted from sweet basil seeds were of the highest average molar mass of 608,240 g/mol.

Introduction

Non-starch polysaccharides (NSP) constitute the main part of dietary fiber in cereal grains and seeds[1]. NSPs, which are commonly found in cereal grains and seeds include arabinoxylans, β-glucans, cellulose, galactomannans, arabinogalactans, xyloglucans and pectic polysaccharides[2]. Non-starch polysaccharides have many positive properties, especially for the food industry including: the ability to bind and retain large amounts of water, increase the viscosity of the solution, solubility, molecular weight and cross-linking ability[3]. In addition, non-starch polysaccharides have positive effects on human health, including supporting the functioning of the digestive system, stimulating the human immune system (they are immunomodulators), exhibiting antioxidant properties and preventing the occurrence of various types of cancer[4]. In the publications to date, there is a noticeable lack of information on the non-starch polysaccharides released during extraction by whole seeds of milk thistle, hemp, and sweet basil. A very small number of publications concerning these seeds, focus on the molecular weight of non-starch polysaccharides included in their composition. The aim of this study was to develop efficient methods for extracting (extraction) non-starch polysaccharides from the seeds of milk thistle, hemp, and sweet basil, and to determine their composition and molecular properties.

The research material was seeds of milk thistle (*Silybum marianum*) denoted as SM, hemp (*Cannabis sativa* L. var. *Sativa*) denoted as CS and sweet basil (*Ocimum basilicum L.*) denoted as OB were purchased from an online store.

Extraction of non-starch polysaccharides were made from 10 g of whole seeds and 10 g of ground seeds. Seeds (whole and ground separately) were poured into separate beakers of 250 mL capacity, then each sample was poured with 200 mL (in the case of sweet basil seeds it was 600 mL due to high water absorption) of water at 70°C. Extraction was carried out for 60 minutes on a magnetic stirrer. After this time, the sample was centrifuged for 10 minutes at 4500 × g (in the case of sweet basil seeds, it was centrifuged three times, after each centrifugation the clear supernatant was collected). The obtained supernatant was poured into plastic beakers, frozen and freeze-dried. The yield of non-starch polysaccharides was calculated as a percent of the amount of used seeds or wholemeal.

The monosaccharide composition of arabinoxylans was determined after acid hydrolysis by adapted HPLC/RI method[5]. For calibration, monosaccharide standards of glucose (Glu), arabinose (Ara), xylose (Xyl), galactose (Gal) and mannose (Man) at varying concentrations (0,1 - 1 mg/mL) were applied. The content of monosaccharides after hydrolysis was calculated in percent of dry mass of the sample as an average of two replications. The distribution of molar masses of the samples was determined by size exclusion chromatography (SEC)[5]. The protein content in the samples was determined by biuret assay. Statistical analysis of the results was conducted using MS Excel and StatSoft Statistica software.

Result and discussion

Table I shows the yield, monosaccharide composition and protein content in preparations polysaccharides from whole and ground milk thistle, hemp and sweet basil seeds extracted at two temperature levels.

Table I: **Monosaccharide and protein composition of preparations from milk thistle (SM), hemp (CS) and sweet basil (OT) seeds**

Preparation	Yield [%]	Sugar composition						Protein [%]
		Glc [%]	Xyl [%]	Gal [%]	Ara [%]	Man [%]	Total sugar content [%]	
SM-W-70	4.9	18.2±0.6e	5.2±0.5c	7.6±0.3c	4.0±0.1c	2.9±0.1c	37.8±1.6d	42.0±7.1e
SM-M-70	31.0	5.7±1.0a	0.2±0.3a	1.9±0.6a	2.0±0.1b	0.9±0.7a	10.8±2.4a	31.3±1.9c
SM-M-RT	21.1	7.0±1.6ab	0.4±0.2a	2.6±0.1a	2.3±0.2b	1.7±0.4b	14.0±2.4b	56.6±2.2f
CS-W-70	3.7	15.3±0.3d	1.5±1.1a	3.7±0.4b	1.1±0.5a	2.9±0.1c	24.4±2.6c	30.6±0.8c
CS-M-70	12.8	10.1±1.6c	0.2±0.3a	3.2±0.9ab	1.4±0.5a	2.1±0.0b	17.0±2.7b	24.6±0.9b
CS-M-RT	11.2	14.5±2.7d	1.0±0.4a	4.0±0.1b	1.4±0.1a	2.7±0.3c	23.5±4.0c	32.3±1.6c
OB-W-70	4.9	16.4±0.4d	15.4±1.0d	23.2±1.5f	15.3±1.0f	0.0±0.3a	70.3±3.8e	5.2±3.0a
OB-M-70	43.9	7.4±0.3b	4.5±0.5c	14.2±1.8e	7.7±1.1e	0.5±0.1a	34.3±3.8d	34.9±0.9d
OB-M-RT	42.8	4.9±0.2a	3.3±0.1b	11.0±0.9d	5.7±0.6d	0.4±0.0a	25.4±1.8c	44.8±0.7e

*SM-W-70 - whole milk thistle seeds extracted with water at a temperature of 70°C; SM-M-70 - ground milk thistle seeds extracted with water at 70°C; SM-M-RT - ground milk thistle seeds extracted with water at 25°C; CS-W-70- whole hemp seeds extracted with water at a temperature of 70°C; CS-M-70- ground hemp seeds extracted with water at a temperature of 70°C; CS-M-RT - ground hemp seeds extracted with water at 25°C; OB-W-70- whole sweet basil seeds extracted with water at a temperature of 70°C; OB-M-70- ground sweet basil seeds extracted with water at a temperature of 70°C; OB-M-RT - ground sweet basil seeds extracted with water at 25°C.

The highest yields of preparations of polysaccharides (42.8-43.9%) were obtained from ground sweet basil seeds, at both temperature levels (Table 1). The yield of polysaccharides from ground sweet basil seeds has not been studied previously. The smallest amounts of preparations (3.7-4.9%) were obtained from water extraction at 70℃ conducted on whole seed of milk thistle (SM-W-70), hemp (CS-W-70) and sweet basil (OB-W-70). The yield of polysaccharides from whole sweet basil seeds (OB-W-70) was similar to the results of Fekri et al., 2008 and Lodhi et. al, 2019[6,7]. The previous publication showed that temperature influenced the yield of polysaccharides. The highest yield of polysaccharides from whole basil seeds was observed at 50°C and started to decrease at ≥ 80°C[8]. The yield of non-starch polysaccharides from ground hemp seeds was 11.2-12.8% (Table 1), which was lower than in the work by Barsby et al., 2021[9].

The higher amount of total sugars (37.8%) was determined for the preparation obtained from whole milk thistle seeds subjected to extraction at 70°C (SM-W-70), compared to preparations from ground seeds of the same plant. The dominant sugar in all polysaccharide samples from milk thistle seeds was glucose (5.7-18.2%). The preparation obtained from ground milk thistle seeds, which were subjected to extraction at 70°C (SM-M-70), was characterized by the lower protein content of 31.3%, and the higher purity, compared to other preparations from milk thistle seeds. The previous studies showed that the total carbohydrate content in milk thistle seeds was 42.2%, of which polysaccharides accounted for 39.7%[10].

The higher amount of total sugars (24.4%) was determined for the preparation obtained from ground hemp seeds subjected to extraction at 70°C (CS-M-70), compared to other preparations from hemp seeds. In addition, in this sample (CS-M-70) glucose was the major sugar (15.3%), and protein accounted for 30.6%. The previous studies showed that polysaccharides from hemp seeds consist of 6.5% glucose, 1.4% ribose, 0.8% galactose, 0.1% arabinose, and 8.3% protein[9]. However, higher amounts of glucose have been detected in this study.

The highest amount of total sugars (70.3%) was determined for the preparation obtained from whole sweet basil seeds subjected to extraction at 70°C (OB-W-70), considering preparations from ground sweet basil seeds and all other. These total sugars included galactose (23.2%), glucose (16.4%), xylose (15.4%) and arabinose (15.3%). In addition, this sample (OB-W-70) had the lowest protein content (5.2%), compared to samples prepared from ground sweet basil seeds. The previous studies showed that polysaccharides from sweet basil seeds consist of 68.1% glucose and galactose, 5.05% mannose, 4.41% xylose, 2.15% arabinose, 1.54% rhamnose[11]. However, lower amounts of glucose, galactose, xylose, and arabinose have been detected in this study, respectively.

In all seeds tested (table 1), water-extracted samples at 70°C obtained from whole seeds had a higher sugar residue content compared to ground seeds heated and extracted at room temperature (25°C).

The preparation extracted from whole basil seeds (OB-W-70), which were subjected to extraction at 70°C, was characterized by the lowest protein content of 5.2%, and the highest purity. The lower protein content in the preparations obtained by the extraction at 70°C was probably due to the fact that under these conditions' protein was partially denatured and not extracted (table 1). As the opposite the ground seeds extracted in water at 25°C (table I) had the lowest purity and high protein content.

Based on the obtained sugar profiles of preparations extracted from the seeds of milk thistle (Table I), it can be assumed that their composition may include polysaccharides such as glucans, arabinogalactans, galactomannans, arabinoxylans. Preparations extracted from hemp seeds may include glucans, galactomannans, arabinogalactans, arabinoxylans. According to information in the literature, polysaccharides from hemp seeds consist of two fractions, which are composed of mannose, glucose, galactose, xylose in a molar ratio of 13.61:58.01:17.03:11.35 and mannose, rhamnose, galacturonic acid, galactose and arabinose in a molar ratio of 1.68:6.61:4.48:17.52:40.93:28.79[12]. Preparations extracted from sweet basil seeds may contain arabinoxylans, galactomannans, glucans. The previous studies showed that polysaccharides from hemp seeds consist of two main fractions: glucomannans (~43%) and a polysaccharide containing a xylan backbone linked by (1 → 4) bonds (~24.3%)[13].

Table II: **Molecular properties of preparations from milk thistle (SM), hemp (CS) and sweet basil (OT) seeds**

Preparation*	M_w [g/mol]	M_n [g/mol]	Đ
SM-W-70	2.200	400	5.5
SM-M-70	3.410	370	9.2
SM-M-RT	4.340	700	6.2
CS-W-70	1.590	330	4.8
CS-M-70	1.620	310	5.2

CS-M-RT	1.170	290	4.0
OB-W-70	565.900	40.980	13.8
OB-M-70	608.240	59.320	10.3
OB-M-RT	419.700	38.590	10.9

*Abbreviations of sample names as in Table I

The molecular parameters i.e., weight average molar mass (M_w), number average molecular mass (M_n) and dispersity (Đ) of polysaccharides from milk thistle, hemp and sweet basil seeds were calculated (Table 2) from the obtained molecular weight distribution profiles (Fig 1-3). The polydispersity index (Đ) was in the range of 4-13.8 for all samples and indicated that all polysaccharides were heterogeneous. Polysaccharides extracted from milk thistle seeds revealed an average molar mass of 2.200-4.340 g/mol[11]. In previous publications, the molecular mass of non-starch polysaccharides extracted from whole and ground milk thistle seeds has not been analyzed.

Polysaccharides extracted from hemp seeds indicated an average molar mass of 1.170-1.630 g/mol (Table II). The previous studies showed that polysaccharides from whole hemp seeds amounts to 864 -77.400 g/mol, which is in accordance with the results obtained in this work[12, 14]. In addition, the Mw of non-starch polysaccharides from ground hemp seeds has not been studied so far.

Polysaccharides extracted from sweet basil seeds, especially the sample obtained from ground seeds extracted with water at 70°C (OB-M-70) revealed the highest average molar mass of 608.240 g/mol. Polysaccharides extracted from whole sweet basil seeds (OB-W-70) revealed an average molar mass of 565.900 g/mol, what was lower than in the work by Naji-Tabasi et al. 2016[11]. In previous publications, non-starch polysaccharides extracted from ground sweet basil seeds in terms of Mw was not described.

The obtained molecular weight distribution profiles of the various polysaccharides from the seeds showed significant differences. The molecular weight distributions from the seeds of milk thistle and hemp (Figs 1 and 2) contain peaks that indicate the present of low molecular weight compounds (mono-, di- and oligosaccharides). The molecular weight distribution profiles of sweet basil seeds (Fig 3) are characterized by distinct peaks in the range of high molar mass, which indicate the present of polysaccharides.

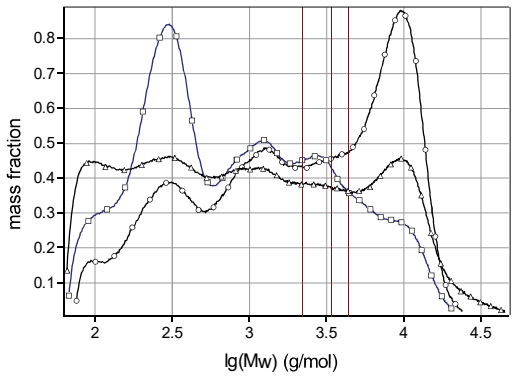

Fig. 1: Molecular weight distribution profiles of milk thistle seed preparations. (-Δ-) ground milk thistle seeds extracted with water at 70°C (SM-M-70), (-○-) ground milk thistle seeds extracted with water at 25°C (SM-M-RT), (-□-) whole milk thistle seeds extracted with water at a temperature of 70°C (SM-W-70).

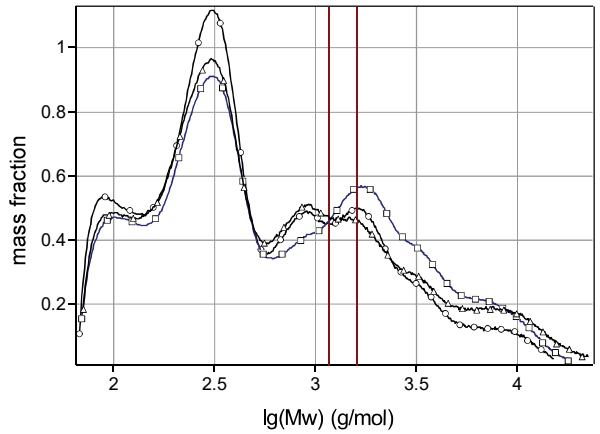

Fig. 2: Molecular weight distribution profiles of hemp seed preparations (-Δ-) ground hemp seeds extracted with water at a temperature of 70°C (CS-M-70), (-○-) ground hemp seeds extracted with water at 25°C (CS-M-RT), (-□-) whole hemp seeds extracted with water at a temperature of 70°C (CS-W-70).

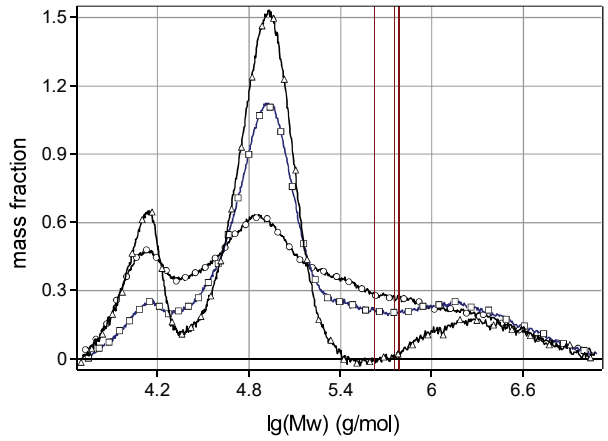

Fig. 3: Molecular weight distribution profiles of sweet basil seed preparations (-Δ-) ground sweet basil seeds extracted with water at 25°C (OB-M-RT), (-○-) whole sweet basil seeds extracted with water at a temperature of 70°C (OB-W-70), (-□-) ground sweet basil seeds extracted with water at a temperature of 70°C (OB-M-70).

Conclusion

The high yields of polysaccharide preparations were observed for the preparations obtained from milled seeds subjected to extraction at 70°C and the lowest yields were determined for the preparations obtained from whole seeds subjected to extraction at 70°C.

The highest content of total sugars (70.3%) was determined for the preparation obtained from whole basil seeds subjected to extraction at 70°C (OB-W-70), and the dominant sugar was galactose (23.2%). The lowest content of total sugars (10.8%) was found in the preparation obtained from ground seeds of milk thistle subjected to extraction at 70°C (SM-M-70) with glucose as the dominant sugar (5.7%).

The preparation extracted from whole basil seeds, which were subjected to extraction at 70°C (OB-W-70), was characterized by the lowest protein content of 5.2%, and the highest purity.

Polysaccharides extracted with water at 70°C from sweet basil seeds (OB-M-70) revealed the highest average molar mass of 608.240 g/mol. Among examined polysaccharides the lowest average molar mass of 1.170 g/mol was determined for saccharides extracted from ground hemp seeds.

REFERENCES

1. Knudsen K.E.B. Carbohydrate and lignin contents of plant materials used in animal feeding. Anim. Feed Sci. Technol. *67*, 319–338 (1997).
2. Choct M. Feed non-starch polysaccharides: Chemical structures and nutritional significance. Feed. Milling Int. *191*, 13–26 (1997).
3. Căpriţă R., Căpriţă A., Călin J. Biochemical Aspects of Non-Starch Polysaccharides. J. Anim. Sci. Biotechnol. *43*, 1, (2010).
4. Nie Y., Lin Q., Luo F. Effects of Non-Starch Polysaccharides on Inflammatory Bowel Disease. Int. J. Mol. Sci. *18*, 1372, (2017).
5. Buksa K., Ziobro R., Nowotna A. et al. Isolation, modification, and characterization of soluble arabinoxylan fractions from rye grain. Eur Food Res Technol. *235*, 385–395 (2012).
6. Fekri N., Khayami M., Heidari R., Jamee R. Chemical Analysis of Flaxseed, Sweet Basil, Dragon Head and Quince Seed Mucilages. J. agric. biol. sci. *3*, 2 (2008).
7. Lodhi B.A., Hussain M.A., Sher M., Haseeb M.T., Ashraf M.U., Hussain, S. Z., Bukhari, S.N.A. Polysaccharide-Based Superporous, Superabsorbent, and Stimuli Responsive Hydrogel from Sweet Basil: A Novel Material for Sustained Drug Release. Adv. Polym. Technol. 1–11 (2019).
8. Nazir S., Wani I. A., Masoodi F. A. Extraction optimization of mucilage from Basil (*Ocimum basilicum* L.) seeds using response surface methodology. J. adv. res., 8, *3* (2017).
9. Barsby J.P., Cowley J.M., Leemaqz S.Y., Grieger J.A., McKeating D.R., Perkins A.V., Bastian S.E.P., Burton R.A., Bianco-Miotto T. Nutritional properties of selected superfood extracts and their potential health benefits. PeerJ. (2021).
10. Denev P.N., Ognyanov M.H., Georgiev Y.N., Teneva D.G., Klisurova D.I., Yanakieva I. Zh. Chemical composition and antioxidant activity of partially defatted milk thistle (*Silybum marianum* L.) seeds. Bulg. Chem. Commun. *52*, 182-187, (2020).
11. Naji-Tabasi S., Razavi S.M.A., Mohebbi M., Malaekeh-Nikouei, B. New studies on basil (*Ocimum bacilicum* L.) seed gum: Part I – Fractionation, physicochemical and surface activity characterization. Food Hydrocoll. *52*, 350–358 (2016).
12. Wen Z.S., Xue R., Du M., Tang Z., Xiang X.W., Zheng B., Qu Y.L. Hemp seed polysaccharides protect intestinal epithelial cells from hydrogen peroxide-induced oxidative stress. Int. J. Biol. Macromol. *135*, 203-211 (2019).
13. Anjaneyalu, Y.V., Gowda, D.C. Structural studies of an acidic polysaccharide from *Ocimum basilicum* seeds. Carbohydr. Res., *75*, 251–256 (1979).
14. Julakanti S., Pradeep Raja Charles A., Syed R., Bullock F., Wu Y. Hempseed polysaccharide (*Cannabis sativa* L.): Physicochemical characterization and comparison with flaxseed polysaccharide. Food Hydrocoll. *143*, (2023).

STRUCTURAL ANALYSIS OF POLYSACCHARIDES FROM MUSHROOM *Hericium erinaceus* MFTCCB 134

ROMAN BLEHA[a*], JANA ČOPÍKOVÁ[a], LEONID SUSHYTSKYI[a, b], LUCA VANNUCCI[b], ANDREJ SINICA[a], MIROSLAV JOZÍFEK[c], IVAN JABLONSKÝ[c], PAVEL KLOUČEK[d]

[a] *Department of Carbohydrates and Cereals, University of Chemistry and Technology, Prague, Technická 5, 16628 Prague, Czech Republic*
[b] *Institute of Microbiology of the Czech Academy of Sciences, Vídeňská 1083, 14220 Prague, Czech Republic*
[c] *Department of Gardening,* [d] *Department of Crop Production, Czech University of Life Sciences, Prague, Kamýcká 129, 16521 Prague, Czech Republic*

blehar@vscht.cz

Abstract

The aim of this research was the structural characterisation of polysaccharides isolated from fruiting bodies of the cultivating medicinal mushroom *Hericium erinaceus* MFTCCB 134. Cold and hot water extracts (CWE, HWE) were obtained and purified, and followed by alkali extraction from the reminder solids. The composition and structure of the fractions were analysed by FTIR spectroscopy, and neutral sugars/linkage analyses were determined by GC/FID and GC/MS, respectively. Galactose, fucose and glucose were found in purified CWE, while glucose predominated in purified HWE.

Introduction

The fruiting bodies of *Hericium erinaceus* have been cultivated and widely used in Asian countries for centuries. They are also known as the source of bioactive compounds such as polysaccharides[1–3]. The polysaccharides of *Hericium erinaceus mushrooms* have several biological activities, such as anti-inflammatory, antitumor, and anti-oxidant[4-7]. In general, all biological activities depend on the monosaccharide composition, structure, and position of glycosidic linkages, branching and molecular weight of tested polysaccahrides[1,2].

This research focuses mainly on the isolation and characterisation of water-soluble polysaccharide fractions from fruiting bodies of *Hericium erinaceus* strain MFTCCB 134. These fractions were characterised by FTIR and GC/FID.

Experimental

Materials and cultivation

The fruiting bodies of the *Hericium erinaceus* strain MFTCCB 134 (originally from Vietnam) were grown in green houses and were provided by Mykoforest (Velčice, Slovak Republic). The substrate is based on the ratio of a mixture of 79 % beech and oak sawdust, 20 % wheat bran and 1 % gypsum. The moisture content was adjusted to 64 %. The 2 kg of substrate were filled into Sac O2 polypropylene bags and steamed at 90 °C for 24 hours. In addition, the bags were cooled and inoculated with 5 to 7% of the granular seedlings that were prepared on sterile wheat grains. Colonisation was carried out at 25 °C for 21–25 days and then the bags were transferred to a lighted grow room (light for 24 hours) for fructification at 18 °C with a relative humidity of 90–95%. The first fruiting bodies (Fig. 1) were harvested after 10–12 days.

Fig. 1: **Fruiting bodies of the mushroom *Hericium erinaceus* MFTCCB 134.**

Preparative Procedures

Lipids and other small molecules were removed from dried and milled fruiting bodies using hexane, ethanol, and acidic ethanol (0.2 mol l^{-1} HCl). Furthermore, the crude extracts were then obtained by successive extractions with cold water, hot water (100 °C under reflux) and an alkali solution (1 mol l^{-1} NaOH, 4 °C) yielding crude extracts CWE, HWE, AE, respectively, and the insoluble part IP.

Aqueous extracts F1 and F2 were concentrated under vacuum and polysaccharide fractions were precipitated with an excess of ethanol (4:1 v/v), centrifuged, washed with 80%, 96% ethanol and acetone and dried in air. The alkaline-soluble and insoluble products F3 and SR were neutralised by washing with acidic ethanol and 80% ethanol until the neutral reaction, then washed with 96% ethanol and dried in air. Protein from the water extracts was removed with a combination of the enzyme's pepsin and pronase, and then the fractions were further purified by columns filled with DEAE Sepharose Fast flow and Sephacryl S-400HR. The fractions collected were dialysed in 1000 Da membranes against distilled water for three days and lyophilised. Two new fractions of CGF (cold water gel filtration) and HGF (hot water gel filtration) and further analysis was performed with FTIR, GC/FID.

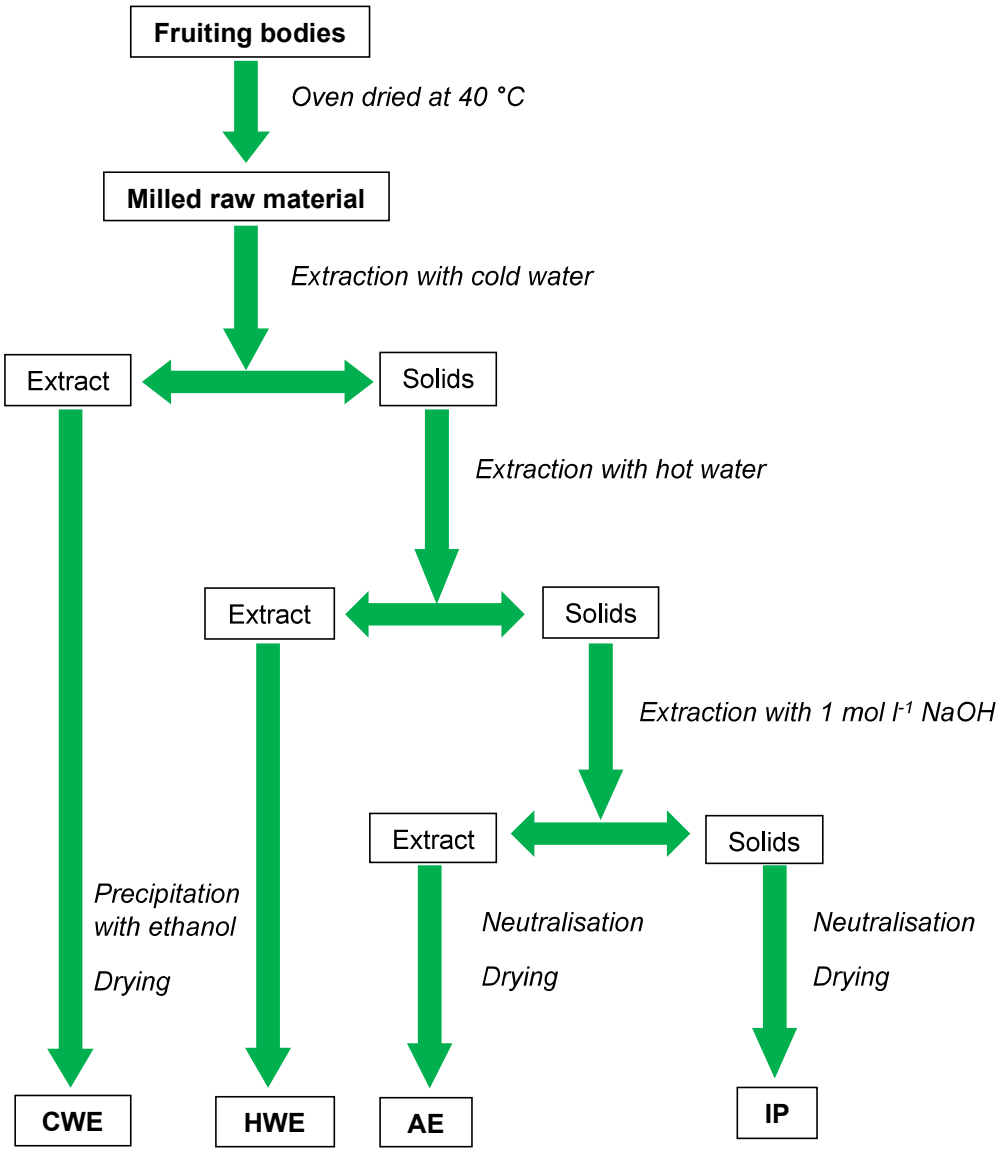

Fig. 2: **Isolation scheme of polysaccharide fractions from fruiting bodies of the *Hericium erinaceus* strain MFTCCB 134**

Analytical Methods

FTIR spectra (400–4000 cm^{-1}) of the fractions were recorded in KBr pellets using a Nicolet 6700 FTIR spectrometer (Thermoscientific, USA); 64 scans were accumulated with a spectral resolution of 2.0 cm^{-1}. The spectra were smoothed, and the baseline was corrected using Omnic 8.0 and 9.0 (ThermoScientific, USA) software and exported in ASCII format to Origin 2019b software (OriginLab Inc., USA) software for graph preparation.

Neutral sugars were analysed in all materials and fractions by hydrolysis in 72% H_2SO_4 and analysed as alditol acetates by GC/FID using a Shimadzu GC2010 (Japan) equipped with a 30 m capillary column DB-225 with an internal diameter of 0.25 mm and a film thickness of 0.15 µm. Injector and detector temperatures were, respectively, 220 °C and 230 °C. The oven temperature programme was followed 200 °C for 1 min, then increased to 220 °C (40 °C/min), temperature 220 °C for 7 min, then increased to 230 °C (20 °C/min) until the final temperature 230 °C for 1 min, total time 9 min.

Results and Discussion

Yields of the crude extracts and solid residues are summarised in Table I. The masses of the products significantly decreased after the treatment with proteolytic enzymes and dialyses with cut off 10 kDa. FTIR spectra of dry raw material and isolated fractions measured in a KBr tablet are shown in Fig. 3. The intense IR bands around 950–1200 cm^{-1} were assigned to stretching vibrations of the C–O and C–C bonds of the glycosidic bonds and the pyranose rings of carbohydrates. This region is characteristic of polysaccharides, which are pronounced in raw material and apparently predominant in all fractions.

Table I: **Yields of the crude fractions obtained from the fruiting bodies of *Hericium erinaceus* MFTCCB 134 and the partially purified extracts after the treatment with proteases and dialysis.**

Fraction	Crude fractions			After proteases and dialysis		
	m (g)	Yield (% w/w)		*m* (g)	Yield (% w/w)	
Raw material	142.66	100				
CWE	1.83	1.29		0.32	0.23	
HWE	9.04	6.34		0.90	0.63	
AE	22.30	15.63		14.64	10.27	
IP	23.39	16.39				

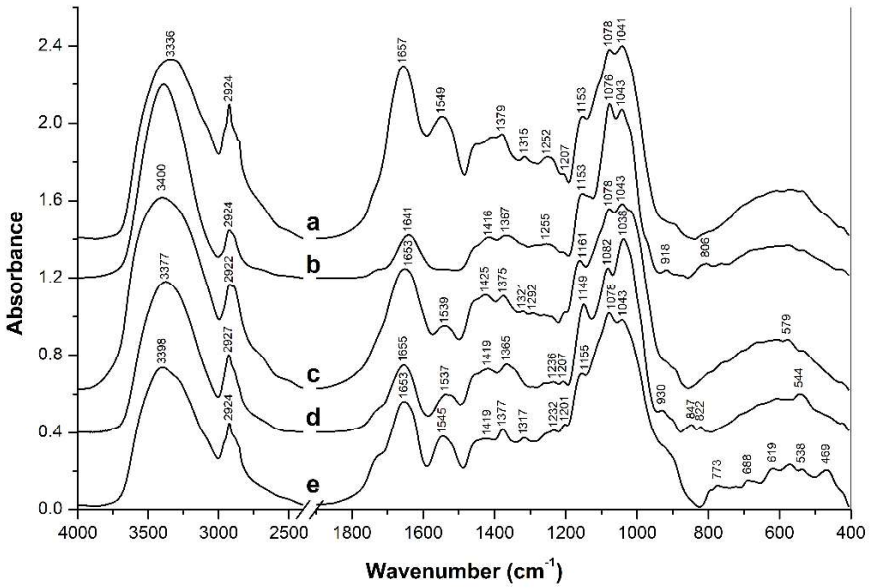

Fig. 3: **FTIR spectra of the raw material (a) and crude fractions CWE (b), HWE (c), AE (d) and IP (e) obtained.**

The bands of the cold water extract around 916, 876 and 802 cm^{-1} (skeletal vibration) indicate the presence of galactan. Previously, Li et al. (2016)[5] described fucogalactan isolated from this mushroom by water extraction. Its backbone consisted of (1→6)-linked *α*-D-galactopyranosyl units, and terminal *α*-L-fucopyranoses were bound at the O-2 position of some backbone units. In contrast, the bands of the hot water extract at 1149, 930, 847, 822 and 544 cm^{-1} confirm the presence of (1→3)-α-D-glucan. A characteristic band of *β*-D-glucans was found as a shoulder around 893 cm^{-1} ($C1_{\beta}H$ deformation vibration) in the raw fruiting bodies, cold, hot water extracts, and SR. The branched (1→3)(1→6)-*β*-D-glucans has been described for fruiting bodies of the mushroom *H. erinaceus* MFTCCB 134[8,9]. The protein bands around 1657 cm^{-1} (amide I) and 1549 cm^{-1} (amide II) are the most prominent in the raw material, but are much weaker than the polysaccharide bands in the obtained fraction. These amide bands were negligible in the case of the cold water fraction, and the contribution of chitin was evident for IP. The bands of symmetric deformation of CH_3 around 1377 cm^{-1} and amide III around 1317 cm^{-1} also confirm the presence of chitin in IP assigned as a chitin-glucan complex of cell walls. A band or shoulder around 1740 cm^{-1} assigned to C=O stretching vibration indicates the presence of ester groups probably from lipid residues.

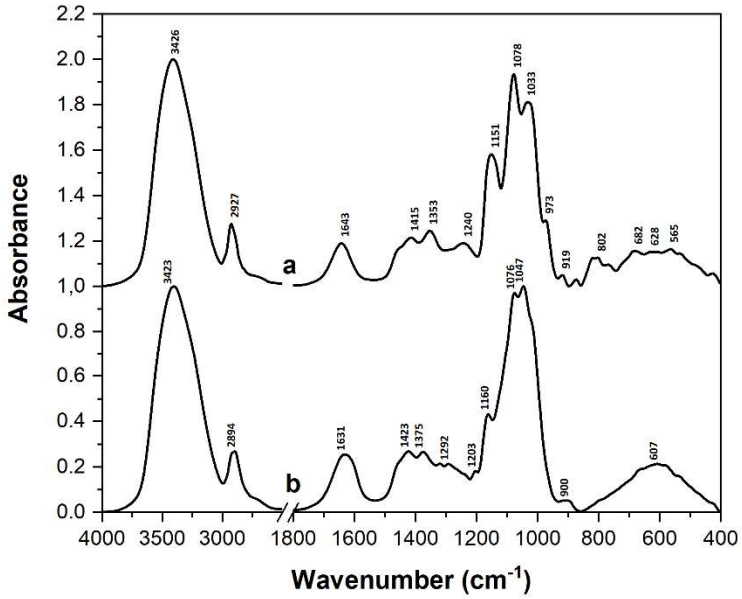

Fig. 4: **FTIR spectra of the purified polysaccharides obtained from CWE (a) and HWE (b).**

FTIR spectra of purified water-soluble soluble fractions are shown in Fig. 4. There purified products were obtained by two step preparative chromatography using DEAE Sepharose Fast flow and Sephacryl S-400HR gels[10]. Strong C-O and C-C stretching bands at 1200–950 cm^{-1} confirmed predominance of carbohydrates. For purified CWE, there are important pyranose bands at 1151 and 1078 cm^{-1}, and the band at 919 cm^{-1} and 873 cm^{-1} arose from glucose and galactose units[11]. The purified HWE demonstrate intense IR band at 1160 cm^{-1}, which is related to the stretching vibration of the glycosidic bonds. The bands at 1076, 1047 and 900 cm^{-1} are characteristic for β-anomeric glucose units and, therefore, β-glucans[12].

The monosaccharide composition of all isolated fractions is summarised in Table II. Glucose was the main monosaccharide in all fractions and in raw fruiting bodies (55–94 mol %). The highest glucose content was found in IP (94 mol %) followed by AE, HWE and CWE (from 91 to 55 mol %). However, IP showed low amount of total neutral sugars due to the contribution of chitin. Crude CWE also demonstrated high amount of galactose (32 mol %) followed by fucose (8 mol %), and the ratios of these sugars increased two times after purification, while the proportion of glucose significantly decreased. Raw material showed significant ratio of mannose (13 mol %), which decreased in all fractions. Thus, mannose is probably a part of mannoproteins, which were removal during the isolation of polysaccharides. Therefore, for all fractions, the main isolated polysaccharides were glucans. Purified HWE contained more glucose (92 mol %) than the crude extract, but purification of CWE led to higher amount of fucogalactans, as has been reported earlier[2,5]. According to methylation analysis, 1,6- and 1,2,6-galactose, 1,6-linked glucose and terminal fucose predominated in purified CWE, while 1,6-, 1,3,6-, 1,3-linked and terminal glucose were found in purified HWE.

Table II: **Monosaccharide composition of the fruiting bodies of mushroom *Hericium erinaceus* MFTCCB 134, crude and purified polysaccharide fractions obtained from them.**

Fraction	Molar ratio [mol %]							Total
	Fuc	Ara	Man	Glc	Gal	Rha	Xyl	[% w/w]
Raw Material	2	0	**13**	**72**	**12**	0	1	71
CWE	8	1	2	**55**	**32**	0	1	91
CWE purified	**16**	0	1	**15**	**67**	0	1	69
HWE	2	0	1	**88**	8	0	0	86
HWE purified	1	0	0	**92**	6	0	0	68
AE	1	0	4	**91**	1	0	2	87
IP	1	0	2	**94**	1	1	1	43

Conclusions

Four crude polysaccharide fractions were isolated from fruiting bodies of cultivated mushroom *Hericium erinaceus* MFTCCB 134. Polysaccharides soluble in cold and hot water were defined mainly as D-glucans and branching fucogalactans. The soluble alkali fraction contained (1→3)-*α*-D-glucans as main products. Insoluble residues were defined as chitin-glucan complexes of cell walls. The water-soluble extracts were further purified and obtained polysaccharides were analysed. This study confirmed that, in addition to proteins, *Hericium erinaceus* MFTCCB 134 is a prominent source of polysaccharides perspective for food and medicinal applications.

Acknowledgements

This work was supported by the Ministry of Agriculture of the Czech Republic (project QK1910209) and Mykoforest (Velčice, Slovak Republic), the company that provided Hericium culture, are greatly acknowledged. MBÚ: the Institutional grant RVO 61388971

REFERENCES

1. Khan M. A., Tania M., Liu R., Rahman M. M.: J. Compl. and Integr. Med. *10*, 253 (2013).
2. Wang X., Zhang D., Yin J., Nie S., Xie, M.: Crit. Rev. Food Sci. Nutr. *59*, S96 (2019).
3. He X., Wang X., Fang J., Chang Y., Ning N., Guo H., Huang L., Huang X., Zhao Z.: Int. J. Biol. Macromol. *97*, 228 (2017).
4. Wang Z., Luo D., Liang Z.: Carbohydr. Polym. *57*, 241 (2004).
5. Li Q. Z., Wu D., Zhou S., Liu Y. F., Li Z. P., Feng J., Yang Y.: Carbohydr. Polym. *144*, 196 (2016).
6. Li X., Wang Z., Wang L., Walid E., Zhang H.: Int. J. Biol. Macromol. *13*, 5801 (2012):
7. Liu Y., Ren Z., Ruihong Y., Chen S., Zhang J., Xu Y., Meng Z., Luo Y., Zhang W., Hunag Y., Qin T.: Int. J. Biol. Macromol. *166*, 1396 (2021).
8. Dong Q., Jia L. M., Fang J. N.: Carbohydr. Res. *341*, 791 (2006).
9. Zhang A., Deng Y., Sun P., Meng X., Zhang J.: J. Food Biochem. *35*, 1680 (2011).
10. Sushytskyi L., Lukáč P., Synytsya A., Bleha R., Rajsiglová L., Capek P., Pohl R., Vannucci L., Čopíková J., Kaštánek P.: Carbohydr. Polym. 246 (2020).
11. Tu, J.; Liu, H.; Wen, Y.; Chen, P.; Liu, Z.: J. Food Biochem., 45 (2021).
12. Bleha, R.; Třešňáková, L.; Sushytskyi, L.; Capek, P.; Čopíková, J.; Klouček, P.; Jablosnký, I.; Synytsya, A.: Molecules, 24 (2019).

REFORMULATION OF CONFECTIONERY PECTIN JELLY WITH *HERICIUM ERINACEUS* WATER EXTRACT

MANON DALLEAU[a], ELODIE MORINAU[b], ROMAN BLEHA[c], ANDREJ SINICA[c], MARKÉTA BERČÍKOVÁ[c], JAN MACHÁČEK[c], JANA ČOPÍKOVÁ[c*]

[a]*Polytech Angers, University Angers, France*
[b]*École Nationale Supérieure de chimie, University of Montpellier, France*
[c]*the University of Chemistry and Technology in Prague*

copikovj@vscht.cz

Introduction

The producing of a confectionery with the higher benefit is an aim of our experiments. The formulation of confectionery pectin jelly was modified with the *Hericium erinaceus* 91 water extract to enrich this product with mushroom polysaccharides and phenolic compounds. FTIR spectroscopy was applied to monitor experimental steps and products. Water soluble polysaccharides *Hericium erinaceus* 99 were characterized by the content of ß-glucan and its composition of monosaccharides. Confectionery pectin jellies were subjected to sensory analysis and their sensory acceptability and elasticity were evaluated.

Experimental

Preparation of *Hericium erinaceus* 91 water extract

The suspension of 750 g of frozen mushroom and 2000 ml of drinking water has been heated to the boiling point under reflux for 5 h. The filtrate of the suspension was used in the formulation of jelly t.

The formulation of confectionery jelly

The formulation of confectionery jelly with water or *Hericium erinaceus* aqueous extracts were prepared according to the Herbstreith&Fox KG recipe (1.3 g pectin DE 56-62 %, e.g. slow set, Danisco//IFF Smirice, 500 g sucrose, 330 g glucose syrup DE 40, 220 g water, 2,5 g sodium citrate, 11 ml citric acid solution 50 %). The evaporation process of sugar solution was completed at the temperature 119 °C. The jelly mass solidified in starch molds at laboratory temperatures 24 h (Tab. I).

Analytical and physical methods of *Hericium erinaceus* 91 and confectionery pectin jelly

The antioxidant activity of *Hericium erinaceum* 91 was determined by the DPPH method[1]. The principle of this method is based on the reaction of the free radical DPPH (2,2-diphenyl-1-picrylhydrazyl) with the antioxidants present in the sample. The antioxidant activity of the sample was expressed in mg TEAC / 100 g sample. The parameter TEAC (Trolox Equivalent Antioxidant Capacity) indicated the concentration of Trolox having antioxidant activity corresponding to the sample (Table II).

The content of total polyphenols in *Hericium erinaceus* was determined according to the method Singleton and Rossi[2]. The total polyphenol content was calculated from the regression equation of the calibration curve for gallic acid and expressed as mg GAE (Gallic Acid Equivalent)/g sample (Table II).

The content of ß-glucan in *Hericium erinaceus* 120 was determined by the method K-YBGL (Neogen Megazyme) (Table II).

The monosaccharide composition (Tab. II) of purified polysaccharide fractions was determined after hydrolysis with 72% H_2SO_4 and analysed as alditol acetates by GC-FID using the chromatograph Shimadzu GC2010 (Japan) equipped with 30 m capillary column DB-225 with internal diameter 0.25 mm and film thickness 0.15 μm. The temperatures of injector and detector were, respectively, 220˚C and 230˚C. The oven temperature program was following: 200˚C for 1 min, then rose to 220˚C (40˚C/min), temperature 220 ˚C for 7 min, then rose to 230 ˚C (20˚C/min) until, final temperature 230 ˚C for 1 min, total time 9 min (Table III).

FTIR spectra were recorded in mode ATR on the Nicolet 6700 FTIR spectrometer (Thermo Scientific, USA) in the spectral range from 4000 to 400 cm^{-1} with a resolution of 2 cm^{-1} and 64 scans. The spectra were processed using Omnic 8.0 and 9.0 (Thermo Scientific, USA) and Origin 2018b (OriginLab, USA and interpreted in the spectral range from 2000 (event. 1800) to 650 cm^{-1}.

When fortifying sweets with non-traditional ingredients, it is necessary to take into account the amount of individual raw materials to maintain the required physical and sensory properties. The formulation of jelly was evaluated by sensory analysis.

Sucrose crystals from the jelly sample were observed and confirmed in the dark field of a polarizing microscope (Nikon Eclipse E400 Pol).

The determination of physical properties of jelly was performed using the Texture Analyser TA.XT. plus equipment (Stable Microsystems, United Kingdom) in the arrangement of two straight one-way compression plates. The sample (cylinder: diameter 1 cm, length 5 cm)) is placed on the bottom plate and it was compressed by the plate with a diameter of 100 mm.

- Speed plate motion before the test: 1 mm / s
- Position at the time when the top plate in contact with the sample (top pattern) designed to overcome the forces of 0.05 N
- Speed of movement in the test plate: 5 mm / s
- The maximum relative deformation: 75% of the initial sample height
- Plate comes to height of the original sample and after a time delay of 5 s sample is compressed again under the same conditions.

Speed of data collection is 500 points per second.

Results and discussion

Confectionery jelly is a typical confectionary mass that contains sucrose, glucose syrup, gelling compounds and about 20 % of water. There is an attractive possibility to enrich the confectionery jelly with aqueous extracts of medicinal plants or mushrooms. Studies on pharmacological activities have revealed that *Hericium erinaceus* polysaccharides possess the potential to help prevent, alleviate, or treat major diseases including cancer, gastric ulcer, diabetes, hyperlipidemia, hepatic injury, and neurodegenerative diseases[1,2].

The composition of *Hericium erinaceus* 91 is presented in Tables I and II. Experimental results are comparable with data from literature[3.4,5]. Fig 1. presents FTIR spectra of *Hericium erinaceus* 91, the lyophilized water extract and the solid after water extraction. The observed bands are interpreted in Table III. All three spectra have the typical ß-glucan region[6,7,8] 1200-860 cm^{1}.

The formulation of pectin jelly is presented in Table IV. All prepared formulations of pectin jelly were subjected to sensory evaluation and the results are shown in Fig. 2. When fortifying sweets with non-traditional ingredients, it is necessary to take into account the amount in which the individual materials can be applied in formulation in order to maintain required physical and sensory properties. There is evidence that the mushroom flavour and taste of pectin jelly were favourably accepted. The sensory analysis was completed with the texture analysis (Tab. V)[10] and the polarizing microscopy (Fig. 3). There is the difference between pectin jelly with water in formulation (jelly No 1) or *Hericium erinaceus* 91 water extract (50 %: 50 %, No 4) in hardness and fracturability, nevertheless the sensory analysis did not show anything perceptible.

Conclusion

Confectionery pectin jelly is common sweets, but the disadvantage of jelly is a high carbohydrates content which does not correspond with balanced diet. However, the production of untraditionally fortified sweets will diversify the offer on the market and provide consumers with healthier product variants. The materials rich on beneficial medicinal mushroom extract can meet this requirement.

Table I: **Properties of *Hericium erinaceus* 91**

Sample	**Content of polyphenols [mg GAE/1 g dry matter]**	**Antioxidant activity [mg TEAC/100 g dry matter]**	**Content of ß-glucans {g/100 g dry matter [**
Hericium erinaceus 91	1.88	77.33	29.77

Table II: **The monosaccharide composition of polysaccharides *Hericium e.* 91– molar ratio [%]**

	Fuc	**Ara**	**Man**	**Glc**	**Gal**	**Rha**	**Xyl**
Hericium erinaceus 91	1	0	5	79	14	0	2

Table III: **Observed bands in the infrared spectra 1800 – 450 cm^{-1} of *Hericium erinaceus* 91, *Hericium erinaceus 91* water extract and *Hericium erinaceus* 91 solid after water extraction**[1,2,3,4]

Hericium erinaceus 91	Hericium erinaceus 91 water extract	Hericium erinaceus 91 solid part	Assigment
1739			C-O lipid ester
1649		1652	Protein Amide I
	1631	1633	
	1593		´-O-H-O bending of bound water
		1556	
1540			Protein Amide II
	1404		
1375		1377	C-O-H bending (pyranose ring)
1153		1155	C-C streching, + C-O streching, +C-H deformation (pyranose ring)
	1081		
1074		1074	
	1053		
1047			C-C strechning
		1041	
920-880			Glucan band (a, ß. anomer C-H deformation)
	910		
		900	

880	878		ß-configuration of sugar units

Table IV: **Formulations of confectionery pectin jelly**

	Water	**Water extract of *H. erinaceus***	**Glucose syrup**	**Sucrose**	**a_w**
	[g]				[1]
Jelly 1	220	0	230	500	0.662
Jelly 2	176	44	230	500	0.668
Jelly 3	132	88	230	500	0.658
Jelly 4	110	110	230	500	0.644
Jelly 5	44	176	230	500	-
Jelly 6	0	250	230	500	0.663

Table V: **Texture analysis of confectionery pectin jelly No 1 and confectionery pectin jelly No 4**

		Hardness [*N*]	**Fracturability [*N*]**	**Springiness**	**Cohesiveness**	**Gumminess**	**Adhesiveness [N.E.C.]**	**Chewiness**	**Resilience**
Jelly 1	**Average:**	**269.53**	**-2.40**	0.52	0.29	77.21	-7.27	41.19	0.11
	Coef. Var.	0.12	-0.45	0.30	0.14	0.22	-0.54	0.45	0.13
	S.D.	32.57	1.07	0.15	0.04	16.97	3.95	18.31	0.01
Jelly 4.	**Average:**	**223.71**	**61.63**	0.71	0.29	65.15	-8.33	46.71	0.11
	Coef. Var.	0.10	0.82	0.25	0.08	0.14	-0.39	0.35	0.10
	S.D.	23.00	50.74	0.18	0.02	9.10	3.27	16.10	0.01

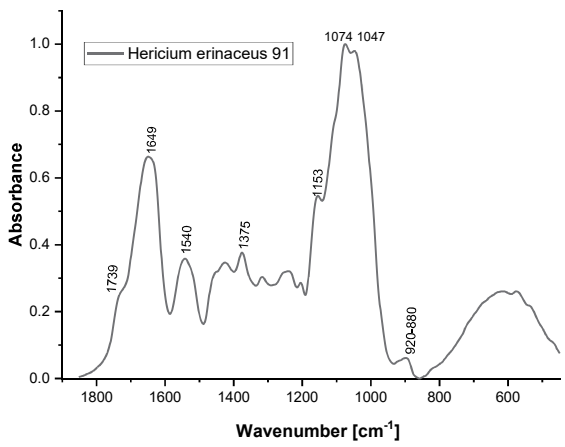

A

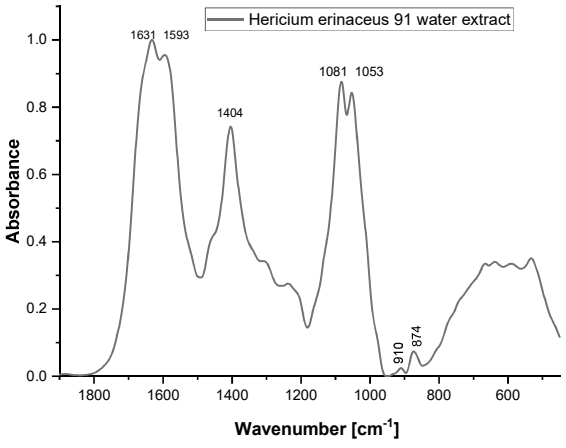

B

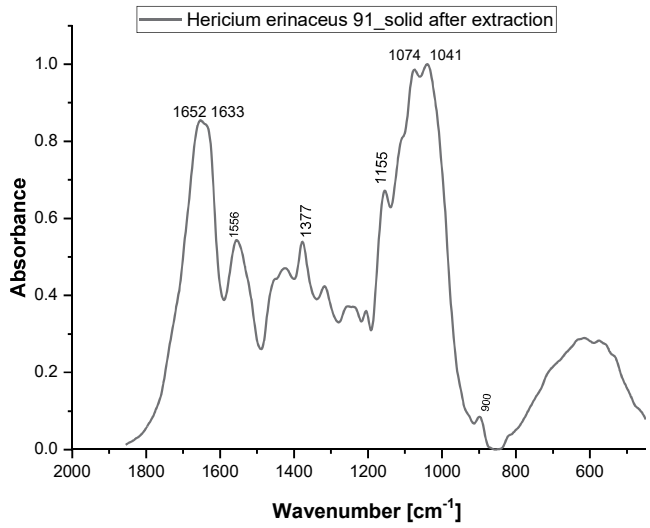

C

Figure 1: **FTIR spectrum of *Hericium erinaceus* 91(A), *Hericium erinaceus* 91 lyophilized water extract (B) and *Hericium erinaceus* 91 solids after extraction (C).**

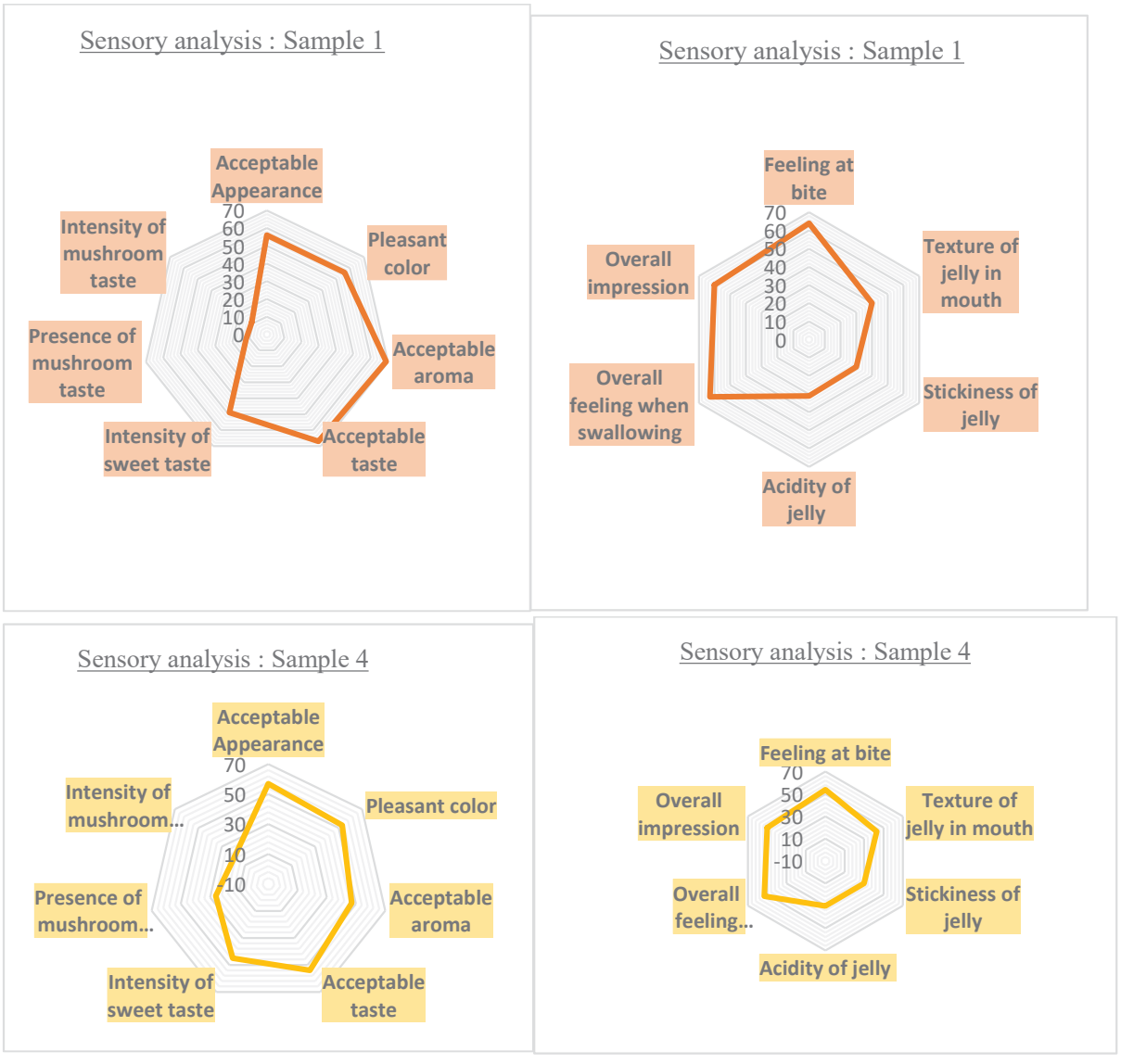

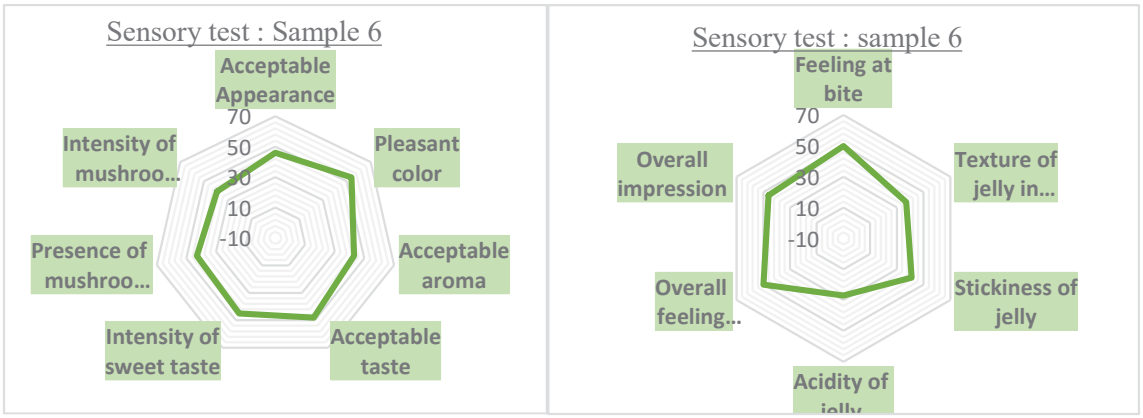

Figure 2: **Sensory evaluation of pectin jelly No. 1,4 and 6**

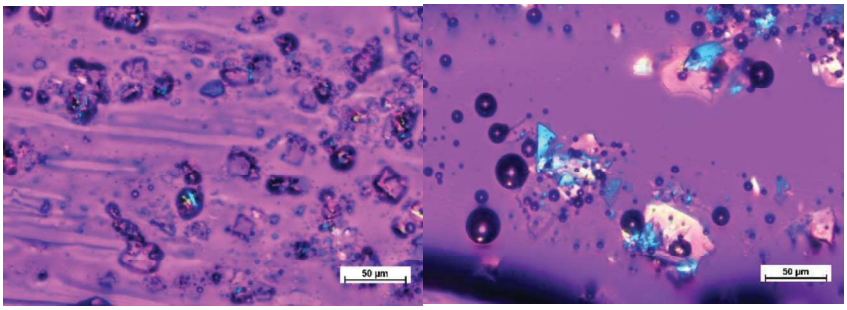

A B

Figure 3: **Polarizing microscopy of pectin jelly No.1 (A) and jelly No.5 (B)**

REFERENCES

1. Chong, P. S.et al.: Int.J. Molecular Sciences. **21**, 16 (2020)
2. Thongbai, B., et al.: Mycol Progress. **14**, 91 (2015).
3. Hou Y., Ding X., Hou W.: *Mol. Medicine Rep*. *11*, 3799 (2015).
4. Li Q.Z. et al.: Carb. Polym. 144, 196 (2016).
5. Yan J.K. et al.: *Carb. Polym*., *193*, 373 (2018).
6. Gomba G. K et al.: *Int.J.Biol.Macromol*. *80*, 271 (2015).
7. He J.Z et al.: *Molecules*, *17*, 4373 (2012).
8. Silva S. et al.: *J. Sci.Food Agric*. *92*, 1826 (2012).
9. Mohaček-Grošev V. et al.: *Spectrochimica Acta Part A 57*, 2815 (2001).
10. Rivero R., et al.: J. Sci.Food Agri. **100**, 1030 (2020)

YEAST GLUCAN PARTICLES AND THEIR CORE

PETR FATKA[a], FILIP ZAVŘEL[a], JAROSLAV HANUŠ[a], FRANTIŠEK ŠTĚPÁNEK*[a]

[a]*Department of Chemical Engineering, University of Chemistry and Technology Prague, Technická 5, Prague 6, 166 28, Czech Republic*

Frantisek.Stepanek@vscht.cz

Abstract

Yeast-derived *β*-glucan particles (GPs) make a promising material for use as a bioactive drug carrier for targeted drug delivery. Data from the literature and our laboratory suggest that such particles contain a residue in their centre, which is never discussed in the literature. Such a residue could represent an obstacle for pharmaceutical use of glucan particles and was, therefore, examined. The composition of the residue remained unknown until the use of Confocal Raman Microscopy, which revealed that it is made of glycogen and protein. Both of these were quantified and attempts to get rid of them were carried out.

Introduction

Yeast *β*-glucans, isolated from cell walls of yeast *Saccharomyces cerevisiae* (baker's yeast) are well known for their immunomodulatory properties for which they are used as food supplements. It has also been reported that it is possible to prepare hollow porous particles from the yeast cells, which retain the closed almost-spherical geometry. Attention has turned towards such particles (called glucan particles, GPs) recently, as they form a promising material for targeted delivery of active substances (drugs) in oral formulations. GPs keep the immunoactivating properties of *β*-glucans and are reported to provide synergy with certain anti-inflammatory drugs (e.g. curcumin). GPs are phagocytosed by intestinal macrophages making them a promising vector for lymphatic drug delivery[1,2].

The preparation process of GPs comprises of alkaline extraction, followed by neutralization and several washing steps (in water and organic solvents – isopropyl alcohol and acetone, typically). It is aimed at removal of cell wall mannoproteins and inner cellular content, while the *β*-glucan component of the cell wall is not decomposed and its closed arrangement is retained[3]. Different images from our laboratory and literature alike (obtained by Laser scanning confocal microscopy and Transmission electron microscopy) suggest that in the centre of GPs prepared this way there is a residue of unknown composition[4-6]. This residue ("core") is never discussed in the literature. In this work, we studied the nature of this residue and possibilities of its removal, in order to obtain hollow particles as they are described in the literature. This should help with obtaining a more uniform material. Uniformity of GPs is crucial, if ever were GPs to undergo an approval process for use in pharmaceutics.

Experimental

Materials

GPs were prepared from dry baker's yeast (Lesaffre, Czech Republic) purchased from local shop. Enzyme α-amyloglucosidase, Bradford reagent solution and Glucose oxidase/peroxidase/*o*-dianisidine assay kit (GAGO20) were purchased from Sigma-Aldrich. All standard chemicals were of analytical grade (purchased form Lach-Ner, Czech Republic or Penta, Czech Republic).

Standard preparation process

The baker's yeast was subjected to a procedure previously described by Šalamúnová *et* al. (2021)[1]. The subsequent description follows the large batch process, in cases when small batch process was used all weights and volumes were 6 times smaller.

First, 150 g of dry yeast were suspended in 600 ml of NaOH solution (1 mol l^{-1} NaOH, 250 g l^{-1} of dry yeast). The suspension was heated at 90 °C for one hour, after which it was centrifuged, the pellet was resuspended in fresh 1 M NaOH solution and the process was repeated two more times (in total 3 alkali extractions were performed). Afterwards, the pellet was resuspended in 400 ml of deionized water and the pH was adjusted to 4 - 5 by dropwise addition of concentrated HCl, and heated at 75 °C for 2 hours. The suspension was again centrifuged and the pellet was washed by water (3 times), isopropanol (4 times) and acetone (2 times), with each washing step consisting of adding 400 ml of fresh solvent. The final glucan particles were left in a fume hood overnight to evaporate the residual organic solvents and then lyophilized for 2 days to remove any remaining moisture.

Glucan particle characterization

Scanning Electron Microscopy (SEM - Jeol JCM-5700), Transmission Electron Microscopy (TEM - Jeol JEM-1010) and Optical Microscopy together with the Laser Scanning Confocal Microscopy (LSCM, Olympus BX41 and Olympus Fluoview FV-1000; 405 and 488 nm lasers used for excitation) were used for the

morphological analysis of the particles. For Attenuated Total Reflectance Fourier Transform Infrared (ATR-FTIR) Spectroscopy, the Nicolet iZ10 FTIR module with a ZnSe ATR accessory was used and the CHNS elemental analysis was carried out using a Vario EL Cube elemental analyzer from Elementar Analysen Systeme GmbH (performed in the UCT Prague Central Laboratories). UV-VIS spectroscopy was carried out in quartz cuvettes with 10 mm path length using Biochrom WPA Lightwave II machine. An upright Raman microscope WITec alpha 300 RSA (WITec, Ulm, Germany) with laser excitation at 532 nm was used for confocal Raman microscopy measurement. For fluorescent dyeing to use with LSCM Calcofluor White and fluorescein isothiocyanate (FITC) was used. In order to improve the contrast of the resulting images sequential scanning was used (blue channel was excited with 405 nm laser and green channel was excited with 488 nm laser).

For microscopic imaging agarose hydrogel was used as a fixative to prevent motion of observed particles. In case of Confocal Raman microscopy, the cover slide was sealed with CoverGrip™ Coverslip Sealant (Biotium) in order to prevent evaporation of solvent and drying of the sample.

Glycogen and protein quantification

Glycogen in GPs was determined according to a protocol that was slightly modified, as the first steps of the process described in the protocol are alkaline permeabilisation of yeast cells followed by acidic treatment[7]. These steps were skipped because they were already performed as a part of the preparation process of GPs from yeast. GP suspensions of different concentrations were preheated (1 ml, pH 5.2 buffer solution, 57°C) and mixed with 40 µl of 20 mg/ml α-amyloglucosidase enzyme solution and the reaction was left to run overnight. Then, samples were centrifuged (Eppendorf™ MiniSpin, 13400 rpm, 10 min) and glucose liberated by the enzymatic reaction was assayed using the oxidase/peroxidase/*o*-dianisidine kit (GAGO20) in the supernatant. Colour change developed by the assay kit was determined by UV-VIS at λ = 540 nm. Glucose solution of known concentration was shipped along with the kit and was used to measure calibration line.

Determination of protein content in GPs was carried out using the Bradford protein assay[8]. 100 µl of GP suspension in pH 6.8 PBS was mixed with 3 ml of Bradford reagent. The mixture was incubated at room temperature for 5 minutes and then the colour change caused by the formation of a protein-dye complex was determined by UV-VIS at λ = 595 nm. Despite the 30 times dilution of the GP suspension with the dye solution turbidity of the sample had to be taken into consideration and correction of its effect was needed to be performed so that the evaluation was accurate. Bovine serum albumin was used as a standard protein to prepare calibration solutions and measure the calibration line.

Additionally, organic CHNS elemental analysis was carried out and nitrogen content was observed.

Preparation process modifications

Double enzymatic degradation

The preparation was initiated as usual (small batch used). All steps up until addition of acid and pH adjustment to 4-5 were performed, including the 2h heating step, which follows the pH adjustment. After this acidic treatment enzymatic decomposition steps were added. To 100 ml of GP suspension in pH 5.2 acetate buffer solution 200 mg of the α-amyloglucosidase enzyme was added. The amount of the enzyme was chosen based on previous glycogen assays and estimated GP yield. Next the solids were separated from the solution by centrifugation and the solids were introduced to 100 ml of pH 7.4 phosphate buffer solution to which 25 mg of trypsin was added. Trypsin was used as an enzyme of first choice. The amount was chosen based on the estimated GP yield and in the ratio from the technical specification of the enzyme at the supplier's website.

After the enzymatic treatment steps the process was finished as usual with the washing and drying steps. Glycogen and protein content were quantified for these modified GPs as well.

Results and discussion

GP preparation

GPs prepared by the standard process show wrinkled surface when examined by SEM (Figure 1). It is possible to see that they retain the closed arrangement with occasional budding necks.

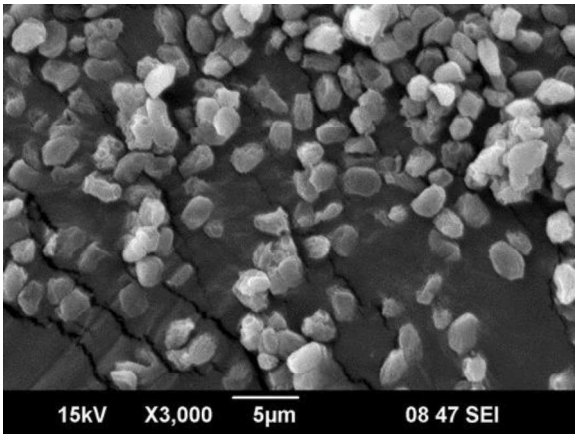

Figure 1. **SEM image of prepared *β*-glucan particles.**

Imaging with optical microscope or LSCM in dry state results in a picture that is difficult to describe. The particles appear wrinkled, but it is difficult to determine to what extent is the image affected by light scattering or diffraction on the particle shell. In aqueous environment GPs swell and it is possible to observe them with LSCM (Figure 2a). In the centre of the particles the unknown core is observed. The core exhibits autofluorescence signal. This core can be observed by TEM as well (Figure 2b, taken from Saloň *et* al. (2016)[6]). This observation, however, still doesn't give any information about the composition of the core.

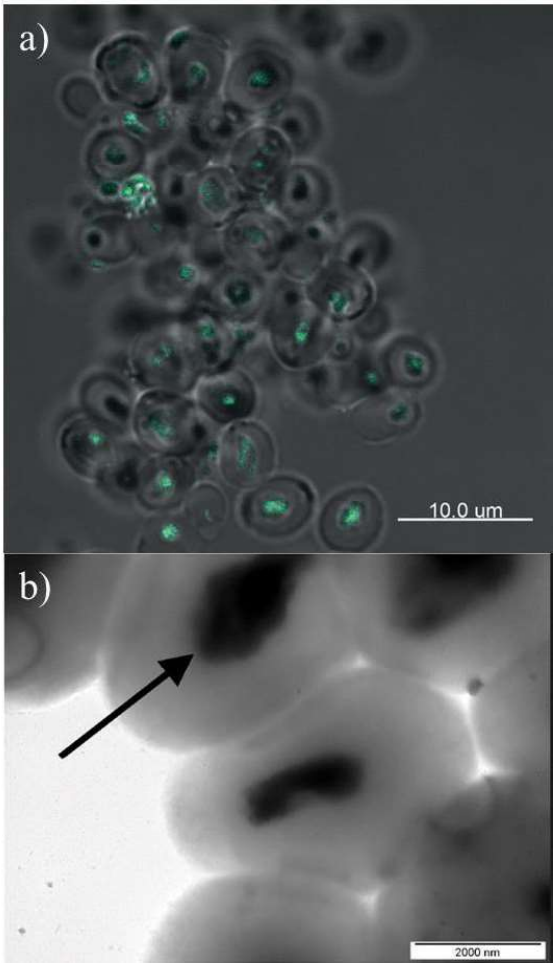

Figure 2. **Images of prepared *β*-glucan particles.** Image a) LSCM image of GPs in aqueous environment, compound transmission and autofluorescence (40× magnification objective) and image b) TEM image of GPs (taken from Saloň *et* al. (2016)[6]). Black arrow shows the core.

Confocal Raman microscopy and fluorescent dyeing of GPs

Before the use of Confocal Raman microscopy, several attempts of GP disruption were made, followed by ATR-FTIR, SEM and LSCM observation. None of these were considered successful, so it was necessary to look for another method that would allow determination of GP core composition. Confocal Raman microscopy was used and it was discovered that in the core of GPs glycogen and further unspecified protein can be found. It was also discovered that the outer layer is made of *β*-glucan as anticipated and that this layer is well hydrated in the aqueous environment. On the contrary, it seems that the core repels water. This rises up the question whether the core wouldn't be a beneficial component of GPs in case of encapsulation of lipophilic compounds. Back-to-back comparison of core-containing and core-free GPs would be needed to test this hypothesis.

The information acquired by Confocal Raman microscopy was confirmed by fluorescent dyeing of GPs by FITC and Calcofluor White (Figure 3). FITC labels proteins and its signal was observed the strongest in the GP core. Calcofluor White labels *β*-polysaccharides with higher affinity to chitin. Signal of Calcofluor White was observed in the *β*-glucan outer layer with stronger response at the budding necks. This is in agreement with previously published information that the budding necks contain chitin in increased concentrations.

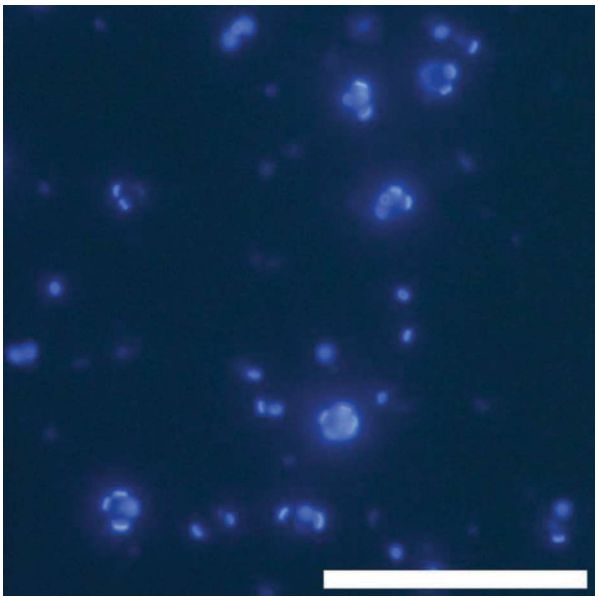

Figure 3. **Wide-field fluorescence image of GPs dyed with Calcofluor White.** Observed with a 40× magnification objective with the use of
U-MWU2 fluorescence cube). Scale bar represents 50 μm.

Glycogen and protein quantification

Confocal Raman microscopy provided qualitative information about the GP core, the logical follow-up was to quantify the glycogen and protein content. The enzymatic decomposition of glycogen followed by assaying liberated glucose was chosen for glycogen quantification, as the same enzyme would be possible to use for the core removal step, if the measurement proved successful.

This approach was used to propose a modified preparation process, which aimed at obtaining core-free GPs.

Results for the original GPs as well as for GPs prepared by a modified method are summarized in Table I.

Table I
Results of glycogen assay, Bradford protein assay and nitrogen content from organic CHNS elemental analysis of GPs obtained by the standard process and the modified process.

	Glucose liberated per 1g GPs	**Protein mass fraction (Bradford)**	**Nitrogen mass fraction (CHNS)**
Standard GPs	140-160 mg	4.5-9.1 %	0.4-2.3 %
Modified GPs	53.2 mg	4.5 %	1.74 %

The amount of glucose liberated from the standard GPs suggest a rather high amount of glycogen, which was not anticipated. In case of both, glycogen and protein, batch-to-batch variability was observed, which is the reason why the numbers in Table I are presented as ranges. In case of the modified preparation process it can be seen that these modified GPs contained approximately 2/3 less glycogen than the original GPs. It is possible that to get rid of all the glycogen higher amount of the enzyme or more than one α-amyloglucosidase step is needed. On the other hand, the protein content still fits in the range of the original GPs as well as the nitrogen content obtained from organic CHNS elemental analysis. This suggests that either trypsin is not a suitable enzyme for the protein remaining in the GP core and a different enzyme/enzyme mixture is needed or that a different approach needs to be tested.

Protein content in the GP core can be the reason why the core still shows autofluorescence, when the modified GPs are observed by LSCM (Figure 4).

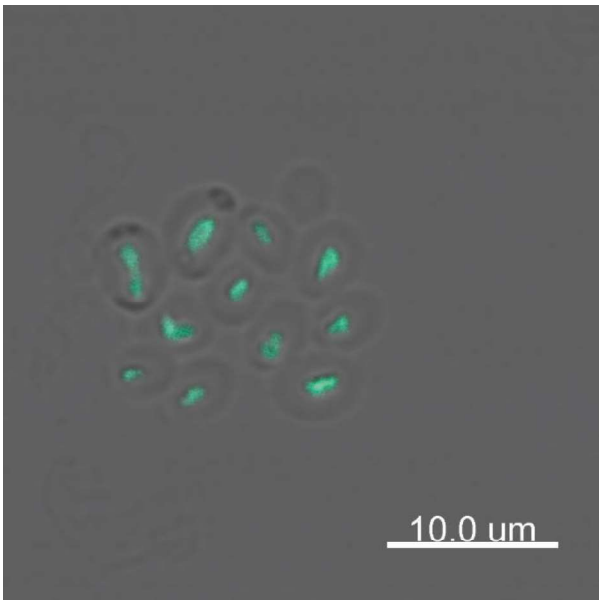

Figure 4. LSCM image of GPs prepared by the modified process. Autofluorescence is still noticeable in the GP core. 40× magnification objective used.

Conclusions

Glucan particles prepared by the standard process are made of β-glucan outer layer and a residue at the centre, which we call "core". Despite the core was not discussed in previously published literature, we decided to investigate it, as such an unidentified part of such a promising material could present an obstacle for potential use in pharmaceutics, where high degree of purity and uniformity of all used substances is required. It was discovered by Confocal Raman microscopy that the core is composed of glycogen and protein. The amounts of glycogen and protein in GPs were quantified. It was discovered that amount of glucose liberated from GPs was in the range 140-160 mg/g of GPs and that the mass fraction of proteins in GPs lied between 4.5-9.1 %. The preparation process was modified based on these data by addition of two enzymatic decomposition steps – α-amyloglucosidase step aimed at glycogen decomposition and removal and trypsin step aimed at protein removal. Glycogen removal was ~65% successful, which makes this approach promising and worth further investigation. Protein removal was not successful, which suggests either wrong choice of enzyme or need for a different approach. Further investigation of the possibilities of core-free particles preparation is subject of ongoing studies. It is a necessary achievement for the possibility to investigate, whether the core is undesired or can be utilized in some cases.

We would like to thank doc. RNDr. Peter Mojzeš, CSc. of the Faculty of Mathematics and Physics of Charles University for introducing us to Raman microscopy, allowing us to use his equipment and help with description of obtained data.
We would like to acknowledge financial support by the Czech Science Foundation (project no. 19-26127X) and by UCT Prague from the grant of Specific university research (project no. A2_FCHI_2023_037).

REFERENCES

1. Šalamúnová P., Saloň I., Ruphuy G., Kroupová J., Balouch M., Hanuš J., Štěpánek F.: *Eur. J. Pharm. Biopharm.*, *168* (2021).
2. Větvička V., Vannucci L., Šíma P., Richter J.: *Molecules*, *24* (2019).

3. Soto E. R., Ostroff G. R.: *Bioconjugate Chem.*, *19*, *4* (2008).
4. D.-Q. Liu, S. Lu, L. Zhang, L.-X. Zhang, M. Ji, X.-G. Liu, Z. Yu, R.-T. Liu: *Nanoscale Adv.s*, **2** , 3494-3506, (2020).
5. X. Zhou, X. Zhang, S. Han, Y. Dou, M. Liu, L. Zhang, J. Guo, Q. Shi, G. Gong, R. Wang, J. Hu, X. Li, J. Zhang: *Nano Lett.* 17, 1056–1064, (2017).
6. Saloň, I.; Hanuš, J.; Ulbrich, P.; Štěpánek, F.: *Food Bioprod. Process.,* ***99***, 128-135 (2016).
7. Chen, Y., Futcher, B.: *Bio-protocol 7*, *13* (2017).
8. Bradford, M. M., *Anal. Biochem.*, *72*, *1*, (1976).

SIMULATION OF CONTINUOUS CHROMATOGRAPHY SEPARATION OF MANNITOL FROM CELERY STALK EXTRACTS

SIMONA GILLAROVÁ*, SVATOPLUK HENKE, DANIEL RŮŽIČKA, PAVLA KRČOVÁ, ZDENĚK BUBNÍK

Department of Carbohydrates and Cereals, University of Chemistry and Technology, Prague, Technická 5, 16628 Prague 6

simona.gillarova@vscht.cz

Abstract

This work deals with the simulation of continuous chromatography separation of mannitol and other carbohydrates from a solution which modelled the composition of carbohydrates in the celery stalk extracts. For these purposes, the measured data from discontinuous chromatography was used. Individual discontinuous chromatography separation took place on two columns of different geometry with the same sorbent (strongly basic anion exchanger) under different experimental conditions. The continuous chromatography was performed using computer simulation in the Aspen Chromatography™.

Introduction

The concept of this follow-up work is based on the chromatographic separation of mannitol from a model aqueous solutions containing another carbohydrate, such as glucose, fructose, and sucrose[1]. The solutions were prepared according to real content of saccharides in the celery stalk extract. The subject of this work was the measurement and acquisition of data from the discontinuous separation of mannitol from the model solutions. Based on these obtained data from the discontinuous chromatographic separation, a computer simulation of the continuous chromatography of mannitol and other saccharides, was subsequently performed. From the results of the simulation of continuous chromatography, which were carried out in the Aspen Chromatography program, it is possible to optimize the process and subsequently to realistically verify the appropriately selected model experimentally, using continuous chromatographic separation at the KCHS-SMB-8-ND chromatography real station (developed at the Department of Carbohydrates and Cereals, UCT Prague).

Materials, equipment, and methods

Preparation of mannitol stock solution for discontinuous separation

For the purposes of discontinuous chromatography separation of mannitol, a solution was prepared, which in its composition modelled the extract of carbohydrates from the celery stalk. The composition of this solution is described in Table I.

Table I: **Composition simulating extract of celery stalk[2].**

	% in dry matter	% in sample	g/ 500 g of solution
Sucrose	5.68	0.91	4.54
Glucose	11.74	1.88	9.39
Fructose	12.80	2.05	10.24
Mannitol	15.24	2.44	12.19
∑	45.46	16.00	36.37

Preparation of solutions for column regeneration

The experiments were carried out on a column filled with a strongly basic anion exchange sorbent Dowex Monosphere 550A (Dow, USA). Before each measurement, it was necessary to perform sorbent regeneration using NaCl and NaOH solutions. For regeneration were used four variants of regeneration of bound functional groups. The composition of individual solutions is shown in Table II.

Table II: **The composition of the individual variants of the regeneration solutions.**

Regeneration variant	Working designation	Regeneration solutions
1	R0	200 mM NaCl, 10 mM NaOH
2	RX1	MIX 200 mM NaCl and 10 mM NaOH
3	RX2	MIX 120 mM NaCl and 20 mM NaOH
4	RX3	MIX 60 mM NaCl and 20 mM NaOH

Discontinuous chromatography separation

Discontinuous separation of aqueous solutions of sucrose, glucose, fructose, and mannitol was performed on two columns of different geometry, which were filled with strongly basic anion exchange sorbent Dowex Monosphere 550A (Dow, USA). But for this contribution it was chosen only data obtained on "small" column XK16/40 with dimensions 1.6 x 40 cm, volume 49 mL, the height of sorbent layer 23.5 cm. And for further simulations of continuous chromatography, the experiment named E08 was chosen. Before each separation, the column was regenerated at a temperature of 25 °C and a flow rate was 1 L/h. The scheme of the discontinuous apparatus is shown in Figure 1. Working conditions during discontinuous separation: injected quantity 2.5 g, mobile phase flow rate 150 mL/h, time of separation 180 min. The analysis of the obtained fractions from the discontinuous separation of samples was carried out on a high-performance liquid chromatograph Dionex DX-500 (Dionex, USA).

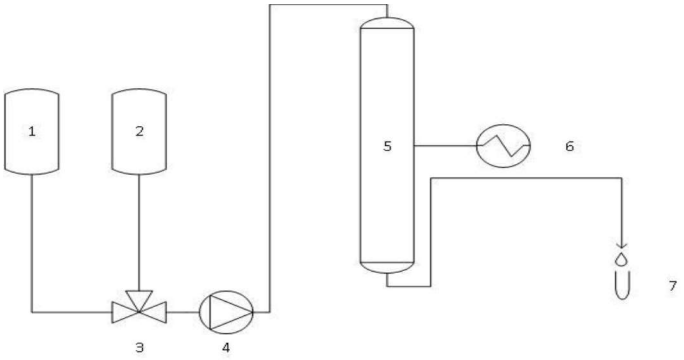

Fig. 1: **Scheme of discontinuous chromatographic apparatus. (1 reservoir of regeneration solution, 2 reservoir of mobile phase, 3 3/2-way solenoid valve, 4 pulse pump, 5 column, 6 thermostat, 7 collection of fractions)**

Continuous chromatography separation

The simulation of continuous chromatography separation was performed using computer simulation in the Aspen Chromatography™ software environment. First, it was necessary to identify a suitable model of the chromatographic process, i.e., to determine the values of the model parameters on the basis of experimental data from discontinuous chromatography. For these purposes, an equilibrium dispersion model with a linear isotherm was chosen.

Firstly, there is a need to identify the model parameters. The input data for the Aspen Chromatography simulation and estimation module include: the initial set of estimated model parameters – the linear adsorption coefficients and dispersion coefficients for all 4 components, the dimensions of the single column – the diameter and length of the chromatographic tube column, the dead volume of the system, the parameters of the packing – internal and external porosity of the bed, the volume flow of the mobile phase, the injected feed volume and the feed concentrations of the compounds. After running of the initial discontinuous separation simulation, the estimation is started resulting in the final set of equilibrium and kinetic parameters of all compounds.

The final set of the model parameters is entered together with the dimensions of the continuous chromatography station into the Aspen Chromatography module for continuous chromatography in the Figure 2, which is representing the model of the continuous chromatographic separator KCHS-SMB-8-ND (UCT, Prague) equipped with 8 columns of the length of 2 m and of the diameter 25 mm. The system is now operating in the SMB mode with the configuration 2 columns per section, but using the flow distributor can operate also in the VariCol mode.

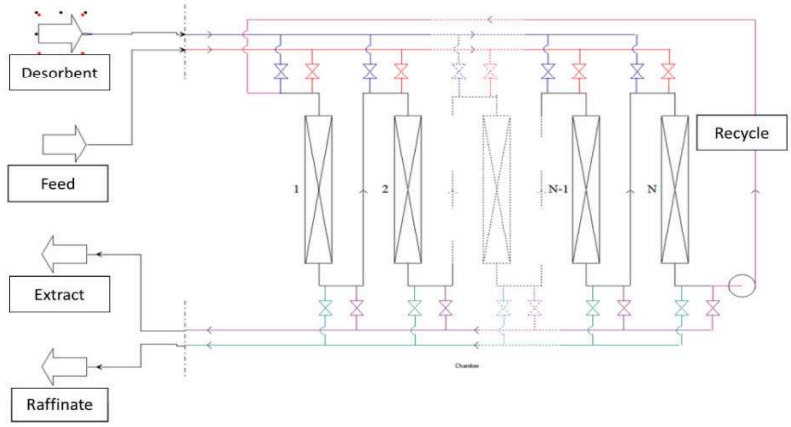

Fig. 2: **Scheme of the real KCHS-SMB-8-ND station for simulation purposes in the Aspen Chromatography environment.**

On the base of the linear adsorption isotherm coefficients, the dimensionless flows of the continuous separation are calculated using the TMB linear theory. With the help of the triangle theory module are the dimensionless values recalculated to the resulting set of the SMB volume flows of the eluent, extract, feed, raffinate and recycle stream, as well as the switch period is calculated. The resulting periodic steady-state showed the characteristic in time periodic changes of the output concentrations in the extract and raffinate stream. For a clear evaluation of the periodically steady state, the average concentrations of the components are calculated in the extract and the raffinate for the last 8 periods, i.e., one cycle, has to be independent on time. In such a case is considered the system to be steady.

Results and discussion

Continuous separation was performed using computer simulation in the Aspen Chromatography™. The simulation was performed on the basis of data from discontinuous experiments, i.e., from obtained chromatograms. First, the parameters of the model were determined, and the simulation was carried out according to them in the continuous SMB mode.

Discontinuous chromatographic separation and identification of chromatographic model identification

The search for operational parameters of continuous separation (i.e., all flow rates and switching period) was carried out using the measured values in the Aspen Chromatography™ working environment, see Figure 3.

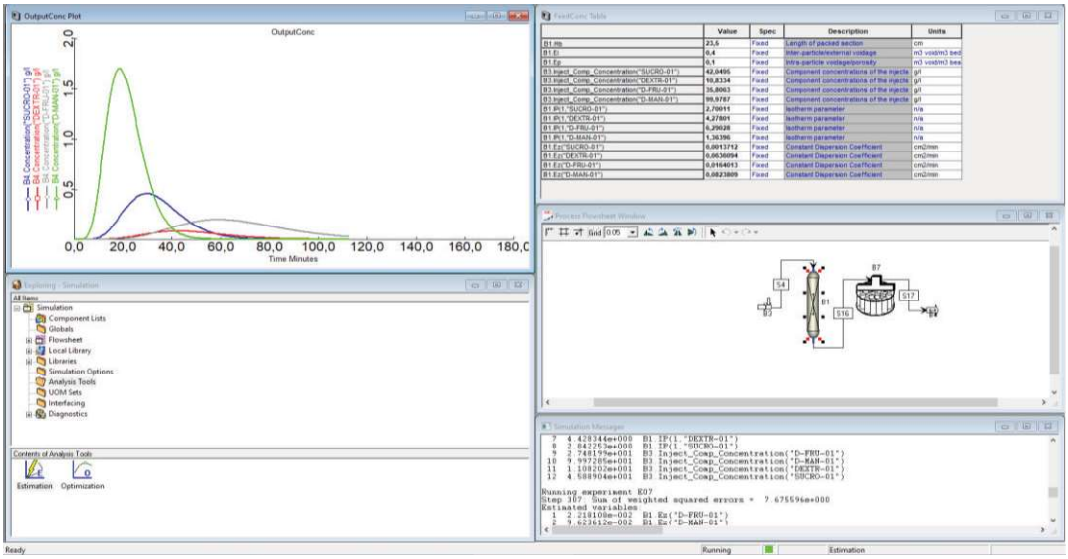

Fig. 3: **A preview of the Aspen Chromatography™ environment for finding model parameters from measured discontinuous chromatograms.**

Experiment E08, i.e., separation on a "small" column, was chosen to identify the parameters of the equilibrium dispersion model (EDM) for the subsequent purposes of calculating the operational parameters for the SMB simulation. The obtained parameters of the model are shown in Table III.

Table III: **Determined model parameters for selected experiment E08 (see Figure 3).**

Exp.	**Flow rate (mL/h)**	**Distribution coefficient (1)**				**Dispersive coefficient (cm^2/min)**			
		Sac	Glc	Fru	ManOH	Sac	Glc	Fru	ManOH
E08	150	3.37	6.58	9.44	1.35	4.16	2.59	3.71	2.03

From Figure 4, it can be seen that the agreement between the simulated and experimentally determined data was achieved.

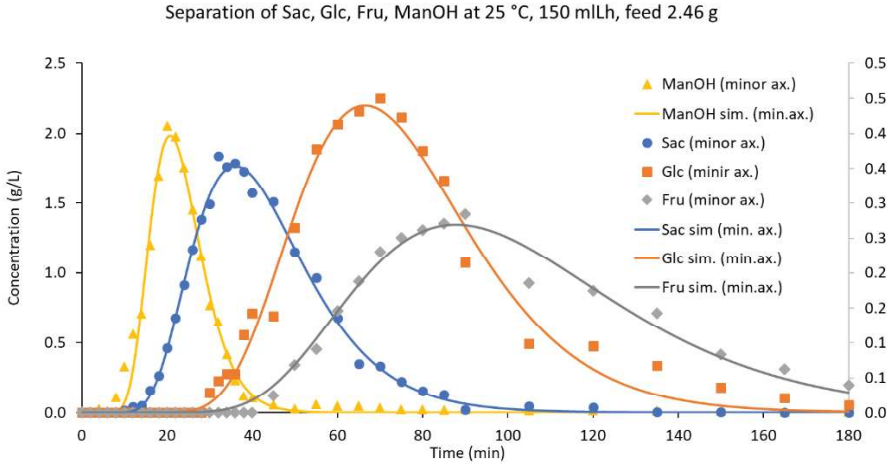

Fig. 4: **Comparison of experimentally determined data and data obtained by computer-simulated discontinuous separation on a "small" column for experiment E08.**

The simulation of continuous SMB chromatographic separation

Continuous separation was performed by simulation for the selected experiment E08 in the Aspen Chromatography with the aim of isolating mannitol from the other components of the mixture. To run the

simulation, operational parameters were calculated for E08, i.e., flow of eluent, extract, feed, raffinate, recycle and switching period, which is summarized in Table IV. Continuous experiments were designated KE08.

Table IV: **Calculated operational parameters for continuous simulation KE08.**

Operational parameters	KE08
Flow of eluent (mL/min)	7.19
Flow of extract (mL/min)	6.59
Flow of feed (mL/min)	28
Flow of raffinate (mL/min)	88
Flow of recycle (mL/min)	5
Switch period (min)	8.64

The simulation was performed for 5000 min and was sufficient for the system to reach a periodic steady state. The simulation environment shows Figure 5.

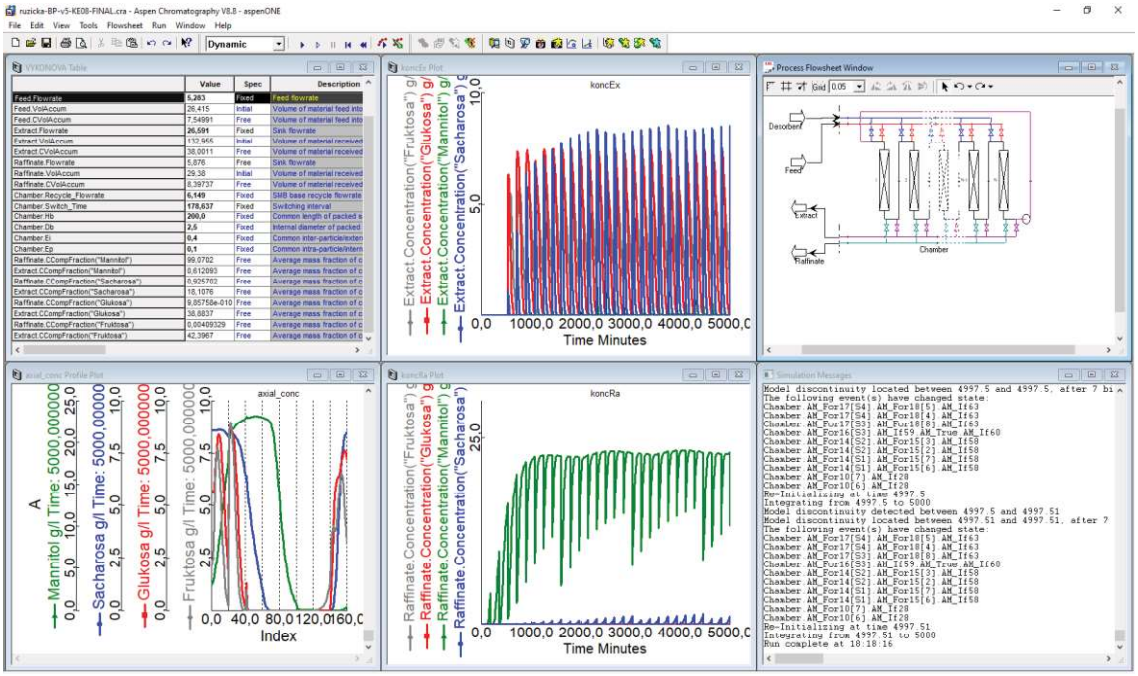

Fig. 5: **Environment for simulation of continuous experiments on the continuous chromatograph model KCHS-SMB-8-ND with eight columns for experiment KE08**

The periodic course of concentrations in the outlet streams of raffinate and extract is illustrated in Figure 6 and Figure 7 for simulation experiment KE08.

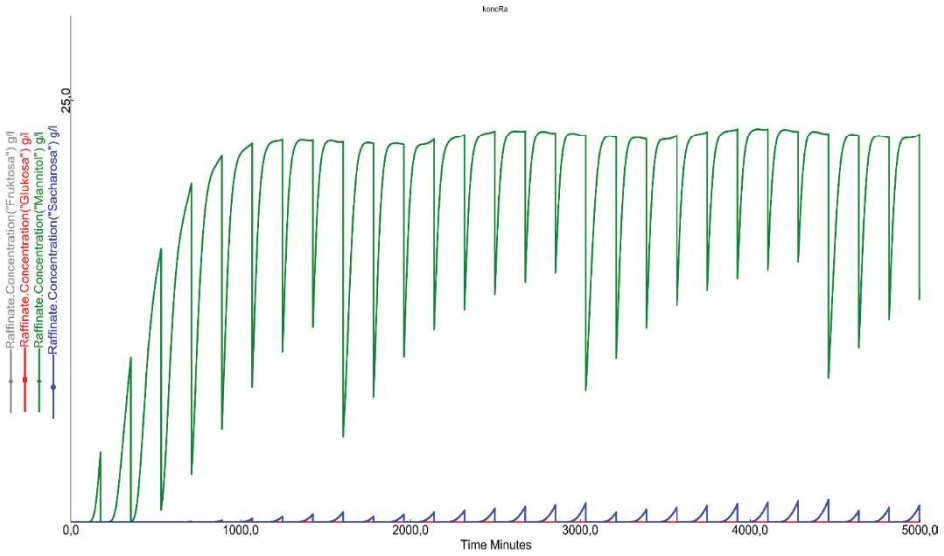

Fig. 6: **Course of the concentration of carbohydrates in the raffinate during the simulation for experiment KE08.**

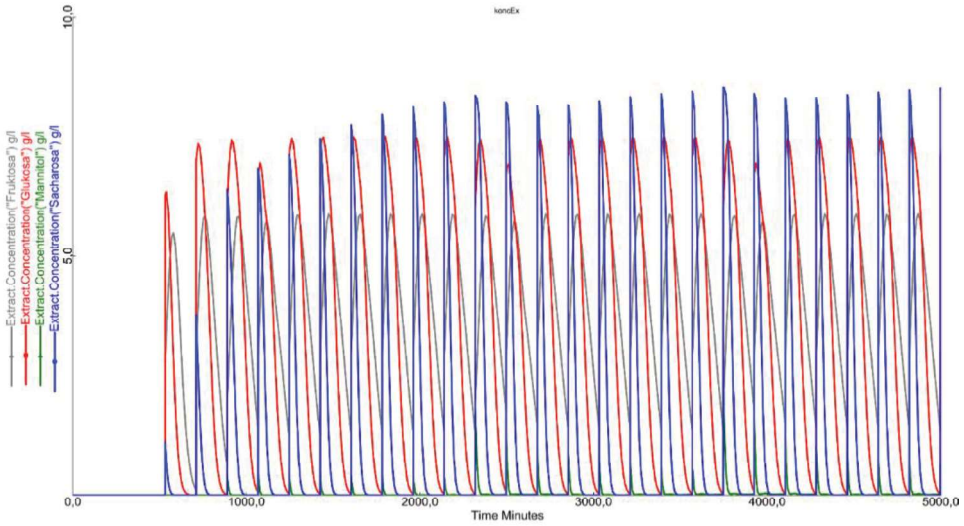

Fig. 7: **Course of the concentration of carbohydrates in the extract during the simulation for experiment KE08.**

The achieved periodic steady states are demonstrated in Figure 8 and Figure 9, which show the steady course of the contents of carbohydrates in the dry matter of the extract and the raffinate during the last cycle.

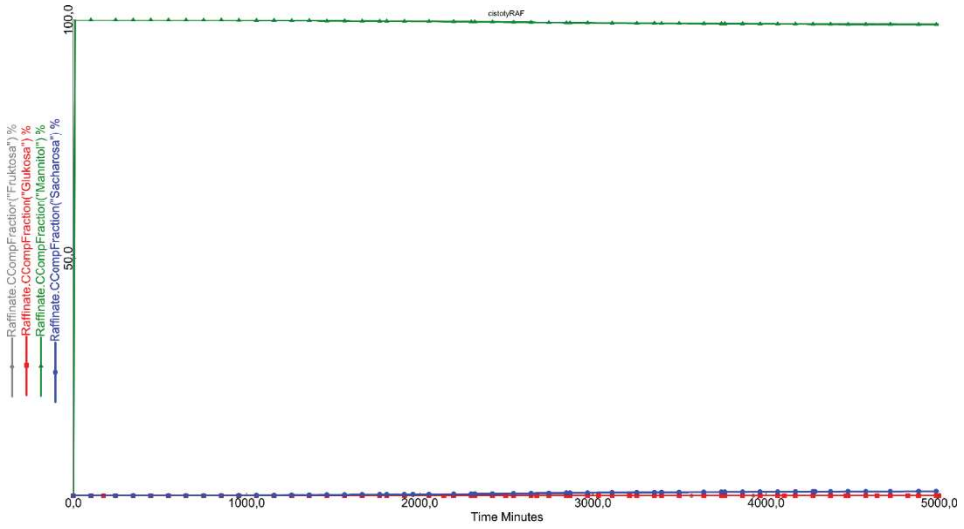

Fig. 8: **Course of the content of carbohydrates in dry matter in the raffinate during the simulation for experiment KE08.**

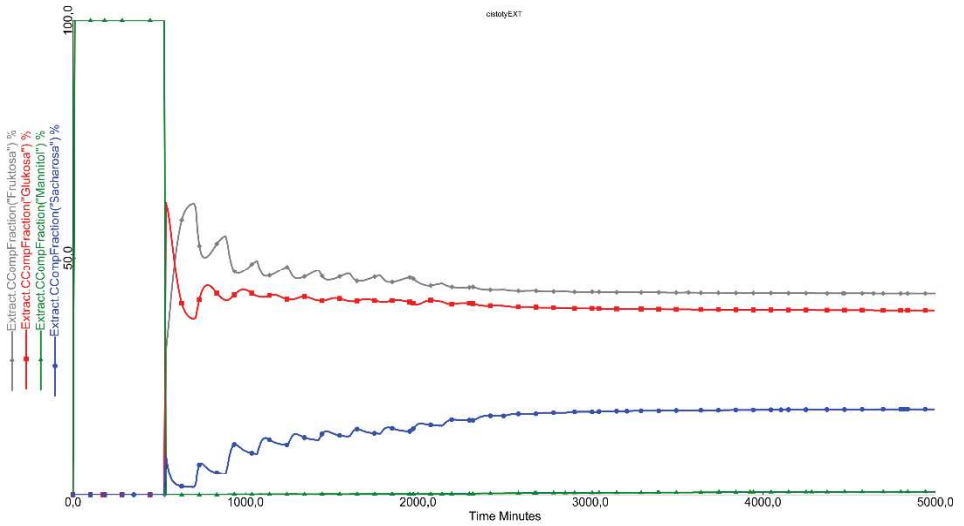

Fig. 9: **Course of the content of carbohydrates in dry matter in the extract during the simulation for experiment KE08.**

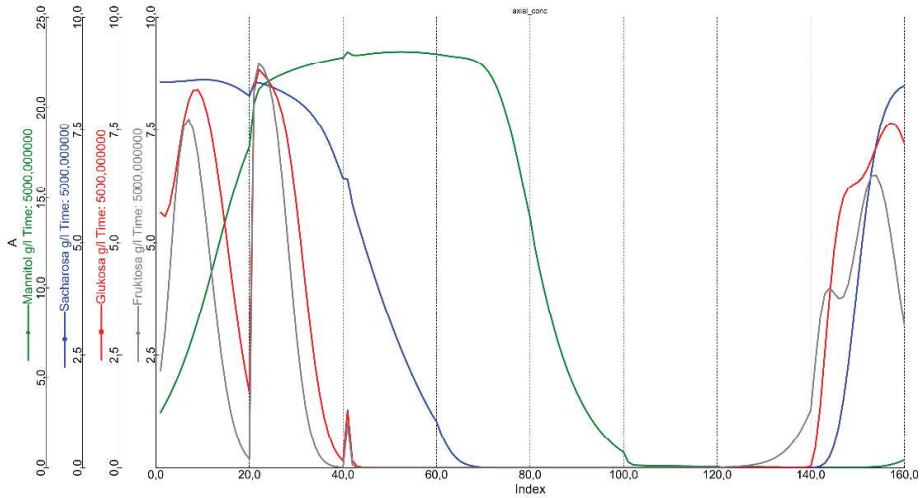

Fig. 10: Concentration profile of carbohydrates in the entire system, i.e., across all 8 columns, for experiment KE08 at the end of the simulation (at 5000 min).

The following Table V clearly shows the composition of the raffinate, and extract expressed by the content of a specific saccharide in the dry matter of the stream for the last cycle at the end of the simulation for experiment KE08. It can be seen that the raffinate stream contains the majority of mannitol at 99.07 % and thus there was an increase compared to the raw material, where it was represented by 33.5 %.

Table V: **Carbohydrate contents in the dry matter of the streams (raffinate and extract) for the last cycle at the end of the simulation for experiment KE08.**

Saccharide (%)	Raw material (Feed)	KE08 Raffinate	KE08 Extract
Mannitol	33.5	99.07	0.61
Sucrose	28.2	0.93	18.11
Glucose	25.8	0.00	38.88
Fructose	12.5	0.00	42.40

Conclusion

Mannitol was successfully isolated by discontinuous separation from a model mixture of carbohydrates, which also contained sucrose, glucose, and fructose. The composition of the used model solution (feed) modelled the carbohydrate extract from celery stalk. Discontinuous separation was carried out on column XK16/40 filled the strongly basic anion exchange sorbent Dowex Monosphere 550A (Dow, USA) at a temperature of 25 °C. The influence of the used sorbent regeneration on the separation of mannitol was monitored, where the optimum was achieved with increasing ionic strength of NaOH in the regeneration solution. The identification of the selected equilibrium dispersion model with a linear isotherm was performed in the Aspen Chromatography™ environment, where a set of equilibrium and kinetic parameters was obtained. These parameters were used to calculate operational parameters for our own continuous separation in the form of simulation on the basis of which an experiment will also be carried out at the chromatography station KCHS-SMB-8-ND (developed at the Department of Carbohydrates and Cereals, UCT Prague).

Acknowledgement

„This work was supported from the grant of Specific university research – grant No A1_FPBT_2023_006“.

REFERENCES

1. Gillarová S., Henke S., Svoboda T. et al.: Czech J Food Sci *39*, 281-288 (2021).
2. Rupérez P., Toledano G.: Eur Food Res Technol *216*, 224-226 (2003).

UTILIZATION OF UV LIGHT/TIO_2 IN THE DEPOLYMERIZATION OF PECTIN AT VARIOUS pH AND TEMPERATURE VALUES

BETIM HAJDARI*, SVATOPLUK HENKE, SIMONA GILLAROVÁ, TOMÁŠ SVOBODA, VLADIMÍR POUR, ZDENĚK BUBNÍK

Department of Carbohydrates and Cereals, University of Chemistry and Technology, Prague, Technická 5, 16628 Prague 6

Hajdari.Betim@vscht.cz

Abstract

Galacturonic acid, as one of the main constituents of pectin backbone, is found to have remarkable prebiotic characteristics and health benefits. This work is focused on the depolymerization of pectin in the presence and absence of UV light/TiO_2 under various pH and temperature values. Additionally, the individual effect of UV light on pectin depolymerization is assessed. The solution of pectin is prepared by mixing lemon peel powder pectin with distilled water. This solution is adjusted to the corresponding pH using H_2SO_4 or NaOH. Subsequently, quantification of galacturonic acid and other saccharides is done by using HPAEC-PAD.

Introduction

Probiotics are non-pathogenic micro-organisms which confer health benefits on the host and prevent or improve some diseases when administered in adequate amounts[1]. In the other case, a prebiotic is a selectively fermented ingredient that allows specific changes in the composition and/or activity of the gastrointestinal microbiota[2]. Thus, the demand for diverse prebiotic ingredients is increasing tremendously. Commercial prebiotics (such as fructooligosaccharides, galactooligosaccharides and isomaltooligosaccharides), are fermented by microbes in the proximal part of the colon and not throughout the colon. Therefore, new products are in need, by giving effects in the distal part of the colon where may be a risk for colon cancer and ulcerative colitis[3].

The main sources of carbohydrates which are consumed by the bacteria in the colon are plant-derived polysaccharides and one of these polysaccharides is pectin. Pectin polysaccharides and oligosaccharides impart a prebiotic effect as long as they are resistant to gastric juice, trypsin, pepsin, rennet, and are fermented slowly in the colon. In the other case, the main monomer of pectin, galacturonic acid, is found to possess remarkable prebiotic characteristics, by selective stimulation of benefit strains of *Lactobacillus reuteri, Streptococcus thermophilus* and by inhibition of pathogenic bacteria[4]. Thus, the characterization of these carbohydrates is of great importance. Several reports have been focused on modification of pectin. Pectin is depolymerized by using acid hydrolysis[3, 5], enzymatic hydrolysis[3, 6, 7], hydrothermal processing[3, 8]. In addition to these processes, depolymerization of pectin using UV light/TiO_2 has also been reported[9].

Pectin is a heterogeneous complex composition of polysaccharides. The principal monomer is galacturonic acid (GalA), which can be free, or methyl esterified at the carboxyl groups at carbon 6. The degree of esterification determines the properties of pectin in food technology as high methoxy pectin can form a gel under acidic conditions (pH ~ 3) in the presence of high sugar concentrations, while low methoxy pectin form gels by interaction with divalent cations (particularly Ca^{2+})[10]. There are three domains of pectin molecule[11]

- **Homogalacturonan**, consisting of GalA units. This polysaccharide represents about 60-70 % of the total pectin[4, 12]. Homogalacturonan is considered to be the smooth region of pectin.
- **Rhamnogalacturonan I**, the main monomers are rhamnose and galacturonic acid branched with galactan, arabinan and arabinogalactan. This polysaccharide is known as the hairy region of pectin.
- **Rhamnogalacturonan II**, the main monomer is galacturonic acid and has a complex branched pattern.

Notwithstanding advancement in the utilization of UV light/TiO_2 on the overall pectin depolymerization, there is a need to understand the individual effect of pH, temperature, UV light and TiO_2 photocatalyst. Thus, in this work we present the depolymerization of pectin under various pH and temperature values. Moreover, the individual effect of UV light is presented.

Equipment, chemicals, and method

Photoreactor

All the experiments were performed using photocatalytic reactor. The photoreactor has two main parts: light source and photocatalyst. The wavelength of this artificial lamp is 272 nm whereas as a photocatalyst we use TiO_2. From the technical point of view, TiO2 matches most of the requirements of photocatalysis. Several layers of catalyst (TiO_2) are applied in the inner surface of glass cylinder. The type of glass cylinder is 13-19. The height of the glass cylinder is 70 mm, the inner and outer diameter are 33 and 36mm. The photocatalyst (TiO_2) is bought in the Czech Republic (Mikropur s.r.o.). The photocatalytic reactor is connected to the feeding vessel and thermometer. Thus, the solution is placed in the feeding vessel and circulates constantly from the feeding vessel to the photoreactor at a determined temperature. For further data evaluation, the pH meter, conductometer and a thermometer are placed in the feeding vessel. Moreover, the temperature of the solution could be controlled from the Almemo device as the maximum/minimum temperature and from thermometer which is connected directly to the tap water. Almemo device shows on its screen all the data (pH, temperature, conductivity of the solution) and transfers/stores in the computer.

Chemicals

Lemon peel powder pectin (purchased in the Czech Republic, Danisco Cultor) is used to prepare the solution of pectin, with the molecular weight of about 400 kDa. H_2SO_4 and NaOH are used to adjust the pH of the solution. Before and after the measurements, the photoreactor is cleaned with H_2O_2 (0.01M). To evaluate the effect of H_2O_2, oxalic acid degradation is measured before and after the measurements. Sodium hydroxide, sodium acetate and degassed water are used to prepare the eluents for HPAEC-PAD. Sodium azide is used for sterilization of injectors in HPAEC.

Method

Lemon peel powder pectin (0.5 g) is mixed with 0.5 L of distilled water. The solution is obtained by using a magnetic stirrer. Acidic and alkaline solutions are obtained by applying H_2SO_4 and NaOH. The neutral solution of pectin is obtained by first boiling the distilled water to 100 °C for 10 min and ultrasonicate for 10 min. The solution is then transferred to the feeding vessel for circulation. So, the solution flows constantly from the feeding vessel through the pipes into the photoreactor by using a power rotating pump. All the measurements are accomplished in the presence of UV light. The exception from this exposure was only when pectin depolymerization is tested in the absence of UV light. Subsequently, as the solution was circulating for 5 h, every 30 min a sample is collected and stored in the fridge. The samples were then melted and filtered (membrane nylon 0.45 μm filter) prior to injection due to any possible pectin residues. The obtained supernatants were placed in the plate of the high-performance anion exchange chromatography coupled with pulsed amperometric detection for galacturonic acid and other saccharides determination. To clean the surface of the photocatalyst from the last experiment, H_2O_2 (0.01M) is prepared and placed in the feeding vessel and let for 30 min to circulate in the photocatalytic reactor and feeding vessel. To be sure that the photocatalyst always has the origin efficiency, degradation of oxalic acid is measured before and after application of H_2O_2. Lastly, the feeding vessel is washed 3 times before each measurement with distilled water.

Chromatographic determination of monosaccharides

High performance anion exchange chromatography coupled with pulsed amperometric detection (HPAEC-PAD) takes advantage of the weakly acidic nature of carbohydrates to give highly selective separations at high pH. HPAE-PAD is extremely selective and specific for carbohydrates because pulsed amperometry detects only those compounds that contain functional groups that are oxidizable at the detection voltage employed[13]. Carbohydrates are detected by measuring the electrical current generated by their oxidation at the surface of a gold electrode. The products of this oxidation reaction also poison the surface of the electrode[13]. Therefore, the electrode is cleaned time by time and this is accomplished by polishing the gold electrode. Dionex HPAEC consists of pump (flow: 1 ml/min), autosampler, column (Dionex CarboPac PA1), detector (PAD with the gold electrode), software (chromeleon). The Dionex CarboPac PA1 is particularly well-suited to the analysis of monosaccharides. The reagents that are used to prepare the mobile phase are:

- ***Distilled water (A).*** The water should be of a high quality. Moreover, it should be as little dissolved CO_2 as possible. On this basis, distilled water is first boiled to about 100 °C for 10 min and then sonicated for 10 min for water degassing (remove CO^2). During these processes (boiling and sonication) a vacuum water aspirator is connected with the volumetric flask. The process is finished when all the bubbles formed disappear.
- ***Sodium hydroxide (B).*** The concentration of 0.2M NaOH is obtained by adding 20.8 mL of 50-52 % solution of NaOH with a plastic pipet into 2 L of degassed water.
- ***Sodium acetate (0.6M) and sodium hydroxide (0.1) mixed (C).*** This solution is prepared by first filling the beaker of 1L with degassed water. Consequently, the solution of water is placed in a magnetic stirrer. Simultaneously, as the water is mixing, 98.4 g of solid sodium acetate is poured. The solution is mixed until the acetate has been dissolved. Next, 10.4 mL of NaOH (50%) is added. All this obtained solution is transferred to volumetric flask and filled with sonicated water up to the mark.

Once the eluents are prepared, they are kept blanked under helium (3.8 psi/26.2 kPa) all the time.

Results

The content of galacturonic acid (GalA) is shown in the following figure, in the presence of UV light/TiO_2 incorporating the effect of different temperature values. The content of galacturonic acid in solution is used as an indicator for pectin depolymerization, meaning that the higher the content of GalA in solution, the higher the depolymerization of pectin has taken place.

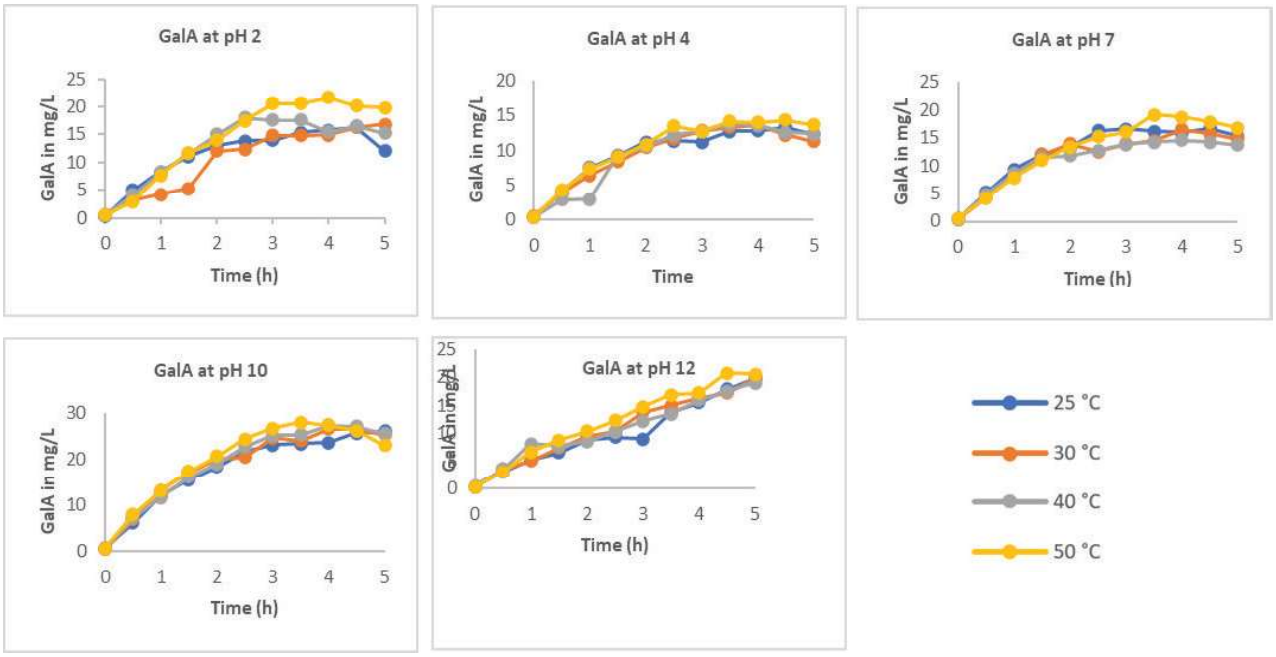

Figure 1: **The content of galacturonic in the depolymerized pectin solution in mg/L for 5 h. The effect of temperature is shown at various pH values.**

For all pH values, the content of GalA is increased by the time exposure to the UV light. For instance, in the 1st figure at pH 2, we can see that the content of GalA, at the beginning of the experiment (1st sample), is 0.35 mg/L, whereas after 5 hours (11th sample) exposure to UV light/TiO_2 is around 15 to 20 mg/L (according to the temperature applied). Likewise, by increasing the temperature a slightly higher content of GalA is observed. Regarding temperature values, the highest content of GalA is provided when pectin is depolymerized at 50 °C, especially at pH 10, by yielding 28 mg/L. At the same conditions, the lowest content of GalA resulted to be at 25 °C being about 26.17 mg/L. So, in this comparison, even if the temperature is increased by 100 %, the content of GalA is increased by only 7 %. At the other pH values, the efficacy percentage is even lower than 7 %. In the following figure, the contribution of different pH values to the overall pectin depolymerization is shown. The measurements are accomplished in the temperature range of 25, 30, 40 and 50 °C but for the purposes of simplicity we will show only the measurements at 25°C.

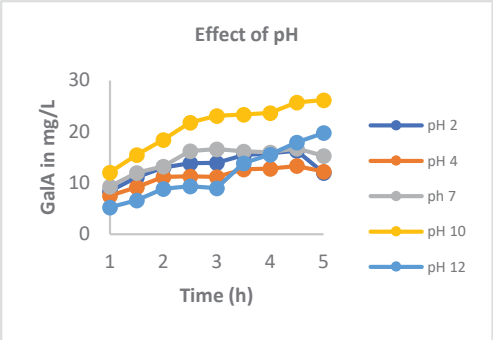

Figure 2: **The content of GalA at various pH values at 25°C.**

The highest content of GalA is provided by alkaline medium of pH 10. This may occur due to the occurrence of β-elimination reaction. In the other hand, the lowest content of GalA is provided in acidic environment of pH 4. This means that the bonds between GalA are considerable stable in an acidic environment. In this comparison, alkaline medium of pH 10 provides 96.32 % higher content of GalA compared to that of acidic environment of pH 4. Moreover, 60.84 % higher content of GalA are provided at pH 10 than the one at pH 2; 56.5 % higher than the one at pH 7 and 32.43 higher than the one at pH 12. So, the data show that pectin is relatively resistant in acidic environments but extremely sensitive to alkali. The results obtained with the photocatalytic process corresponds with those which are obtained by Jankana Burana et al [9]. The authors state that a pH value of 10 afforded the most rapid degradation of pectin with 71.2% decrease in molecular weight. In the next following figure, the individual contribution of UV light is presented.

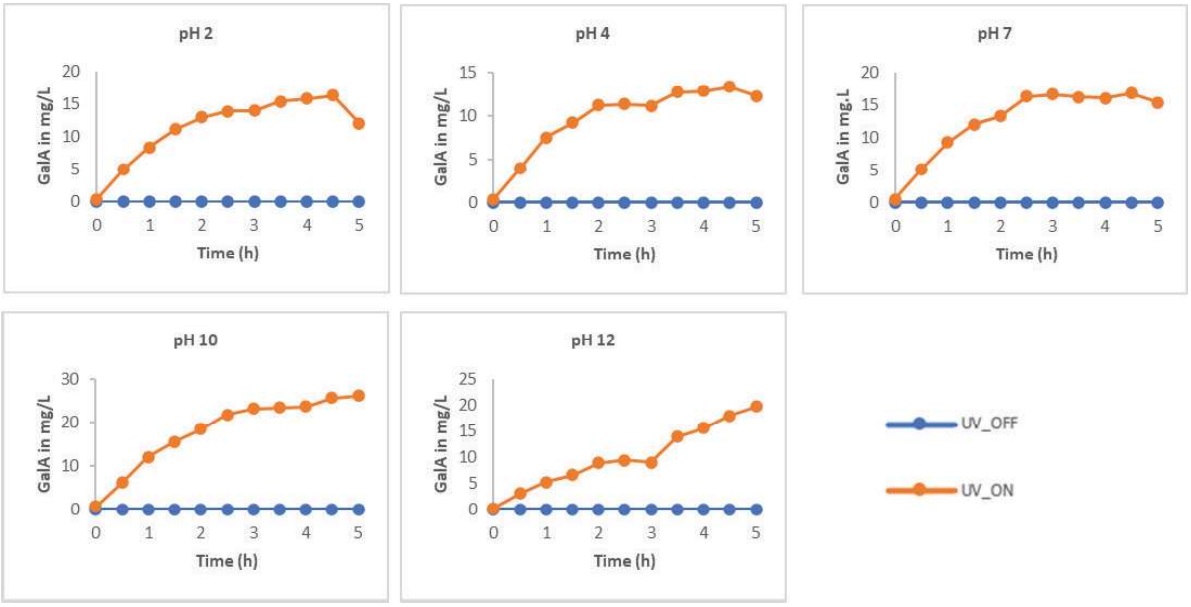

Figure 3: **The individual contribution of UV light at various pH values (25°C)**

As is clearly observable in the above figure, there is a considerable effect of UV light/TiO_2 in the overall pectin depolymerization. For example, in the presence of UV light/TiO_2, at pH 2, the highest content of GalA is about 16 mg/L, whereas the highest content of GalA at the same conditions, in the absence of UV light, is 0.25 mg/L. So, the efficiency of UV light in releasing GalA from pectin solution is about 64-fold higher compared with the depolymerization of pectin in the absence of UV light. As we have shown previously, higher content of GalA is obtained when depolymerization of pectin takes place in alkaline medium of pH 10. In this case, the contribution of UV light is also of great importance, by yielding 116 times higher content of GalA compared with the one in the absence of UV light. The same trend is observed at other pH values.

Next, in addition to GalA, as the main monomer of pectin polysaccharides, the content of other saccharides will be shown such as, rhamnose, arabinose, galactose and glucose. The content of these saccharides is shown in various pH values at 25°C.

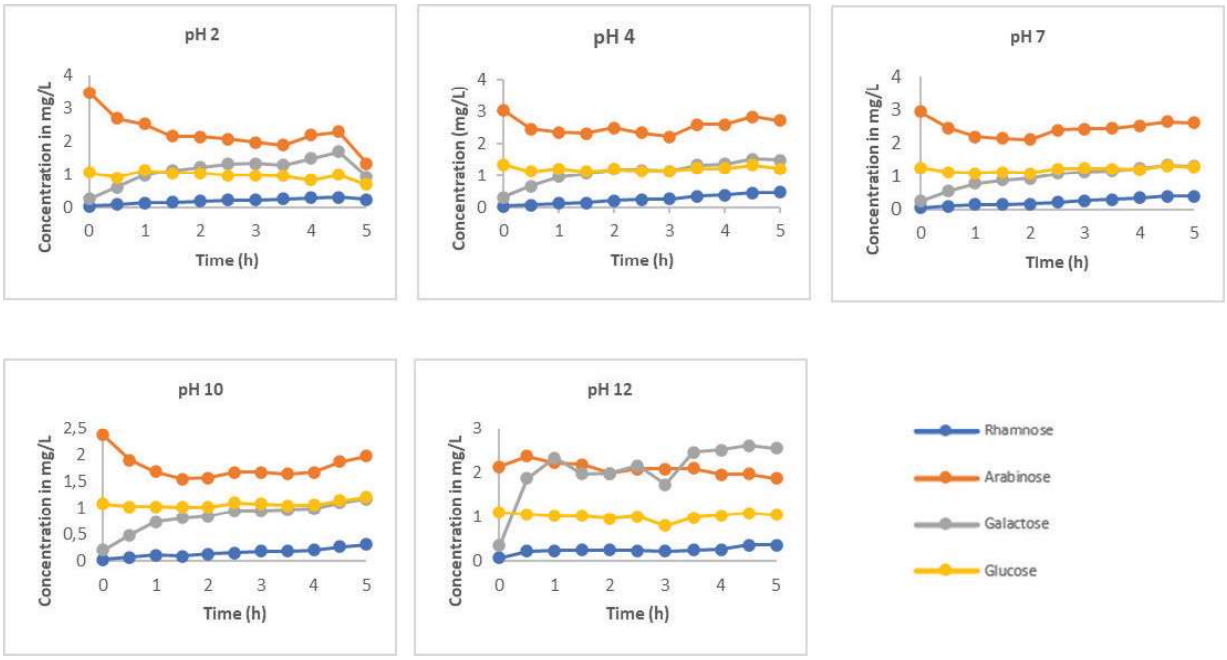

Figure 4: **The content of saccharides at various pH values during the depolymerization of pectin.**

The release of the saccharides is not realized at the same rate for each carbohydrate. Apparently, in acidic and neutral conditions, arabinose resulted to be present in the highest concentration. The lowest content of arabinose, compared to other pH values, resulted to be in alkaline environment of pH 12. Contrarily, of all pH values, rhamnose resulted to be in the lowest concentration. This may occur due to the strong bond between rhamnose and galacturonic acid. However, the highest content of rhamnose is released in acidic environment of pH 4, being about 0.5 mg/L. Likewise, glucose has its maximum concentration at pH 4, whereas galactose has its maximum concentration in strongly alkaline medium of pH 12. Interestingly, the concentration of galactose at pH 12 in comparison to the other pH values is increased by about 73.3 %.

Conclusion

In addition to our previous findings, we have found that the alkaline medium of pH 10 is the best medium concerning pectin depolymerization, by providing the highest content of GalA. This may occur due to the occurrence of β-elimination reaction. Therefore, pectin under UV light/TiO_2 in the alkali medium is highly sensitive. In the other hand, in an acidic environment, the glycosidic bonds between GalA seems to be very stable, providing the lowest amount of GalA. This means that the glycosidic bonds between galacturonic acid are relatively resistant in an acidic environment. Moreover, by increasing the temperature, the content of GalA is increased. However, the content of galacturonic acid is increased by only 7 %, even though the temperature is doubled. Furthermore, the individual contribution of UV light in the presence of TiO_2 resulted to be 116 times higher (pH 10) compared when pectin is depolymerized in the absence of UV light. Galacturonic acid can be utilized in the food industry (as acidic agent), chemical industry (as washing powder agent) and in pharmaceutic industry (for production of vitamin C). In the other hand, arabinose resulted to be in the highest concentration compared to the other saccharides. This neutral sugar can be utilized for diagnostic purposes in bacteriology. In addition to the findings, it will be necessary to further distinguish how the TiO_2 catalyst contributes to the overall pectin depolymerization rate. Moreover, it will be necessary to determine the content of oligosaccharides in the chromatogram or any other quantification method to specify the possible applications.

Acknowledgement
„This work was supported from the grant of Specific university research – grant No A1_FPBT_2023_006“.

REFERENCES

1. Figueroa-González, I., et al.: J Sci Food Agric. (2011).

2. Tingirikari, J.M.R.: Food Funct. (2018).
3. Gullón, B., et al.: Trends Food Sci. (2013).
4. Nadia, E.K., Nasser, S.M.: J Pure Appl Microbiol. (2016).
5. Grohmann, K., Cameron, R., Buslig, B.: Bioresour. Technol. (1995).
6. Combo, A. M. M., Aguedo, M., Goffin, D., Wathelet, B., Paquot, M.: Food Bioprod Process. 588-596. (2012).
7. Olmos, J. C., Hansen, M. Z.: Chem. Eng. J. 29-36. (2012).
8. Martínez, M., Gullón, B., Yáñez, R., Alonso, J. L., Parajó, J. C.: Chem. Eng. J. 480-486. (2010).
9. Burana-osot, J., Soonthornchareonnon, N., Hosoyama, S., Linhardt T. Toida, R. J.: Carbohydr. Res. 1205-1210. (2010).
10. Blanco-Pérez, F., Steigerwald, H., Schülke, S., Vieths, S., Toda, M., Scheurer, S.: Curr Allergy Asthma Rep. 43. (2021).
11. Velisek, J.: The Chemistry of Food, (2014).
12. Míguez, B., et al.: Probiotics and prebiotics in human nutrition and health, 301-330 (2016).
13. Rohrer, J.: Technical Note, *20*(1), 1-12 (2012).

USE OF ESSENTIAL OILS IN THE PRODUCTION OF BAKERY PRODUCTS

LUCIE JURKANINOVA, MATEJ BOZIK

Czech University of Life Sciences Prague, Department of Food Science, Kamýcká 129, 165 00 Praha – Suchdol, Czech Republic

jurkaninova@af.czu.cz

INTRODUCTION

Bakery products have become integral to people's daily diets worldwide due to rapid socioeconomic development[1]. These products, constituting staple foods globally, are produced at a staggering rate of over 9 billion kilograms annually, with an average consumption of about 70 kilograms per person each year[2]. The primary ingredients for bakery products are flour, water, leavening agents like yeast, and salt. To enhance dough handling and create specialty items with improved nutritional value, optional ingredients are added[3].

The process of making bakery products can be simplified into dough preparation, maturation, and baking. The optimal procedure varies depending on the specific product and the desired final properties[4]. Key quality aspects for baked goods encompass a substantial loaf volume, uniform texture, and an extended shelf life[2].

Shelf life of baked goods

Certain bakery products, such as bread, have a limited shelf life and undergo changes in texture, taste, and appearance due to physical, chemical, and microbial factors during storage. Microbial spoilage, driven by the growth of bacteria, molds, and yeasts, results in an undesirable appearance[1]. This microbial activity can produce unpleasant odors and toxic metabolites, posing risks to health and causing economic losses for the baking industry and consumers[5]. Food molds and their toxic byproducts account for approximately 25 % of global agricultural food loss, according to the Food and Agriculture Organization of the United Nations[6].

Several factors influence the spoilage of bakery products, including product characteristics, processing conditions, packaging, and storage conditions. Product attributes like ingredients, nutritional composition, oxidative stability, moisture, water activity, and pH play a critical role. The processing phase involves baking time, temperature, cooling, and production environment hygiene. Storage factors such as temperature, light exposure, relative humidity, and microbial content are carefully monitored. Packaging characteristics are also significant, considering mechanical properties, thermal stability, gas permeability, UV barrier, gas composition, antioxidants, and antimicrobial activity[1].

Physical methods such as ultraviolet light, infrared radiation, microwave heating, and ultra-high pressure treatment are employed to prevent spoilage, although they have limitations[1]. Conventional methods rely on preservatives, with a common choice being a combination of calcium propionate and sorbic acid to inhibit undesirable microorganisms in bakery products.

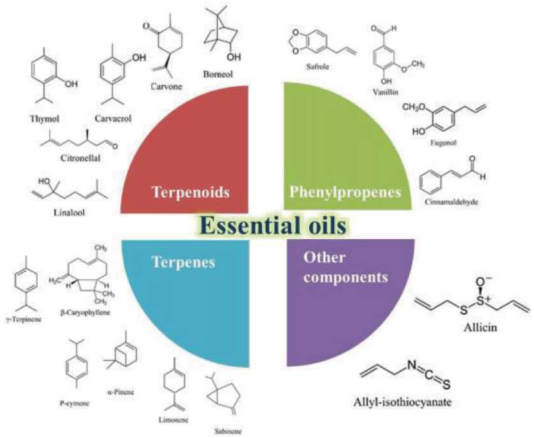

Figure 1. Selected components of essential oils with antimicrobial activity[7]

Preservatives

Preservatives are added to food products to enhance or maintain their nutritional value and quality, thereby extending shelf life and bolstering consumer acceptance[8]. The composition and quantity of each preservative are subject to regulation[7]. Preservatives are classified as either chemical or natural. Chemical preservatives include synthetic substances like benzoates, sorbates, nitrites, nitrates, sulphites, glutamates, glycerides, and others. For

instance, sorbic acid, propionic acid, and propionic acid salts are approved for use in bakery products. Sulphur dioxide and its salts can be added to crisps and crackers[9]. The second group comprises substances derived from natural sources, such as salt, sugar, vinegar, honey, spices, and more[8].

Consumers' growing interest in healthy lifestyles and diets has led to a desire to reduce the use of common chemical preservatives. Essential oils, known for their antioxidant, antibacterial, antifungal, antiviral, antiparasitic, and insecticidal properties, have gained attention as alternatives[10]. These oils, produced by various parts of aromatic plants, contain a complex mixture of volatile compounds. They serve to protect the plants against bacteria, viruses, fungi, and insects[11].

Essential oils are clear, volatile liquids that are sparingly colored and soluble in fats and organic solvents. They consist of terpene compounds, alcohols, acids, esters, epoxides, aldehydes, ketones, amines, and sulphides, with aromatic and terpene compounds being the two main categories. Essential oils typically contain about 20-60 different components, with a few dominant ones accounting for 20-70 %, while the rest are present in trace amounts. Major components are primarily responsible for their biological effects, although the minor components also contribute[6]. Differences in chemical composition and biological activity are influenced by factors such as climatic conditions, cultivation strategies, plant variety, fertilization, water supply, and extraction processes[12].

However, essential oils have limitations. They can cause allergic reactions, exhibit toxicity at higher concentrations, and lack well-documented exposure guidelines. Additionally, their chemical variability and lipophilic nature present challenges. Despite these limitations, essential oils are widely used in cosmetics, perfumery, pharmaceuticals, and as food preservatives[13].

Spices and essential oils are employed in the food industry to enhance flavor and prolong the shelf life of products. Components found in cloves, cinnamon, oregano, garlic, coriander, rosemary, parsley, lemongrass, sage, and vanilla have demonstrated potent antimicrobial effects[14].

In the context of baking, essential oils are valued for their antimicrobial and antioxidant properties. They can be incorporated directly into bakery product recipes or packaging materials to extend shelf life[7].

In recent years, research into the antimicrobial activity of essential oils, their mechanisms of action, and their potential against pathogenic microorganisms has gained significance. This antimicrobial effect is influenced by chemical compounds within the oils, with oxygenated terpenoids, particularly phenolic terpenes, phenylpropanoids, and alcohols, playing a key role. Substances with a high percentage of phenols include carvacrol, thymol, menthol and eugenol. Essential oils from mustard, cinnamon, and cloves have been found to slow down the spoilage process, and lemon grass, cinnamon, clove, and thyme essential oils exhibit fungicidal activity. Some, like turmeric and cloves, have been shown to inhibit mold growth in butter cakes, primarily due to their sesquiterpenes, monoterpene hydrocarbons, eugenol, and phenolic compounds[15].

In conclusion, essential oils and their active components can effectively preserve various baked goods by offering antimicrobial and antioxidant properties. These oils may also enhance the flavor and aroma of bakery products. Their synergistic effects with traditional chemical preservatives or physical processes promise to extend shelf life and reduce the need for chemical additives. Further research is needed to determine essential oils' optimal use, concentrations, and synergies for preserving bakery products.

The Biostore project (QK21010064) is supported by the Ministry of Agriculture, National Agricultural Research Agency.

REFERENCES

1. Qian M, Liu D, Zhang X, Yin Z, Ismail BB, Ye X, Guo M. 2021. A review of active packaging in bakery products: Applications and future trends. Trends in Food Science & Technology 114:459–471.
2. Gu M, Hong T, Ma Y, Xi J, Zhao Q, Xu D, Jin Y, Wu F, Xu X. 2022. Effects of a commercial peptidase on rheology, microstructure, gluten properties of wheat dough and bread quality. LWT 160:113266.
3. Dewettinck K, van Bockstaele F, Kühne B, van de Walle D, Courtens TM, Gellynck X. 2008. Nutritional value of bread: Influence of processing, food interaction and consumer perception.
4. Dziki D, Różyło R, Gawlik-Dziki U, Świeca M. 2014. Current trends in the enhancement of antioxidant activity of wheat bread by the addition of plant materials rich in phenolic compounds. Trends in Food Science & Technology 40:48–61. Elsevier.
5. Axel C, Zannini E, Arendt EK. 2017. Mold spoilage of bread and its biopreservation: A review of current strategies for bread shelf life extension. Critical Reviews in Food Science and Nutrition 57.
6. Mutlu-Ingok A, Devecioglu D, Dikmetas DN, Karbancioglu-Guler F, Capanoglu E. 2020. Antibacterial, Antifungal, Antimycotoxigenic, and Antioxidant Activities of Essential Oils: An Updated Review. Molecules 2020, Vol. 25, Page 4711 25:4711. Multidisciplinary Digital Publishing Institute.
7. Gavahian, M., Chu, Y. H., Lorenzo, J. M., Mousavi Khaneghah, A., & Barba, F. J. (2020). Essential oils as natural preservatives for bakery products: Understanding the mechanisms of action, recent findings,

and applications. Critical Reviews in Food Science and Nutrition, 60(2), 310–321. https://doi.org/10.1080/10408398.2018.1525601.
8. Dwivedi S, Prajapati P, Vyas N, Malviya S, Kharia A. 2017. A Review on Food Preservation: Methods, harmful effects and better alternatives. Asian Journal of Pharmacy and Pharmacology 3.
9. Příhoda J., Humpolíková P., Novotná D. (2003): Základy pekárenské technologie. 1. vyd. Pekař a cukrář s.r.o., Praha.
10. Ahmed LI, Ibrahim N, Abdel-Salam AB, Fahim KM. 2021. Potential application of ginger, clove and thyme essential oils to improve soft cheese microbial safety and sensory characteristics. Food Bioscience 42.
11. Bakkali F, Averbeck S, Averbeck D, Idaomar M. 2008. Biological effects of essential oils - A review.
12. Tavares L, Zapata Noreña CP, Barros HL, Smaoui S, Lima PS, Marques de Oliveira M. 2022. Rheological and structural trends on encapsulation of bioactive compounds of essential oils: A global systematic review of recent research. Food Hydrocolloids 129:107628. Elsevier.
13. Napoli E, Di Vito M. 2021. Toward a New Future for Essential Oils. Antibiotics 10:207.
14. Tajkarimi MM, Ibrahim SA, Cliver DO. 2010. Antimicrobial herb and spice compounds in food. Food Control 21:1199–1218.
15. Soumya C, Sudha ML, Vijaykrishnaraj M, Negi PS, Prabhasankar P. 2017. Comparative study on batter, quality characteristics and storage stability of muffins using natural ingredients (preservatives) and synthetic preservatives. Journal of Food Processing and Preservation 41:e13242. John Wiley & Sons, Ltd.

STRUCTURAL ANALYSIS OF CRUDE POLYSACCHARIDE FRACTIONS FROM MUSHROOM *Hericium erinaceus* F 5242

KRISTÝNA KLÁROVÁ[a*], ROMAN BLEHA[a], JANA ČOPÍKOVÁ[a], MIROSLAV JOZÍFEK[b], ANDREJ SINICA[a], PAVEL KLOUČEK[c]

[a]Department of Carbohydrates and Cereals, University of Chemistry and Technology, Prague, Technická 5, 16628 Prague, Czech Republic
[b]Department of Gardening, [c] Department of Crop Production, Czech University of Life Sciences, Prague, Kamýcká 129, 16521 Prague, Czech Republic

Kristyna.Klarova@vscht.cz

Abstract

The aim of this work was the isolation and structural characterisation of the crude polysaccharide fractions of *Hericium erinaceus* strain f 5242. Crude polysaccharide fractions were obtained by subsequent extractions with cold water, hot water, and alkali solution. The chemical composition and structure of the crude polysaccharide fractions isolated were analysed by spectroscopic and separation methods.

Introduction

Mushrooms *Hericium erinaceus* have been cultivated and used in countries such as Japan, China, and South Korea for centuries. They are used as a source of bioactive compounds such as phenolics, fatty acids, proteins, and polysaccharides. The polysaccharides of *Hericium erinaceus* have biological activities such as immunomodulating, antiaging, anti-inflammatory, antitumor and anti-oxidant[1-2]. In general, these biological activities are mainly related to the monosaccharide composition, structure, and position of glycosidic linkages, the branching, and the molecular weight of polysaccharides[3].

This work focusses on the isolation and characterisation of crude polysaccharide fractions from fruiting bodies of mushroom *Hericium erinaceus* f 5242. These fractions were characterised by FTIR spectroscopy and GC/FID.

Experimental

Materials and cultivation

The fruiting bodies of *Hericium erinaceus* strain f 5242 were grown in cooperation with the Czech University of Life Sciences in green houses and were provided by the Crop Research Institute. The substrate is based on the ratio of a mixture of 79 % beech-oak sawdust, 20% wheat bran and 1 % gypsum. The moisture content was adjusted to 64 %. The 2 kg of substrate were filled into Sac O_2 polypropylene bags and steamed at 90 °C for 24 hours. Additionally, the bags were cooled and inoculated with 5 to 7% of the granular seedlings that were prepared on sterile wheat grains. Colonisation was carried out at 25 °C for 21–25 days and then the bags were transferred to a lighted grow room (light for 24 hours) for fructification at 18 °C with a relative humidity of 90–95%. The first fruiting bodies (Fig. 1) were harvested after 10–12 days.

Fig. 1: **Frozen (top) and oven dried (bottom) fruiting bodies of *Hericium erinaceus* strain f 5242**

Preparative Procedures

Lipids, oligosaccharides, and polyphenols were removed from dried and milled material with hexane, ethanol, and acidic ethanol (0.2 mol l^{-1} HCl). Furthermore, the crude extracts were obtained by extractions with cold water, hot water (100 °C under reflux) and an alkali solution (1 mol l^{-1} NaOH, 4 °C) yielding crude extracts F1, F2 and F3 and solid residues SR. The polysaccharides were precipitated from the crude extracts with an excess of ethanol (4:1 v/v), centrifuged, washed with 80%, 96% ethanol and acetone and dried in air. The soluble and insoluble alkaline products F3 and SR were neutralised by washing with acidic ethanol and 80% ethanol until the neutral reaction, then washed with 96% ethanol and dried in air. All fractions were analysed by FTIR and GC/FID (neutral sugars)[4].

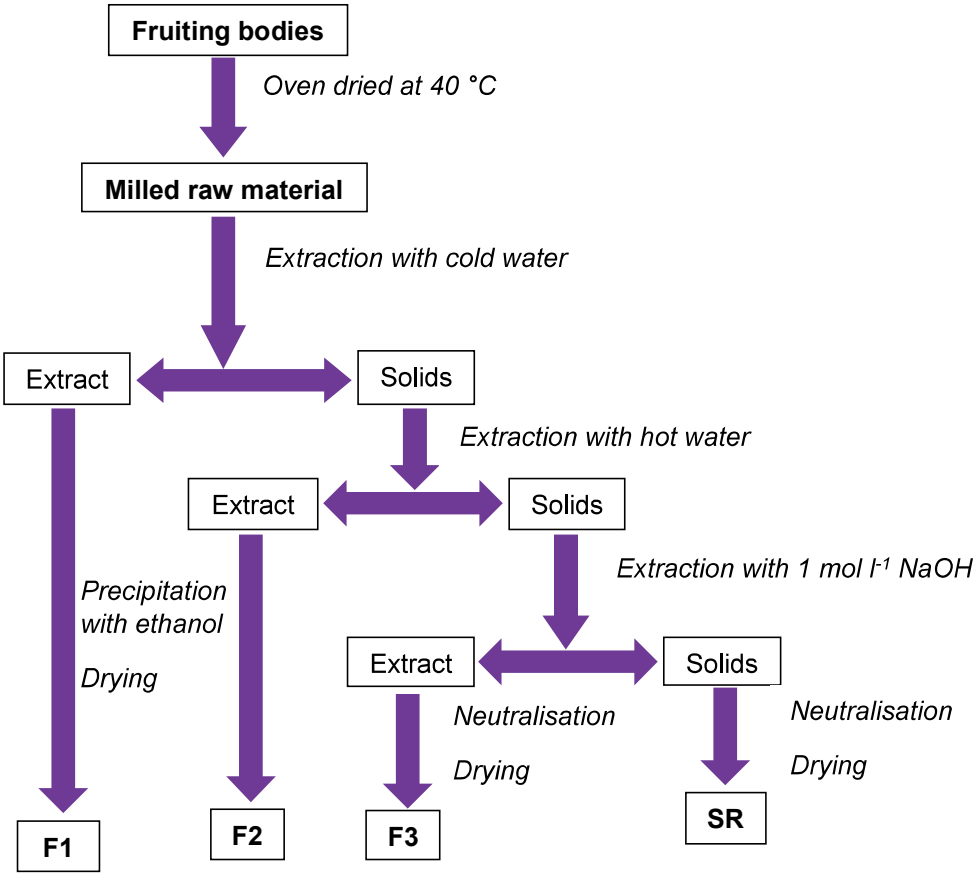

Fig. 2: **Isolation scheme of crude polysaccharide fractions from fruiting bodies of *Hericium erinaceus* strain f 5242**

Analytical Methods

FTIR spectra (400–4000 cm^{-1}) of the fractions were recorded in KBr pellets using a Nicolet 6700 FTIR spectrometer (Thermoscientific, USA); 64 scans were accumulated with a spectral resolution of 2.0 cm^{-1}. The spectra were smoothed and the baseline was corrected using Omnic 8.0 and 9.0 (ThermoScientific, USA) software and exported in ASCII format to Origin 2019b software (OriginLab Inc., USA) software for graph preparation.

Neutral sugars were analysed in all materials and fractions by hydrolysis in 72% H_2SO_4 and analysed as alditol acetates by GC/FID using a Shimadzu GC2010 (Japan) equipped with a 30 m capillary column DB-225 with an internal diameter of 0.25 mm and a film thickness of 0.15 µm. The injector and detector temperatures were, respectively, 220 °C and 230 °C. The oven temperature programme was followed 200 °C for 1 min, then increased to 220 °C (40 °C/min), temperature 220 °C for 7 min, then increased to 230 °C (20 °C/min) until the final temperature 230 °C for 1 min, total time 9 min.

Results and Discussion

Yields of the crude extracts and solid residues are summarised in Table I. The mass of fruiting bodies decreased more than two times after washing and about 4.5 times after all extractions. The yields of the crude extracts significantly increased in the order of F1, F2 and F3.

The monosaccharide composition of all isolated fractions is summarised in Table II. Glucose was the main monosaccharide in all fractions (55–93 mol %). The highest glucose content was found in solid residues (SR) (93 mol %), but lower values were found in fraction F2 (hot water extract) (92 mol %) and alkali extract (89 mol %). The F1 fraction (cold-water extract) had the lowest glucose content (54 mol. %) but also the highest galactose content (35 mol %) and fucose (8 mol %). Fucose, mannose, and xylose were found to be minor sugars in most fractions. Therefore, the main isolated polysaccharides should be glucans, but in the case of cold water also fucogalactans, as has been reported earlier[6].

Table I: **Yields of the crude fractions obtained from the fruiting bodies of mushroom *Hericium erinaceus* f 5242**

Fraction	Weight [g]	Yields [% w/w]
Raw material	250.12	100
Washed	112.93	45 %
F1	2.96	2.62
F2	13.53	12.00
F3	31.79	28.15
SR	24.93	22.08

Table II. **Monosaccharide composition of the crude fractions obtained from fruiting bodies of mushroom *Hericium erinaceus* f 5242.**

Fraction	Molar ratio [mol %]							Total
	Fuc	Ara	Man	Glc	Gal	Rha	Xyl	[% w/w]
F1	**8**	0	2	**54**	**35**	0	0	63
F2	3	1	1	**92**	3	0	0	61
F3	2	0	**6**	**89**	1	0	**1**	69
SR	4	1	2	**93**	1	0	0	32

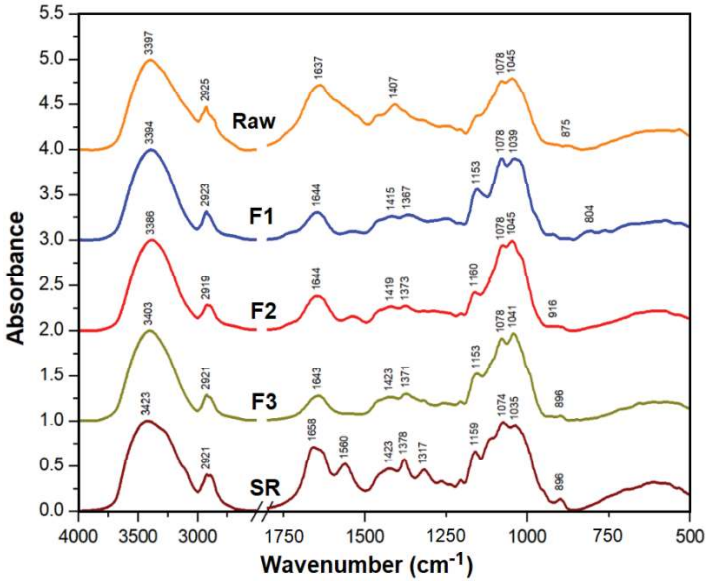

Fig. 3: **FTIR spectra of the crude polysaccharide fractions obtained from mushroom *Hericium erinaceus* f 5242**

The FTIR spectra of dry raw material and isolated crude polysaccharide fractions were measured in KBr pellets and are shown in Fig. 3. The IR bands with high intensity around 950-1200 cm $^{-1}$ belong to stretching vibrations of the C-O, C-C bonds of glycosidic bonds and pyranose rings of carbohydrates[5]. This region is characteristic of polysaccharides and is called the 'envelope', which is pronounced in raw material and apparently predominant in all fractions. This is followed by a region of 900-700 cm^{-1} representing deformation vibrations of the C-H groups sensitive to the anomeric structure of carbohydrates[5].

The skeletal vibration bands of F1 around 919, 874 and 804 cm^{-1} the presence of galactan. Previously, Li et al. (2016)[7] described fucogalactan isolated from this mushroom by water extraction with the backbone of (1→6)-linked α-D-galactopyranosyl units, and terminal α-L-fucopyranoses bound at the O-2 position of some backbone units. In contrast, the bands of F2 at 1160, 1078, 1045 and 896 cm^{-1} (shoulder) confirm the presence of (1→3)(1→6)-β-D-glucans. A characteristic band of β-D-glucans was found at 896-898 cm^{-1} (C1$_\beta$H deformation vibration) in the spectra of F2, F3 and SR. The chitin bands around 1658 cm^{-1} (amide I), 1560 cm^{-1} (amide II), 1378 cm^{-1} (symmetric deformation of CH_3) and 1317 cm^{-1} (amide III) are the most prominent in SR.

Conclusions

Four crude polysaccharide fractions were isolated from fruiting bodies of cultivated mushroom *Hericium erinaceus* f 5242. Polysaccharides soluble in cold and hot water were defined mainly as glucans and branched fucogalactans. The soluble alkali fraction contained glucans and proteins as the main products. Insoluble residues were defined as chitin-glucan complexes of mushroom cell walls. The selected fractions will be further purified and isolated polysaccharides will be analysed. This work confirmed that the mushroom *Hericium erinaceus* f 5242 could be a promising source of polysaccharides.

Acknowledgements

This work was supported by the Ministry of Agriculture of the Czech Republic (project QK1910209) and the *Crop Research Institute (Prague-Ruzyně, Czech Republic) which provided Hericium culture are greatly acknowledged.*

REFERENCES

1. He X., Wang X., Fang J., Chang Y., Ning N., Guo H., Huang L., Huang X., Zhao Z.: Int. J. Biol. Macromol. *97*, 228 (2017).
2. Friedman M.: J. Agric. Food Chem. *63*, 32 (2015).
3. Synytsya A., Novák M.: Carbohydr. Polym. *92*, 1 (2013).

4. Bleha R., Třešňáková L., Sushytskyi L., Capek P., Čopíková J., Klouček P., Jablosnký I., Synytsya A.: Molecules *24* (2019).
5. Novais, Â., Freitas, A. R., Rodrigues, C., Peixe, L.: J. Clin. Microbiol. Infect. Diseas. *38* (2019).
6. Wang X.-Y., Z. D.-d., Yin J.-Y., Nie S.-P., Xie M.-Y.: Crit. Rew. In Food sci. and nutrition *59*, S1 (2019).
7. Li Q. Z., Wu D., Zhou S., Liu Y. F., Li Z. P., Feng J., Yang Y.: Carbohydr. Polym. *144*, 196 (2016).

THE USE OF POLYSACCHARIDES IN THE EMULSION TECHNOLOGY

IVETA KLOJDOVA*, ABDUL MUIZ, NUJAMEE NGASAKUL, ALI KOZLU, DIANA KARINA BAIGTS ALLENDE

DRIFT-FOOD, Faculty of Agrobiology, Food and Natural Resources, Czech University of Life Sciences, Kamýcká 129, 165 21 Praha-Suchdol

klojdova@af.czu.cz

Abstract

Many food and cosmetic products are based on emulsions. The preparations of emulsion systems require the appropriate emulsifiers and stabilizers. In particular, molecular-based emulsifiers are used for this purpose and their effectiveness is crucial for the overtime stability of the final products. During the past few decades, there has been a tendency to use particle-based alternatives to form and stabilize "Pickering emulsions." These so-called "Pickering particles" are often based on polysaccharides or their complexes. Additionally, by-products from the food industry can be utilized for the preparation of Pickering particles.

Introduction

The importance of polysaccharides in the emulsion technology is unexceptionable. They can act as emulsifiers, stabilizers, or co-stabilizers of various emulsion systems[1]. In general, emulsions are systems of at least two normally immiscible (unmixable or unblendable) owing to liquid-liquid phase separation. The two simple systems are o/w (oil in water) and w/o (water in oil) emulsions. More complex systems are then multiple emulsions w/o/w (water in oil in water) and o/w/o (oil in water in oil). In general, molecular-based emulsifiers are used for the preparation of emulsions. However, some emulsifiers are not very effective at preventing product destabilization under some environmental conditions such as mechanical treatment and temperature conditions[2]. The current trend in the preparation of emulsions and foams is the stabilization by solid (or soft) particles, called Pickering particles. So stabilized emulsion systems are then called Pickering emulsions. This approach to stabilization was first described by Ramsden in 1903[3] and current progress in this field can be called the "neo-Pickering era"[4]. The stabilization of simple o/w emulsion by Pickering particles is shown in Fig. 1.

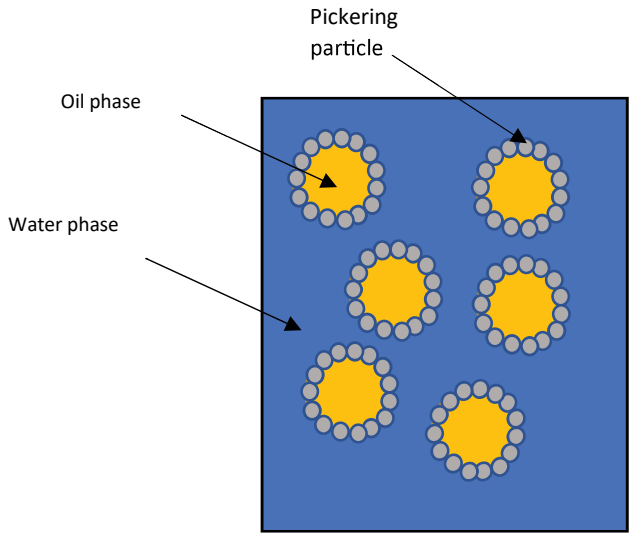

Fig. 1: Stabilization of o/w emulsions by Pickering particles.

Stabilization of Pickering and conventional emulsions by polysaccharides

Traditionally, Pickering emulsions have been stabilized by inorganic particles such as metal oxide-, metal hydroxide-, metal sulfate-, silica-, clay- and carbon-based particles, etc. Unfortunately, these emulsions do not have a big potential for applications in pharmacy, food, and cosmetic products[5]. For this reason, there has been interest in using biopolymer-based particles that are promising for those applications to form Pickering emulsions. Most Pickering particles are generally fabricated from polysaccharide materials, often in combination with protein-

based materials[6]. Usually, the behaviour of polysaccharide-based materials is somewhere between Pickering particles and molecular-based emulsifiers. In the beginning, some polysaccharides may create distinct particles in one separated phase of the emulsion and after the mixing, they are deformed and act as an adsorbed barrier at the oil-water interface[7]. Moreover, in food formulations, hydrocolloids are used for increasing food consistency, improving the gelling effect, and controlling the microstructure, texture, flavour, and shelf life. Hydrocolloids (often named gums) are defined as complex polysaccharides that can be dissolved or dispersed in a water phase and contribute to the stabilization of emulsion systems. Interactions of polysaccharides between themselves, with molecular-based emulsifiers or proteins may also provide additional stabilization effects [8,9]. Some gums such as Arabic gum, locust bean (carob) gum, konjac gum have been used in food and other technologies for decades, and the others are still found, namely e.g., gum ghatti, etc. [10]

Nutritional effects and encapsulation efficiency of emulsions stabilized by polysaccharides

In recent years, there has been a trend to use emulsions to encapsulate sensitive bioactive compounds and improve the nutritional value of foods. Additionally, encapsulation is a promising tool in pharmacy and medicine for targeting deliveries of drugs. The improved and modified structure of food matrices based on emulsions may facilitate the development of functional foods and formulations for targeted deliveries of nutrients or drugs. Highly potent but poorly soluble drugs are often the main obstacle in the development of new formulations. However, this problem may be overcome by the application of systems based on lipid emulsions (emulsions with at least one oil phase). The main advantage of polysaccharide stabilized emulsions is the high resistance to low pH. The low pH in the stomach is a barrier for some administrations. It means that they can be used as preservatives of emulsions for administrated bioactive compounds for targeted therapies of some diseases such as intestinal inflammations or even cancer[11].

Nutritional value

The preparation of food products with reduced energy intake remains a big challenge for researchers. Although considerable attention was paid to developing new and improved nutritional and dietary approaches to regulate energy intake, the number of people suffering from obesity are still rising. So, the addition of polysaccharides in food products based on fat/oil emulsions may help not only to stabilize these systems but also improve the dietary profile. A very promising approach is the incorporation of dietary fibers such as cellulose, resistant starch, inulin, lignins, chitins, pectins, beta-glucans, etc. in food products. Polysaccharide-based materials can reduce/manage lipid digestion in general and work as fat replacers[12].

Encapsulation efficiency

The additional benefit of emulsions stabilized by polysaccharides (in the form of Pickering particles or a coating layer) is their encapsulation efficiency of sensitive compounds and resistance to the conditions in the stomach. Some sensitive compounds such as bioactive proteins are denaturated at low pH (1-3) in the stomach and encapsulation techniques can help to protect them. Those compounds are then released in the intestine. Usually, the main force for the release is the action of lipases. Hence, the oil barrier is disrupted, and water phase with bioactive compounds is released. The very effective systems for the delivery are multiple emulsions. Multiple emulsions are systems of emulsions in emulsions and stabilizations by polysaccharides play an important role in their preparations. They can act as natural emulsifiers/co-emulsifiers or stabilizers of internal (simple) emulsions or multiple (outer) emulsions. There is also a big effort to use polysaccharide-based Pickering particles for the stabilization of multiple emulsions.

The use of by-products

There is a trend to use by-products from the food-industry as a source of natural food additives. By-products are secondary products from agro-food productions that are cheap and often rich in bioactive ingredients such as peptides, carotenoids, and phenolic compounds. These compounds can be extracted and incorporated into foodstuffs and work as antimicrobial, antioxidant, and food colorant agents. Often, these by-products contain high amounts of polysaccharides. So, they can be effectively used as stabilizers or natural (co)emulsifiers in emulsions. Consumers' demand for healthier food and green cosmetics has increased over the last years and by-products may be a novel approach to healthier technology of emulsion-based products. The promising sources of polysaccharide-based by-products are brewers spent grain, peels from fruits, etc [13].

Conclusions

Polysaccharides have been used in the technology of emulsions because of their stabilization properties such as thickening properties, creation of an additional layer, and interaction with molecular. In the last decade, there has been a growing trend to use solid particles (Pickering particles) for preparations and stabilizations of emulsions. In general, food emulsions prepared with polysaccharides may improve the nutritional value of final products. They may increase fiber content and regulate the digestion process. Additionally, they may be used for the encapsulation of sensitive bioactive compounds and the target administration in the intestine. Similarly, emulsions based on polysaccharides can be incorporated into natural cosmetic products or even pharmaceuticals. Moreover, the use of polysaccharide-based by-products from the food industry remains a big challenge for researchers. This area of polysaccharide-based by-product applications in the emulsion technology has a big research potential and contributes to sustainability in the whole production chain.

Acknowledgement: This research was funded by the European Union's Horizon 2020 Research and Innovation Program under grant agreement No 952594 (ERA Chair project DRIFT-FOOD).

REFERENCES

1. Cui F, Zhao S, Guan X, McClements DJ, Liu X, Liu F, et al. Polysaccharide-based Pickering emulsions: Formation, stabilization, and applications. Vol. 119, Food Hydrocolloids. 2021.
2. Muschiolik G. Multiple emulsions for food use. Vol. 12, Current Opinion in Colloid, and Interface Science. 2007.
3. Ramsden W. Separation of solids in the surface-layers of solutions and "suspensions." Proceedings of the Royal Society of London. 1903;72.
4. Dickinson E. Advances in food emulsions and foams: reflections on research in the neo-Pickering era. Vol. 33, Current Opinion in Food Science. 2020.
5. Aveyard R, Binks BP, Clint JH. Emulsions stabilised solely by colloidal particles. Adv Colloid Interface Sci. 2003;100–102(SUPPL.).
6. Li XM, Xie QT, Zhu J, Pan Y, Meng R, Zhang B, et al. Chitosan hydrochloride/carboxymethyl starch complex nanogels as novel Pickering stabilizers: Physical stability and rheological properties. Food Hydrocoll. 2019;93.
7. Cui F, Zhao S, Guan X, McClements DJ, Liu X, Liu F, et al. Polysaccharide-based Pickering emulsions: Formation, stabilization, and applications. Vol. 119, Food Hydrocolloids. 2021.
8. Klojdová I, Troshchynska Y, Štětina J. Influence of carrageenan on the preparation and stability of w/o/w double milk emulsions. Int Dairy J. 2018;87.
9. Gawai KM, Mudgal SP, Prajapati JB. Stabilizers, colorants, and exopolysaccharides in yogurt. In: Yogurt in Health and Disease Prevention. 2017.
10. Dłuzewska E, Jakubczak K, Florowska A. Effect of gum Arabic and gum ghatti on the stability of beverage emulsions. Italian Journal of Food Science. 2014;26(2).
11. Klojdová I, Milota T, Smetanová J, Stathopoulos C. Encapsulation: A Strategy to Deliver Therapeutics and Bioactive Compounds? Pharmaceuticals. 2023 Feb 27;16(3):362.
12. Belluco CZ, Mendonça FJ, Zago ICC, Di Santis GW, Marchi DF, Soares AL. Application of orange albedo fat replacer in chicken mortadella. J Food Sci Technol. 2022;59(9).
13. Faustino M, Veiga M, Sousa P, Costa EM, Silva S, Pintado M. Agro-food byproducts as a new source of natural food additives. Vol. 24, Molecules. 2019.

POROUS TITANIA CERAMICS PREPARED BY STARCH CONSOLIDATION CASTING (SCC) WITH POTATO OR CORN STARCH – MICROSTRUCTURE AND ELASTIC PROPERTIES

LUCIE KOTRBOVÁ*, VOJTĚCH NEČINA, WILLI PABST

Department of Glass and Ceramics, University of Chemistry and Technology, Prague (UCT Prague), Technická 5, 166 28 Prague, Czech Republic

lucie.kotrbova@vscht.cz, pabstw@vscht.cz

Abstract

Starch consolidation casting (SCC) is used to prepare porous titania ceramics using 15–45 % of potato or corn starch. After firing at 1300 °C, porosities are in the range 36–52 % and 32–45 % for ceramics prepared with potato and corn starch, respectively. The porosity dependence of Young's modulus, determined via impulse excitation, corresponds to the exponential prediction, and the temperature dependence of Young's modulus can be described by a master curve. Based on these results, it is possible to prepare porous titania ceramics with Young's modulus in the range 37–112 GPa and to predict their temperature dependence up to 1000 °C.

Introduction

Titania, i.e., titanium dioxide (TiO_2), is an important material for preparing functional ceramics. Apart from its high dielectric constant, which makes it a useful capacitor material[1,2], in porous form it is widely applied as a catalyst[3-5] and as a gas sensor[6-8]. Now starch consolidation casting (SCC) is a well-established shaping technique for preparing porous ceramics since more than two decades[9-12]. It is based on the ability of native starch to swell in hot water and finally gelatinize[13,14], i.e. in contrast to other pore formers of comparable size that can be used for the preparation of porous ceramics, e.g. lycopodium spores[15], starch acts not only as a pore former but also as a consolidation agent because the swelling starch granules absorb water from the suspension and press the ceramic particles into close contact without requiring dewatering via the semipermeable interface as in the case of traditional ceramic slip casting into porous plaster molds. The SCC process thus allows the shaping of ceramics by casting starch-containing suspensions into non-porous metal molds. Consequently, SCC has become popular as a versatile shaping method for alumina, zirconia, and other types of oxide ceramics. After demolding and drying, during firing in an oxidizing atmosphere, e.g., air, the starch granules or gel burns out, leaving a pore space whose volume fraction (porosity) can be controlled by the amount of starch, while the pore size and shape is determined by the type of starch. The general principles, practical possibilities, and optimization (fine-tuning) of SCC have been treated in detail in previous papers[16-18].

Although in the literature there are many papers concerning starch-based polymers containing titania particles as a filler (e.g. as an opacifier or a photocatalyst), applications of starch to prepare titania ceramics are very scarce so far and no work is available that would focus on the possibilities of controlling microstructures and tailoring properties of titania ceramics using starch as a pore former. To the best of our knowledge, SCC has not yet been used for this purpose at all. Therefore, in this work we systematically compare the microstructures of porous titania ceramics made with two types of native starches: potato starch (the largest of the commonly available starches) and corn starch (a commonly available starch of intermediate size).

Although titania ceramics are used in functional applications (dielectrics, catalysts, gas sensors), the mechanical properties are of fundamental important for the performance and long-term stability of ceramic components. Moreover, since porous titania ceramics are often used at high temperatures, it is essential to know its high-temperature behavior, including the temperature dependence of mechanical properties, e.g., elastic properties. Now one of the most suitable methods for determining elastic properties such as Young's modulus is the impulse excitation technique (IET)[19]. This non-destructive testing technique allows Young's modulus to be determined from the resonant frequency of flexural vibrations of long bars or slender rods. The experimentally determined Young's modulus values can subsequently be compared with theoretical predictions for the porosity dependence of Young's modulus, with experimental results[20-25], or with the results of numerical modelling[26-30], where it has been consistently found that porous ceramics with convex pores have higher elastic moduli than those with concave pores. In particular, for many types of ceramics prepared by SCC, e.g., e.g., alumina ceramics, zirconia ceramics and alumina-zirconia composite ceramics, it has been found that the porosity dependence of

Young's modulus follows approximately an exponential prediction[20-22]. For titania ceramics this has not been checked so far. The present contribution fills this gap. Moreover, using temperature-dependent IET measurements, the temperature dependence of Young's modulus will be determined and fitted to obtain a master curve for future work and predictions.

Experimental

The raw materials used in this work was nanocrystalline titania (TiO_2) powder in the form of anatase (Perches, Czech Republic) with a density of 3.83 g/cm^3 and a particle (crystallite) size of 60 nm, potato starch (Natura, Czech Republic) with a median granule diameter of 45–50 µm and corn starch (Dr. Oetker, Slovakia) with a median granule size of around 14 µm. Using distilled water and small amounts of a dispersant for the ceramic powder (Dolapix CE64, Zschimmer and Schwarz, Germany), aqueous suspensions were prepared from the anatase powder, and starch was then added in amounts (so-called nominal starch contents) ranging between 15 and 45 vol.% related to the total volume of solids (i.e. ceramics and starch), assuming a starch density of 1.5 g/cm^3. After casting into preheated metal molds, see Figure 1, the suspensions were heated in a laboratory drier at 80 °C for 4 h. Due to starch swelling and gelatinization the ceramic suspension is transformed into a soft (gel-like) body that can be demolded and subsequently dried (2 h at 40, 60, 80 and 100 °C). This process is called starch consolidation casting / SCC. After complete drying (overnight) the samples were fired in an electric furnace at 1300 °C with a heating rate of 2 °C/min and a dwell time of 2 h at the maximum temperature. Since firing is performed in air, i.e., an oxidizing atmosphere, the starch burns out (in the temperature range 300–600 °C) without leaving any residues in the ceramics. After starch burnout the space occupied by the swollen starch granules and the starch gel remains empty (pore space), and since the starch granules are much larger than the ceramic particles (crystallites) the large pores due to starch burnout do not close during sintering of the ceramics, so that the result is a porous ceramic body. During firing and sintering, the anatase, which is the low-temperature polymorph of titania, is transformed into rutile, the high-temperature polymorph of titania.

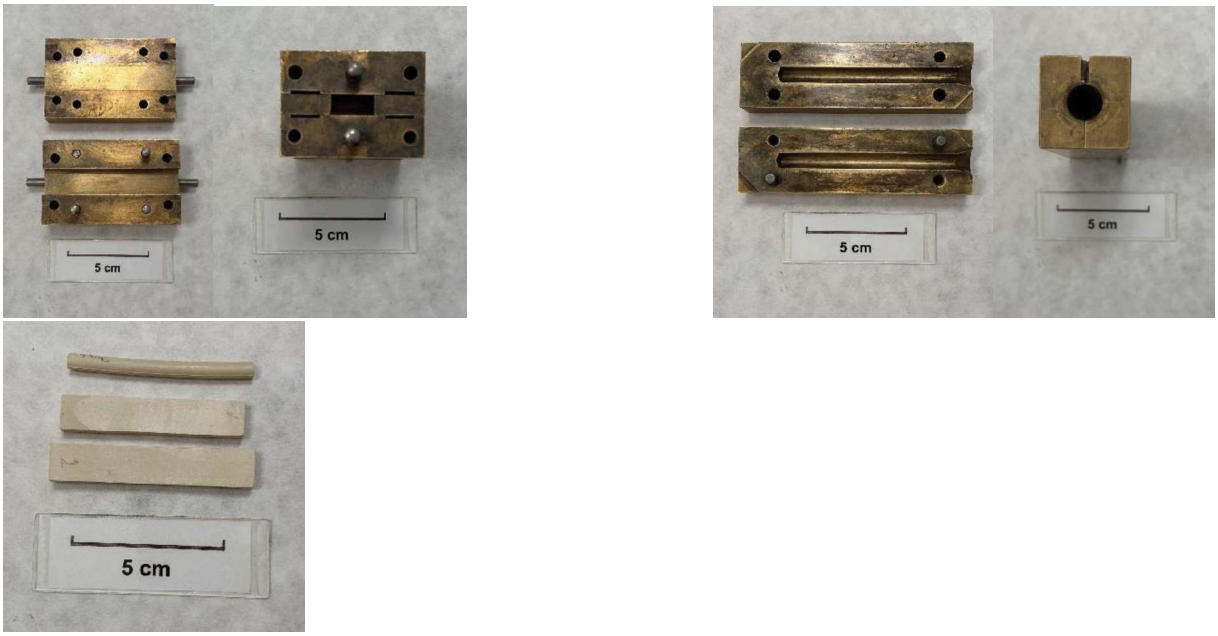

Figure 1: **Metal molds for bar-shaped samples (left), rod-shaped samples (middle), and porous titania ceramics prepared by SCC (right).**

After firing the linear shrinkage of the porous ceramics was determined by a slide caliper. Basic microstructure characterization was performed by the Archimedes method (bulk density and open porosity). The total porosity was calculated using the bulk density and the theoretical density of rutile (density 4.24 g/cm^3). Scanning electron microscopy / SEM (Lyra 3, Tescan, Czech Republic) based on fracture surfaces was used to study the details of the microstructure of the ceramics prepared. Elastic property measurements were performed via the impulse excitation technique / IET, using a Resonant Frequency and Damping Analyzer (RDFA23, IMCE, Belgium), both

at room temperature and during thermal cycling from room temperature to 1300 °C (heating and cooling with rates of 5 °C/min). Young's modulus was determined from the resonant frequencies of flexural vibrations[19].

Results and Discussion

Figure 2 shows the linear shrinkage of porous titania ceramic bodies due to firing, related to the sample dimensions before firing (but after drying), as a function of the nominal starch content in the suspension (before starch swelling). The shrinkage values for each specimen (rods or bars) have been calculated as weighted averages by weighting the dimensional changes in the length and diameter (for rods) or length, width and height (for bars) according to the dimensions, i.e. the strongest statistical weight is assigned to the dimensional change in the length direction of the samples, which can be assumed to be the most accurate one, because the length is the largest absolute dimension of the samples, while the weakest statistical weight is assigned to the diameter (for rods) and the height (for bars), which are the smallest absolute dimensions of the samples and thus their relative changes can be assumed to be prone to the largest errors. Table 1 lists the corresponding average shrinkage values of 2–3 samples. The error bars in Figure 2 show the minimum and maximum values.

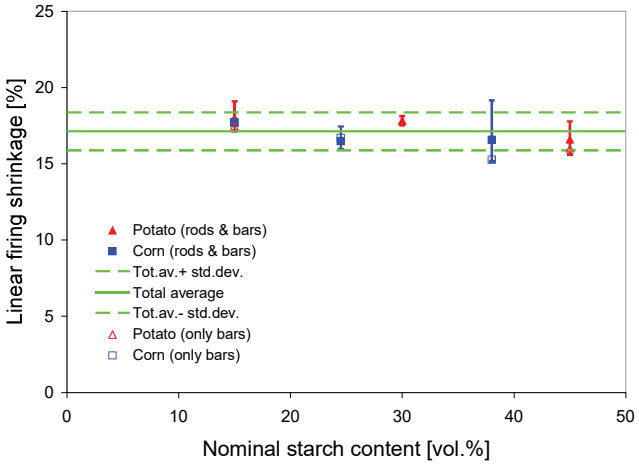

Figure 2: **Linear firing shrinkage of porous titania ceramic bodies prepared by starch consolidation casting (SCC) with potato starch (15, 30 and 45 vol.%) and corn starch (15, 24.5, 38 vol.%) versus nominal starch content.**

From the data points in Figure 2 and the values in Table I it is evident that the shrinkage values are quite similar, but those for the samples prepared with potato starch seem to be slightly higher (16.0–18.0 %) than for the samples prepared with corn starch (15.3–17.7 %). Moreover, for both starch types there is possibly a slightly decreasing trend with increasing nominal starch content, but this would need to be confirmed by a larger number of measurements on more samples. It is quite remarkable that the starch content has obviously almost no influence on the shrinkage (otherwise the shrinkage would increase with increasing starch content). However, this finding fully confirms earlier findings on porous ceramics prepared by starch consolidation casting (SCC)[16-18]. The explanation is that the pores resulting from the starch burnout are so large compared to the ceramic particles that they are essentially unsinterable. That means, usually these pores cannot be eliminated by sintering and do not contribute to the overall shrinkage. The shrinkage of these pores is usually just dictated by the shrinkage of the titania ceramic matrix. The total average of the firing shrinkage of all samples is 17.1 ± 1.2 %. According to the preceding explanations, this value can be considered to be approximately identical to the firing shrinkage of the titania ceramic matrix itself, i.e., of dense titania ceramics (without starch as a pore former). Interestingly, this value is much lower than the value obtained when the same TiO_2 (anatase) powder is shaped by uniaxial pressing, where after firing at 1300 °C for 2 h a shrinkage of 32.4 % has been obtained[31]. The reason is that in uniaxial pressing polyethylene glycol (PEG) is used as a binder for the preparation of a ready-to-press granulate. In contrast to starch, PEG does not form large pores but covers the particle surfaces and occupies the interparticle voids. From this point of view the shaping technique used in the present work (starch consolidation casting / SCC based on aqueous slips) is actually more efficient for achieving a tight packing of anatase particles than dry pressing. This

is a consequence of the good dispersion achieved for the anatase particles in water achieved in this work. It should be recalled that the anatase particles used in the present work are nanosized and thus prone to agglomeration, so that dry pressing may be generally less suitable for obtaining dense ceramic bodies from this powder than water-based shaping techniques.

Table I: **Linear firing shrinkage of porous titania ceramic bodies prepared by starch consolidation casting (SCC) with potato starch (15, 30 and 45 vol.%) and corn starch (15, 24.5, 38 vol.%) versus nominal starch content.**

Starch type	Nominal starch content [vol.%]	Linear firing shrinkage [%] (average of rods and bars)	Linear firing shrinkage [%] (average of bars only)
Potato	15	18.0	17.5
Potato	30	17.8	17.8
Potato	45	16.6	16.0
Corn	15	17.7	17.7
Corn	24.5	16.5	16.7
Corn	38	16.6	15.3

Figure 3 shows the porosity of the porous titania ceramics (after firing) as a function of the nominal starch content in the suspension (before starch swelling), and Table II lists the corresponding values, together with the values of the bulk density. The values listed in the table show that the open porosity of the porous titania ceramics is in the range 36.4–51.5 % when prepared with potato starch and 31.5–44.8 % when prepared with corn starch. With such high porosities (> 30 %) it can be expected that almost all the porosity is open, i.e., closed porosity should be almost absent, and the open porosity should be approximately equal to the total porosity. This is indeed the case: the closed porosity ranges from 0 to maximally 2.8 % and decreases with increasing nominal starch content (from 2.8 to 1.2 % for potato starch and from 1.4 to 0 % in the case of corn starch). It is obvious from Figure 3 that the porosity (pore volume fraction) attained in the porous ceramics is usually significantly higher than the nominal starch content (i.e. the volume fraction of starch granules related to the solids in the suspension, i.e. ceramic particles and starch granules), and only for very high starch contents the former approaches or even crosses the latter. This result is typical for starch consolidation casting (SCC)[16-18] and is caused mainly by the swelling of the starch granules[13,14] (even the crossover of the two curves for higher contents of corn starch has been observed in previous work on other types of ceramics[18]). The principles of this process have been investigated and quantified in several previous papers[13,16-18]. Since the degree of swelling is much larger for potato starch than for corn starch (swelling factors 3.7 and 2.3, respectively[14]), the final porosity in the ceramics made with potato starch is larger than that of ceramics with corn starch. For the purpose of practical technology, the following fit relations can be used for the controlled preparation of porous titania ceramics via starch consolidation casting (SCC)

- with potato starch (coefficient of determination 0.9995): $\phi = 0.3236 + 0.0045 \cdot x$,
- with corn starch (coefficient of determination 0.8518): $\phi = 0.2702 + 0.0039 \cdot x$,

where ϕ is the target value of the total porosity (here in volume fractions) and x is the nominal starch content (here in volume percentages).

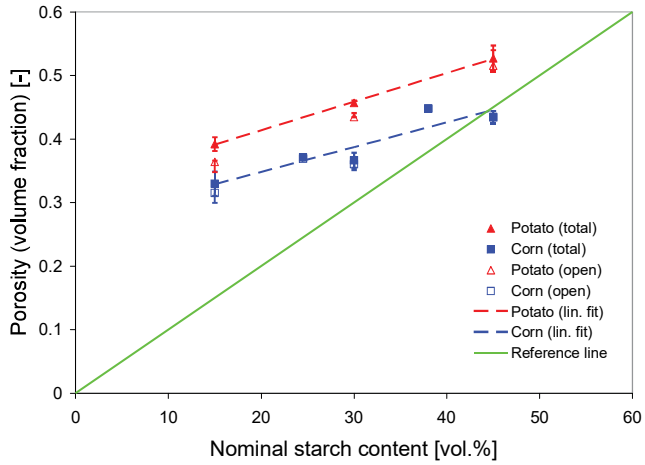

Figure 3: **Porosity of porous titania ceramic bodies prepared by starch consolidation casting (SCC) with potato starch (15, 30 and 45 vol.%) and corn starch (15, 24.5, 30, 38, 45 vol.%) versus nominal starch content, the green line is a guide to the eye.**

Table II. **Bulk density and open porosity (determined via the Archimedes technique), total porosity (calculated from the theoretical density of rutile 4.24 g/cm^3) and closed porosity (calculated as the different of total and open porosity) for porous titania ceramics prepared by starch consolidation casting (SCC) with potato starch (15, 30 and 45 vol.%) and corn starch (15, 24.5, 30, 38 and 45 vol.%) versus nominal starch content (the total porosity from the mass-volume ratio is only for recheck, with the asterisk denoting damaged or deformed specimens).**

Starch type	Nominal starch content [vol.%]	Bulk density [g/cm^3]	Open porosity [%] (Archimedes)	Total porosity [%] (Archimedes)	Total porosity [%] (mass-vol.-ratio, only for recheck)	Closed porosity [%]
Potato	15	2.578 ± 0.038	36.4 ± 0.2	39.2 ± 1.1	38.6	2.8
Potato	30	2.303 ± 0.017	43.4 ± 0.6	45.7 ± 0.4	46.6	2.2
Potato	45	2.006 ± 0.085	51.5 ± 2.5	52.7 ± 2.0	53.7	1.2
Corn	15	2.842 ± 0.081	31.5 ± 1.6	33.0 ± 1.9	36.4*	1.4
Corn	24.5	2.667 ± 0.002	36.9 ± 0.0	37.1 ± 0.0	40.5*	0.2
Corn	30	2.686 ± 0.050	36.3 ± 0.9	36.6 ± 1.2	36.8	0.3
Corn	38	2.342 ± 0.018	44.8 ± 0.4	44.8 ± 0.4	46.6*	0
Corn	45	2.401 ± 0.043	43.5 ± 0.9	43.4 ± 1.0	43.4	0

Figure 4 shows the Young's modulus of porous titania ceramic bodies prepared by starch consolidation casting (SCC) with potato starch (15, 30 and 45 vol.%) and corn starch (15, 24.5, 30, 38, 45 vol.%) versus (total) porosity (average volume fraction for individual specimens). It is evident that the majority of measured data are close to the exponential prediction (except for one data point which is closer to the power-law prediction). This confirms previous findings for other types of ceramics prepared by starch consolidation casting (SCC) or by traditional ceramic slip casting with starch as a pore former[22]. The exponential relation is indeed known to provide the most realistic predictions for the elastic moduli (and other properties such as thermal conductivity) of porous ceramics with convex pores. All predictions are based on the value of 285 GPa for the Young's modulus of dense (pore-free)

titania ceramics (rutile ceramics), E_0, which can be calculated from the elastic tensor (stiffness matrix) of rutile monocrystals[32]. The theoretical predictions shown in Figure 4 are the upper Paul bound (Voigt bound), the upper Hashin-Shtrikman bound, the power-law relation, and the exponential relation, which can be written respectively as

$$\frac{E}{E_0} \le 1-\phi\,, \qquad \frac{E}{E_0} \le \frac{1-\phi}{1+\phi}\,, \qquad \frac{E}{E_0} = (1-\phi)^2\,, \qquad \frac{E}{E_0} = \exp\left(\frac{-2\phi}{1-\phi}\right).$$

The theoretical background and physical details of these predictions can be found in previous papers[20-30].

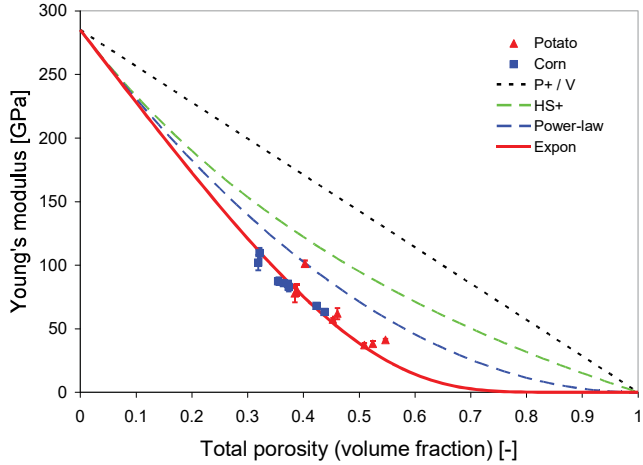

Figure 4: **Young's modulus of porous titania ceramics prepared by starch consolidation casting (SCC) with potato starch (15, 30 and 45 vol.%) and corn starch (15, 24.5, 30, 38, 45 vol.%) versus total porosity (volume fraction for individual specimens), compared to theoretical predictions (upper Paul bound = Voigt bound, upper Hashin-Shtrikman bound, power-law prediction, exponential prediction).**

Figures 5 and 6 show selected SEM micrographs of fracture surfaces of the porous titania ceramics prepared in this work. Apart from the clear differences in porosity and pore size (which are due to the different starch content before firing and the different size of granules of potato starch and corn starch), it is evident that in the case of potato starch the pores are not simple empty voids but are usually filled with fragments of ceramic shells or even hollow spheres that are obviously relics of ceramic powder that was in direct contact with the (gelatinized relics of) starch granules during shrinking together with the ceramic particles that covered their surface. The low-magnification images of Figure 5 shows the overall changes in porosity due to changes in the nominal starch content, while the high-magnification detail micrographs in Figure 6 show the changes in pores size and shape due to the choice of the starch type: the large isolated cavities resulting from the burnout of potato starch and the much smaller interconnected cavities resulting from the burnout of corn starch are compared to the final grain size of the ceramic particles (grains, crystallites). The connectivity of the pore space is determined by a complex interplay of the starch content and the starch type.

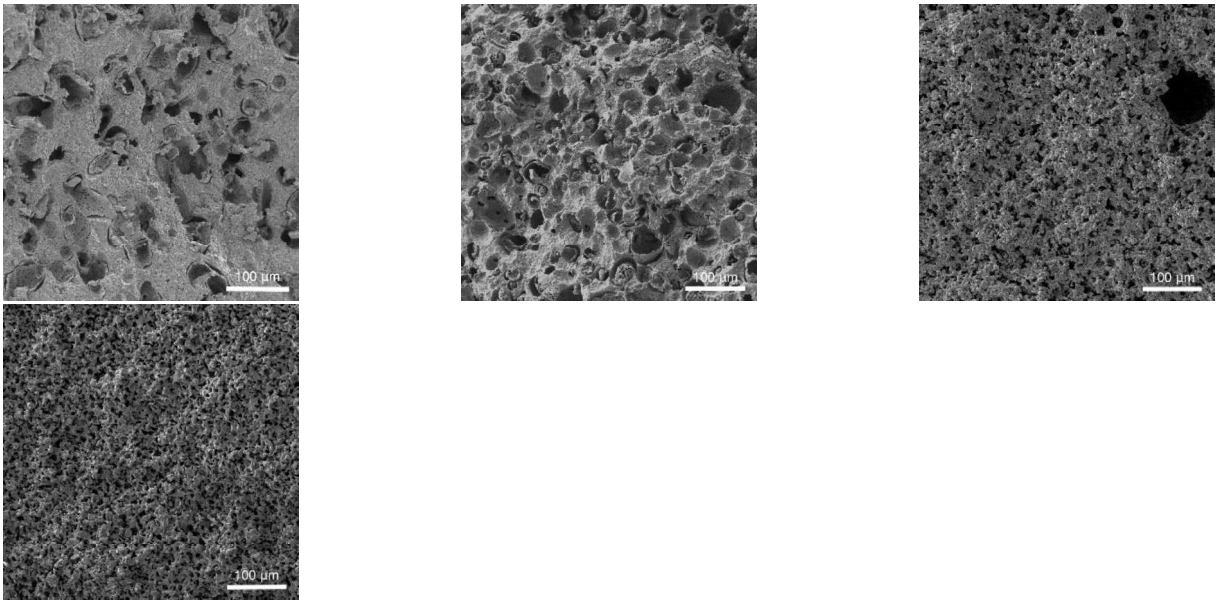

Figure 5: **SEM micrographs of fracture surfaces of porous titania ceramics prepared by starch consolidation casting (SCC) with potato starch (left hand side) and corn starch (right hand side) with nominal starch contents of 15 and 45 vol.%, respectively.**

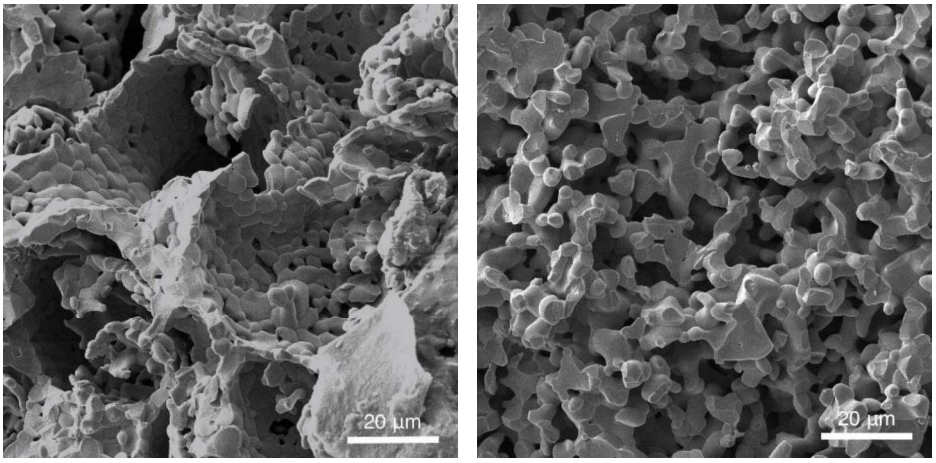

Figure 6: **SEM micrographs of fracture surfaces of porous titania ceramics prepared by starch consolidation casting (SCC) with potato starch (left hand side) and corn starch (right hand side) with a nominal starch content of 45 vol.%.**

Figure 7 shows the temperature dependence of Young's modulus for porous titania ceramics prepared by SCC with 30 % potato starch after sintering at 1300 °C. The heating curve decreases with increasing temperature, with an elastic anomaly between 1000–1200 °C, while the cooling curve shows almost exactly reversible behavior. The origin of the elastic anomaly is not clear but can be related to a residual content of anatase (i.e., the low-temperature polymorph of titania) in the titania ceramics (whose main phase is rutile (i.e., the high-temperature polymorph of titania). When these curves (heating and cooling branches) are normalized with respect to the room temperature value of Young's modulus and fitted in the range from room temperature (RT) up to 1000 °C, the master curve of the temperature dependence of Young's modulus can be obtained in the form of a third-order polynomial as

$$\frac{E(T)}{E_{RT}} = 1 - 0.169 \cdot 10^{-3} T + 0.0267 \cdot 10^{-6} T^2 - 0.00936 \cdot 10^{-9} T^3 .$$

This master curve (with T in °C) is characteristic for all titania ceramics prepared from the anatase powder used in this work and can thus be used to calculate the temperature dependence of Young's modulus for any specimens of arbitrary porosity.

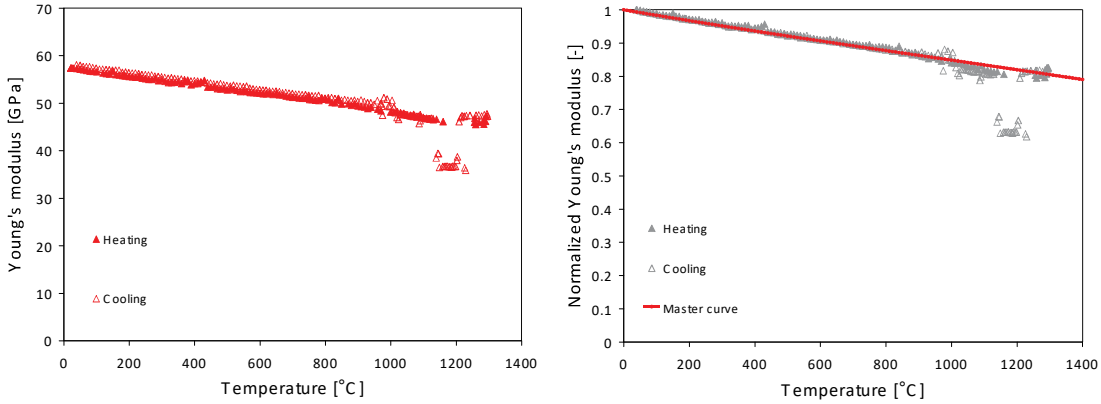

Figure 7: **Temperature dependence of Young's modulus for porous titania ceramics prepared by starch consolidation casting (SCC) with 30 vol.% potato starch (left hand side) and the same dependence for the normalized Young's modulus (normalized to the room temperature value), together with the master curve obtained by fitting this dependence in the range from room temperature to 1000 °C.**

Summary and Conclusion

Starch consolidation casting (SCC) has been used to prepare porous titania ceramics from nanocrystalline anatase powder using potato or corn starch with nominal starch contents in the range 15–45 vol.% (related to the solids in the suspension). After starch burnout and firing at 1300 °C (heating rate 2 °C/min, dwell time 2 h) the firing shrinkage of the ceramics is in the range 15.3–18.0 %, with a total average 17.1 ± 1.2 % (virtually independent of the nominal starch content and the starch type). Open porosities of the porous titania ceramics are in the range 36.4–51.5 % when prepared with potato starch and 31.5–44.8 % when prepared with corn starch, and total porosities are only insignificantly higher, because closed porosities are very low (0–2.8 %). Technologically relevant linear fit relations are given that allow a reasonable control of the total porosity via the nominal starch content, i.e., these fit relations provide the nominal content of potato or corn starch for achieving selected target porosity in the titania ceramics.

The microstructure of the porous titania ceramics has been investigated via scanning electron microscopy (SEM) of fracture surfaces, from which it is evident that the starch content determines the porosity, while the starch type determines pore size and shape and the connectivity of the pore space is determined by a complex interplay of both the amount and the type of starch. The porosity dependence of Young's modulus, determined via the impulse excitation technique (IET) at room temperature, is found to be in good agreement with the exponential prediction. On the other hand, the temperature dependence of Young's modulus, determined via temperature-dependent IET, shows a nonlinear decrease with increasing temperature, for which a third-order polynomial fit has been given for the range from room temperature up to 1000 °C. Therefore, based on the results of this work, it is possible to prepare porous titania ceramics with selected target values of Young's modulus in the range 37–112 GPa at room temperature and to predict their temperature dependence up to 1000 °C.

This work is part of the project "Impulse excitation as an unconventional method for monitoring phase changes and microstructure evolution during thermal loading of materials" (project GA22-25562S), supported by the Czech Science Foundation (GAČR).

REFERENCES

1. Diebold U.: Surf. Sci. Rep. *48*, 53 (2003).
2. Fröhlich K.: Mater. Sci. Semicond. Processing *16*, 1186 (2013).
3. Kim A., Debecker D. P., Devred F., Dubois V., Sanchez C., Sassoye C.: Appl. Catalysis B *220*, 615 (2018).
4. Guo H., Sen T., Zhang J., Wang L.: J. Colloid Interf. Sci. *538*, 248 (2019).
5. Mao H., Zhang F., Du M., Dai L., Qian Y., Pang H.: Ceram. Int. *47*, 25177 (2021).
6. Savage N., Chwieroth B., Ginwalla A., Patton B., Akbar S. A., Dutta P.: Sensors Actuators B *79*, 17 (2001).
7. Miyazaki H., Hyodo T., Shimizu Y., Egashira M.: Sensors Actuators B *108*, 467 (2005).

8. Zhang M., Ning T., Sun P., Zhang D., Yan Y., Li Z.: Sensors Actuators B *268*, 77 (2018).
9. Lyckfeldt O., Ferreira J. M. F.: J. Eur. Ceram. Soc. *18*, 131 (1998).
10. Pabst W., Týnová E., Mikač J., Gregorová E., Havrda J.: J. Mater. Sci. *21*, 1101 (2002).
11. Týnová E., Pabst W., Gregorová E., Havrda J.: Key Eng. Mater. *206-213*, 1969 (2002).
12. Sandoval M. L., Talou M. H., Martinez A. G. T., Camerucci M. A., Gregorová E., Pabst W.: Ceram. Int. *44*, 3893 (2018).
13. Týnová E., Pabst W., Mikač J.: Macromol. Symp. *203*, 295 (2003).
14. Živcová Z., Gregorová E., Pabst W.: Starch / Stärke *62*, 3 (2010).
15. Živcová Z., Gregorová E., Pabst W.: J. Mater. Sci. *42*, 8760 (2007).
16. Gregorová E., Pabst W.: J. Eur. Ceram. Soc. *27*, 669 (2007).
17. Gregorová E., Živcová Z., Pabst W.: Starch / Stärke *61*, 495 (2009).
18. Pabst W., Gregorová E., Sedlářová I., Černý M.: J. Eur. Ceram. Soc. *31*, 2721 (2011).
19. ASTM 1876-01: Standard test method for dynamic Young's modulus, shear modulus, and Poisson's ratio by impulse excitation of vibration, ASTM International, West Conshohocken 2001.
20. Pabst W., Gregorová E., Tichá G., Týnová E.: Ceram. Silik. *48*, 14 (2004).
21. Pabst W., Tichá G., Gregorová E., Týnová E.: Ceram. Silik. *49*, 77 (2005).
22. Živcová Z., Černý M., Pabst W., Gregorová E.: J. Eur. Ceram. Soc. *29*, 2765 (2009).
23. Gregorová E., Pabst W., Nečina V., Uhlířová T., Diblíková P.: J. Eur. Ceram. Soc. *39*, 1893 (2019).
24. Gregorová E., Nečina V., Hříbalová S., Pabst W.: J. Eur. Ceram. Soc. *40*, 2063 (2020).
25. Gregorová E., Semrádová L., Sedlářová I., Nečina V., Hříbalová S., Pabst W.: J. Eur. Ceram. Soc. *41*, 3559 (2021).
26. Pabst W., Uhlířová T., Gregorová E., Wiegmann A.: J. Eur. Ceram. Soc. *38*, 2694 (2018).
27. Uhlířová T., Nečina V., Pabst W.: J. Eur. Ceram. Soc. *38*, 3004 (2018).
28. Pabst W., Uhlířová T., Gregorová E.: Ceram. Int. *44*, 8100 (2018).
29. Pabst W., Uhlířová T.: J. Eur. Ceram. Soc. *41*, 7967 (2021).
30. Uhlířová T., Šimonová P., Pabst W.: J. Eur. Ceram. Soc. *42*, 2946 (2022).
31. Lietavec J.: Mikrostruktura a elastické vlastnosti porézní TiO_2 keramiky připravené částečným slinováním. M.Sc. thesis, UCT Prague 2023.
32. Isaak D. G., Carnes J. D., Anderson O. L., Cynn H.: Phys. Chem. Minerals *26*, 31 (1998).

PHYSICOCHEMICAL AND SENSORY EVALUATION OF CHOCOLATES SUPPLEMENTED WITH MANNANPRO®, A HIGH PURITY POLYSACCHARIDE DERIVED FROM ALOE VERA

VERONIKA KOTRCOVÁ[a*], PRAKASH EKAMBARANELLORE[b], MARCELA SLUKOVÁ[a]

[a]*University of Chemistry and Technology Prague, Department of Carbohydrates and Cereals, Technická 5, 166 28 Praha 6-Dejvice, Czech Republic*
[b]*Dazzeon Biotech Co., Ltd, No.1, 5F-2, Wuquan1st road, Xinzhuang District, New Taipei City, 248624, Taiwan*

veronika.kotrcova@prazskacokolada.cz

Abstract

Acemannan is a polysaccharide isolated from Aloe vera, well known for its immunomodulatory, antiviral, antitumor features, and tissue regeneration effects. Following the traditional method, two bean-to-bar chocolates were prepared with the supplementation of 1 % and 5 % MannanPRO® a high-purity acemannan isolated using a proprietary fractionation technology. The physical and chemical analyses of the chocolates demonstrated an increase in viscosity with particle sizes up to 20 and 60 μm with 1% and 5% supplementation of MannanPRO®, respectively. The addition MannanPRO® also enhanced the antioxidant activity of the chocolates. No significant changes were observed in the profile of volatile compounds and infrared spectroscopy with the addition of MannanPRO®. The aroma and mouthfeel were observed to be excellent for chocolates with 1% supplementation of MannanPRO®, while chocolates with 5% MannanPRO® offered a strong flavour and taste. Further studies on developing functional chocolates with MannanPRO® are underway.

Introduction

Cocoa is obtained from the seeds of Theobroma cacao tree, which is commonly found in tropical regions. These seeds contain a variety of natural compounds, with polyphenols being the most abundant among them. Cocoa has been associated with a wide range of biological benefits, including its potential as antioxidant, antiproliferative, antiapoptotic, anti-inflammatory and anti-cancer properties. Furthermore, cocoa has been investigated in different health conditions, including heart diseases, dyspepsia, nervous system diseases, circulation problems, and many others[1].

Acemannan, β-(1-4)-acetylated polymannose, is a major polysaccharide extracted from aloe vera. Acemannan functions as an immunomodulator and regenerative biomaterial[2]. With unique acetylated mannose molecules, this polysaccharide induces growth factors and synthesis of extracellular matrix, and mineral deposition[3].

Materials and methods

The cocoa beans used are 100% Criollo and come from the Carmelo Farm of Juan Diego Suarez in the Tolima region of Colombia. Acemannan used for these analyses was provided by Dazzeon Health Sciences, Taiwan. Coconut sugar (Indonesia) and cocoa butter (Dominican Republic) were used as the remaining ingredients. The ingredients were mixed following a strict recipe (Table I, Table II). The chocolate stone melangeur was used for preparing of the samples (Premier Lifestyle Chocolate Refiner). Tempering was carried out manually on a marble table, following the chocolate tempering curves (Picture 1). The chocolate was then poured onto stainless steel plates and placed into the cooling conservator for 24 hours. The chocolate plates were manually broken into several pieces. Those well-tempered chocolate with the shiny surface and the smooth breakage were used for the analyses.

Table I: **Ingredients for sample ACE 1**

ACE 1	Content [%]	Content [g]
Cocoa beans	52	520
Coconut sugar	32	320
Cocoa butter	15	150
MannanPRO®	1	10

Table II: **Ingredients for sample ACE 5**

ACE 5	Content [%]	Content [g]
Cocoa beans	52	520
Coconut sugar	28	280
Cocoa butter	15	150
MannanPRO®	5	50

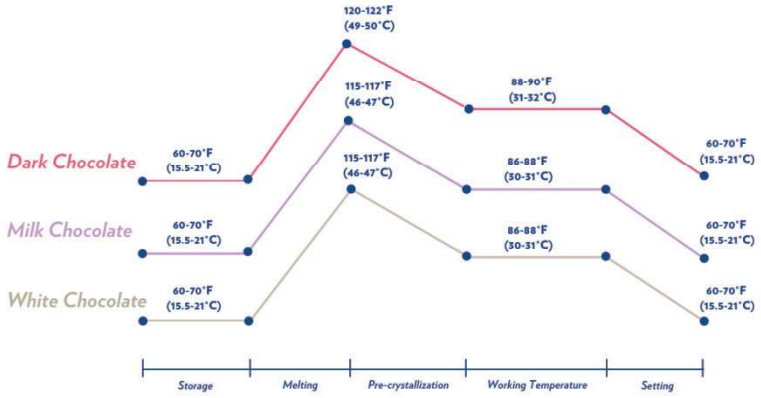

Picture 1: Tempering seeding method[4]

Particle size

For each sample, three replicates were performed, and each replicate was measured five times. A quantity of 2 g of each chocolate sample was mixed in 30 ml of isopropanol. The mixture was then vortexed for 3 minutes. Background noise measurements were taken before measuring each sample. The program in Table 3 was applied:

Table III: **Program for measuring of particle size.**

Analysis model	General purpose
Broadcast model	Mie
Dispersant used	Propan-2-ol
Dispersant refractive index	1.390
Particle refraction index	1.590
Particle absorption index	0.010

Viscosity

The study of viscosity was carried out to determine the rheological properties of different chocolate samples. Both samples were placed into an oven at 50 °C for 24 hours. Viscosity was measured using a HAAKE Viscotester iG rotary rheometer. Measurements were carried out in a coaxial cylinder arrangement at 40 °C. A sufficient quantity of chocolate (15 g) was placed in the preheated stator so that the rotor was fully immersed. The rotor was attached to the viscometer.

The viscosity program follows:

- *heat the sample to 40 °C for 5 minutes*
- *shear rates increase from 0 to 5 s^{-1} in 1 minute*
- *endurance at a given shear rate of 5 s^{-1} for 4 minutes*
- *shear rate increase from 5 to 60 s^{-1} in 3 minutes*
- *endurance at a given shear rate of 60 s^{-1} for 30 seconds*
- *decrease shear rate from 60 to 5 s^{-1} in 3 minutes*
- *decrease shear rate from 5 to 0 s^{-1} in 30 seconds*

To determine the flow behaviour and stress of non-Newtonian fluids, the Casson model was run. The ascending and descending branches of the flow curve were always measured. The results are expressed in terms of Casson dynamic viscosity (η_{CA}) and Casson yield stress (τ_{CA}). Casson's model was chosen for the calculation of the results, the equation can be written in the following mathematical relation:

$\sqrt{\tau} = \sqrt{\tau_0} + \sqrt{(\eta_C \cdot \dot{\gamma})}$, τ … shear stress [Pa], τ_0 … flow limit [Pa], η_C … Casson viscosity [Pa.s], $\dot{\gamma}$ … shear rate [s^{-1}]

Antioxidant activity

To determine the antioxidant activity of the samples, the TEAC (Trolox equivalent antioxidant capacity) method with DPPH was carried out. DPPH (2,2-diphenyl-1-picrylhydrazyl) is a stable, purple-coloured radical with an absorbance maximum at 517nm, absorbance was read at this wavelength. Antioxidant compounds are able to transfer an electron, causing the solution to change colour from purple to yellow.

For each sample, three replicates were performed.

A calibration curve was first prepared using a Trolox standard (3,4-dihydro- 6-hydroxy2,5,7,8-tetramethyl-2H-1-benzopyran-2-carboxylic acid). By successive dilution, concentrations of 20, 40, 80, 120 and 160 mg/l were prepared. As with the samples, absorbance at 517nm was measured for each concentration, and 3 measurements were taken for each concentration.

Sensory evaluation

Judges were given two unknown samples of chocolates. The samples were at the same temperature, the evaluators tested the samples in random order. Water and bread were used to neutralize the flavours between the tested samples. Coffee beans were used to neutralize the aroma.

Volatile substances

For the analysis of chocolate samples was used mass spectrometer ISQ (Thermo Scientific).

Table IV: **Conditions for determination of volatile substances**

MS	
Electron ionization:	EI +70 eV
Temperature:	230 °C
Scanning range:	29 – 450 Da
Scan speed:	4 scans per second

SPME:	
HS vial:	20 ml
Sample weight:	2.1 g ± 1 mg
SPME filament:	50/30μmDVB/CAR/PDMS (Divinylbenzen/ Carboxen/ Polydimethylsiloxane)
Extraction to SPME filament:	30 min, 60 °C

GC:	
Instrument:	TRACE GC ULTRA (Thermo Scientific)
Column:	DB-5MS UI (60 m x 0.32 mm, film 1.0 μm)
Injection:	250 ºC – split 1:20
Carrier gas:	helium 6.0
Constant flow rate:	1.5 ml/min
Temperature program:	40 ºC (5 min) –> 15 ºC/min –> 290 ºC (5 min)

Results and Discussion

Particle size

The key finding from the data obtained is that both chocolate samples contain a comparable quantity of particles measuring up to 3 μm in size and a similar number of particles up to 8 μm in size. These results indicate that both chocolates were crafted with great precision. Notably, the most significant distinction lies in the presence of the largest particles. In the case of chocolate containing 1% MannanPRO® (referred to as ACE 1 in this study), these large particles measure around 20 μm, while in the chocolate with 5% MannanPRO® (referred to as ACE 5), these particles can reach up to approximately 50 μm. This suggests that achieving perfect homogenization of acemannan in a melangeur is more challenging at higher MannanPro® concentrations. Interestingly, this variability

in particle size was not mentioned by the evaluators during the sensory analysis, and they rated the chocolate as of very high quality.

Viscosity

The viscosity comparison results clearly indicate that the presence of MannanPRO® has a substantial impact on the chocolate's fluidity and its flow limit. Specifically, for the ACE 1 sample, the viscosity is approximately only 0.67 times that of the ACE 5 sample.

When incorporating up to 5 % MannanPRO® into the recipe, it can significantly influence the technological processing of the product. To address this, it might be necessary to make adjustments to the formula by including additional ingredients such as cocoa butter or lecithin.

Antioxidant activity

The assessment of the antioxidant activity in chocolate samples containing 1 % and 5 % MannanPRO® revealed intriguing results. The measurements indicated that the antioxidant activity increased when 5 % of MannanPRO® was added. This finding is noteworthy because chocolate typically possesses a naturally high level of antioxidant activity, and when additional ingredients are introduced, it usually experiences a decline in this property.

Table V: **Antioxidant activity of ACE 1 and ACE 5**

	Antioxidant activity (mg equivalent of ascorbic acid/100 g of sample)*	Average	Inhibition of DPPH (%)*	Average
ACE 1_1	741	772	60.8	63.4
ACE 1_2	818		67.3	
ACE 1_3	757		62.2	
ACE 5_1	802	796	66.0	65.5
ACE 5_2	750		61.6	
ACE 5_3	836		68.8	

* Uncertainty of the measurement: 10 %

Sensory evaluation

The chocolate with 5 % MannanPRO® received significantly higher ratings, with 89 % of evaluators preferring ACE 5 over ACE 1. The acidic and fruity taste of the final chocolate was particularly well-received. The balance of sweetness was also highly rated. In contrast, for the ACE 1 sample, evaluators noted a slightly bitter and astringent aftertaste, but no unpleasant or foreign flavours were detected in either sample.

The mouthfeel of both samples was evaluated similarly, with ACE 1 being described as smoother. However, the aroma was better rated for ACE 1 chocolate. This difference in aroma perception is attributed to ACE 5 having a stronger and more pronounced flavour, which had a more significant impact on the taste and olfactory experience. Generally, evaluation for both chocolates – rich aroma, followed by a sweet red-black berry, coffee and tobacco leaf flavour note, the richness and bitterness of the dark chocolate have been very well balanced by the use of coconut sugar.

Table VI: **Sensory evaluation of ACE 1 and ACE 5 samples**

Chocolate with 1 % of MannanPRO®	Chocolate with 5 % of MannanPRO®
➢ Dark shiny bar with a good snap, which has initial bitter taste and complex palette of taste of red fruits. The judges felt the high astringency aftertaste that may have been slightly overshadowed by the fruitiness in the	➢ A dark bar that has an initial quite strange earthy flavour that gives way to a rich fruitiness. The taste is strong, fruity and the judges did glean some cherry notes on the palate.

second sample ACE 5. This astringency increased towards the end. ➢ The flavour is well balanced and not too sweet, and the alternative ingredients do work, and give an overall good flavour with good cocoa notes and a full taste.	➢ Good looking bar with an impressive shine and moderate snap. The melt is smooth and creamy, and the judges enjoyed the notes of richness from the beans. The great fruitiness of the taste stands out, which is probably due to the greater amount of added MannanPRO®.

Volatile substances

Based on the analysis of aromatic volatiles, it was determined that the aroma profiles of both chocolates are quite similar. The most prominent compound in both is acetic acid. The significant difference observed lies in the butanediol content, which is higher in ACE 5.

It is worth noting that while the chocolates may have slightly different smells, their mass spectrometry results are the same. This variation in aroma could be attributed to the presence of different isomers (R/S) of certain compounds. One isomer may have an unpleasant odour, while the other might have a pleasant or neutral scent. Unfortunately, the device used for analysis cannot distinguish between these isomers. This fact underscores the importance of sensory evaluation by human evaluators in such cases.

Table VII: **Retention time of volatile substances and their names**

Retention time [min]	Chemical compound
4.68	ethanol
5.37	acetone
5.64	formic acid
7.72	acetic acid
9.37	isovaleraldehyde
10.49	acetoin
11.07	isobutyric acid
11.85	2,3-butanediol
12.59	isovaleric acid
12.75	2-methylbutyric acid
15.34	trimethylpyrazine
15.79	d-limonene
16.35	tetramethylpyrazine
16.60	$C_{10}H_{18}0$
17.20	pyranone
18.28	phenylethyl acetate

Infrared spectroscopy

There are no significant differences between spectra of chocolates with 1 % and 5 % content of MannanPRO®.

Conclusion

In conclusion, the incorporation of MannanPRO® a high purity acemannan into new functional chocolates presents a promising avenue for enhancing their health benefits. Chocolate, already known for its pleasurable taste, has demonstrated numerous positive impacts on health, including heightened antioxidant activity. The addition of acemannan, a compound derived from aloe vera, offers an exciting opportunity to further augment these sensory and health-promoting properties. The combination of chocolate's inherent properties and acemannan's potential health benefits may result in a novel and synergistic way to support overall well-being. Further research and clinical

studies warrant to fully explore and validate the potential health benefits of acemannan-infused chocolates, while the preliminary findings suggest a promising future for this innovative fusion of taste and health.

REFERENCES

1. Smith, D. F. Benefits of flavanol-rich cocoa-derived products for mental well-being: A review. Journal of functional foods 2013, (5), 10–15.
2. Thant, A. A., et al. Characterization of a bioscaffold containing polysaccharide acemannan and native collagen for pulp tissue regeneration. Int. J. Biol. Macromol. 2023, (225), 286–297.
3. S. Songsiripradubboon, S. Kladkaew, C. Trairatvorakul, P. Sangvanich, K. Soontornvipart, W. Banlunara, et al., Stimulation of dentin regeneration by using acemannan in teeth with lipopolysaccharide-induced pulp inflammation, J. Endod. 43 (7) (2017) 1097–1103.
4. Tempering seeding method. Guittard chocolate company. https://www.guittard.com/in-the-kitchen/article/science-of-chocolate (accessed Sept 14, 2023).

DEVELOPMENT OF CHITOSAN FILMS FROM EDIBLE LESSER MEALWORMS (*Alphitobius diaperinus*)

ALI KOZLU[a], ABDUL MUIZ[a], NUJAMEE NGASAKUL[a], IVETA KLOJDOVÁ[a], ANNA MASCELLANI[b], JAROSLAV HAVLIK[b], DIANA KARINA BAIGTS-ALLENDE[a*]

[a]DRIFT-FOOD Center, Faculty of Agrobiology, Food and Natural Resources, Czech University of Life Sciences Prague, Prague 16500, Czech Republic
[b]Department of Food Science, Faculty of Agrobiology, Food and Natural Resources, Czech University of Life Sciences Prague, Kamycka 129, 165 00 Prague 6 – Suchdol,
Czech Republic

kozlu@af.czu.cz, muiz@af.czu.cz, ngasakul@af.czu.cz, klojdova@af.czu.cz, mascellani@af.czu.cz, havlik@af.czu.cz, baigts_allende@af.czu.cz[*]

Abstract

Chitin is one of the most abundant biopolymers present mainly in crustaceans (shells) and arthropods (exoskeletons) with a similar structure to vegetable fiber (cellulose). Chitosan, the deacylated derivative of chitin, is appreciated in different sectors (medical, pharmaceutical, packing) because of its biodegradability, non-toxicity, antimicrobial and mechanical properties. In this study, chitin from lesser mealworms (*Alphitobius diaperinus*) was obtained to produce chitosan. Chitosan's degree of deacetylation was determined by the Nuclear Magnetic Resonance (NMR) technique and was used for edible film production. The mechanical properties and color of chitosan films were evaluated and compared with commercial chitosan films (from crustaceans). Our results showed that edible lesser mealworms are a potential source of good-quality chitosan.

Introduction

The consumption of edible insects, known as entomophagy, has been a part of the dietary habits of various cultures worldwide through the years. Edible insects in Western countries are gaining attention due to their nutritional composition, sustainability, and reduced environmental impact compared to traditional livestock [1, 2]. However, from the safety point of view, just some edible insect species have been approved by EFSA, which is the case of the lesser mealworm (*Alphitobius diaperinus)*, recently authorized as novel food either frozen, dried, and or as powder form [3]. Edible insects are a valuable nutritional food source regarding high content and quality protein with a well-balanced profile of essential amino acids, essential fatty acids including omega 6 and 9, and micronutrients (mainly vitamins) [4, 5]. Edible insects have considerable insoluble fiber in their composition, present as chitin in their exoskeleton. Chitin is a complex polysaccharide commonly found in nature, particularly in crustaceans, fungal cell walls, and insect cuticles. It has been reported that chitin may benefit the immune system by providing prebiotic properties to the gut flora and slowing down the growth of some potentially pathogenic microorganisms [6, 7]. Chitin is a long-chain polymer made of N-acetylglucosamine units, while chitosan is a derivative of chitin [8]. Chitosan is produced by deacetylating chitin, which partially removes some acetyl groups from the chitin molecule. The degree of deacetylation depends mainly on the conditions used during the procedure and is commonly used to determine the type of polymer, chitosan, requiring a degree of deacetylation higher than 50% [9]. Therefore, this parameter directly affects this polymer's properties in many applications, including biological, physical, chemical, and mechanical properties. Chitosan has great potential for use as active films with potential applications as food packaging due to its antimicrobial, antioxidant, nontoxic, biocompatible, biodegradable, and edible properties in the food industry [10].

In this study, we obtained chitin from the larval exoskeleton of *A. diaperinus*; the deacetylation step was applied to obtain chitosan. The degree of deacetylation was evaluated by NMR, and edible films were prepared. The developed edible films were characterized by color and mechanical properties (texture) and compared to standard samples (commercial).

Materials and methods

Materials

The lesser mealworms (*Alphitobius diaperinus*) were purchased from a local insect-rearing farm (PAPEK, Prague, Czechia). This study used residues of processed lesser mealworm (other proposes) to extract chitin. All chemicals used in experiments were reagent grade. Sodium hydroxide and hydrochloric acid (≥98%) were supplied by Lachner (Hungary). Commercial chitosan (≥75% of deacetylation degree), glycerol, and acetic acid were purchased from Sigma-Aldrich (Germany) and VWR Chemicals (Belgium).

Methods

The extraction process of chitosan

The extraction process of chitosan includes three main steps (demineralization, deproteinization, and deacetylation). Chitosan extraction was carried out according to [11]. Sodium hydroxide and hydrochloric acid solutions eliminated protein and minerals, respectively. In the case of deacetylation, NaOH (high molarity) solutions and temperature control were applied. Lastly, chitosan was washed using distilled water until neutral and air-dried overnight at 45 °C.

The degree of deacetylation (DD) by NMR

The degree of deacetylation (DD) was calculated using proton nuclear magnetic resonance spectroscopy (^{1}H NMR), according to [12]. Five milligrams of dry chitosan were briefly solubilized with 0.5 mL of 2% DCl solution in D_2O and heated at 70 °C for 1.5 h. The solution was transferred to a 5 mm NMR tube. ^{1}H NMR spectra were acquired on a Bruker Avance III spectrometer equipped with a broadband fluorine observation SmartProbeTM with z-axis gradients (Bruker BioSpin GmbH, Rheinstetten, Germany) operating at a proton NMR frequency of 500.18 MHz. The temperature was set to 298 K (25 °C). Acquisition time (AQ) and relaxation delay (D1) were set at 1 and 12 s, respectively. When 90° pulses were used, 128 scans were acquired. DD values were determined from the relative integrals of acetyl (N-acetyl and AcOH) and combined H2-H6 protons. Integration was based on 1.7–2.4 and 2.7–4.4 ppm intervals.

Edible Film Preparation

The production of chitosan-based edible films was carried out using the method described by [13] with some modifications. Chitosan edible films were prepared by dissolving 0.5 % w/v of chitosan in a stirred mixture of 1 % (v/v) acetic acid aqueous solution containing 1 % w/v glycerol as a plasticizer on the magnetic stirrer. These solutions were cast on plastic petri dishes and dried at room temperature (25 °C) for 48 h in an incubator. The dried films obtained were stored at 25 °C and, after that, analysed for color and mechanical properties (texture).

Color measurement

Color values of samples were determined by a colorimeter (Konica Minolta CM700d, Japan). The CIE Lab scale was used, and lightness (L*) and chromaticity parameters (a* and b*) were measured. L* values range from 0 (black) to 100 (white); a* values range from −80 (greenness) to 100 (redness); and b* values range from −80 (blueness) to 70 (yellowness). Chroma (C) and Hue angle (h°) were calculated using the following equations (Eqs. (1), (2))

$$C = \sqrt{a^2 + b^2} \quad (1)$$

$$h° = \tan^{-1}\left(\frac{b}{a}\right) \quad (2)$$

Mechanical properties

The film's strength was measured using a texture analyser with a load cell of 50 N (EZ-SX, Shimadzu, Japan) and a puncture probe of 2 mm in diameter. The film sample was placed on a circular holder (r=2 cm), and the probe was driven (speed was 1.0 mm/sec) through the film until it punctured. The force (N) at the point of rupture was recorded as maximum strength.

Results and discussion

Chitosan characterization

Deacetylation degree

According to Table I, the degree of deacetylation obtained for edible insect chitosan obtained from lesser mealworms was 69.29%, slightly lower than the commercial chitosan (shrimp source) 74.45% analysed as a reference.

Chitosan color

Table I shows that commercial chitosan samples demonstrated higher L*, C, and h°values than insect-based chitosan samples (Fig 1). Color values of chitosan polymer may change depending on the source type and the procedure for its obtaining. The differences between color values may also be related to the fact that the decolorization process was not performed, and the natural color of the insect is brown.

Chitosan films characterization

Films color

It was observed that insect-based edible films exhibited lower L*values (82.04 ± 0.03) than commercial chitosan films (87.37 ± 0.05) (Fig 2). Likewise, C and h° values for insect-based edible films (2.38 ± 0.05 and 76.31± 0.05, respectively) were lower than commercial chitosan films (4.96 ± 0.02 and 88.38 ± 0.09, respectively). Differences in strength values could be attributed to the different nature and characteristics of sources used and the treatments applied.

Films strength

Insect-based edible films demonstrated a lower strength than control samples (0,21 ± 0,02 and 0,30 ± 0,02 N, respectively). These differences might be mainly related to the degree of deacetylation of the samples.

The product obtained in the present study can be considered chitosan since the average value of the degree of deacetylation is greater than 50%. This data indicated that lesser mealworm residues could be an alternative and promising source for chitosan production with desirable bioplastic properties. However, improvement in deacetylation processing could enhance the insect chitosan properties.

Figure 1: **Chitosan samples (A: Insect-based chitosan, B: Commercial chitosan)**

Figure 2: **Chitosan-based edible films (A: Insect-based chitosan films, B: Control chitosan films)**

Table I: **Color and degree of deacetylation of insect-based chitosan and commercial chitosan.**

	Insect based chitosan	**Commercial chitosan**
L*	62.32 ± 0.02	89.87 ± 0.02
C	14.50 ± 0.06	15.25 ± 0.00
h°	74.82 ± 0.06	87.11 ± 0.09
NMR (Degree of Deacetylation)	69.29 ± 3.01	74.45 ± 0.16

Acknowledgement: This research was funded by European Union's Horizon 2020 Research and Innovation Program under grant agreement No 952594 (ERA Chair project DRIFT-FOOD).

REFERENCES

1. Baigts-Allend D. K., & Stathopoulos C.: Eur. Food Res. Technol., *249*, 849-860. (2023).
2. Hartmann C., Shi J., Giusto A., & Siegrist M.: Food Qual. Prefer., *44*, 148-156. (2015).
3. Puteri B., Jahnke B., & Zander K.: Appetite, 106594. (2023)
4. Van Huis A.: J. Insects as Food Feed., *6*, 27-44. (2020).
5. Bessa L. W., Pieterse E., Sigge G., & Hoffman L. C.: J. Sci. Food Agric., *100*, 5017-5022. (2020).
6. da Silva Lucas A. J., Oreste E. Q., Costa H. L. G., López H. M., Saad C. D. M., & Prentice, C.: Food Chem., *343*, 128550. (2021).
7. Lopez-Santamarina A, Mondragon A. D. C., Lamas A., Miranda J. M., Franco C. M., & Cepeda A.: Foods, *9*, 782. (2020).
8. Van Huis, A., Rumpold, B., Maya, C., & Roos, N.: Annu. Rev. Nutr, *41*, 551-576. (2021)
9. El Knidri H., Belaabed R., Addaou A., Laajeb A., & Lahsini A.: Int. J. Biol. Macromol., *120*, 1181-1189. (2018).
10. Bakshi P. S., Selvakumar D., Kadirvelu K. & Kumar N. S.: Int. J. Biol. Macromol., *150*, 1072-1083. (2020).
11. Baigts-Allend D. K., Alva A. P., Haro M. S., Martínez A. S., & Ojeda J. M.: INNOTEC, (19 ene-jun), 97-108. (2020).
12. Fernandez-Megia E., Novoa-Carballal R., Quiñoá E., & Riguera R.: Carbohydr. Polym., *61*, 155-161. (2005).
13. Chen S, Wei X, Sui Z, Guo M, Geng J, Xiao J, Huang D.: Insects, *12*, 53. (2021)

THE QUALITY OF VEGAN FERMENTED PLANT BASED BEARAGES STABILIZED BY CITRUS PECTIN

PATRYCJA JANKOWSKA[a], JACEK LEWANDOWICZ[b], HANNA MARIA BARANOWSKA[c], JOANNA LE THANH-BLICHARZ[a*]

[a]Department of Food Concentrates and Starch Products, Prof. Wacław Dąbrowski Institute of Agriculture and Food Biotechnology—State Research Institute, 40 Starołęcka Street, 61-361 Poznań, Poland
[b]Institute of Logistics, Poznań University of Technology, 2 Jacka Rychlewskiego Street, 60-965 Poznan, Poland
[c]Department of Physics and Biophysics, Poznan University of Life Sciences, 60-637 Poznań, Wojska Polskiego Str. 38/42

joanna.lethanh-blicharz@ibprs.pl

Abstract

The aim of the work was to evaluate the quality of vegan alternatives to yoghurts produced with assistance of citrus pectin. Five different commercial plant-based beverages manufactured form oat, soy, rice, coconut, and almonds, were used for production of working material. Cow milk with 3.2% fat content was used as reference. Yoghurts were evaluated in terms of their rheological properties, molecular properties, texture, color, acidity, and stability.

Introduction

Yoghurt according to Codex Alimentarius is a milk product obtained by fermentation of milk using suitable microorganisms that results in reduction of pH and coagulation[1]. A plant-based lifestyle is becoming increasingly popular, and people are more often looking for plant-based alternatives to animal based products[2]. Global market of vegan alternatives to yoghurt was estimated at over 2 billion dollars in 2020 and forecasted to grow with compound annual growth rate of 18.9% up to 2027[3]. Moreover almost 200 new vegan alternatives to yoghurt were launched in the EU market only in 2020[4].

The production process of vegan alternatives to yoghurt is quite similar to natural yoghurt. However instead of milk, aqueous extracts from different plant materials are used, also known as plant based bevarages[5]. Among major challenges associated with production of vegan alternatives to yoghurt, are poor appearance and texture that is result of phase separation[6]. This phenomenon is almost identical, but less evident as in case of common yoghurts. Nevertheless, yoghurts are thermodynamically unstable two-phase systems that are classified as oil in water emulsions[7]. Moreover, during fermentation thixotropic gel structure is formed[8,9]. For the above reason different hydrocolloids are used to improve stability and thus quality of fermented milk products[10,11].

The aim of the work was to evaluate quality of vegan alternatives to yoghurt stabilized by citrus pectin, produced form different plant-based beverages.

Materials and methods

The experimental material consisted of five natural yoghurts varying in plan beverage used for their production. Commercial plant-based beverages sold under band name Inka (Grana sp. z o.o., Skawina, Poland) manufactured form oat, soy, rice, coconut, and almonds were used. Cow milk with 3.2% fat content was used as reference (SM "Mlekpol," Grajewo, Poland). Vivo vegan yoghurt starter culture was used for fermentation (Gama-Tech, Warszawa, Poland). All reagents used were of analytical grade.

Yoghurts were prepared in 160 cm3 portions with 1% addiction of citrus pectin. Fermentation was performed using yoghurt maker JG3523 (Severin Elektrogeräte GmbH) for 12 hours. After the fermentation yoghurts were matured for 24 hours at temperature of 4±2°C.

Syneresis was determined by centrifugation. Yoghurt samples of roughly 10 cm3 were placed into 15 cm^3 scaled test tubes and centrifuged with acceleration of 250 x g for 30 minutes. Synereis was calculated in percent according to volume of separated whey in reference to the whole sample.

Titratable acidity was determined by neutralization of accurately weighted 25 g yoghurt sample using 0.25 mol/dm3 sodium hydroxide solution using phenolphthalein as indicator. Obtained results were expressed as Soxhlet-Henkel degrees (°SH) as well as lactic acid content using conversion ratio of 1°SH = 0.0225% of lactic acid[12].

Universal texture profile (Texture Profile Analysis) of yoghurts was determined with a TA-XT2 texturometer (Stable Micro Systems, England). A "double bite test" was performed with a 35 mm aluminium cylindrical probe on a depth of 20 mm with a speed of 0.5 mm/s. Hardness (N), adhesiveness (N·s), cohesiveness, springiness, and gumminess (N) were determined.

Rheological properties of yoghurts were determined using RotoVisco1 rheometer (Haake Technik GmbH, Germany) before the measurement samples were rested in the measuring cylinder for 5 min. Measurements were performed using Z20 DIN Ti coaxial measurement system within 0.05-600 s^{-1} shear rate. Obtained flow curves were fitted to the Ostwald de Waele model. Data collection and calculations were made using RheoWin 3.61 software.

Results and discussion

One of the key quality factors of fermented products is their acidity. Titrable acidity and pH of investigated fermented plant-based beverages is presented in Table I. All of investigated products did not reach recommended acidity levels published within Codex Alimentarius[1]. Moreover, the acidity did not correlate with carbohydrate content of investigated plant beverages, which was 0.1, 2.6, 7.6 and 11.0 for almond, both soy and coconut, oat, and rice, respectively. Considering low amount of carbohydrates and relatively high acidity of soy and coconut beverages, they seem to be the best matrix for preparation of fermented drinks. On the other hand, the pH values were comparable to fermented milk drinks with fruit extracts[13].

Syneresis values ranged between 2 and 52% and were comparable to natural yoghurts produced form cow milk, but with varying fat content. Lewandowicz[14] found that yoghurt produced from fully skimmed milk gave product with highest syneresis of above 50%, while form semi skimmed milk the syneresis was of around 25%, whereas products with full fat milk resulted in syneresis below 10%. Moreover, commercially produced yoghurts are characterized by syneresis below 10%[12]. In view of that, only the coconut-based beverage met the market requirements. When considering the use of other plant beverages, one should consider addition of other hydrocolloids (apart from pectin) to improve the fermented beverage stability.

Table I: **Physicochemical properties of vegan yoghurts**

Plant beverage	Titratable acidity °SH	Lactic acid g·100 g^{-1}	pH	Syneresis %
Oat	3.1	0.07	5.21	46
Rice	0.4	0.01	5.53	52
Coconut	4.4	0.10	4.44	5
Soy	7.1	0.16	5.49	26
Almond	0.9	0.02	5.47	25
Reference	9.8	0.22	5.58	2

The variability of color of investigated plant-based beverages was relatively low (Table II). This is especially evident when considering lightness parameter (L) and a parameter, which corresponds to greenish hue (as samples adopted negative a value). Higher variability was observed for b parameter, in case of which a shift in both direction of the color axis was observed, when compared to reference sample. All vegan beverages were almost 10% darker than reference natural yoghurt and slightly less green with shift in a parameter below 3 units. Oat and soy based fermented beverages were significantly more yellow, whereas rice, coconut and almond based were less yellow than reference sample. The above observations are reflected in the most important color benchmark for yoghurt i.e., whiteness index (WI), indicating the perception of how white the product is. Coconut based beverage had the highest WI among vegan beverages, what was the result of relatively high L and low b value of parameter. Rice

and almond beverages gave similar, but slightly worse color characteristics. Whereas oat and soy-based beverages were significantly more yellow, thus contributing to low WI.

Table II: **Color parameters of vegan yoghurts**

Plant beverage	L	a	b	Whiteness index %
Oat	77.05	-3.77	15.45	72.08
Rice	77.34	-2.21	7.85	75.92
Coconut	78.31	-2.82	4.06	77.76
Soy	77.94	-2.87	16.56	72.27
Almond	77.54	-2.55	6.36	76.52
Reference	86.31	-4.70	10.30	82.24

Table III includes considered universal texture profile (TPA) parameters of plant-based beverages. The investigated products varied mostly between hardness, adhesiveness, and gumminess. This type of TPA characteristics is common for semi-solid food products. It should be also noted that gumminess is a secondary TPA parameter, which is a product of hardness and cohesiveness. Therefore, the observed differences in gumminess are mostly influenced by hardness. The reference sample had quite stiff (high hardness), but smooth texture (low adhesiveness). Similar texture profile was observed in case of soy-based plant beverage, however it had more undesired adhesive properties. This product was followed by coconut and almond ones, which had lower hardness, but more comparable adhesiveness to reference sample. Rice based beverage had almost liquid like texture with lowest hardness, highest cohesiveness, springiness equal to unity, and lack of adhesiveness. Oat based beverage had significantly different TPA profile from other products. Moreover, with rather undesired properties with relatively low hardness, cohesiveness, springiness, and gumminess, but high adhesiveness.

Table III: **Universal texture profile of vegan yoghurts**

Plant beverage	Hardness N	Adhesiveness N·s	Cohesiveness -	Springiness -	Gumminess N
Oat	0.44	0.23	0.64	0.93	0.28
Rice	0.43	0.00	0.76	1.00	0.33
Coconut	0.50	0.17	0.74	0.97	0.37
Soy	0.62	0.31	0.68	0.95	0.42
Almond	0.47	0.14	0.67	0.95	0.31
Reference	0.65	0.16	0.69	0.96	0.45

Parameters of Ostwald de Waele model that indicate rheological properties of investigated vegan beverages are listed in Table IV. The rheological study was in accordance with results obtained during TPA. The highest consistency index (K) was recorded for soy, coconut, and reference sample, respectively. Whereas almond rice and oat-based beverages had K value below 2. The highest value of flow behavior index n (indicating how similar to Newtonian fluid the product is), was calculated for coconut, almond and reference sample. Taking into consideration relatively high K and n value of coconut beverage, it had the most desired rheological properties. Moreover, this product was similar in terms of its rheological properties to reference sample. At the same time coconut-based beverage had the lowest thixotropy value (indicating good rheological stability).

Table IV: **Ostwald de Waele model parameters of vegan yoghurts**

Plant beverage	K $Pa \cdot s^n$	n -	Thixotropy $Pa \cdot s^{-1}$
Oat	1.32	0.410	1158
Rice	1.57	0.377	682
Coconut	2.47	0.416	-121

Soy	3.73	0.380	2336
Almond	1.78	0.415	1345
Reference	2.38	0.412	2391

Conclusions

Yogurts are one of the most popular foods eaten all over the world. Due to the increasing demand for milk alternatives, plant-based beverages have been widely introduced to the market in recent years. Moreover, there is growing interest in fermented plant-based beverages that aim to substitute natural yoghurts. To improve the quality of those products, different hydrocolloids can be added, including pectin. A comprehensive assessment of the quality of fermented plant beverages manufactured form different plant sources was made in terms of their physicochemical features such as: acidity, pH, syneresis, color, texture, and rheological properties. It was stated that with the assistance of citrus pectin, plant-based beverages are suitable base for production of "yoghurt" like products. Obtained fermented beverages were slightly: less acidic, darker, weaker in term of texture and rheological properties and had higher syneresis. The most similar product in terms of all investigated physicochemical properties to the reference sample that was prepared from full fat cow milk, was obtained based on coconut plant-based beverage.

REFERENCES

1. FAO/WHO: Standard for fermented milks, CXS 243-2003, 2023.
2. Fehér A., Gazdecki M., Véha M., Szakály M., Szakály Z.: Sustainability *12*, 4136 (2020).
3. Grand View Research: Vegan Yogurt Market 2020–2027. Available online: https://www.grandviewresearch.com/industry-analysis/vegan-yogurt-market.
4. Boukid F., Lamri M., Dar B.N., Garron M., Castellari M.: Foods *10*, 2782 (2021).
5. Brückner-Gühmann M., Benthin A., Drusch S.: Food Hydrocoll. *86*, 146 (2019).
6. Grasso N., Alonso-Miravalles, L.; O'Mahony J.A.: Foods *9*, 252 (2020).
7. Lewandowicz J., Le Thanh-Blicharz J., Śmigielska H., in: *Current Trends in Quality Science - quality design of food products*, p. 78. Instytut Technologii i Eksploatacji – PIB, Poland, 2019.
8. Dołhańczuk-Śródka A., Nabrdalik M., Maślak N., Wąsiewicz N., Ziembik Z.: Proc. ECOpole *9*, 193 (2015).
9. Plaskota D.: Zywn-nauk. Technol. Ja. *12*, 88 (2004).
10. Szwedziak K., Antczak, D.: Postępy Techniki Przetwórstwa Spożywczego *1*, 19 (2016).
11. Nastaj M., Gustaw W.: Zywn-nauk. Technol. Ja. *13*, 217 (2005).
12. Wichrowska D., Wojdyła T.: Inż. Ap. Chem. *53*, 421 (2014).
13. Papademas P., Ioannou I., Aspri M.: Appl. Sci. *13*, 9243 (2023).
14. Lewandowicz J., in: *Current Trends in Quality Science - design, quality and safety of products*, p. 231. Instytut Technologii i Eksploatacji – PIB, Poland, 2022.

ZETA POTENTIAL & DYNAMIC LIGHT SCATTERING MEASUREMENTS – A NEW TOOL FOR POLYSACCHARIDES STUDIES

GRAŻYNA LEWANDOWICZ[a*], KRZYSZTOF DWIECKI[b]

[a]*Department of Biotechnology and Food Microbiology, Poznan University of Life Sciences, 60-627 Poznań, Poland*
[b]*Department of Food Biochemistry and Analysis, Poznan University of Life Sciences, 60-623 Poznań, Poland*

grazyna.lewandowicz@up.poznan.pl; krzysztof.dwiecki@up.poznan.pl

Abstract

Due to the development of nanotechnology, dynamic light scattering (DLS) and ζ potential measurements have gained enormous popularity in recent years, especially for studying liposomes and other nanoparticles of therapeutic relevance. This short review presents the potential of these techniques for the study of polysaccharides. The principles of zeta potential and DLS measurements were briefly presented, as well as limitations of these analyses. The correlation between dynamic and static light scattering in relation to analyses of dimension of macromolecules in colloid dispersed systems was also mentioned.

Introduction

Commercialization of nanotechnology supported development in other fields of sciences and technology, primarily in medicine and electronics, but also in food technology, energy, and environment protection[1,2]. The nanoscale materials include among other nanotubes, fullerenes, nanorods, quantum dots, liposomes. According to the European Commission recommendation nanomaterials have a size of 1-100 nm at least in one dimension[3]. However, it should be emphasized that in the essence, nanomaterials are distinguished by fact that below a certain size, quantum effects significantly affect the properties and behavior of particles. This implies the need to use specific analytical techniques to study this type of systems. Particular challenges arise when studying liposomes and other lipid nanoparticles[4,5]. Interface and colloid science has made a significant contribution to the development of this research. Particles dispersed in colloids can be recognized as a special type of nanoparticles as their size is in the range of approximately 1 nanometre to 1 micrometer[6].

The stability of colloidal dispersion systems depends mostly on the surface potential of the dispersed particles. It can be estimated by ζ potential measurements using commonly available instruments. This analysis is based on electrokinetic phenomena, and the obtained results depend primarily on pH and ionic strength of the dispersion. The concentration of the dispersed phase also has some effect[7,8]. ζ -potential measurements at different pH-values can be made both for polymer solutions and suspension. They give information about the type and amount of dissociated or adsorbed charged species. The shape of ζ-potential curves is different for polymers carrying acidic and basic surface groups, and for non-polar, non-dissociating ones. In case of protein molecules that carry both acidic and basic groups the ζ-potential vs pH course is of sigmoidal shape with the intersection of the abscissa axis at isoelectric point. If polymer molecules carry only acidic or only basic groups ζ-potential reveal only negative or positive values, respectively. By analysis of non-polar polymers the line decrease with the increase of pH is observed[9,10]. It is generally assumed that an absolute ζ potential value of 0 to 5 mV indicates that the system is flocculating or coagulating; 10 to 30 mV indicate incipient instability; 30 to 40 mV moderate stability; 40 to 60 mV good stability and greater than 60 mV excellent stability[11]. Using the same apparatus, it is possible to measure the hydrodynamic radius (or diameter) and diffusion coefficient of dispersed particles, what corresponds to their dimensions. This method consists in dynamic light scattering (DLS) or quasi-elastic light scattering and is also known as photon correlation spectroscopy. Concentration of sample and its preparation conditions, fluorescence and colour of sample, shape, agglomeration, and rotational diffusion of nanoparticles affect the measurement result[7,8]. Static light scattering signal measurements should also be mentioned here. They are proportional to molar mass, the concentration of polymer and refractive index increment of the solution. They are designed to determine the molecular mass of polymers. However, for proper analyses a molecular dispersion of macromolecules in solution is necessary[12,13].

Cellulose

Cellulose is the most abundant natural polymer all over the world. It is primarily used for papermaking and production of cardboard. Moreover, it is used for the production of coatings, laminates, optical films basing on cellulose regenerate fibers and films, as well as different cellulose esters and ethers. The more recent, currently developed cellulose processing areas include, among others, immobilization of biologically active substances or separation of enantiomeric molecules[14]. This technological progress creates the need for the development of analytical techniques such as DLS and ζ potential measurements. As cellulose is in principle insoluble in water environment, the analyses of the surface of polymer particles are the most widely used for its study. By applying this technique, it is possible not only to determine the amount of adsorbed or dissociated charged species but also some physicochemical properties of cellulose fibers such as swelling ability. By hydration, the diffusion layer becomes wider and ζ potential changes. Thanks to this, it is possible to analyse the differences between cellulose fibers obtained from different sources, using different chemicals and in different processing processes. Moreover, the presence of different surfactants also reveals significant effect[9]. Much attention has been devoted in recent years to the preparation and characterization of cellulose nanocrystals. Importantly, the DLS data on the size of nanoparticles of cellulose are consistent with those obtained employing various microscopic methods such as transmission electron microscopy (TEM), scanning electron microscopy (SEM) or atomic force microscopy (AFM)[15-19].

Starch

There is a correlation between particle size and their zeta potential. This phenomenon has been observed for nanoparticles obtained by homogenization of high amylose corn starch. By reduction of original diameter of corn granules from a few microns to tens of nanometres the ζ potential changes from -35 mV to -62 mV[20]. Analyses of the ζ potential of granular starch make possible not only to define their physical properties but to make more deep insight into chemical composition of the surface layer. One of the very first studies on the ζ potential of wheat and potato starch granules has shown that they contain in the surface layer low molecular substances that define their surface electric charge[21]. Wheat starch in its native form reveals typical for zwitterionic polymers sigmoidal shape of the profile of ζ potential vs pH . This curve has positive values for pH below 4. In a more alkaline medium, the ζ potential becomes negative. After extraction with EDTA the sigmoidal curve runs within negative ζ potential values in the entire range. It is related to the complexation of cations present in the starch suspension. Further extraction with the mixture of chloroform and methanol results in removal of phospholipids and in consequence the reduction of the ζ potential above pH 3 is observed. This proves the presence of acidic carboxyl groups on the surface of the granules. In case of potato starch the sigmoidal curve of the profile of ζ potential vs pH runs is within negative ζ potential value range. The effect of EDTA extraction as in case of wheat starch results in significant decrease of ζ potential values which corresponds to complexation of cations. Further extraction with the mixture of chloroform and ethanol results in extraction of lipids and seemingly unexpected constant zeta potential of -11 mV for all pH values in the range 2.5 – 10. It is due to the fact that phosphates in starch granules are mainly in the form of diester that is no titratable in the pH 2 – 10 regions. Summing up this study proves the presence of surface protein, phosphate, and lipid in wheat starch granules whereas surface phosphate and lipid in case of potato starch[21]. Moreover, the degree of chemical modification of starch, especially with regards to its cross-linking can be analysed using DLS techniques. More cross-linked starches reveal lower ability to swell, which results in significant changes in results of DLS analysis by the course of gelatinisation[22].

Special attention should be paid to the starch pastes as they do not constitute solution or suspension. Starches after pasting constitute a complex colloidal system being the mixture of dissolved molecules and granules swollen to different degrees[23]. In our previous study we proved that both ζ potential and DLS values of chemically modified starches pastes are mainly affected by environment and secondly by the type of chemical modification[24]. In the distilled water environment ζ potential of starch pastes, except E 1412, has negative values. In contrast, in buffers, including that of pH=7.0, all pastes reveal negative ζ potential values even that of cationic starch. Special attention should be paid to the DLS data presented in Fig. 1. In the distilled water the highest hydrodynamic diameter is revealed by molecules of native starch and the lowest those of oxidised starch. This latter finding is in line with the expectations. Cross-linked starch E 1412 reveals the highest hydrodynamic diameter only in buffers solutions. This points that deionised water it is not conducive to the dissolution of distarch phosphate macromolecules.

Partially degraded macromolecules of oxidised starch reveal the smallest hydrodynamic diameter in neutral and acidic environment. On the other hand, buffer of pH value of 9.5 causes more extensive solvation of oxidised starch macromolecules due to the presence of acidic carboxyl groups in its structure.

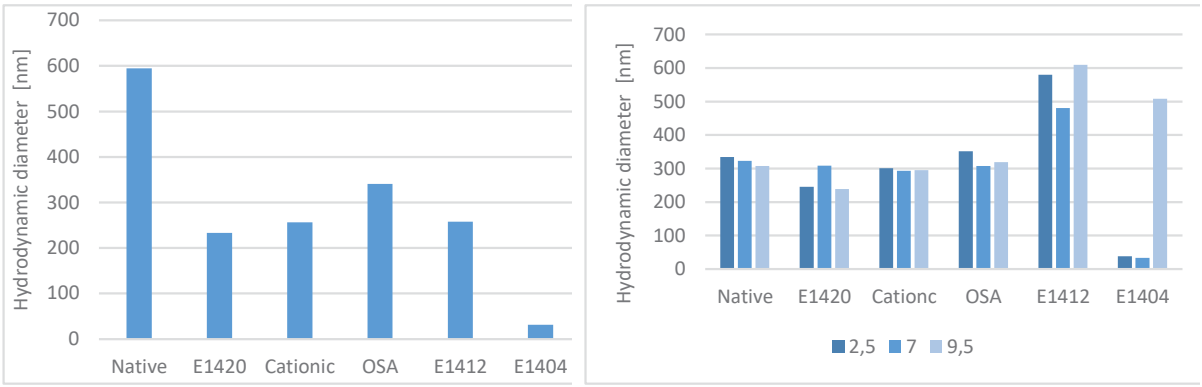

A B

Fig. 1: **Hydrodynamic diameter of chemically modified starch pastes at the concentration of 1% in different environment. A) distilled water; B) buffers of different pH (based on Makowska A.et al.[24]).**

As, in 2022, there were published data, gained with size exclusion chromatography with triple detection, regarding chemically modified starches[25], it became possible to compare data from the DLS and SLS studies. PCA analysis taking into consideration ζ potential values, hydrodynamic diameter (derived from DLS analysis), number-, weight-, and z-average molecular masses, polydispersity, intrinsic viscosity, radius of gyration and hydrodynamic radius (derived from SEC analysis) shows excellent almost 100% coverage of the data. A very interesting seems to be primarily the relationship between parameters determined based on light scattering phenomena. There is a strong correlation between hydrodynamic diameter (derived from DLS) and z-average molecular mass (derived from SLS, but only for unbuffered paste). It is in line with expectation as the unbuffered paste most closely reproduces the conditions of SEC analysis. Moreover, a strong correlation has been observed between:

- ζ potential value at pH = 2.5 and intrinsic viscosity
- ζ potential value at pH = 7.0 and radius of gyration
- ζ potential value at pH = 9.5 and weight average molecular mass.

However further studies are necessary to verify if these relationships are the rule.

REFERENCES

1. Younus Wani M., Ganie N.A., Dar K.A., Dar S.Q., Khan A.H., Khan N.A., Zahmatkesh S., Manzar M.S., Banerjee R.: Int. J. Biol. Macromol. *239*, 124350 (2023).
2. Kumar P., Mahajan P., Kaur R., Gautam S.: Mat. Today Chem. *17* 100332 (2020).
3. COMMISSION RECOMMENDATION of 18 October 2011 on the definition of nanomaterial (2011/696/EU). Off. J. Eur. Union.
4. Hallan S.S., Sguizzato M., Esposito E., Cortesi R.: Pharm. *13*, 549 (2021).
5. Bryła A., Juzwa W., Weiss M., Lewandowicz G.: Int. J. Pharm. *520*, 149–157 (2017).
6. IUPAC reports; https://old.iupac.org/reports/2001/colloid_2001/manual_of_s_and_t/node33.html
7. Bhattacharjee S.: J. Control. Rel. *235*, 337–351 (2016).
8. Cano-Sarmiento C., Téllez-Medina D.I., Viveros-Contreras R., Cornejo-Mazón M., Figueroa-Hernández C.Y., García-Armenta E., Alamilla-Beltrán L., García H.S., Gutiérrez-López G.F.: Food Eng. Rev. *10*, 113–138 (2018).
9. Reischl M., Stana-Kleinschek K., Ribitsch V.: Macromol. Symp. *244*, 31–47 (2006).
10. Jamróz E., Parab G., Jachimska B., Szczepanowicz K., Warszyński P., Para A.: Coll. Surf. A: Physicochem. Eng. Aspects *441*, 880– 884 (2014).
11. Kumar A., Kumar Dixit CH.: Advances in Nanomedicine for the Delivery of Therapeutic Nucleic Acids 43-58, 2017.

12. Gilbert R.G., Gidley, M.J.; Hill, S.; Kilz, P.; Rolland-Sabaté, A.; Stevenson, D.G.; A., C.R. Cer. Food. World *55*, 139–143 (2010).
13. Gidley M.J.; Hanashiro I., Hani N.M., Hill S.E., Huber A., Jane J.-L., Liu Q., Morris G.A., Rolland-Sabaté A., Striegel A.M., et al. Carbohydr. Polym. *79*, 255–261 (2010).
14. Klemm D., Heublein B., Fink H.P., Bohn A.: Angew. Chem. Int. Ed. *44*, 3358 – 3393 (2005).
15. Wu G., Li Q., Jin C., Kong Z., Wang S. Tappi Journal *18*, 4 (2019).
16. Boluk Y., Danumah Ch.: J. Nanopart. Res. *16*, 2174 (2014).
17. Fuster M.G., Moulefera I., Muñoz M.N., Montalbán M.G., Víllora G.S.: Polym. *15*, 382 (2023).
18. Rovera C., Carullo D., Bellesia T., Büyükta D., Ghaani M., Caneva E., Farris S.: Food Syst. *6*, 1087867 (2023).
19. Naduparambath S., Jinitha T.V., Shaniba V., Sreejith M.P., Balan A.K., Purushothaman E.: Carb. Polym. *180*, 13–20 (2018).
20. Liu D., Wua Q., Chen H., Chang P.R.: J. Coll. Int. Sci. *339*, 117–124 (2009).
21. Marsh R.A., Waight S.G.: Starch/Stärke *34*, 5, 149-152 (1982).
22. Desam G.P., Li J., Chen G., Campanella O., Narsimhan G.: Carb. Polym. *199*, 331–340 (2018).
23. Błaszczak W., Lewandowicz G.: Foods *9*, 670 (2020).
24. Makowska A., Dwiecki K., Kubiak P., Baranowska H.M., Lewandowicz G.: Polym. *14*, 2977 (2022).
25. Lewandowicz J., Le Thanh-Blicharz J., Szwengiel A.: Process. *10*, 938 (2022).

PICKERING O/W EMULSIONS STABILIZED BY BREWERS' SPENT GRAIN

ABDUL MUIZ, IVETA KLOJDOVÁ*, DIANA KARINA BAIGTS ALLENDE, NUJAMEE NGASAKUL, ALI KOZLU

DRIFT-FOOD, Faculty of Agrobiology, Food and Natural resources, Czech 6 University of Life Sciences, 165 21 Prague, Czechia

muiz@af.czu.cz, klojdova@af.czu.cz. Baigts_Allende@af.czu.cz, ngasakul@af.czu.cz, kozlu@af.czu.cz

Abstract

An emulsion is a mixture of two or more immiscible liquids that coexist in one system. Emulsions are thermodynamically unstable systems and must be stabilized by emulsifiers. A sustainable approach to stabilizing emulsion is the use of Pickering particles prepared from by-products. Brewer's spent grain (BSG), a by-product from the brewery industry, can be used as a source of Pickering particles after its modification by milling and acid hydrolysis. The particle size of BSG and emulsions was significantly affected by modification methods and storage time.

Introduction

An emulsion is a complex mixture of at least two immiscible liquids that are dispersed in one system [1]. Emulsions are thermodynamically unstable and can undergo Oswald ripening[2], creaming [3], and coalescence [4]. Conventionally, emulsions are stabilized by emulsifiers which decrease the surface tension between phases and can increase the steric hindrance and electrostatic repulsion between droplets [5, 6]. However, some synthetic emulsifiers have been found to cause health issues such as inflammation, skin rashes, irritation of eyes, hemolysis, and environmental problems[7, 8]. A sustainable approach for the stabilization of emulsions may be the use of Pickering particles (PPs). PPs are solid particles that are absorbed in the oil–water interface, making a barrier to stabilize emulsions and avoid instability phenomena.

By-products from the food industries are promising materials for the preparation of PPs. Often, these by-products are sources of many bioactive compounds. BSG is the major by-product of the brewing industry, representing around 85% of the total by-products generated in the brewery. BSG is a lignocellulosic material containing about 17% cellulose, 28% non-cellulosic polysaccharides, mainly arabinoxylans, and 28% lignin. BSG has been used in animal feeding, food raw materials, energy production, and biotechnological processes [9].

BSG can be modified using different methods for the preparation of PPs. The modification of particles is provided to reduce the particle size and change the surface properties of particles to allow the preparation of a specific type of emulsion (o/w or w/o). The commonly used methods for the preparation of particles are treatment with octenyl succinic anhydride (OSA) [10], acid hydrolysis [11], milling [12], high-pressure treatment [13], and nanoprecipitation [14].

Acid hydrolysis is a heterogeneous process that involves the diffusion of acids into the fibers and the cleavage of the glycosidic bonds [15].This method is particularly used to produce nanoparticles with some specific properties. Wet milling (also called wet grinding) is a procedure where shearing or crushing is applied to reduce and disperse particles suspended in a liquid slurry. So prepared particles can be used without any additional modification d, or they can be dried and separated if needed [16].

II. Material and method

Material

BSG was collected from local breweries, freeze-dried (-54°C, 3 days), and stored at -20°C until use. All chemicals used in experiments were reagent grade. Dimethyl sulfoxide (DMSO) was supplied by VWR Chemicals (France). Sodium hydroxide, and hydrochloric acid (≥98%) were supplied by Lachner (Hungary). Sulfuric acid was purchased from Penta (Czechia).

Method

Wet milling was provided according to the method [17] with some modifications . Before milling process, BSG was grinded using a blender A11 (IKA, Germany) for 2–4 min and sieved through a 212μm - sieve to obtain

a fine powder. After sieving, rotor-stator homogenizer (IKA, Germany) was used for wet milling. Milling experiments were performed by varying the rotation speed between 12000 and 20000 rpm for 2-3 min. Milled BSG particles were named M-BSG.

Acid hydrolysis was provided according to [11] with minor modifications. Firstly, BSG was treated with a 5 M NaOH (125 mL) aqueous solution at 90 °C for 3 hours, washed with distilled water, and then air-dried. Subsequently, it was immersed in 125 mL of DMSO under the same conditions, washed with distilled water, and air-dried. The obtained substance was hydrolyzed with a mixed acid solution (260 mL) at 75 °C for 8 h in an ultrasonic bath (Fisher Sonicator, ELMA Germany). The mixed acid solution was prepared by mixing sulfuric acid (98% *w*/w), hydrochloric acid (37% w/w), and distilled water at a ratio of 3:1:6 (*v*/v). After hydrolysis, the obtained suspension was centrifuged (universal 320, Hettich, Germany) at 7500 rpm for 25 min at room temperature, and the supernatant was removed. Acid-hydrolyzed BSG particles were named AH-BSG

Preparation of o/w emulsion

After milling and acid hydrolysis, 5 % BSG Pickering particles were dissolved in distilled water to prepare an aqueous phase. Then the aqueous phase was mixed with oil phase (canola oil) at 20000 rpm for 2 min at room temperature to prepare 5% o/w emulsion.

BSG particle size and droplet size of o/w emulsions

The particle size of BSG and droplets size of emulsions was determined by a laser diffraction method using a Malvern Mastersizer 3000 (Malvern instruments, UK). The measurements of freshly prepared BSG particles and o/emulsions were provided. Additionally, the droplet sizes of o/w emulsions after 1 week were also evaluated.

A refractive index 1.47 and absorption index 0.01 were used for the calculations of the particle size. Particle size measurements are reported as average mean diameters (Dx 50, μm). All the measurements were done in triplicates and the average data was reported [18].

Statistical analysis

All measurements were performed in triplicate, and data were expressed as the mean ± SD. ANOVA analysis was performed at a significant difference level of $p < 0.05$ by IBM SPSS Statistic.

Results

Particle size of BSG

The average particle size distribution of BSG after milling and acid hydrolysis is shown in Fig 1. M-BSG had multimodal distribution and a bigger particle size (58.8 μm), while AH-BSG particles had a lower particle size (9.62 μm). The lower value of the mean particle size of AH-BSG could be explained by shorter chains after sonication [19]. Acid hydrolysis involves the diffusion of acid into the cellulose fibers and the subsequent cleavage of glycosidic bonds. In the early stage of hydrolysis, the acid diffused preferentially into the non-crystalline portions of cellulose and hydrolyzed the available glycosidic bonds. After the hydrolysis, further reaction occurred much slowly at the reducing end and at the surface of the residual crystalline regions, i.e., the cellulose micro crystallites. As the hydrolysis time increases, surface charge increases and the particle size decreases due to cleavage of glycosidic bonds [20].

The changes in conformation and morphology after sonication could result in improved physicochemical properties and functions. As previously reported by [21], the shape and size of particles had a significant impact on the emulsion stability. It was found that smaller particles formed emulsions with smaller droplets.

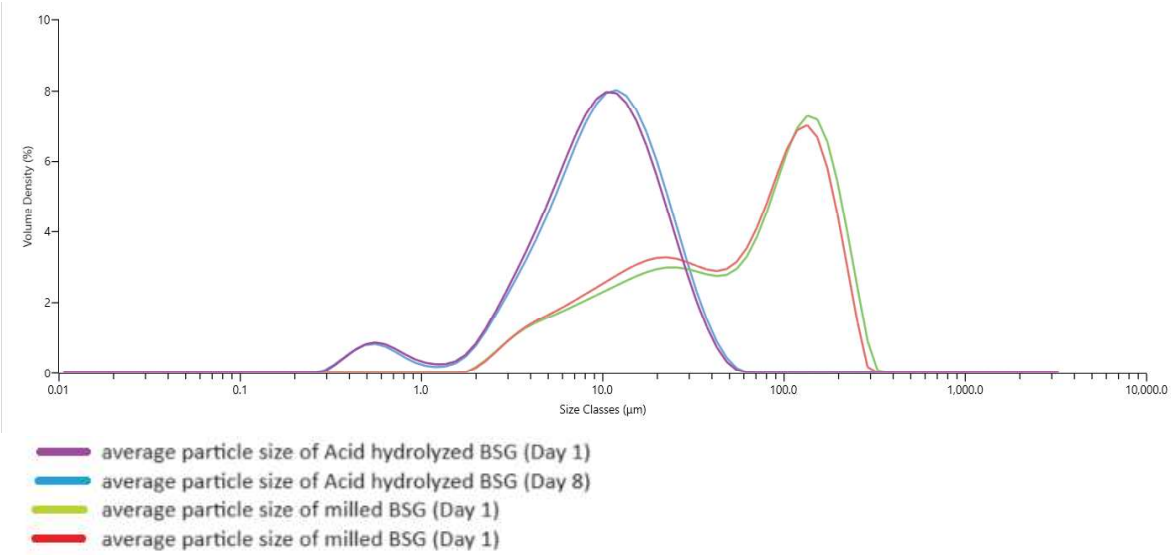

Fig. 1: **Average particle size of milled and acid hydrolysis BSG**

Droplet size of o/w emulsions

The droplet size of o/w emulsions was significantly affected by storage time and modification method of particles. The droplet size distribution of freshly prepared emulsions and after storage for 7 days is shown in Fig 2. Larger droplet size was observed in M-BSG emulsion after 7 days compared to AH-BSG emulsions. After storage, D_x50 of AH-BSG emulsions increased from 11.70 to 12.0 µm, while D_x50 of M-BSG emulsions increased from 34.0 to 35.6 µm. According to Stokes' law, emulsion stability may be ensured by increasing continuous phase viscosity, decreasing droplet size, or decreasing difference in densities between the disperse and the continuous phase[22].

Lower molecular weight and more flexible chains of AH-BSG may form a films that could cover droplets and prevent oil droplets coalescence [23].

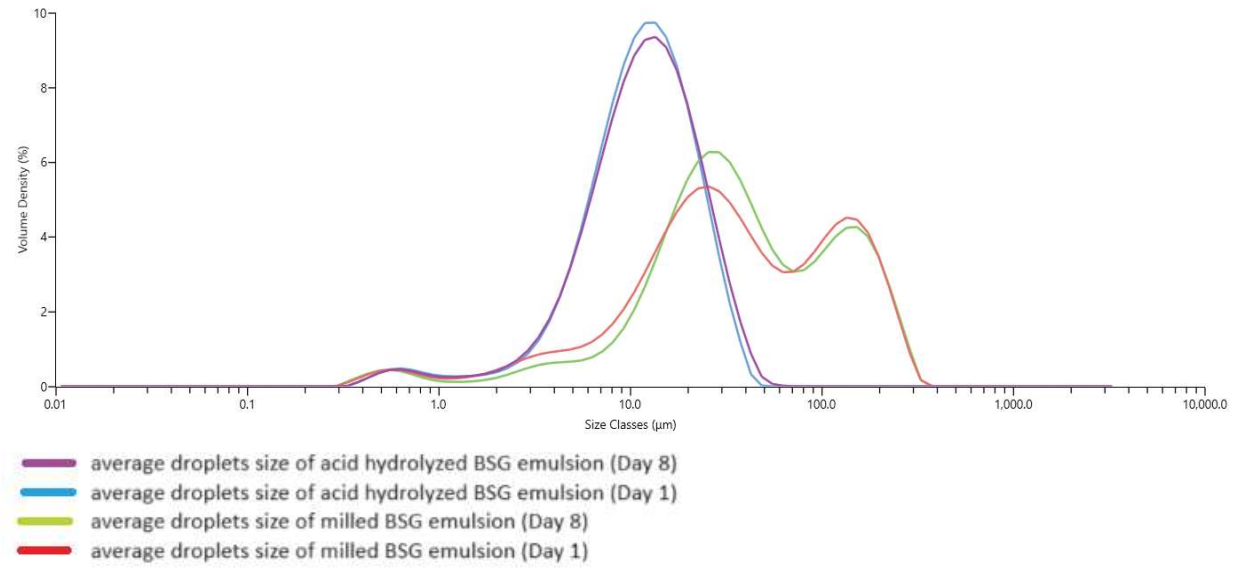

Fig. 2: **Average droplet size of milled and acid hydrolysis BSG emulsions**

Acknowledgement: This research was funded by European Union's Horizon 2020 Research and Innovation Program under grant agreement No 952594 (ERA Chair project DRIFT-FOOD).

REFERENCES

1. J. Jiao and D. J. J. A. P. Burgess, "Rheology and stability of water-in-oil-in-water multiple emulsions containing Span 83 and Tween 80," vol. 5, pp. 62-73, 2003.
2. H. Lamba, K. Sathish, L. J. F. Sabikhi, and B. Technology, "Double emulsions: emerging delivery system for plant bioactives," vol. 8, pp. 709-728, 2015.
3. N. Krog, "Additives in Dairy Foods| Emulsifiers," 2011.
4. N. Leister, H. P. J. C. Karbstein, and Interfaces, "Evaluating the stability of double emulsions—A review of the measurement techniques for the systematic investigation of instability mechanisms," vol. 4, no. 1, p. 8, 2020.
5. M. Rayner *et al.*, "Biomass-based particles for the formulation of Pickering type emulsions in food and topical applications," vol. 458, pp. 48-62, 2014.
6. H. Jiang, Y. Sheng, T. J. C. O. i. C. Ngai, and I. Science, "Pickering emulsions: Versatility of colloidal particles and recent applications," vol. 49, pp. 1-15, 2020.
7. R. H. Steele, S. Limaye, B. Cleland, J. Chow, and M. G. Suranyi, "Hypersensitivity reactions to the polysorbate contained in recombinant erythropoietin and darbepoietin," (in eng), *Nephrology (Carlton),* vol. 10, no. 3, pp. 317-20, Jun 2005.
8. C. K. Nielsen, J. Kjems, T. Mygind, T. Snabe, and R. L. Meyer, "Effects of Tween 80 on Growth and Biofilm Formation in Laboratory Media," (in English), Original Research vol. 7, 2016-November-22 2016.
9. S. I. Mussatto, G. Dragone, and I. C. Roberto, "Brewers' spent grain: generation, characteristics and potential applications," *Journal of Cereal Science,* vol. 43, no. 1, pp. 1-14, 2006/01/01/ 2006.
10. A. Marefati, M. Bertrand, M. Sjöö, P. Dejmek, and M. J. F. H. Rayner, "Storage and digestion stability of encapsulated curcumin in emulsions based on starch granule Pickering stabilization," vol. 63, pp. 309-320, 2017.
11. H. Dong, Q. Ding, Y. Jiang, X. Li, and W. Han, "Pickering emulsions stabilized by spherical cellulose nanocrystals," *Carbohydrate Polymers,* vol. 265, p. 118101, 2021/08/01/ 2021.
12. X. Lu, J. Xiao, and Q. Huang, "Pickering emulsions stabilized by media-milled starch particles," *Food Research International,* vol. 105, pp. 140-149, 2018/03/01/ 2018.
13. G. Villamonte, V. Jury, and M. J. F. H. de Lamballerie, "Stabilizing emulsions using high-pressure-treated corn starch," vol. 52, pp. 581-589, 2016.
14. Y. Qin, C. Liu, S. Jiang, L. Xiong, Q. J. I. C. Sun, and Products, "Characterization of starch nanoparticles prepared by nanoprecipitation: Influence of amylose content and starch type," vol. 87, pp. 182-190, 2016.
15. X. Lu, H. Zhang, Y. Li, and Q. Huang, "Fabrication of milled cellulose particles-stabilized Pickering emulsions," *Food Hydrocolloids,* vol. 77, pp. 427-435, 2018/04/01/ 2018.
16. Senieer. (2022, 09 Sep). *A comparative study of Dry milling vs Wet milling*. Available: https://www.senieer.com/a-comparative-study-of-dry-milling-vs-wet-milling/
17. C. V. Luciani, E. W. Conder, and K. D. Seibert, "Modeling-Aided Scale-Up of High-Shear Rotor–Stator Wet Milling for Pharmaceutical Applications," *Organic Process Research & Development,* vol. 19, no. 5, pp. 582-589, 2015/05/15 2015.
18. A.-I. Yeh, Y.-C. Huang, and S. H. Chen, "Effect of particle size on the rate of enzymatic hydrolysis of cellulose," *Carbohydrate Polymers,* vol. 79, no. 1, pp. 192-199, 2010/01/05/ 2010.
19. L. Liu, M. Chen, T. E. Coldea, H. Yang, and H. Zhao, "Emulsifying properties of arabinoxylans derived from brewers' spent grain by ultrasound-assisted extraction: structural and functional properties correlation," *Cellulose,* vol. 30, no. 1, pp. 359-372, 2023/01/01 2023.
20. X. M. Dong, J.-F. Revol, and D. G. Gray, "Effect of microcrystallite preparation conditions on the formation of colloid crystals of cellulose," *Cellulose,* vol. 5, no. 1, pp. 19-32, 1998/03/01 1998.
21. J. Wu and G. H. J. S. Ma, "Recent studies of Pickering emulsions: particles make the difference," vol. 12, no. 34, pp. 4633-4648, 2016.
22. I. Kalashnikova, H. Bizot, P. Bertoncini, B. Cathala, and I. J. S. M. Capron, "Cellulosic nanorods of various aspect ratios for oil in water Pickering emulsions," vol. 9, no. 3, pp. 952-959, 2013.
23. F. Ravera, K. Dziza, E. Santini, L. Cristofolini, L. J. A. i. C. Liggieri, and I. Science, "Emulsification and emulsion stability: The role of the interfacial properties," vol. 288, p. 102344, 2021.

RECOVERY OF BIOACTIVE COMPOUNDS FROM BREWER SPENT GRAINS USING DEEP EUTECTIC SOLVENT EXTRACTION

NUJAMEE NGASAKUL, IVETA KLOJDOVÁ*, ABDUL MUIZ, ALI KOZLU, DIANA K. BAIGTS-ALLENDE, CONSTANTINOS E. STATHOPOULOS, AND SUWIMOL CHOCKCHAISAWASDEE

DRIFT-FOOD Center, Faculty of Agrobiology, Food and Natural Resources, Czech University of Life Sciences Prague, Prague 16500, Czech Republic

ngasakul@af.czu.cz, klojdova@af.czu.cz, muiz@af.czu.cz, kozlu@af.czu.cz, baigts_allende@af.czu.cz, stathopoulos@af.czu.cz, chockchaisawasdee@af.czu.cz

Abstract

Brewers' spent grain (BSG) is the by-product derived from the brewing industry, which contains many valuable components. In the present study, three choline chloride-based deep eutectic solvents (DESs) were prepared to extract phenolic compounds using ultrasound-assisted extraction., The antioxidant activity of the extracts was evaluated. Choline chloride-based DES with levulinic acid showed the highest DPPH inhibition activity ($p \leq 0.05$), while the other two DES systems exhibited no significant difference in inhibition activity compared to those of the conventional solvents. The results suggested that DESs could be used as green solvents to substitute organic solvents.

Introduction

Brewers' spent grain (BSG) is the major by-product derived from the first step of beer manufacturing and accounts for approximately 85% of the total by-products generated[1]. BSG is mainly composed of fibrous materials since the cell wall components of BSG are the association of polysaccharide polymers, accounting for 30-70% (w/w), such as cellulose and hemicellulose surrounded by a lignin sheath[2]. Hemicellulose is the major polymeric fraction found in BSG, contributing to 20-40% of the lignocellulosic composition[3]. BSG can be used as an alternative protein source as it contains approximately 15-30% protein[3]. Additionally, it contains lipids, minerals, vitamins, and amino acids[4, 5]. Since barley malt contains grain husks and pericarp, BSG is a rich source of polyphenols[6]. Many studies reported the polyphenol compounds found in BSG, such as phenolics and flavonoids[6-11]. These compounds can possess bioactive activities, including antioxidant, anti-inflammatory, antiproliferative, and antimicrobial activities[5]. Previous studies on antioxidants have reported free radical scavenging activities (DPPH and ABTS), ferric reducing power (FRAP), or oxygen radical absorbance capacity (ORAC). Due to this, BSG has also been used as a raw material for the recovery and isolation of high-value components. In recent years, the use of deep eutectic solvents (DESs) to replace organic solvents in the extraction of bioactive compounds from various food materials have been reported[12, 13]. DESs are new alternative extraction solvents comprising a combination of two or more chemicals that act as hydrogen bond acceptor (HBA) and hydrogen bond donor (HBD)[14, 15]. This study aimed to extract bioactive compounds from BSG by using different DESs systems, and to evaluate their extraction efficiencies.

Materials and methods

BSG was obtained from local breweries and freeze-dried at -55°C for 72 h. The dried BSG was ground to powder with particle sizes of < 400 μm ($d_{(50)}$ value) and stored at -20°C until use. To extract bioactive compounds from BSG, different DES systems were prepared based on previous work. The composition of the DESs used in this study is shown in Table I. Each DES mixture was prepared in a closed bottle with heating and stirring at 70-75°C until a transparent liquid was formed.

Table I: **The composition of DESs.**

	HBA	HBD	Molar ratio	Water content (%v/v)	Reference
DES 1	Choline chloride	Ethylene glycol	1:2	25	López-Linares et al.[16]
DES 2	Choline chloride	Levulinic acid	1:2	30	Wu et al.[17]
DES 3	Choline chloride	Urea	1:2	50	Deniz et al.[18]

Extraction of polyphenolic compounds was performed by mixing 0.4 g of dried BSG with 4 mL of DES in a centrifuge tube. The extraction was carried out at 60 °C for 2 h in an ultrasound bath (Elmasonic Easy 100 H, Fisherbrand) with a frequency of 37 kHz[18]. Then, the supernatant was collected by centrifuging at 5,000 rpm for 10 min and filtered through a 0.2 µm membrane, as the protocol in Fig. 1. To compare the extraction efficiency, distilled water, and organic solvents (absolute methanol and 50%v/v ethanol) were used control solvents.

Figure 1: **Protocol for the extraction of polyphenolic compounds from BSG.**

DPPH radical scavenging activity

The DPPH (2,2-Diphenyl-1-picrylhydrazyl) radical scavenging activity of BSG extracts were determined using the method previously described by Hidalgo et al.[19]. Briefly, 100 µL of the diluted sample and 100 µL of DPPH solution (0.1 mM 2,2-Diphenyl-1-picrylhydrazyl in ethanol) were placed in a 96-well microplate and mixed well. After incubation at room temperature in the dark for 30 min, the absorbance was measured at 517 nm by a spectrophotometric microplate reader (Synergy H1, BioTek), using methanol as a blank. The radical scavenging activity was reported as the inhibition percentage using equation (1), where S is the absorbance of the sample solution and B is the absorbance of the blank solution (methanol).

$$\text{DPPH inhibition (\%)} = 1 - (S/B) \times 100 \qquad (1)$$

Results and discussion

The percentage of DPPH inhibition of BSG extract obtained from three different DES solvents is shown in Fig. 2. DPPH assay is well-known technique for analysing the antioxidant activity using reagent 2,2-diphenyl-1-picrylhydrazyl (DPPH). It is a simple and rapid method with accuracy and precision. DPPH is a free radical; when it interacts with antioxidants or radical species, the violet solution of DPPH will change to pale yellow or colourless. The absorbance of the solution at 517 nm indicates the potential antioxidant properties of the sample in terms of hydrogen-donating capacity[20]. The intensity of the violet solution decreased when the sample had a high anti-oxidation ability. From the data obtained, DES 2 extracts exhibited the highest DPPH inhibition level ($p \leq 0.05$), reaching 51.70%, while distilled water extract showed the lowest level of inhibition at 34.24% ($p \leq 0.05$). This result was in agreement with the study by Meneses et al.[21], who extracted BSG with different solvents and found that distilled water showed a lower percentage of DPPH inhibition (3.33%) compared to methanol, ethanol, and acetone in some concentrations. It has been reported that the cell walls of plant materials, including BSG, have

an unpolar character. This material is usually more soluble in less polar solvents, allowing the extraction of the antioxidant compounds more efficiently. It explains why the extracts obtained using water demonstrated both lower total phenolic content and antioxidant potential than using the organic solvents, owing to water's high polarity[22, 23].

However, comparing the three DES systems showed that DES 2 extract was more effective in inhibiting free radical DPPH than those obtained from the other two DES systems. Many previous studies have reported similar trends; the high antioxidant capacity of DES extracts was obtained from acidic DESs[24-27]. This can be attributed to their intermolecular interactions, mostly due to hydrogen bonds between the solvent and the acidic phenolics presented in BSG extracts. The interaction could reduce oxidative degradation by decreasing the movement of solute molecules and consequently reducing the contact with oxygen, which can stabilize the phenolic compounds[28].

The inhibition activities of DES 1 and DES 3 extracts were not significantly different from those of methanol and 50% ethanol ($p>0.05$). The measured values were in the range of 40.24-43.58%. In comparison, Meneses et al.[21] found that BSG extracts produced with solid-to-liquid extraction using organic solvents such as ethanol, methanol, and acetone presented DPPH inhibition potential varied from 0-20.55%, which were lower than the results of this study. A study on the antioxidant activity of brewing waste, malt bagasse, also reported a low value of DPPH, which was 12.86%[29]. BSG obtained from different types of malt and kilning temperatures were studied on DPPH radical scavenging activity and exhibited values between 22.56-26.77%[30]. These expected differences could be due to the composition of raw material, BSG, and the type of solvent specificity to the target compound[6]. Additionally, Moreira et al.[31] found that the light malt extracts presented higher scavenging activities towards the radicals DPPH and ABTS than the dark malt extracts. It could be related to the increasing degree of malt color and kilning temperature. However, Kumari et al.[32] found that the FRAP and DPPH radical scavenging activity level in dark BSG was 8 and 9 times higher than in light BSG, respectively. It may indicate that free phenolics are less abundant in light BSG, possibly due to degradation or extraction during fermentation or their cell-bound nature. However, a high value of DPPH inhibition indicates an efficient antioxidant activity of BSG, which may result from the phenolic composition. This composition has been revealed to affect the free radical-scavenging activity of the sample significantly[31]. Thus, the high content of phenolic compounds could be expected in this study because of the high inhibition activity found in the BSG extract.

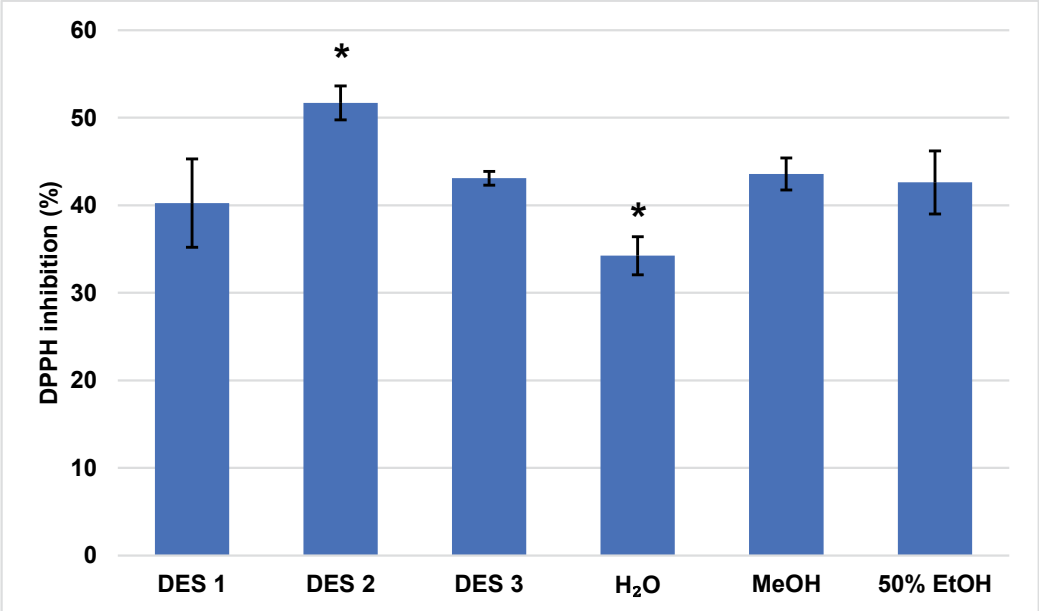

Figure 2: **Percentage of DPPH inhibition of BSG extract obtained from different solvents. DES 1: choline chloride-ethylene glycol (1:2), DES 2: choline chloride-levulinic acid (1:2), and DES 3: choline chloride-urea (1:2).**

Conclusion

DES 2 (choline chloride: levulinic acid; 1:2) was the most efficient in the extraction of polyphenolic compounds from BSG in comparison to the conventional solvents and the other DESs systems investigated in this study. The DPPH inhibition of BSG extract obtained from such mixture was higher (51.70%) than that obtained from both mixtures of choline chloride with urea (43.09%) and ethylene glycol (40.24%). It was observed that DESs could be a potential alternative to conventional organic solvents for extraction of bioactive compounds from plant materials. For further work, it would be interesting to evaluate extraction efficiency of other DESs.

Acknowledgement: This research was funded by the European Union's Horizon 2020 Research and Innovation Program under grant agreement No 952594 (ERA Chair project DRIFT-FOOD).

References

1. Aliyu, S., and Bala, M.: 'Brewer's spent grain: a review of its potentials and applications', Afr. J. Biotechnol., *10*, 3, (2011), pp. 324-331
2. Rodriguez, L.M., Camina, J.L., Borroni, V., and Pérez, E.E.: 'Protein recovery from brewery solid wastes', Food Chem., *407*, (2023), pp. 134810
3. Agrawal, D., Gopaliya, D., Willoughby, N., Khare, S.K., and Kumar, V.: 'Recycling potential of brewer's spent grains for circular biorefineries', Curr. Opin. Green Sustain. Chem., *40*, (2023), pp. 100748
4. Rachwał, K., Waśko, A., Gustaw, K., and Polak-Berecka, M.: 'Utilization of brewery wastes in food industry', PeerJ, *8*, (2020), pp. e9427
5. Yu, D., Sun, Y., Wang, W., O'Keefe, S.F., Neilson, A.P., Feng, H., Wang, Z., and Huang, H.: 'Recovery of protein hydrolysates from brewer's spent grain using enzyme and ultrasonication', Int. J. Food Sci. Technol., *55*, 1, (2020), pp. 357-368
6. Bonifácio-Lopes, T., M. G. Castro, L., Vilas-Boas, A., Campos, D., Teixeira, J.A., and Pintado, M.: 'Impact of gastrointestinal digestion simulation on brewer's spent grain green extracts and their prebiotic activity', Food Res. Int., *165*, (2023), pp. 112515
7. Bonifácio-Lopes, T., Vilas-Boas, A., Machado, M., Costa, E.M., Silva, S., Pereira, R.N., Campos, D., Teixeira, J.A., and Pintado, M.: 'Exploring the bioactive potential of brewers spent grain ohmic extracts', Innov. Food Sci. Emerg. Technol., *76*, (2022), pp. 102943
8. Naibaho, J., Wojdyło, A., Korzeniowska, M., Laaksonen, O., Föste, M., Kütt, M.-L., and Yang, B.: 'Antioxidant activities and polyphenolic identification by UPLC-MS/MS of autoclaved brewers' spent grain', LWT, *163*, (2022), pp. 113612
9. Naibaho, J., Pudło, A., Bobak, Ł., Wojdyło, A., López, Á.A., Pangestika, L.M.W., Andayani, S.N., Korzeniowska, M., and Yang, B.: 'Conventional water bath heating on undried brewer's spent grain: Functionality, fatty acids, volatiles, polyphenolic and antioxidant properties', Food Bioscience, *53*, (2023), pp. 102523
10. Petrón, M.J., Andrés, A.I., Esteban, G., and Timón, M.L.: 'Study of antioxidant activity and phenolic compounds of extracts obtained from different craft beer by-products', J. Cereal Sci., *98*, (2021), pp. 103162
11. Herbst, G., Hamerski, F., Errico, M., and L. Corazza, M.: 'Pressurized liquid extraction of brewer's spent grain: Kinetics and crude extracts characterization', Journal of Industrial and Engineering Chemistry, *102*, (2021), pp. 370-383
12. del Mar Contreras-Gámez, M., Galán-Martín, Á., Seixas, N., da Costa Lopes, A.M., Silvestre, A., and Castro, E.: 'Deep eutectic solvents for improved biomass pretreatment: Current status and future prospective towards sustainable processes', Bioresour. Technol., *369*, (2023), pp. 128396
13. Ling, J.K.U., and Hadinoto, K.: 'Deep Eutectic Solvent as Green Solvent in Extraction of Biological Macromolecules: A Review', Int. J. Mol. Sci., *23*, 6, (2022), pp. 3381
14. Abbott, A.P., Capper, G., Davies, D.L., Rasheed, R.K., and Tambyrajah, V.: 'Novel solvent properties of choline chloride/urea mixtures', Chem. Commun., 1, (2003), pp. 70-71
15. Trivedi, T.J., Lee, J.H., Lee, H.J., Jeong, Y.K., and Choi, J.W.: 'Deep eutectic solvents as attractive media for CO2 capture', Green Chem., *18*, 9, (2016), pp. 2834-2842

16. López-Linares, J.C., Campillo, V., Coca, M., Lucas, S., and García-Cubero, M.T.: 'Microwave-assisted deep eutectic solvent extraction of phenolic compounds from brewer's spent grain', J. Chem. Technol. Biotechnol., *96*, 2, (2021), pp. 481-490
17. Wu, L., Li, L., Chen, S., Wang, L., and Lin, X.: 'Deep eutectic solvent-based ultrasonic-assisted extraction of phenolic compounds from Moringa oleifera L. leaves: Optimization, comparison and antioxidant activity', Sep. Purif. Technol., *247*, (2020), pp. 117014
18. Deniz, S., Ünlü, A.E., and Takaç, S.: 'Ultrasound-assisted natural deep eutectic solvent extraction of phenolic compounds from apple pomace', Sep. Sci. Technol., *58*, 2, (2023), pp. 302-313
19. Hidalgo, M., Sánchez-Moreno, C., and de Pascual-Teresa, S.: 'Flavonoid–flavonoid interaction and its effect on their antioxidant activity', Food Chem., *121*, 3, (2010), pp. 691-696
20. Baliyan, S., Mukherjee, R., Priyadarshini, A., Vibhuti, A., Gupta, A., Pandey, R.P., and Chang, C.M.: 'Determination of Antioxidants by DPPH Radical Scavenging Activity and Quantitative Phytochemical Analysis of Ficus religiosa', Molecules, *27*, 4, (2022)
21. Meneses, N.G.T., Martins, S., Teixeira, J.A., and Mussatto, S.I.: 'Influence of extraction solvents on the recovery of antioxidant phenolic compounds from brewer's spent grains', Sep. Purif. Technol., *108*, (2013), pp. 152-158
22. Dorta, E., Lobo, M.G., and Gonzalez, M.: 'Reutilization of Mango Byproducts: Study of the Effect of Extraction Solvent and Temperature on Their Antioxidant Properties', J. Food Sci., *77*, 1, (2012), pp. C80-C88
23. Kim, D.-O., and Lee, C.Y.: 'Extraction and Isolation of Polyphenolics', Current Protocols in Food Analytical Chemistry, *6*, 1, (2002), pp. I1.2.1-I1.2.12
24. Alsaud, N., Shahbaz, K., and Farid, M.: 'Application of deep eutectic solvents in the extraction of polyphenolic antioxidants from New Zealand Manuka leaves (Leptospermum Scoparium): Optimization and antioxidant activity', J. Mol. Liq., *337*, (2021), pp. 116385
25. Chanioti, S., and Tzia, C.: 'Extraction of phenolic compounds from olive pomace by using natural deep eutectic solvents and innovative extraction techniques', Innov. Food Sci. Emerg. Technol., *48*, (2018), pp. 228-239
26. Rashid, R., Mohd Wani, S., Manzoor, S., Masoodi, F.A., and Masarat Dar, M.: 'Green extraction of bioactive compounds from apple pomace by ultrasound assisted natural deep eutectic solvent extraction: Optimisation, comparison and bioactivity', Food Chem., *398*, (2023), pp. 133871
27. Zannou, O., Pashazadeh, H., Ibrahim, S.A., Koca, I., and Galanakis, C.M.: 'Green and highly extraction of phenolic compounds and antioxidant capacity from kinkeliba (Combretum micranthum G. Don) by natural deep eutectic solvents (NADESs) using maceration, ultrasound-assisted extraction and homogenate-assisted extraction', Arab. J. Chem., *15*, 5, (2022), pp. 103752
28. Dai, Y., Rozema, E., Verpoorte, R., and Choi, Y.H.: 'Application of natural deep eutectic solvents to the extraction of anthocyanins from Catharanthus roseus with high extractability and stability replacing conventional organic solvents', J. Chromatogr. A, *1434*, (2016), pp. 50-56
29. Saraiva, B.R., Agustinho, B.C., Vital, A.C.P., Staub, L., and Matumoto Pintro, P.T.: 'Effect of brewing waste (malt bagasse) addition on the physicochemical properties of hamburgers', J. Food Process. Preserv., *43*, 10, (2019), pp. e14135
30. Farcas, A.C., Socaci, S.A., Chiș, M.S., Pop, O.L., Fogarasi, M., Păucean, A., Igual, M., and Michiu, D.: 'Reintegration of Brewers Spent Grains in the Food Chain: Nutritional, Functional and Sensorial Aspects', Plants, *10*, 11, (2021), pp. 2504
31. Moreira, M.M., Morais, S., Carvalho, D.O., Barros, A.A., Delerue-Matos, C., and Guido, L.F.: 'Brewer's spent grain from different types of malt: Evaluation of the antioxidant activity and identification of the major phenolic compounds', Food Res. Int., *54*, 1, (2013), pp. 382-388
32. Kumari, B., Tiwari, B.K., Walsh, D., Griffin, T.P., Islam, N., Lyng, J.G., Brunton, N.P., and Rai, D.K.: 'Impact of pulsed electric field pre-treatment on nutritional and polyphenolic contents and bioactivities of light and dark brewer's spent grains', Innov. Food Sci. Emerg. Technol., *54*, (2019), pp. 200-210

ISOLATION AND STRUCTURAL ANALYSIS OF EXOPOLYSACCHARIDE PRODUCED BY PERSPECTIVE STRAIN *Limosilactobacillus fermentum* MM1V

ANDREJ SINICA[a*], ROMAN BLEHA[a], ŠÁRKA HORÁČKOVÁ[b], BLANKA VRCHOTOVÁ[b], PETRA SMRČKOVÁ[a], TAMILLA BABAYEVA[a], JIŘÍ ŠTĚTINA[b]

[a]*Department of Carbohydrates and Cereals, University of Chemistry and Technology Prague, Technická 5, 16628 Prague, Czech Republic*

[b]*Department of Dairy, Fat and Cosmetics, University of Chemistry and Technology Prague, Technická 5, 16628 Prague, Czech Republic*

sinicaa@vscht.cz

Abstract

Lactic acid bacteria can produce exopolysaccharides (EPS) that influence the texture of dairy products and could exhibit prebiotic properties. *Limosilactobacillus fermentum* MM1V was isolated as perspective EPS production strain from human milk. Subsequently, EPS were isolated after 36 h cultivation MM1V in MRS broth: skimmed milk (1:1) at 37 °C in 5 % v/v CO_2 atmosphere. The obtained EPS were characterised by spectroscopic and separation methods. They consisted mainly of mannose, galactose, and glucose at the molar ratio of 2:2:1, and also contained *N*-acetylated amino sugars.

Introduction

The positive effects of probiotics on digestion are often attributed to exocellular polysaccharides (EPS) that microorganisms produce to the medium. Numerous studies have documented the beneficial effect of these bacterial metabolites on human health, such as anti-cancer, antimicrobial, or immune stimulating activity[1-3]. Their prebiotic effect is also significant[4,5]. EPS-producing strains can also modify the rheological properties and consistency of fermented milk products, where they increase the viscosity. These bacterial polysaccharides provide a source of stabilizing, thickener, emulsifying, and water-binding substances applicable as natural food additives[6-8].

Many EPS have been successfully isolated, purified, and chemically characterized[8,9], but their low yield is still a problem. For practical and economic reasons, it is effective to use EPS-producing strains, such as widely used lactic acid bacteria or bifidobacteria, which have the "GRAS" (generally recognized as safe) status[10].

This work focuses on characterisation of *Limosilactobacillus fermentum* MM1V from human milk as a perspective EPS production strain. EPS were isolated from the cultural medium and characterised by spectroscopic and separation methods.

Materials and methods

Strain and cultivation

Limosilactobacillus fermentum MM1V was isolated from human milk and characterised as a perspective EPS production strain according to Congo red testing method (mucoid appearance). This strain was cultivated in the mixture of MRS broth: skimmed milk (1:1) using 4 % v/v inoculum at 37 °C in 5 % v/v CO_2 atmosphere.

Isolation of EPS

EPS were isolated from the cultivation medium (400 ml) after 36 h cultivation. Firstly, proteins were precipitated by trichloroacetic acid (final concentration 20 % w/v), and precipitate of denatured proteins was separated by centrifugation. Crude EPS were isolated from the supernatant by ethanol precipitation (1:3 v/v) followed by centrifugation. Obtained pellet was dissolved in re-distilled water and dialysed (cut off 12–14 kDa). After subsequent ethanol precipitation, the final product (80 mg) was dried at 55 °C. The obtained EPS were characterised by spectroscopic and separation methods.

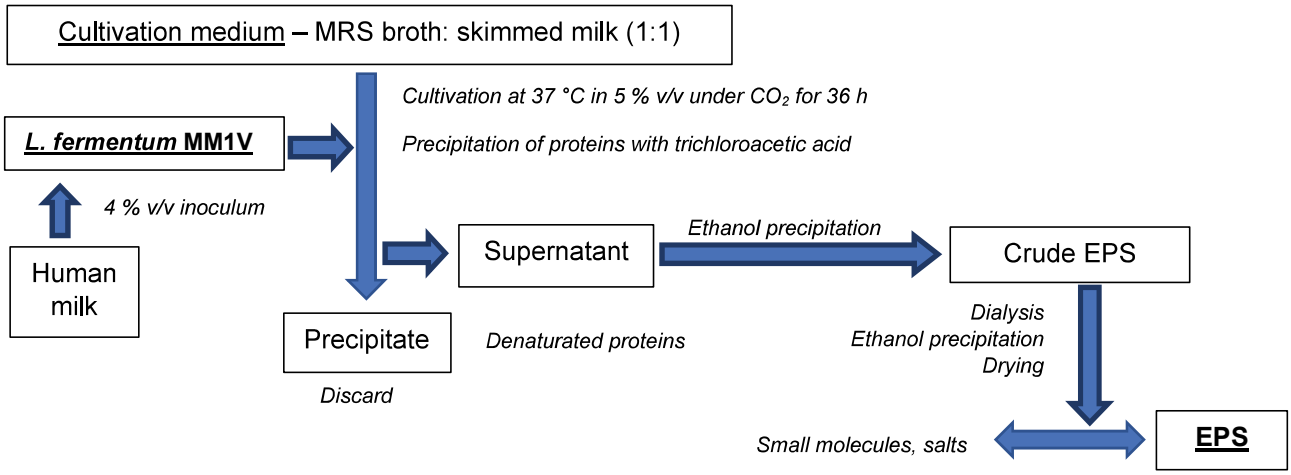

Figure 1: **Scheme of *Limosilactobacillus fermentum* MM1V cultivation and isolation of EPS from the cultivation medium.**

Analytical methods

FTIR spectrum (400–4000 cm^{-1}) of EPS was recorded in KBr pellets using a Nicolet 6700 FTIR spectrometer (Thermoscientific, USA); 64 scans were accumulated with a spectral resolution of 2.0 cm^{-1}. The spectrum was smoothed, and the baseline was corrected using Omnic 8.0 and 9.0 (ThermoScientific, USA) software and exported in ASCII format to Origin 2019b software (OriginLab Inc., USA) software for graph preparation.

The ^{1}H and ^{13}C APT NMR spectra were recorded on a Bruker Avance III TM 600 MHz (Bruker, USA) in D_2O solutions and processed in MestReNova 10.0 software (Mestrelab Research S.L., Spain) software. All the spectra were exported to Origin 6.0 software (Microcal Origin, USA) software for graph preparation. Correlation spectroscopy ^{1}H, ^{1}H COSY, ^{1}H, ^{13}C HMQC and ^{1}H, ^{13}C HMBC experiments were applied for the assignments of proton and carbon signals.

Molecular weight of EPS was determined using analytical HP GPC. The samples were dissolved in mobile phase (0.1 mol L^{-1} phosphate buffer with 0.1 mol L^{-1} $NaNO_3$ and 0.02 % sodium azide) for 12 h at room temperature at concentration of 5 g L^{-1}, transported to 2 mL inject vials and 30 µL of each were injected after preheating to 40 °C, temperature of columns preset to 40 °C. HP GPC was performed on OMNISEC (Malvern Panalytical, UK) equipped with YMC-Pack Diol-300 and YMC-Pack Diol 120 (YMC Europe GmbH, Germany) columns and four detectors (RI, LALS, RALS and viscosimeter). Signals from all detectors were collected and injections were performed in triplicate for each sample and eluted at the flow rate 0.7 ml min^{-1} for 55 min. Analysis of molecular weights was performed on the basis of known concentration using narrow pullulan standard (6.13×10^4 g mol^{-1}).

Neutral sugars were analysed in all materials and fractions by hydrolysis in 72% H_2SO_4 and analysed as alditol acetates by GC/FID using a Shimadzu GC2010 (Japan) equipped with a 30 m capillary column DB-225 with an internal diameter of 0.25 mm and a film thickness of 0.15 µm. The injector and detector temperatures were, respectively, 220 °C and 230 °C. The oven temperature programme was followed 200 °C for 1 min, then increased to 220 °C (40 °C min^{-1}), temperature 220 °C for 7 min, then increased to 230 °C (20 °C min^{-1}) until the final temperature 230 °C for 1 min, total time 9 min.

Results and discussion

The monosaccharide composition of EPS is summarised in Table I. Mannose (40.7 mol %) and galactose (36.7 mol %) were the main monosaccharides followed by glucose (17.8 mol %) and fucose (4.3 mol %). Arabinose, rhamnose and xylose were found at trace amounts. Therefore, the main isolated product should be heteropolysaccharide, probably galactoglucomannan, or a mixture of polysaccharides.

Table I: **Monosaccharide composition of EPS produced by *Limosilactobacillus fermentum* MM1V.**

Sample	Molar ratio [mol %]							Total
	Fuc	Ara	Man	Glc	Gal	Rha	Xyl	[% w/w]
EPS	4.3	0.3	40.7	17.8	36.7	0.2	0.1	50.7

The FTIR spectrum of EPS measured in KBr pellets is shown in Fig. 2. The bands at 2925 and 3408 cm^{-1} arose from stretching vibrations of C–H and O–H bonds, respectively. The overlapped intense IR bands at 950–1200 cm^{-1} were assigned to stretching vibrations of the C–O, C–C bonds of glycosidic bonds and pyranose rings of polysaccharides[11,12]. The bands at 800 cm^{-1}, 872 cm^{-1} (shoulder) and 899 cm^{-1} represented skeletal vibrations of *β*-D-glucopyranosyl, *β*-D-galactopyranosyl and *α*-D-mannopyranosyl units, respectively[12]. The IR bands at 1643 cm^{-1} (amide I), 1547 cm^{-1} (amide II), 1383 cm^{-1} (symmetric deformation of CH_3) and 1317 cm^{-1} (amide III) indicated the presence of *N*-acetylated amino sugars. Band at 1257 cm^{-1} (C–O–C stretching vibration) and a shoulder at 1739 cm^{-1} (C=O stretching vibration) were assigned to *O*-acetyl ester groups.

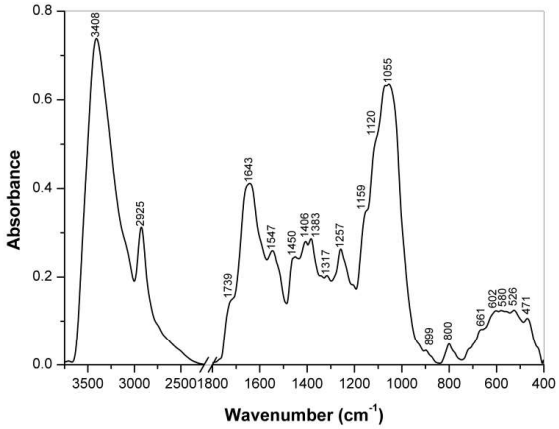

Figure 2: **FTIR spectrum of EPS produced by *Limosilactobacillus fermentum* MM1V.**

Three HP GPC chromatograms of EPS recorded form RI, RALS and viscosimetry detectors are shown in Fig. 3. The chromatograms indicated two peaks corresponding to molecular masses of 3.10×10^5 g mol^{-1} and 6.05×10^4 g. Possibly EPS consists of two polysaccharides of different molecular masses, e.g., *β*-D-glucogalactan and *α*-D-mannan. It is unclear how these polysaccharides can be connected to each other and what place galactofuranose and *N*-acetyl amino sugar units occupy in this structure. Further structural analysis is required to elucidate the exact structure of this EPS.

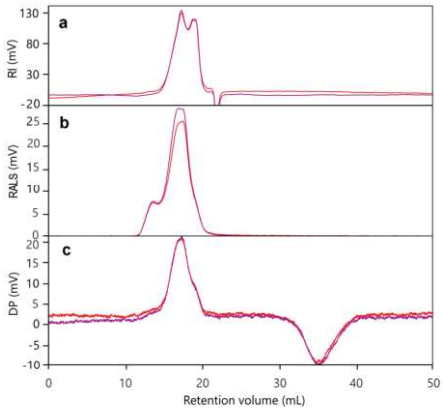

Figure 3: **HP GPC chromatograms of isolated EPS recorded from RI (a), RALS (b) and viscometer (c).**

Proton and ^{13}C APT NMR spectra of EPS are represented in Fig. 3a, b. Resonance signal assignments are summarised in Table II. Individual sugar units are assigned as **a** – **i**, and the most pronounced of them were terminal

α-Man*p* (**c**), *β*-Glc*p* (**h**) and *β*-Gal*p* (**h**) that confirmed highly branched structure of EPS. Minor units of *β*-Gal*f* (**b**) and *α*-Gal*p*NAc (**e**) were also observed.

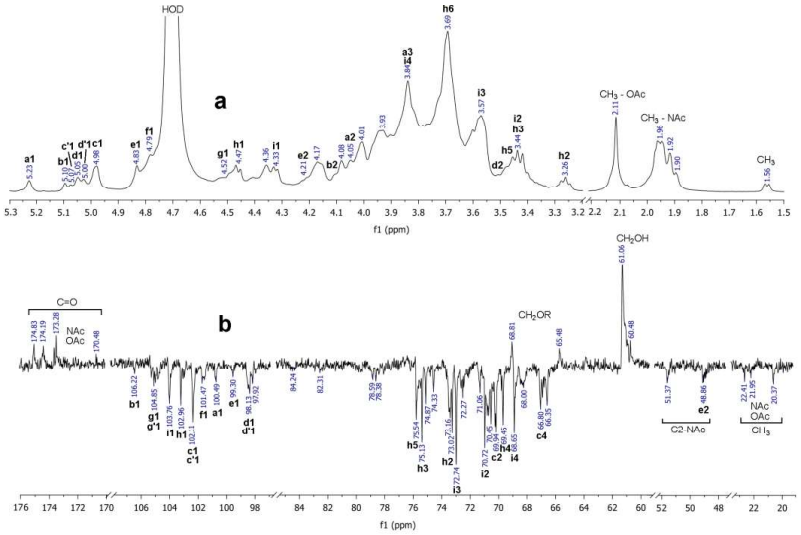

Figure 4: **^{1}H (a) and ^{13}C APT (b) NMR spectra of EPS produced by *Limosilactobacillus fermentum* MM1V.**

Table II: **Proton and carbon resonance signal assignments for EPS**

Unit	Structure	δ (ppm)							
		H1/C1	H2/C2	H3/C3	H4/C4	H5/C5	H6/C6	CH_3	C=O
a	2,6-*α*-Man*p*	5.23	4.05	3.91	3.74	3.71	3.62; 4.07		
		100.51	78.38	70.23	66.36	71.39	65.48		
b	*β*-Gal*f*	5.10	4.11	4.17	3.95				
		106.23	86.46	75.27	82.34				
c	*α*-Man*p*	4.98	4.01	3.75	3.55	3.70	3.70; 3.85		
		102.12	69.92	70.23	66.87	73.24	61.04		
d		5.05	3.51						
		98.13							
e	*α*-GalpNAc	4.84	4.21	3.89				1.56	
		99.29	48.86					15.33	170.48
f		4.79	3.92						
		101.40							
g	4,6-*β*-Gal*p*	4.52	3.69	3.77	3.92	3.57	3.79; 4.16		
		104.57	73.15	73.26	78.63	73.96	68.82		
h	*β*-Glc*p*	4.46	3.26	3.44	3.34	3.47	3.70		
		102.97	73.21	75.52	69.51	75.52	61.04		
i	*β*-Gal*p*	4.32	3.44	3.57	3.84	3.59	3.69		
		103.77	70.86	73.02	68.56	75.13	61.23		

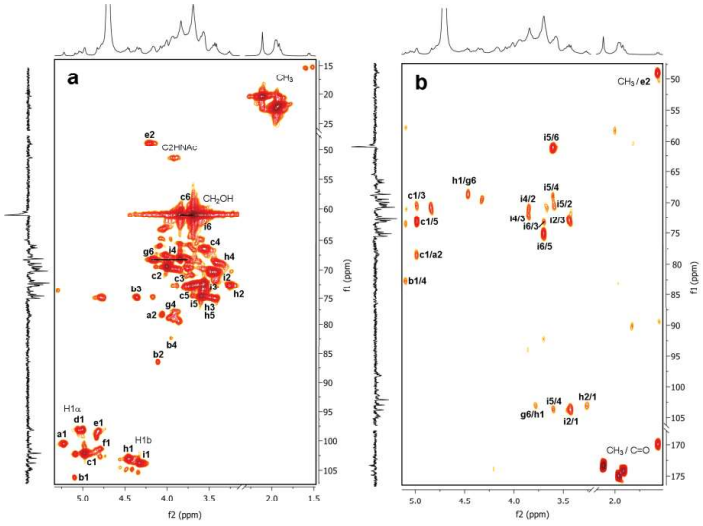

Figure 5: **^{1}H, ^{13}C HMQC (a) and ^{1}H, ^{13}C HMBC (b) NMR spectra of EPS produced by *Limosilactobacillus fermentum* MM1V.**

Proton signals at 1.56–2.11 ppm and corresponding carbon signals at 20.37–22.41 ppm arose from CH_3 groups in *O*-Ac and *N*-Ac attached to the sugar units. Carbon signals at 48.86 and 51.37 correspond to C-2 carbons carrying *N*-Ac groups. Intense positive carbon APT signals at ~60–61 ppm were assigned to C-6 of CH_2OH groups, while the downfield shifted signals at 65.48 and 68.81 ppm corresponded to glycosylated CH_2OR groups. Weak negative carbon APT signals at 78.38 and 78.59 ppm indicated substituted CHOR groups. The correlation HMQC and HMBC spectra of EPS (Fig. 4a, b) confirmed the assignment of the main carbohydrate units and two inter-unit connections: (i) between terminal *α*-D-Man*p* (**c**) and 1,2,6-linked *α*-D-Man*p* (**a**) and (ii) between terminal *β*-D-Glc*p* (**h**) and 1,4,6-linked *β*-D-Gal*p* (**g**).

Conclusions

The product obtained in the cultivation medium of *Limosilactobacillus fermentum* MM1V was identified as EPS (3.10×10^5 g mol^{-1}) consisted mainly of mannose, galactose, and glucose at the molar ratio of 2:2:1, and also contained galactofuranose and *N*-acetylated amino sugars. This polysaccharide will be characterised as potential prebiotic for food applications.

This work was supported by the Ministry of Agriculture of the Czech Republic (project QK22010186) and by Specific university research – grant No A1_FPBT_2023_006.

REFERENCES

1. Rajoka M. S. R., Shi J., Zhu J., Shao D., Huang Q., Yang H., Jin, M.: Appl. Microbial. Biotechnol. *101*, 35 (2017).
2. Mahdhi A., Leban N., Chakroun I., Chaouch M. A., Hafsa J., Fdhila K., Majdoub H.: Microb. Pathogenesis *109*, 214 (2017).
3. Chabot S., Yu H. L., De Léséleuc L., Cloutier D., Van Calsteren M. R., Lessard M., Oth D.: Le Lait *81*, 683 (2001).
4. Hongpattarakere T., Cherntong N., Wichienchot S., Kolida S.: Carbohydr. Polym. *87*, 846 (2012).
5. Salazar N., Ruas-Madiedo P., Kolida S., Collins M., Rastall R., Gibson G., de los Reyes-Gavilan C. G.: Int. J. Food Microbiol. *135*, 260 (2009).
6. Patel A. K., Michaud P., Singhania R. R., Soccol C. R., Pandey A.: Food Technol. Biotechnol. *48*, 451 (2010).
7. Sasikumar K., Vaikkath D. K., Devendra L., Nampoothiri K. M.: Bioresour. Technol. *241*, 1152 (2017).
8. Sørensen H. M., Rochfort K. D., Maye S., MacLeod G., Brabazon D., Loscher C., Freeland B.: Nutrients *14*, 2938 (2022).
9. Nguyen P. T., Nguyen T. T., Bui D. C., Hong P. T., Hoang Q. K., Nguyen H. T.: AIMS Microbial. 6, 451 (2020).
10. Mattia A., Merker R.: Clin. Infectious Diseases *46*, S115 (2008).
11. Hong T., Yin J. Y., Nie S. P., Xie M. Y.: Food Chem. X *12*, 100168 (2021).
12. Wiercigroch E., Szafraniec E., Czamara K., Pacia M. Z., Majzner K., Kochan K., K., Kaczor A., Baranska M., Malek K.: Spectrochim. Acta A Mol. Biomol. Spectrosc. *185*, 317 (2017).

THE INFLUENCE OF EXTRUSION COOKING ON THE FORMATION OF LIPIDO-AMYLOSE COMPLEXES

PETRA SMRČKOVÁ*, EVŽEN ŠÁRKA, MILENA KOSTENNIKOVA

UCT Prague, Department of Carbohydrates and Cereals, Technická 3, 166 28 Prague 6, Czech Republic

Petra.Smrckova@vscht.cz

Extruded corn grids with addition either amylose, stearic acid, or oleic acid were prepared on the KE 19/24 single-screw extruder. The extrusion process parameters were compression ratio of 2:1, screw speed of 110 rpm and die diameter of 4 mm. Milled extrudates were characterized by dry matter content, water absorption index (WAI), and water-soluble index (WSI), total and resistant starch. The pasting properties was measured using RVA. The change in crystallinity was verified using ATR-FTIR. The largest amount of amylose-lipid complexes is formed using 3% of stearic acid and 10% of amylose.

Introduction

The extrusion cooking is a technological process associated with heat treatment of raw materials. During the extrusion cooking the raw enzyme degradation, the naturally toxin and degradation and inactivation and the microbial load reduction took place. The raw material for extrusion cooking are mostly cereals, legumes, and native starches. The hot extrusion process converts the complex starches into the simple form and increase the glycaemic index of extruded products[2].

Although cereals and native starches are typically low in lipid content, small changes in lipid content can modify extrudate quality. Complexes between starches and lipids are due to the ability of the amylose fraction of starches to bind lipids such as fatty acids[1].

Fatty acids form inclusion complexes with amylose, and possibly with longer outer chains of amylopectin. Such complexes are not easily leached from the granule and inhibit entry of water into the starch granule. The amylose –lipid complexes also limits retrogradation by interfering with the formation of junction zones between starch molecules[6].

The extent of amylose-lipid complexes formation are depended upon the type of fatty acid (saturated or unsaturated) and the amylose content. It is also affected by the extrusion process parameters (screw speed and temperature) and the average particle size of raw materials[4].

Amylose-lipid complexes belong to resistant starch type 5 (RS5), which resists digestive enzymes and is thermostable. Resistant starch (RS5) is important for health, has properties similar to soluble dietary fibre, contributes to reducing body weight and serves to prevent cardiovascular diseases and the development of colorectal cancer[3].

The aim of this study was to prepare extruded products with a high content of resistant starch type 5 (RS5) and to analyse the effects of added fatty acids on resistant starch, on the structural and textural properties of corn-grid-based extrudates.

Materials and methods

Materials

Fine corn grits were kindly provided by the KONKORDIA Ltd. corn mill, Mrzkovice, Czech Republic. Armis olive oil (Greek) was bought on the local market. Stearic acid ≥ 98 % was obtained from Roth Ltd. (German). Amylose powder was purchased from Koch-light laboratories Ltd. (England).

Premix preparation

At first the corn grids were mixed with 18 % of water. In the next step, 0% or 10% amylose and the stearic or oleic acid 1.5 % and 3% were added, respectively. All ingredients mixed carefully over a 5-minute interval and

then left standing for 2 hours at laboratory room temperature. Composition of input mixtures for extrusion cooking is in tab. I.

Table I: **Composition of premixes for extrusion cooking**

Sample	Corn grids (g)	Amylose (g)	Stearic acid (g)	Oleic acid (g)	Water (g)
K	400	-	-	-	32
KS1.5	400	-	6	-	32
KS3.0	400	-	12	-	32
KO1.5	400	-	-	6	32
KO3.0	400	-	-	12	32
KA	400	48	-	-	35.8
KAS1.5	400	48	6.72	-	35.8
KAS3.0	400	48	13.44	-	35.8
KAO1.5	400	48	-	6.72	35.8
KAO3.0	400	48	-	13.44	35.8

The extrusion cooking processes

The extrusion of the wetted premix was achieved using a laboratory Compact KE 19/25 single-screw extruder (Brabender, Germany). The extruder consisted of a screw having a 2:1 compression ratio of 19 mm in diameter and 475 mm in length. An extruder screw speed of 120 rpm was used with a 4 mm die. The dosing screw was adjusted to 15 rpm. The temperature profil in the barrel held almost constant.

Moisture content

For determination RVA viscosity profile, WAI and WSI, the evaluation of moisture content of extruded products were necessary because its dose is dependent on the weight fraction of water present. In this study, the Precisa HA60 drying balance (Dietikon, Switzerland) was used, and 5.00 g of each sample was analysed in advance in two repetitions (operation time of a single measurement approx. 10 min).

Expansion index (EI)

The expansion index is used to express the expansion of extrudates. It is defined as the ratio of the diameter of the extrudate to the diameter of the die. Ten samples were measured nine times and an average was calculated. A digital Vernier calliper with a length measurement accuracy of ±0.01 mm was used. The expansion index (EI) was calculated by equation (1):

$$ER = \frac{D^2}{d^2} \qquad (1)$$

where D is the extrudate diameter (mm) and d is the die diameter (mm).

Water adsorption capacity (WAI) and water solubility index (WSI)

The WAI and WSI were measured following a method developed for cereals[4]. The extrudate was ground by a Perten 3100 laboratory mill (Sweden). The ground extrudates (2.000 ± 0.005 g) were then suspended in 25 ml of water at laboratory temperature and gently stirred. After 30 minutes the slurry was centrifuged at 3000 x g for 15 min. The supernatant was decanted into a dish of known weight and dried at 105°C for 12h. The WAI is

calculated as the weight of gel obtained after the removal of the supernatant per unit weight of dry origin sample. The WSI is expressed as gram of dissolved solid in supernatant per gram of solid dry samples.

RVA pasting properties measurement

The pasting properties of extrudates were determined on the Rapid Viscosity Analyser (RVA 4500, Perten Instruments, Australia). To measure the pasting properties the RVA method 13.04 was used. 3 g of finely-ground samples with moisture content14 % were mixed with 25 g of water in the aluminium container. Twenty-minute profile, with a lowered initial idle temperature were applied.

Resistant starch determination

To determine resistant starch, the "Resistant starch assay procedure" enzyme kit from Megazyme (Ireland) was used. The assay procedure is based on standard international methods (AOAC method 2002.02 and AACC Method 32-40.01). Briefly, the samples were incubated with pancreatic α-amylase and amyloglucosidase. The non-resistant starch was solubilized and hydrolysed to D-glucose. D-glucose was washed out from samples by aqueous ethanol solution (50% v/v), followed by centrifugation. Supernatant was removed and collected to determine non-resistant starch. The RS remains in the pellets. The pellets were treated by 2 M KOH to involved RS. After the neutralization by an acetate buffer and addition of amyloglucosidase the RS starch hydrolyses to glucose took place. D-Glucose in collected supernatants and in hydrolysed pellets were measured after addition of glucose oxidase/peroxidase reagent on the UV/VIS spectrometer at wavelength 510 nm. The content of total starch was calculated as sum of non-resistant content and resistant starch content.

FTIR-ATR

A Fourier transform infrared spectrometer (FTIR spectrometer Nicolet 6700, Thermo Fisher Scientific, USA) and an attenuated total reflection (ATR) technique were used to characterize the molecular and structural properties of the milled extrudates. The tablet contains a small amount of the analysed sample and KBr were prepared on the manual press. The spectra were measured in the wavenumber range 4000-400 cm-1 with a resolution of 2 cm^{-1} and with the number of scans 64.

Statistical analysis

The data as both characteristic points and curve data lines were set as averages; before that, ANOVA was applied at the probability level P = 95%, using the Statistica 13.1 software (Tulsa, USA).

Results and discussion

This chapter deals with the evaluation of the results of analyses performed on a set of samples that were prepared using extrusion cooking. Premixes for this extrusion cooking were prepared by mixing cornmeal with either stearic acid or oleic acid and amylose. The description of individual samples prepared by extrusion cooking is given in tab. 1.

The measured values of dry matter and moisture are shown in tab. II. The moisture content of the extrudates ranged from 8.62 to 11.03%. The lowest moisture content was recorded for sample K (without addition of acid), on the contrary, the highest for sample KAO3.0 (addition of 3% oleic acid and amylose).

Tab. II: **Analyses results of Dry matter content, WAI, WSI, RS a TS**

sample	Dry matter content (%)	WAI (-)	WSI (-)	*x*RS (%)	*x*TS (%)
K	88.97 a	5.08 a	0.28 d	1.00 e	71.47 b
KS1.5	89.32 a	5.11 a	0.25 cd	2.96 d	77.10 acd
KS3.0	89.73 ab	5.00 a	0.21 bc	3.29 ad	71.97 b

KO1.5	89.75	ab	5.40	cd	0.16	ab	2.49	f	73.36	ab
KO3.0	89.82	ab	5.32	c	0.16	ab	3.48	ab	77.23	acd
KA	90.12	ab	5.46	d	0.19	ab	6.83	c	76.41	ac
KAS1.5	90.04	ab	4.81	b	0.16	ab	7.07	c	74.92	ab
KAS3.0	90.36	ab	4.73	b	0.16	a	7.19	c	73.94	ab
KAO1.5	90.37	ab	5.95	f	0.17	ab	3.45	ab	81.34	d
KAO3.0	91.38	b	5.59	e	0.18	ab	3.79	b	80.60	cd

a-f) for individual tested samples means with the same label are not statistically different (P = 95%)

The water solubility index (WSI) is an indicator of the degree of conversion and molecular degradation of starch, it measures the content of soluble components released from starch after extrusion. Addition of free fatty acids reduce WSI because amylose–lipid complexes are insoluble[5].

The fatty acids content increases caused the WAI value decreases, due to insolubility of amylose-lipid complexes. The formation of amylose-lipid complex during extrusion is higher for stearic acid than for oleic acid. We consider the differences in WSI values to be statistically insignificant on α=0.5 significance level.

The calculated values of the content of resistant and total starch are shown in tab. 1. The content of total starch was statistically significantly affected by the addition of amylose, but the addition of fatty acid was no effect.

The highest content of resistant starch was recorded in sample KAS3.0 (addition of 3% stearic acid and amylose) and is equal to 7.19%, while the lowest content is 1.00% in sample K (without fatty acid addition). In general, as the addition of fatty acids increases, the content of resistant starch increases, and more amylose-lipid complexes are formed in case addition of stearic acid.

Extrusion cooking is a process in which the starch present in corn grids is thermally and mechanically modified. The starch material liquefied by high temperature and pressure inside the extrusion barrel is pushed through the die and immediately expanded. This process is associated with the formation of a disordered (amorphous) structure of starch. It caused the partial starch solubility in cold water. On the RVA curve, it corresponds to the Cold Peak (CP) parameter. CP is a viscosity on the start of test at the temperature of 25 °C. Due to the relatively low water content in the premixes, a small amount of starch in the extrudates does not gelatinize and remain in the granular form. This is resulted on the RVA curve in the Raw peak (RP). RP is a maximum of hot paste viscosity at temperature between 90 and 95 °C.

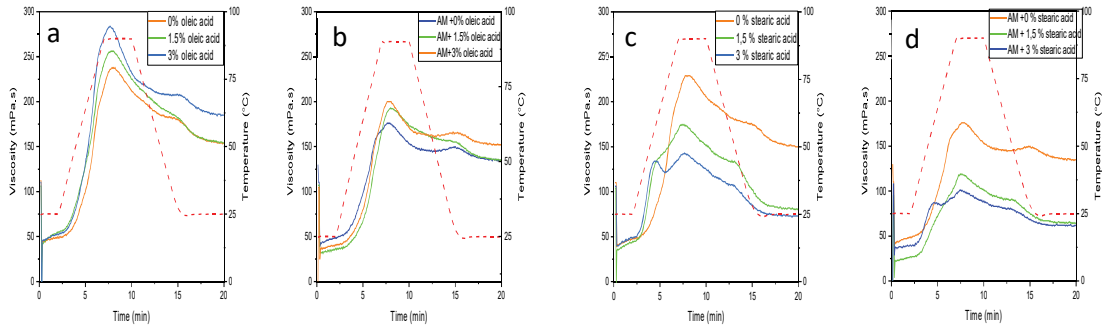

Fig. 1: **Viscosity profiles of extrudates: a) addition of 0, 1.5 and 3% oleic acid b) additions of 0, 1.5 and 3% oleic acid and amylose c) addition of 0, 1.5 and 3% stearic acid d) additions of 0, 1.5 and 3% of stearic acid and amylose.**

The addition of fatty acids and amylose to the extrusion mixtures affected the rheological properties of the extruded products. Viscosity profiles of extrudates with different fatty acids and added amylose are shown in Fig.

1. A significant effect ($p < 0.05$) of extrusion cooking on the RP was observed. A decrease in RP and the FV was observed for samples containing stearic acid on the other hand oleic acid do not decrease these parameters significantly. Cervantes-Ramírez et al.[7] refer similar behaviours in their study.

Thachil et. al.[4] suggested that the addition of a lipid component to the extrusion mixture would result in increased hydrophobicity of the granules, leading to a reduced ability of the granules to take up water as well as reduced swelling of the starch granules during gelatinization.

The final viscosities of tested samples showed different behaviour depending on the type of fatty acids and the amount of amylose added. Gelatinization temperatures of extruded corn grits with the addition of oleic acid and amylose were statistically the same as the paste temperatures of samples without fatty acids and amylose. However, for stearic acid, the degreasing temperature is not defined, suggesting that starches interacted with lipids and prevented starch hydration. Similar results were reported in a study by Cervantes-Ramírez et al[7].

FTIR-ATR Spectroscopy provides information on the chemical composition and structure of the material, FTIR can help optimize processing conditions and improve the quality of the final product[9].

The region of the infrared spectrum from 1200 to 700 cm^{-1} is called the fingerprint region, which indicates the presence of carbohydrate fragments.

The range of frequencies around 1000–1100 cm^{-1} is mainly attributed to starch groups. The major bands associated with proteins are generally associated with peaks at 1640 cm^{-1} and are attributed to amide bonds.

According to Wang[9] the adsorption bands at 1705 cm^{-1} and 2845 cm^{-1} correspond to the vibration of the carbonyl group and the asymmetric vibration of the CH_3 and CH_2 fatty acid groups. Bands at 2922, 2853 cm^{-1} (symmetric and asymmetric stretching of CH_2) and 1745 cm^{-1} (stretching of carbonyl group esters) are associated with bond vibrations originating from lipids present in the samples[10].

One of the main changes in the FTIR spectra during the extrusion cooking process is indicated by Cueto[10] the disappearance of the adsorption band at 1710 cm^{-1} and the formation of a new one at 1745 cm^{-1} (after extrusion cooking). This could be related to the ester carbonyl vibration of lipids interacting with other components (proteins or carbohydrates) that are altered by the extrusion cooking process and shift the signal to higher wavenumbers.

Specific values of adsorption bands for individual samples are shown in tab. III and Fig 2.

Tab. III: **Wavenumber of characteristic vibrations of the main bonds and groups of extrudates**

Wavenumber (cm^{-1})	Wavenumber interval	Band assignments	Band description	Next bands
3415	3550 - 3230	ν(OH)	-OH, dimers a polymers	1440-1290
2922	2955 - 2915	$\nu_{as}(CH_2)$	-(C)-CH_2-, -(O)-CH_2	2880-2835
2853	2895 - 2840	$\nu_s(CH_3)$	-(C)-CH_3-, -(O)-CH_3	1470 - 1385
1745	1750 - 1720	ν(C=O)	-CO-O-stretching of carbonyl group esters	1300 - 1150
1646	1650 - 1615	$\delta(H_2O)$	H–O–H (bend)	-
1021	1085 - 1050	ν_s(COC)	R-CO-O-R', saturated.	-
933	955 -915	γ(OH)	skeletal mode vibration of α-1,4 glycosidic linkage (C–O–C)	-

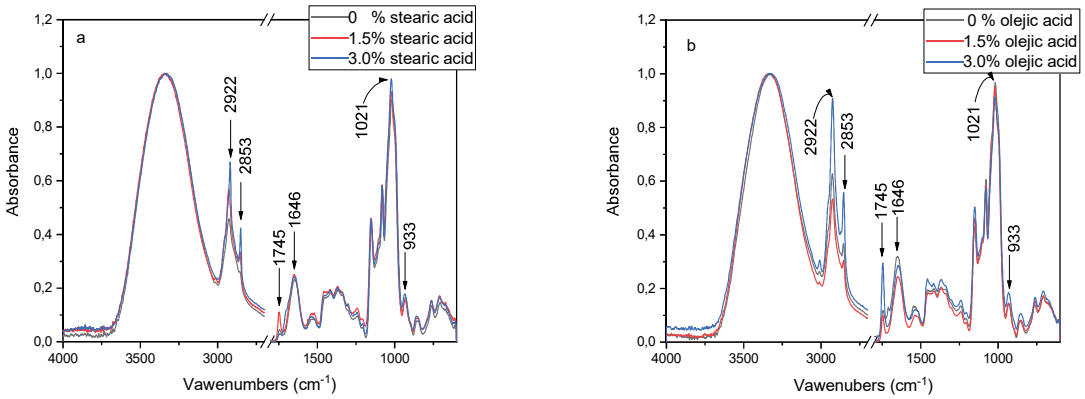

Fig. 2: **FTIR spectra of extruded samples a) addition of 0, 1.5 and 3% stearic acid, b) addition of 0, 1.5 and 3% oleic acid**

Conclusion

The analyses performed in this study showed that stearic acid (a saturated fatty acid) more easily forms complexes with amylose than oleic acid (an unsaturated fatty acid), more amylose-lipid complexes were formed under the influence of stearic acid with the addition of amylose to corn grits, which was also manifested by a significant increase in the content of resistant starch in the extrudate with the addition of amylose and stearic acid (7.19%).

The addition of free fatty acids reduces WSI and WAI because the amylose–lipid complexes are water insoluble. The rheological properties of the extruded products were tested on the rapid viscosity analyser (RVA). The addition of fatty acids and amylose to the extrusion mixtures affected the Raw Peak (RV) and Final Viscosity (FV).

The addition of saturated fatty acids to cereal materials with high amylose content may improve the health benefit of extruded products. Some of the saturated fatty acids in the foodstuff are considered to be of little in the nutritional benefit. The amylose- lipid complexes formation in foodstuff during extrusion can reduce both the energy value of the extruded products and their health risk.

REFERENCES

1. Bhatnagar S. and Hanna M. A.: Cereal Chem., *71*, 582 (1994).
2. Shelar G. A. and Gaikwad S. T.: The Pharma Innovation Journal, *2,* 8, (2019).
3. Panyoo A. E. and Emmambux M. N.: Starch - Stärke, *7-8,* 69, (2017).
4. Thachil M. T., Chouksey M. K., and Gudipati V.: International Journal of Food Science & Technology, *2,* 49, (2014).
5. Desrumaux. A., Bouvier J. M., and Burri J.: Cereal Chem., *76*, 699 (1999).
6. Daniel J. R., Whistler R. L., Röper H., and Elvers B. in*: Ullmann's Encyclopedia of Industrial Chemistry,* Starch, p. 6. John Wiley & Sons, Hoboken, New Jersey, USA, 2007.
7. Cervantes-Ramírez, J.E; Cabrera-Ramirez, A.H, Morales-Sánchez, E.; Rodriguez-García, ME; Reyes-Vega, M.D.; Ramírez-Jiménez, AK; Contreras-Jiménez, BL; Gaytán-Martínez, M.: Carbohydrate Polymers, *246*, p. 116 (2020).
8. Yan, X.X.; Kou, L.H.; Wei, H.Y.; Ren, L.L.; Zhou, J.: Industrial Crops and Products, 145, p. 112 (2020).
9. Wang, S.; Li, C.; Zhang, X.; Copeland, L.; Wang, S.: Scientific Reports, *6*, p. 209 (2016).
10. Cueto M., Farroni, A., Rodriguez S. D., Schoenlechner R., Schleining G., Buera P.: Food and Bioprocess Technology, 11, pp. 1586 (2018).

EXTRACTION AND CHARACTERIZATION OF POLYSACCHARIDES FROM RYE BRAN

BARBORA STÝBLOVÁ*, ROMAN BLEHA, ANDREJ SINICA, MARCELA SLUKOVÁ, IVAN ŠVEC, PAVEL SKŘIVAN

Department of Carbohydrates and Cereals, University of Chemistry and Technology Prague, Technická 5, 16628 Prague, Czech Republic

Barbora.Styblova@vscht.cz

Abstract

This work aimed to isolate and determine the structure of crude, mainly water-soluble, polysaccharide fractions from rye bran. Crude cold and hot water extracts were obtained and purified with a combination of pepsin and amylase to remove proteins and starch, and then alkaline extraction was carried out. The crude polysaccharide fractions were analysed for purity, chemical composition, and structure using FTIR spectroscopy, and the neutral sugars and linkages were determined by GC/FID and GC/MS, respectively.

Introduction

Rye is a traditional cereal in Europe using to bake bread[1]. Whole rye grains contain various polysaccharides, including starch, cellulose, "mixed-linkage" β-glucans and arabinoxylans (AXs)[2-4]. There are two groups of AXs, e.g., water-soluble (extractable with water) and insoluble (extractable with alkali solution like 1M NaOH)[5]. Both groups exhibit several biological activities such as antioxidant, immunomodulation, and antiglycemic6.

The present study focused on isolation and structural characterisation of crude polysaccharide fractions obtained from rye bran using spectroscopic and separation methods.

Experimental

Samples

Commercial rye bran was provided by Natural Jihlava JK s.r.o. (Jihlava, ČR).

Preparative Procedures

Lipids and other molecules, such as phenolic compounds and oligosaccharides, were removed from milled rye bran by successive washing with hexane, ethanol, and acidic ethanol (0.2 mol l^{-1} HCl). Furthermore, the crude extracts were then obtained by successive extractions with cold water, hot water (100 °C under reflux) and an alkali solution (1 mol l^{-1} NaOH, 4 °C) (Fig. 1).

The aqueous extracts CWE – cold water and HWE – hot water was precipitated with an excess of ethanol (4:1 v/v), centrifuged, washed with 80%, 96% ethanol and acetone and dried in air. The alkaline soluble and insoluble products AE and SR were neutralised by washing with acidic ethanol and 80% ethanol until the neutral reaction, then washed with 96% ethanol, acetone and dried in air. The proteins of the cold-water extracts were removed with the enzyme pepsin, the collected fraction was dialysed in 1000 Da membranes against distilled water for three days and lyophilised. A similar procedure was used for HWE, but in this case α-amylase was used to remove starch and was also dialysed. These two purified fractions were further analysed with FTIR, GC/FID, and GC/MS.

Analytical Methods

FT-IR spectra (a spectral region 400–4000 cm^{-1}) of purified extracted fractions were recorded in KBr pellets using a Nicolet 6700 FT-IR spectrometer (ThermoScientific, USA); 64 scans were accumulated with a spectral resolution of 2.0 cm^{-1}. The spectra were smoothed, and the baseline was corrected using Omnic 8.0 and 9.0 (ThermoScientific, USA). Finally, all spectra were exported in ASCII format to Origin 6.0 (Microcal Origin, USA) software for preparation of the final graphs[7].

The chemical analysis of the extracts was performed by neutral sugar analysis. Sugars were released by acid hydrolysis in 72% H_2SO_4 and analysed as alditol acetates by GC/FID using a Shimadzu GC2010 (Japan) equipped with a 30 m capillary column DB-225 with an internal diameter of 0.25 mm and a film thickness of 0.15 µm.

Injector and detector temperatures were, respectively, 220 ˚C and 230 ˚C. The oven temperature programme was as follows: 200 ˚C for 1 min, then rose to 220 ˚C (40 ˚C/min), temperature 220 ˚C for 7 min, then increased to 230 ˚C (20 ˚C/min) until, the final temperature 230 ˚C for 1 min, total time 9 min[7].

A Shimadzu GC2010 SE gas chromatograph (Japan) was coupled to a mass spectrometer with EI ionisation 70 eV and mass range 50 to 650 amu using a scan time of 1 s. Sugar linkage analysis of polysaccharide fractions was performed using the Ciucanu's and Purdie's methods[8,9]. The permethylated products were hydrolysed with 2M TFA at 120 °C for 1 h, followed by reduction with $NaBD_4$ and acetylation. The partially methylated alditol acetates were analysed by GC/MS.

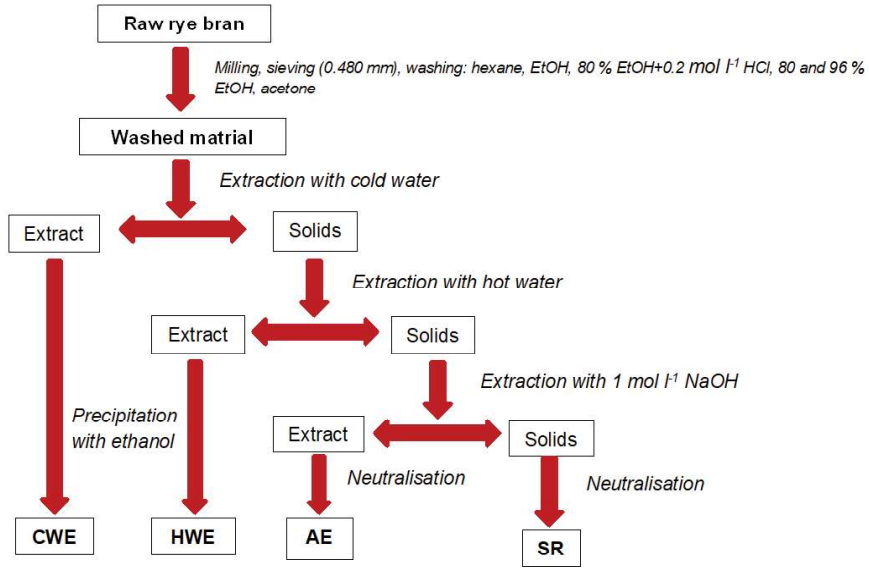

Fig. 1: **Extraction of crude polysaccharide fractions from rye bran**

Results and Discussion

Yields of the crude extracts CWE, HWE and AE and solid residues SR are demonstrated in Table I. The masses of the water-soluble products significantly decreased after the treatment with hydrolytic enzymes. On the basis of the proposed extraction and purification procedure, the main non-starch polysaccharide fractions were obtained.

The monosaccharide composition of the crude products is shown in Table II. Glucose was the main monosaccharide in HWE (89 mol %) and SR (66 mol %), while xylose predominated in CWE (47 mol %) and AE (66 mol %). High amount of glucose confirmed the presence of water-soluble glucans in HWE and cellulose in SR. CWE also has high amount of arabinose (29 mol %) followed by glucose (21 mol %). By contrast, AE contained many glucose (27 mol %) but only few arabinose. Thus, AX is the major component of CWE, but HWE probably contained xylan and xyloglucan. SR also contained comparable amounts of xylose, arabinose, and mannose (8–15 mol %) originated from hemicelluloses.

According to the results of the methylation analysis, the purified CWE is mainly AX with some glucans and composed mainly of 1,4-linked Xyl*p*, 1,3,4-linked Ara*f*, 1,4-linked Glc*p*, t-Ara*f* and 1,3-linked Glc*p*. These results are similar to those of Fadel et al.[3] However, purified HWE was structurally different. The main part was t-Glc*p*, 1,4-linked Glc*p*, 1,4-linked Xyl*p*, t-Ara*f*, 1,6-linked Glc*p*, fully substituted Xyl*p* and, as minors, t-Ara*p*, t Gal*p*, 1,3,4-linked Xyl and 1,4,6-linked Glc. These results confirm the previous description from neutral sugar determination and FTIR. These results are supported by Fadel et al.[3] where they describe the presence of starch and β-glucan.

Table I: **Yields of the crude and purified fractions obtained from rye bran**

Fraction	Crude fractions		After proteases	
	m (g)	Yield (% w/w)	*m* (g)	Yield (% w/w)
Raw rye bran	133.12	100		
Washed rye bran	87.18	65.49		
CWE	1.46	1.10	0.62	0.46
HWE	9.05	6.80	0.18	0.13
AE	1.71	1.28		
SR	1.37	1.03		

Table II: **Monosaccharide composition of rye bran, crude and purified fractions obtained from them**

Fraction	Molar ratio [mol %]						
	Fuc	Ara	Man	Glc	Gal	Rha	Xyl
CWE	1	**29**	0	**21**	1	1	**47**
HWE	2	4	0	**89**	0	0	5
AE	1	4	1	**27**	1	0	**66**
SR	2	**11**	8	**61**	2	0	**15**

The FTIR spectra of the crude fractions obtained from the rye bran (Fig. 2) all have a distinct band for the O-H stretching vibration centred at 3396-3419 cm^{-1}. The band at 2921-2927 cm^{-1} is related to the stretching vibration of C-H bonds[11]. Two bands at 1652-1658 and 1531-1542 cm^{-1} indicate the presence of proteins in some crude extracts. Bands in the range 1450-1200 cm^{-1} corresponded to in-plane ring deformations of C-OH, O-CH, or C-C-H groups[12].

According to González-Estrada[15], typical absorption bands of polysaccharides appear between 1200 and 800 cm^{-1}. The rye bran and fractions have the first prominent band in this region at 1153-1160 cm^{-1}, which corresponds to C-O-C stretching in glycosidic bonds[11], and a distinct band at 1078-1081 cm^{-1}, which represents the stretching vibration of C-O and C-C bonds. CWE and AE also have the most pronounced peak of AX at 1043 cm^{-1} representing the coupled stretching vibration of C-O and C-C bonds and C-OH deformations in the ring[13], while the rye bran and HWE demonstrated a starch band at 1022-1027 cm^{-1}, which also represents the valence vibration of CO bonds[16]. The bands at 850-856 and 896-900 cm^{-1} are related to the (1→4) bonds in α-anomeric and β-anomeric forms of carbohydrates, respectively[11,14]. The band at 825 cm^{-1} for rye bran and 808 cm^{-1} for CWE corresponds to skeletal vibrations[17].

FTIR spectra of crude and purified CWE compared to the spectrum of AX standard prove that this fraction is almost pure AX, but when neutral sugars are determined, the presence of glucans is also evident. In contrast, the FTIR spectrum of untreated HWE has many starch bands compared to the spectrum of this polysaccharide. After purification, the starch bands have decreased or disappeared, but some starch residue is still present. We should repeat the purification step but with pullulanase after α-amylase. HWE more or less lacks proteins and AX.

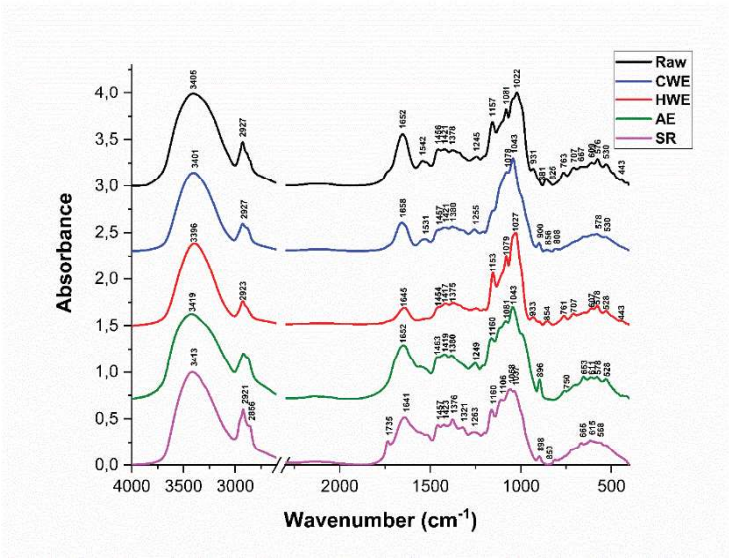

Fig. 2: **FTIR spectra of raw rye bran and derived crude extracts CWE, HWE and AE and insoluble solids SR.**

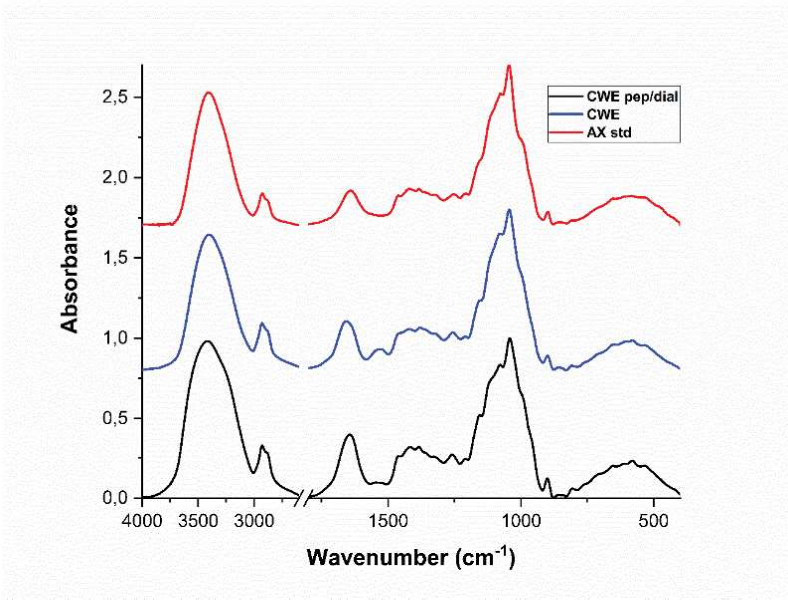

Fig. 3: **FTIR spectra of crude and purified CWE compared to the standard of AX**

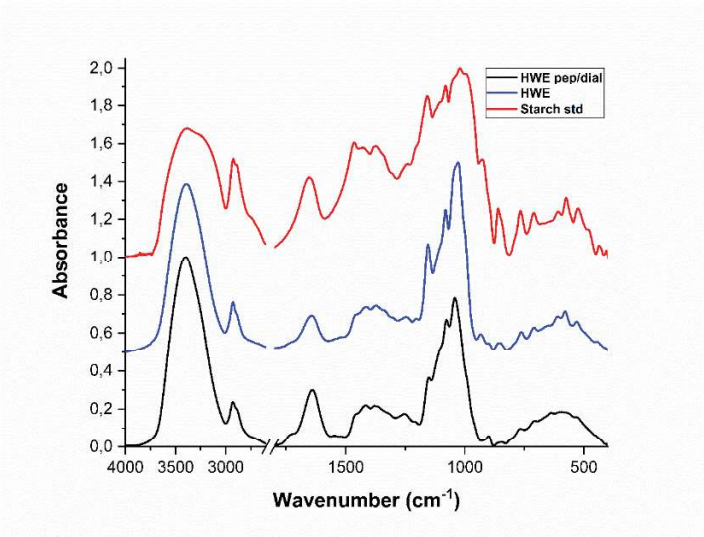

Fig. 4: **FTIR spectra of crude and purified HWE compared to the standard of starch**

Conclusions

The water-soluble and insoluble polysaccharides of the rye bran were extracted and partially characterised. Comparing the FTIR spectra of raw rye bran and crude extracts as well as purified extracts with standard polysaccharides and the results of monosaccharide composition and linkage analysis, the identified polysaccharides were as follows: (i) cold water extract was a mixture of arabinoxylan and "mixed-linkage" β-glucan, (ii) hot water extract consisted mainly of α-glucan (starch), which was then partially removed by amylase, (iii) alkaline extract contained xylans or xyloglucans, (iv) solid residues consisted of cellulose and hemicelluloses such as branched arabinoxylan retained in the solid state after alkaline extraction.

REFERENCES

1. Hansen H. B., Rasmussen C. V., Knudsen K. E. B., Hansen A.: J. Sci. Food Agric. *83* (2003).
2. Hansen H. B., Moller B., Andersen S. B., Jorgensen J. R., Hansen A.: J. Agric. Food Chem. *52*, 8 (2004).
3. Fadel A., Mahmoud A. M., Ashworth J. J., Li W., Ng Y. L., Plunkett A.: Int. J. Biol. Macromol. *109* (2018).
4. Muralikrishna G., Subba Rao M. V. S. S. T.: Crit. Rev. Food Sci. Nutr. *47* (2007).
5. Vinx C. J. A., Delcour J. A.: J. Cereal Sci. *24* (1996).
6. He H.-J., Qiao J., Liu Y., Guo Q., Ou X., Wang X.: J. Agric. Food Chem. *69*, 51 (2021).
7. Bleha, R.; Třešňáková, L.; Sushytskyi, L.; Capek, P.; Čopíková, J.; Klouček, P.; Jablosnký, I.; Synytsya, A.:
8. Molecules, *24* (2019).
9. Ciucanu, I., Kerek, F.: Carbohydr. Res. *131* (2), 209 1984.
10. Purdie, T., Irvine, J. C.: J. Chem. Soc. Trans. *83*, 1021 (1903).
11. Wang L., Zhang L., Qiu S. et al.: J. Cereal Sci. *88* (2019).
12. Kowalska G., Rosicka-Kaczmarek J., Miśkiewicz K. et al.: Food Bioprod. Proces. *130* (2021).
13. Paz-Samaniego R., Méndez-Encinas M., Fierro-Islas J.M. et al. (2014): Ferulated arabinoxylans recovered from low-value maize by-products: Gelation and antioxidant capacity (151-164).
14. Morales-Ortega A., Carvajal-Millan E., López-Franco Y. et al.: Molecules *18*, 7 (2013).
15. González-Estrada R., Calderón-Santoyo M., Carvajal-Millan E. et al.: Molecules *20*, (6) (2015).
16. Argun M.Ş., Kılınç B., Yazıcı E. et al.: J. Cereal Sci. *109* (2023).
17. Agil R., Hosseinian F.: J. Food Compos. Anal. 34, 1 (2014).

PHYSICAL PROPERTIES AND ANTIOXIDANT ACTIVITY OF SODIUM ALGINATE-BASED EDIBLE FILMS INCORPORATED WITH KOMBUCHA

BILGE TASKIN*

DRIFT-FOOD, Faculty of Agrobiology, Food and Natural Sources, Czech University of Life Sciences Prague, Kamycka 129 Prague Suchdol 165 00

taskin@af.czu.cz

Abstract

This research explores developing edible films based on sodium alginate incorporated with green tea kombucha (10%, 20%, and 30%, v/v), assessing their physical characteristics, color, and antioxidant activity. Kombucha incorporation at high levels significantly reduced film thickness and puncture strength, potentially due to altered intermolecular interactions. Films exhibited altered color, becoming darker and less reddish, notably with higher incorporation levels resulting in more pronounced color changes. Importantly, a substantial enhancement of antioxidant activity in films was determined as the kombucha content increased, indicating its preventive potential against free radicals.

Introduction

Edible films and coatings have the potential to replace synthetic and traditional packaging since they are more ecologically friendly, biodegradable, and safer than typical polymeric materials [1]. These are the formulations of solutions containing different components such as solvents, polymers, plasticizers, surfactants, active compounds, and enhancement ingredients [2]. The target effect of the edible films mostly depends on the type, nature, and structure of the foods to apply, and the function of the films can be modified or improved by incorporation of various agents. The addition of active agents from different sources to these packaging materials may act as oxygen and carbon dioxide blockers [3], improve barrier features [4], modify the physicochemical properties [5], and contribute nutritional value as well as sensorial quality [2,6]. The inclusion of antimicrobial agents and antioxidants may slow down food spoiling and increase shelf life [7], therefore, embracing alternative sources of bioactive compounds will make valued contributions.

The importance of nutrition in preserving well-being and optimal health is becoming more well-known. In addition to providing them with vital nutrients, consumers anticipate that the goods will contain biologically active ingredients that are good for their health. Kombucha is one of them that has emerged among consumers with this perspective. It is a tea beverage that is fermented using a bacterial and yeast symbiotic culture, usually resulting in a suspending layer of microbial cellulose mass [8]. Detoxification, energizing, and immune-stimulating are some of the evidenced physiological activities [9], besides the antioxidative, antimicrobial, antibacterial and antiproliferative potential [10]of kombucha drinks, as was also the case for acting on blood glycaemia, diabetes-induced weight loss, and gastric disorders [11]. Kombucha of different raw materials, nutritional features and sensory characteristics is being served to consume in the markets. It is well reported that phenols, polyphenols, organic acids, alcoholic compounds, vitamins, minerals, and antioxidant power of kombucha drinks are prominent, however, the degree and content of these are showing great variability depending on the substrate, microbial composition, fermentation time, and conditions [12]. Sodium alginate (SA) is a polymer extracted from algae that has a high film-forming ability which makes it a promising natural edible film material. There are some attempts to improve the physiochemical or nutritional characteristics of edible films or coatings made up of sodium alginate or its composite forms [13–15]. The aim of this study was to develop a novel edible film based on sodium alginate incorporated by green tea kombucha. The effects of adding kombucha on some physical properties, color, and antioxidant activity were evaluated.

Material and method

Materials

Sodium alginate was purchased from AppliChem Panreac (Darmstadt, Germany). Kombucha from green tea was produced according to a previous method [16] . The culture for fermentation was obtained from local producers.

Glycerol bidistilled and sodium carbonate, calcium chloride, and methanol were obtained from VWR International (Leuven, Belgium), and Folin-ciocalteu reagent was purchased from VWR International (France). 2,2-diphenyl-1-picrylhydrazyl (DPPH) reagent, trolox (Thermo Fisher Scientific, USA) and gallic acid (sigma, Steinheim, Germany) were the other used chemicals.

Film preparation

Edible films were prepared according to a previously published method [17], with modifications. For this, 2 g of sodium alginate was mixed with 100 mL distilled water and stirred at 50 °C for 30 min to dissolve it completely. Then, 1.2 g of glycerol as a plasticizer was added to the mixture and stirred for 15 min. The prepared kombucha liquid (at the second day of fermentation, filtered) was added to the resulting mixture at the concentrations of 0% (SA), 10% (SA10), 20% (SA20), and 30% (SA30) (v/v of mixture), and the final mixture was homogenized (11000 rpm) using a high-speed homogenizer (Ultra turrax, IKA T 25 Digital). The degassing function of the ultrasound machine (Elmasonic Easy 100H, Fisherbrand) was used to remove the bubbles formed. Finally, 25 gr of film-forming solutions were poured into a series of acrylic petri dishes (diameter 9 cm) and were dried at 25 °C and at 55% relative humidity (RH) for 36 h. Dried films were peeled-off and conditioned in a desiccator at room temperature for 2 days before testing.

Thickness

The thickness of the films was determined using a caliper micrometre (Kinex, model 6000, Czech Republic). For this purpose, measurements were made at five different points in each film and the results were calculated on average.

Puncture strength

The puncture strength was measured according to a method described earlier [18]. A texture analyser with a load cell of 50 N (EZ-SX, Shimadzu, Japan) and a puncture probe of 2 mm in diameter was employed to test. The film was placed on a circular holder (r=2 cm), and the probe was driven (speed was 1.0 mm/sec) through the film until it punctured. The force (N) at the point of rupture was recorded as puncture strength.

Color and transparency

The values of *L** (100: lightness, 0: darkness), *a** (+*a*: redness, -*a*: greenness), and *b** (+*b*: yellowness, -*b*: blueness) of obtained films were measured with a spectrophotometer (Konica Minolta CM 700d, NC, Japan). Five replicate measurements were taken from different points for each sample, and before each replication set the colorimeter was calibrated.

The film transparency was determined by following the method of Kurt and Kahyaoglu (2014) [19]. The samples were cut into pieces of circular shape that fit on the plate's test wells and placed over these test wells. The absorbance was read at 600 nm (Synergy H1 Hybrid Reader, BioTek, Vermont, USA) and the empty test well was used for reference value as a blank. The transparency was calculated from the equation below,

$$T = A_{600} / t$$

where T is the transparency (Abs /mm), A600 is the absorbance at 600 nm, and t is the thickness of the film in mm. High T values signify a high degree of opacity and poor transparency. The average results of three applied replicates were taken.

DPPH free radical scavenging assay

A previous method[17] was followed with slight modifications. Thirty mg of film, 3 mL of distilled water and 3 mL of methanol were mixed and centrifuged at 7000 rpm for 5 min after totally dissolved. A sample of 100 µL supernatant and 4 mL of DPPH solution (0.1mM, in methanol) was mixed and kept in the dark for 20 min before reading its absorbance at 515 nm in the spectrophotometer. A volume of 50 µL water and 50 µL methanol was mixed with 4 mL of DPPH solution (0.1mM, in methanol) to prepare the control solution. The DPPH inhibition percentage was calculated as per the following equation where, Ac is the absorbance of the control solution and as is the absorbance of sample, at 515 nm.

DPPH radical inhibition (%) = ((Ac-As)/Ac))*100

Statistical analysis

All experiments were carried out at least in triplicates. The experimental data were given as mean ± standard deviation. Data was subjected to the analysis of variance (ANOVA) using SPSS 22 (IMB, NY, USA). The statistical significance of the terms and comparison of the means were determined by using Duncan's multiple range test at the significance level of p = 0.05.

Results and discussion

Thickness and puncture strength of the films

Table 1 presents the effects of different concentrations of kombucha media on the thickness, puncture strength, color, transparency, and DPPH antioxidant activity properties of sodium alginate films. The incorporation of kombucha affected the thickness of the films significantly ($p<0.05$), and the addition of a higher amount of kombucha liquid resulted in thinner films. It is possible that the addition of kombucha liquid (v/v) led to more dilute film solutions, thereupon reducing the thickness content of the films due to declining solids concentration. This finding could be related to the less organized network [20] of soldium alginate films produced at the highest kombucha levels. Shahrampour et al. (2020) Also observed a reduction in film's thickness by increasing the alginate ratio from 25 to 75%. Similar to our findings, in another study thicker films that were based on gum ghatti were obtained at higher plasticizer (glycerol and sorbitol) concentrations [21]. The thickness of a film is determined by its composition, nature, and preparation process, as well as drying conditions [15]. Also, it is known that prominent compounds like polyphenols and bacteria can interfere with the creation of biopolymer networks and/or change the solids content of the films [20,22].

The mechanical properties i.e., puncture strength, are worthy for understanding material behavior. Puncture resistance, which describes film rigidity, is the greatest force required to break the film by a penetrating tip. The addition of kombucha had a significant negative impact ($p<0.05$) on the puncture strength which is related to the mechanical strength of the films. The lowest puncture strength was measured with the highest incorporation level (30%) (Table I). It is possible that, in acidic conditions, the carboxylic acid groups in sodium alginate can become protonated, leading to weakened intermolecular interactions between polymer chains. This can result in a reduction in the overall strength of the film, making it more susceptible to puncture. Low puncture strength [23], and low mechanical strength [24] at low pH levels were recorded before, and high-molecular-weight organic acids were found to impair intermolecular reactions which lower the film strength. It was found that high kombucha incorporation levels would impair the puncture strength of the film which is supposed to protect the food during handling, storage, or transportation.

Table I: **Thickness, puncture strength, color, transparency, and DPPH inhibition properties of edible films**

Sample code	Thickness (mm)	Puncture strength (N)	*L** value	*a** value	*b** value	ΔE	T (Abs/mm)	DPPH inhibition (%)
SA	0.13 ± 0.009[a]	7.36 ± 0.82 [a]	54.52 ± 1.03 [a]	0.413 ± 0.02 [a]	0.71 ± 0.04[d]	2.77 ± 0.24 [c]	0.754 ± 0.022 [c]	5.40 ± 1.1[d]
SA10	0.13 ± 0.008 [a]	4.96 ± 0.88 [b]	53.03 ± 0.93 [ab]	0.39 ± 0.05 [a]	1.96 ± 0.11[c]	3.01 ± 0.68 [bc]	0.783 ± 0.005 [c]	28.14 ± 2.0[c]
SA20	0.11 ± 0.009 [b]	3.84 ± 0.47 [c]	52.53 ± 0.92 [b]	0.161 ± 0.04 [b]	2.45 ± 0.24[b]	3.67 ± 0.25 [b]	0.913 ± 0.020 [b]	39.65 ± 2.3[b]
SA30	0.10± 0.011 [c]	3.04 ± 0.60 [c]	50.66 ± 0.81 [c]	0.092 ± 0.02 [c]	3.69 ± 0.23 [a]	5.51 ± 0.46 [a]	1.263 ± 0.043 [a]	52.28 ± 1.6[a]

Values are presented as mean ± standard deviation. Data in the same column with different superscript letters are statistically different ($p<0.05$). SA: sodium alginate film without kombucha, SA10, SA20, SA30: sodium alginate films with 10%, 20%, and 30% kombucha, respectively. T: transparency.

Color and transparency of the films

Color and transparency of the edible films are critical parameters as they affect the food quality, appearance, and consumer perception. The addition of kombucha liquid significantly ($p<0.05$) decreased the value of L^* and a^* while increasing the value of b^* (Figure 1). These indicate that the incorporated film samples became darker, yellowish, and less reddish compared to control films SA (0%). Further, the inclusion of 30% created the highest total color difference among the films. While there were slight changes in the color and brightness of SA-kombucha films, the overall alteration in appearance was relatively limited (Figure 2).

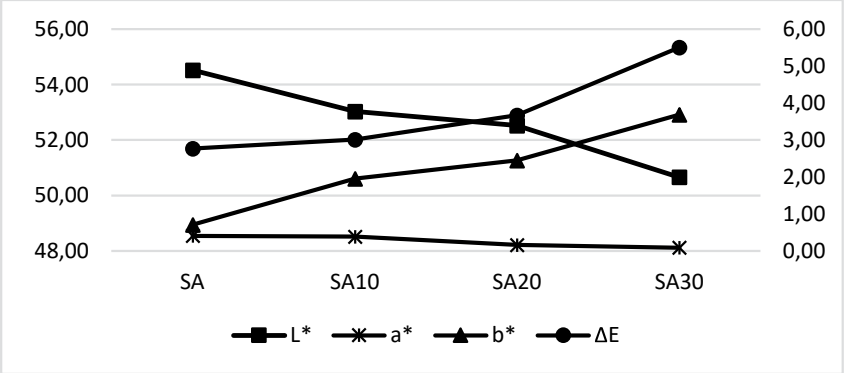

Figure 1: ***L*, a*, b** and ΔE values of the edible films. SA: sodium alginate film without kombucha, SA10, SA20, SA30: sodium alginate films with 10%, 20%, and 30% kombucha, respectively.**

Kombucha is composed of various chemical constituents, including metallic elements (e.g., iron, manganese, nickel, and copper), CO_2, organic food acids, polyphenols, vitamins (ascorbic acid and vitamin B), amino acids like lysine, dietary fiber, sugars, hydrolytic enzymes, and ethanol [25]. Table 1 lists the transparency values of the films, where high T values signify a low degree of transparency and high opacity. Kombucha significantly reduced the transparency of the SA films. This might be due to the interaction of various compounds coming from kombucha (polymeric compounds, polyphenols such as catechins, organic acids, etc.) with SA in the film matrix. These could act as a crosslinking agent, resulting in aggregates and low transmittance, as in the case of epigallocatechin gallate incorporation [14]. Also, it was reported that the existence of a greater number of heterogeneous structures promotes the scattering of light and leads to a reduction in transparency [26]. Films with low transparency may help to delay the oxidation reactions on food surfaces.

a) b)

Figure 2: **Dried edible films a) before being peeled off the petri dishes and conditioned in a desiccator (0%, 10%, 20%, and 30% kombucha incorporated, respectively from left to right), b) after being peeled off the dishes.**

DPPH free radical scavenging activity

The antioxidant activity of the SA films increased significantly as the kombucha content was risen ($p<0.05$). Although it was known that sodium alginate possesses some antioxidant capacity [27], the free radical scavenging activity of its film (5.40 %) was increased about 10 times when combined with the kombucha drink (Figure 3). In particular, films with the highest incorporation content showed the highest free radical inhibition capacity. In this study, the kombucha drink was fermented with sugared green tea. Previous studies reported that the addition of tea polyphenols enhanced the DPPH scavenging activity of alginate based edible films [14,17], possibly as a result of binging with sodium alginate by using the benefit of their hydrophilic structure. Catechins and epicatechins are the main polyphenols abundant in green tea and are mostly the major contributors to the radical scavenging antioxidant power of kombucha tea [28]. The free-radical scavenging potent of these comes from the 3-hydroxy group on an unsaturated C ring in their structure, and donation of OH groups [16]. Additionally, the organic acids and vitamin C are some of the other factors that improve or modify the free-radical scavenging ability, since a significant correlation was reported with this antioxidant capacity [29]. Interestingly, a correlation ($r=0.79$) was detected between DPPH radical scavenging activity and transparency of the films, which may indicate that higher opacity can result in enhanced antioxidant capability. As a result, edible film with a comparatively high kombucha concentration was more likely to exhibit strong antioxidant performance.

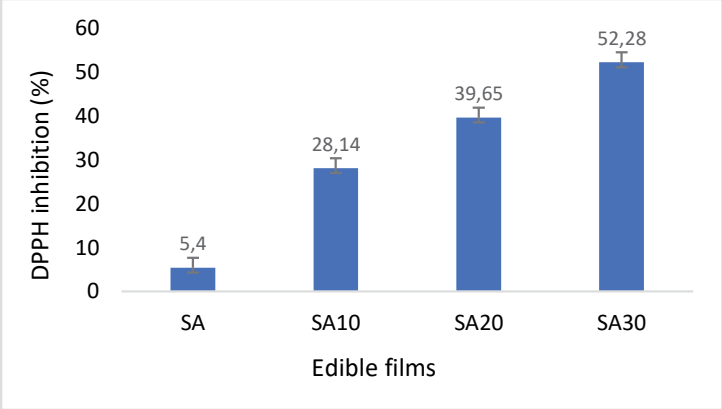

Figure 3: **DPPH radical inhibition activity of edible films. SA: sodium alginate film without kombucha, SA10, SA20, SA30: sodium alginate films with 10%, 20%, and 30% kombucha, respectively.**

In conclusion, the incorporation of green tea kombucha into sodium alginate-based edible films had significant effects on their physical properties, color, and antioxidant activity. While thinner films with reduced puncture strength were observed at higher kombucha levels, the films exhibited enhanced opacity and antioxidant potential, making them a potential candidate for packaging materials with protective properties.

REFERENCES

1. Hanani, Z.A.N., Roos, Y.H. & Kerry, J.P. *Int J Biol Macromol* 71, 94–102 (2014).
2. Ribeiro, A.M., Estevinho, B.N. & Rocha, F. *Food Bioproc Tech* 14, 209–231 (2021).
3. Galus, S. et al. *Coatings* 11, 745 (2021).
4. Shivangi, S., Dorairaj, D., Singh Negi, P. & Shetty, N.P. *Food Hydrocoll* 121, 107046 (2021).
5. Pérez, P.F., Ollé Resa, C.P., Gerschenson, L.N. & Jagus, R.J. *Food Bioproc Tech* 14, 262–271 (2021).
6. Atta, O.M. et al. *Polymers (Basel)* 13, (2021).
7. Koirala, P. et al. *Food Packag Shelf Life* 38, (2023).
8. Laureys, D., Britton, S.J. & De Clippeleer, J. *Journal of the American Society of Brewing Chemists* 78, 165–174 (2020).
9. Vina, I., Semjonovs, P., Linde, R. & Deniņa, I. *J Med Food* 17, 179–188 (2014).
10. Rezende Cardoso, R. et al. (2019). doi:10.1016/j.foodres.2019.108782
11. Dimidi, E., Cox, S.R., Rossi, M. & Whelan, K.doi:10.3390/nu11081806
12. Bortolomedi, B.M., Paglarini, C.S. & Brod, F.C.A. *Food Chem* 385, (2022).

13. Tavassoli-Kafrani, E., Shekarchizadeh, H. & Masoudpour-Behabadi, M. *Carbohydr Polym* 137, 360–374 (2016).
14. Ruan, C. et al. *Int J Biol Macromol* 134, 1038–1044 (2019).
15. Mahcene, Z. et al. *Int J Biol Macromol* 145, 124–132 (2020).
16. Jayabalan, R., Subathradevi, P., Marimuthu, S., Sathishkumar, M. & Swaminathan, K. *Food Chem* 109, 227–234 (2008).
17. Dou, L., Li, B., Zhang, K., Chu, X. & Hou, H. *Int J Biol Macromol* 118, 1377–1383 (2018).
18. Soradech, S., Nunthanid, J., Limmatvapirat, S. & Luangtana-Anan ⇑, M. (2011). doi:10.1016/j.jfoodeng.2011.07.019
19. Kurt, A. & Kahyaoglu, T. *Carbohydr Polym* 104, 50–58 (2014).
20. Shahrampour, D., Khomeiri, M., Razavi, S.M.A. & Kashiri, M. *LWT* 118, (2020).
21. Zhang, P., Zhao, Y. & Shi, Q. *Carbohydr Polym* 153, 345–355 (2016).
22. Biao, Y. et al. *Food Hydrocoll* 97, (2019).
23. Eswaranandam, S., Hettiarachchy, N.S. & Johnson, M.G. *J Food Sci* 69, (2004).
24. Ismillayli, N., Hadi, S., Tri Dharmayani, N.K., Sanjaya, R.K. & Hermanto, D. *IOP Conf Ser Mater Sci Eng* 833, (2020).
25. Mousavi, S.M. et al. *Evidence-based Complementary and Alternative Medicine* 2020, (2020).
26. Fabra, M.J., Falcó, I., Randazzo, W., Sánchez, G. & López-Rubio, A. *Food Hydrocoll* 81, 96–103 (2018).
27. Sellimi, S. et al. *Int J Biol Macromol* 72, 1358–1367 (2015).
28. Teixeira Oliveira, J. et al. *Food Chem* 408, (2023).
29. Malbaša, R. V., Lončar, E.S., Vitas, J.S. & Čanadanović-Brunet, J.M. *Food Chem* 127, 1727–1731 (2011).

EuChemS

European Chemical Society

EuChemS, the European Chemical Society, aims to nurture a platform for scientific discussion and to provide a single, unbiased European voice on key policy issues in chemistry and related fields.

Representing more than 160,000 chemists from more than 40 Member Societies and other chemistry related organisations, EuChemS relies on a unique network of active researchers involved in all the fields of chemistry. Through this network, EuChemS organises several specialised academic conferences as well as the biannual EuChemS Chemistry Congress, the European congress of chemical sciences. EuChemS also promotes the role and image of the chemical sciences among the general public and policy-makers through social media, newsletters and through the organisation of conferences and workshops open to the society.

Through the promotion of chemistry and by providing expert and scientific advice, EuChemS aims to take part of the solution to today´s major societal challenges.

For more information about the European Chemical Society (EuChemS), please visit www.euchems.eu or contact us at:

EuChemS aisbl
Rue du Trône 62
1050 - Brussels
Belgium

Phone: +32 2289 25 67 | +32 2289 26 90

Email: secretariat@euchems.eu

http://on.fb.me/1B8Qa0n

https://twitter.com/EuCheMS